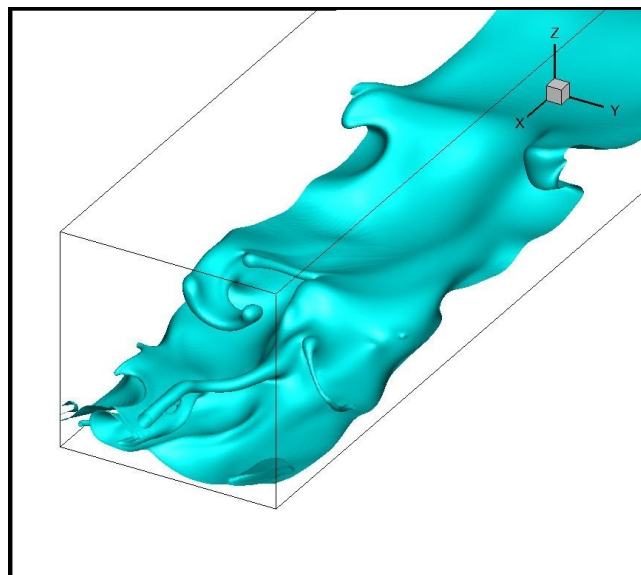University College Dublin
An Coláiste Ollscoile, Baile Átha Cliath

**School of Mathematics and Statistics
Scoil na Matamaitice agus Staitisticí
Advanced Fluid Mechanics (ACM 40890)**

Dr Lennon Ó Náraigh

Advanced Fluid Mechanics (ACM40890)

- Subject: Applied and Computational Mathematics

- School: Mathematical Sciences

- Module coordinator: Dr Lennon Ó Náraigh

- Credits: 5

  Note: This module was called ACM40740 in a previous incarnation. ACM40740 was a 10-credit module with additional coursework; the present version is a 5-credit module.

- Level: 4 (Masters)

- Semester: Second

This module introduces advanced concepts and methods in Fluid Dynamics. The main focus is on viscous incompressible flows, under the following broad headings.

Canonical examples of fluid instability: Eigenvalue analysis of linear instability in the Rayleigh–Benard, Rayleigh–Taylor, and Kelvin–Helmholtz systems. Eigenvalue analysis of parallel flow instability leading to the Orr–Sommerfeld equation. **Parallel flow instability beyond the temporal theory:** Absolute and convective instability, transient growth **Weakly nonlinear stability theory:** Stuart–Landau theory applied to the Cahn–Hilliard and Kuramoto–Sivishinsky equation **Turbulence:** Problems in turbulence. Kolmogorov spectra. Wall-bounded turbulence and Reynolds averaging. Closure models. Discussion of direct numerical simulation and large-eddy simulation. The notion of wall-functions in large-eddy simulation. **Introduction to High-Performance computing:** Solving sparse linear problems iteratively. Applications of such methods to Computational Fluid Dynamics. Introduction to multithread and multicore programming in Fortran.

What will I learn?

On completion of this module students should be able to

1. Write down the eigenvalue problem for the canonical physical systems of Fluid Dynamics

2. Derive the Orr–Sommerfeld equation and compute exact solutions in certain cases

3. Describe the subtle features of linear stability theory beyond temporal eigenvalue analysis

4. Carry out a Stuart–Landau analysis on simple nonlinear equations

5. Characterize turbulence using the Kolmogorov and Reynolds-averaged theories.

6. Solve sparse linear problems iteratively and implement their solution in Fortran.

In addition to the study of sparse linear systems and their role in Computational Fluid Dynamics, a number of mini-projects will form part of this module. Therefore, on completion of this module students should gain much familiarity with computational methods in fluids. In particular, students should further be able to

1. Perform an Orr–Sommerfeld stability analysis of Poiseuille flow using spectral methods in Matlab

2. Solve nonlinear wave equations numerically to test for the applicability of Stuart–Landau theory

3. Implement an existing parallel flow solver to study large-eddy simulations in turbulent channel flow

4. Analyse the turbulent statistics emanating from the simulations under point (4) above.

Editions

First edition: January 2015 (As ACM40740)

This edition: January 2016 (As ACM40890)

This edition: January 2018 (As ACM40890)

Contents

Chapter 0

Introduction

0.1 Overview

The focus of this module is on developing advanced analytical and numerical techniques to deal with incompressible viscous flow. This is a fairly restricted aim, since many interesting phenomena arise in treating of the other flow regimes. For example, a study of compressible flow leads to important topics in acoustics, gas dynamics, and shockwave theory, while a study of incompressible inviscid flow leads (in two dimensions) to the very beautiful theory of vorticity as described using complex analysis and conformal-mapping theory. However, it is sensible to maintain a fairly restricted focus, especially because the proposed research plan aligns with the present lecturer's expertise. Thus, we will study the following topics in detail:

- Linear stability analysis for the canonical physical systems of Fluid Dynamics

- Orr–Sommerfeld theory for parallel flow instability, including exact solutions in certain cases

- The subtle features of linear stability theory beyond temporal eigenvalue analysis

- Stuart–Landau analysis for simple nonlinear equations

- Introduction to turbulence using the Kolmogorov and Reynolds-averaged theories.

- Introduction to Computational Fluid Dynamics

0.2 Learning and Assessment

Learning

- One or two lectures per week

- As this is an advanced module, heavy emphasis is placed on independent study. This will be guided by lecture notes, recommended textbooks, problem sheets, and computational exercises.

Assessment

- One final exam, counting for 50%. The exam will run locally.

- Two computational mini-projects, counting for 50% in total.

- **Other exercises** can be found throughout the book of lecture notes. They may be attempted for practice. The final exam will be based almost entirely on these exercises.

Textbooks

Material and exercises for this module will be taken from the following textbooks:

- Hydrodynamic and Hydromagnetic Stability, S. Chandrasekhar (Dover edition, 1981) [Cha61]

- Hydrodynamic Stability, P. G. Drazin, W. H. Reid (Cambridge University Press, 2004 edition) [DR81]

- Stability and Transition in Shear Flows, P. J. Schmid and D. S. Henningson (Springer, 2001) [SH01]

- Turbulent Flows, S. Pope (Cambridge University Press, 2000) [Pop00]

Other material comes either from the top of my head or from published articles, referred to in the remainder of the lecture notes.

Chapter 1

Rayleigh–Bénard Convection

Overview

You have already studied parallel flow instability from the point of view of linear theory. There, the governing equation is the Orr–Sommerfeld equation, the eigenvalues of which determine the stability of the parallel flow to small-amplitude disturbances. In general, there are no closed-form solutions to the Orr–Sommerfeld equation, either for the eigenfunctions or the eigenvalues. Therefore, the aim in these lectures is to look at a non-trivial but highly relevant physical system where the linear theory admits analytical expressions. This is the case of Rayleigh–Bénard instability.

The idea behind the Rayleigh–Bénard instability is to take a uniform homogeneous fluid sandwiched between two plates, and to heat the bottom plate so that a density gradient emerges, with a cooler, denser layer lying on top of a hotter, less dense layer, thereby inducing an unstable stratification. Beyond a threshold values, this configuration becomes unstable, triggering a convective motion that counteracts the unstable stratification. The mathematics of this flow instability is introduced in these lectures.

1.1 Governing equations

We start with the governing Navier–Stokes equations of incompressible flow in an arbitrary domain:

$$\rho \left(\frac{\partial u_i}{\partial t} + u_j \frac{\partial u_i}{\partial x_j} \right) = -\frac{\partial p}{\partial x_i} + \mu \nabla^2 u_i + \rho g_i,$$

where all the symbols have their usual meaning and the gravity vector is $(g_1, g_2, g_3) = (0, 0, -g)$, such that gravity points in the negative z-direction. The Navier–Stokes equation is supplemented

with the incompressibility condition

$$\frac{\partial \rho}{\partial t} + \frac{\partial}{\partial x_i}(\rho u_i) = 0.$$

To close the Navier–Stokes equations, further conditions (in addition to the incompressibility relation) are required. In particular, it is necessary to prescribe the behaviour of the density function. In the present application, we are interested in fluid behaviour in the presence of a temperature gradient, so it is sensible to focus on a model where the density depends on temperature (T), wherein the simplest possible model is a linear relation:

$$\rho = \rho_0 + \delta\rho, \qquad \delta\rho = -\rho_0 \alpha (T - T_0),$$

where ρ_0 is the reference density, $\delta\rho$ is a fluctuation which depends linearly on temperature. Also, T_0 is the reference temperature, with $T = T_0 \iff \rho = \rho_0$. Finally, the quantity $\alpha > 0$ is the coefficient of volume expansion. We are not done yet: the evolution of temperature field $T(\boldsymbol{x}, t)$ must be precribed. However, this can be accurately modelled by an advection-diffusion equation:

$$\frac{\partial T}{\partial t} + u_i \frac{\partial T}{\partial x_i} = \kappa \nabla^2 T,$$

where $\kappa > 0$ is the thermal diffusivity. We assemble all our equations into a single mathematical model:

$$\rho \left(\frac{\partial u_i}{\partial t} + u_j \frac{\partial u_i}{\partial x_j} \right) = -\frac{\partial p}{\partial x_i} + \mu \nabla^2 u_i + \rho g_i, \tag{1.1a}$$

$$\frac{\partial \rho}{\partial t} + \frac{\partial}{\partial x_i}(\rho u_i) = 0, \tag{1.1b}$$

$$\rho = \rho_0 + \delta\rho, \qquad \delta\rho = -\rho_0 \alpha (T - T_0), \tag{1.1c}$$

$$\frac{\partial T}{\partial t} + u_i \frac{\partial T}{\partial x_i} = \kappa \nabla^2 T, \tag{1.1d}$$

In practice, the density variations are quite small, and an approximation can be made wherein **density variations are considered only in the buoyancy (gravity) term**. This is called the **Boussinesq Approximation** (for a full justification of this approximation, see pages 16-17 in [Cha61]. Thus, Equations (1.1a)–(1.1b) simplify to

$$\frac{\partial u_i}{\partial t} + u_j \frac{\partial u_i}{\partial x_j} = -\frac{1}{\rho_0} \frac{\partial p}{\partial x_i} + \nu \nabla^2 u_i + \left(1 + \frac{\delta\rho}{\rho_0} g_i \right), \qquad \nu = \mu/\rho_0, \tag{1.2a}$$

$$\frac{\partial u_i}{\partial x_i} = 0, \tag{1.2b}$$

while the density and temperature laws remain unchanged. This is a great simplification, as the density in the Navier–Stokes equations is now 'almost' a constant.

1.2 The base state

We study a time-independent base state involving no flow, with $u_i = 0$ and a static temperature distribution, such that

$$\nabla^2 T = 0.$$

We also focus on a two-dimensional geometry for now, in the (x, z) plane, such that the solution of the Laplace equation for temperature reads

$$T = T_0 + Ax + Bz,$$

where A and B are constants. However, we specialize without loss of generality to a situation where the temperature gradient is imposed in the z-direction only, such that $A = 0$. Also, we focus on the more interesting case of an **adverse** temperature gradient, such that $B = -\beta$, with $\beta > 0$, and such that

$$T = T_0 - \beta z.$$

Thus, compared to a baseline at $z = 0$ where the temperature is T_0, high up where $z > 0$ it is relatively colder and low down where $z < 0$ it is relatively hotter. Next, using $\rho = \rho_0 + \delta\rho = \rho_0 - \alpha\rho_0(T - T_0)$ we obtain

$$\rho = \rho_0(1 + \alpha\beta z).$$

Again, compared to a baseline at $z = 0$ where the density is ρ_0, high up where $z > 0$ the fluid is both relatively cool and relatively **more dense** while low down where $z < 0$ it is relatively hot and less dense. This is the notion of an adverse temperature gradient - the temperature and density gradients are going in opposite directions. The last part of the characterization of the base state is the determination of the pressure. We have the w-velocity equation:

$$\frac{\partial w}{\partial t} + u\frac{\partial w}{\partial x} + w\frac{\partial w}{\partial z} = -\frac{\partial p}{\partial z} - \rho_0 g(1 + \alpha\beta z) + \nu\nabla^2 w.$$

With $w = 0$ this gives

$$\frac{\partial p}{\partial z} = -\rho_0 g(1 + \alpha\beta z). \tag{1.3}$$

The analogous u-velocity equation gives $\partial p/\partial x = 0$. Note that Equation (1.3) is the equation of **hydrostatic balance**: the pressure drop and the gravity force are balanced. Solving Equation (1.3) gives

$$p = -\rho_0 g\left(z + \tfrac{1}{2}\alpha\beta z^2\right).$$

We now characterize the base state in full by assembling our results in one place:

$$u_i = 0, \qquad p = -\rho_0 g\left(z + \tfrac{1}{2}\alpha\beta z^2\right). \tag{1.4a}$$

$$T = T_0 - \beta z, \qquad \rho = \rho_0(1 + \alpha\beta z). \tag{1.4b}$$

1.3   Linear stability analysis

Equations (1.4) are the time-independent **base state** of the problem. This solution would appear to be unstable as the stratification is (apparently) itself unstable: a denser fluid sits on top of a less dense fluid. The idea of the remainder of this chapter is to investigate this stability problem. We do so by introducing perturbations:

$$u_i = \underbrace{0}_{\text{base state}} + \underbrace{u_i}_{\text{perturbations}}$$

and

$$T' = \underbrace{T_0 - \beta z}_{\text{base state}} + \underbrace{\theta}_{\text{perturbations}} .$$

We assume that the perturbations are **small** in the sense that the equations of motion for (u_i, T') can be **linearized** without any loss of accuracy in the modeling. The linearized equations of motion read

$$\frac{\partial u_i}{\partial t} = -\frac{\partial}{\partial x_i}\left(\frac{\delta p}{\rho_0}\right) + \delta_{i,z}g\alpha\theta + \nu\nabla^2 u_i, \tag{1.5a}$$

$$\frac{\partial u_i}{\partial x_i} = 0, \tag{1.5b}$$

$$\frac{\partial \theta}{\partial t} = w\beta + \kappa\nabla^2\theta. \tag{1.5c}$$

Here, δp is the perturbation pressure.

Exercise 1.1 *Prove Equation* (1.5) *by carrying out the relevant linearization.*

In incompressible flow wherein the density is a fixed constant, the pressure is always a 'bad' variable because it does not have its own equation (it is determined implicitly via the relation $\partial_i u_i = 0$). Thus, we always try to eliminate the pressure from the equations of motion. We do that here by

considering again the momentum equations:

$$\frac{\partial u}{\partial t} = -\frac{\partial}{\partial x}\left(\frac{\delta p}{\rho_0}\right) + \nu\nabla^2 u, \tag{1.6}$$

$$\frac{\partial w}{\partial t} = -\frac{\partial}{\partial z}\left(\frac{\delta p}{\rho_0}\right) + g\alpha\theta + \nu\nabla^2 w, \tag{1.7}$$

and by taking $\partial_z(1.6) - \partial_x(1.7)$; the result is

$$\frac{\partial}{\partial t}\left(\frac{\partial u}{\partial z} - \frac{\partial w}{\partial x}\right) = -g\alpha\frac{\partial\theta}{\partial x} + \nu\nabla^2\left(\frac{\partial u}{\partial z} - \frac{\partial w}{\partial x}\right). \tag{1.8}$$

We take $\partial_x(1.8)$ and obtain

$$\frac{\partial}{\partial t}\left(\frac{\partial^2 u}{\partial x\partial z} - \frac{\partial^2 w}{\partial x^2}\right) = -g\alpha\frac{\partial^2\theta}{\partial x^2} + \nu\nabla^2\left(\frac{\partial^2 u}{\partial x\partial z} - \frac{\partial w}{\partial x^2}\right). \tag{1.9}$$

We use the incompressibility condition $\partial_x u + \partial_z w$ to write

$$\frac{\partial^2 u}{\partial x\partial z} = -\frac{\partial^2 w}{\partial z^2}.$$

Hence, Equation (1.9) becomes

$$\frac{\partial}{\partial t}\left(-\frac{\partial^2 w}{\partial z^2} - \frac{\partial^2 w}{\partial x^2}\right) = -g\alpha\frac{\partial^2\theta}{\partial x^2} + \nu\nabla^2\left(-\frac{\partial^2 w}{\partial z^2} - \frac{\partial w}{\partial x^2}\right). \tag{1.10}$$

Finally then, we obtain

$$\frac{\partial}{\partial t}\nabla^2 w = +g\alpha\frac{\partial^2\theta}{\partial x^2} + \nu\nabla^4 w.$$

We now assemble here in one place the two closed stability equations for the perturbation velocity and temperature:

$$\frac{\partial}{\partial t}\nabla^2 w = +g\alpha\frac{\partial^2\theta}{\partial x^2} + \nu\nabla^4 w, \tag{1.11a}$$

$$\frac{\partial\theta}{\partial t} = w\beta + \kappa\nabla^2\theta \tag{1.11b}$$

At this point, it is appropriate to discuss boundary conditions. We assume that the flow is unbounded in the x-direction, with $-\infty < x < \infty$, and that the flow is confined in the z-direction by two parallel plates, located at $z = 0$ and $z = d$. The temperature is maintained at fixed values at the plate walls, such that the temperature perturbations vanish at those walls:

$$\theta = 0, \qquad z = 0, d.$$

Also, because of the no-flux/no penetration conditions at the walls, we have

$$w = 0, \qquad z = 0, d.$$

Now, the equation to solve is fourth-order in w, so further boundary conditions are required. Because of no-slip, we have $u = 0$ on the walls, hence $\partial u / \partial x = 0$ on the walls. By continuity, this means that

$$\frac{\partial w}{\partial z} = 0, \qquad z = 0, d,$$

and this gives the required number of boundary conditions necessary to solve Equations (1.11).

1.4   Normal-mode solution

Because of the translational invariance of the equations (1.11) in the x-direction, it makes sense to introduce a trial solution $w \propto \mathrm{e}^{\mathrm{i}kx}$ and $\theta \propto \mathrm{e}^{\mathrm{i}kx}$ representing a plane wave, where k is the wavenumber. Indeed, it also makes sense to introduce exponential time dependence (in a standard way) such that the following **normal-mode solution** is proposed:

$$w = \mathrm{e}^{pt+\mathrm{i}kx}W(z), \tag{1.12a}$$
$$\theta = \mathrm{e}^{pt+\mathrm{i}kx}\Theta(z). \tag{1.12b}$$

Substitution of Equations (1.12) into Equations (1.11) yields

$$p\left(\partial_z^2 - k^2\right)W = \nu\left(\partial_z^2 - k^2\right)^2 W - g\alpha k^2\Theta,$$
$$p\Theta = \beta W + \kappa\left(\partial_z^2 - k^2\right)\Theta.$$

Before going any further, we reduce the number of parameters in these equations by rescaling as follows:

$$\left(\partial_z^2 - k^2 - \frac{p}{\kappa}\right)\Theta = -\frac{\beta}{\kappa}W, \tag{1.13a}$$
$$\left(\partial_z^2 - k^2\right)\left(\partial_z^2 - k^2 - \frac{p}{\nu}\right)W = +\frac{g\alpha}{\nu}k^2\Theta. \tag{1.13b}$$

We introduce a non-dimensional z-coordinate $\widetilde{z} = z/d$, with

$$\frac{d}{dz} = \frac{d\widetilde{z}}{dz}\frac{d}{d\widetilde{z}} = \frac{1}{d}\frac{d}{d\widetilde{z}},$$

and the equations (1.13) become

$$\left(\partial_{\widetilde{z}}^2 - d^2 k^2 - \frac{pd^2}{\nu}\frac{\nu}{\kappa}\right)\Theta = -\frac{\beta d^2}{\kappa}W, \tag{1.14a}$$

$$\left(\partial_{\widetilde{z}}^2 - d^2 k^2\right)\left(\partial_{\widetilde{z}}^2 - d^2 k^2 - \frac{pd^2}{\nu}\right)W = +\frac{g\alpha d^2}{\nu}(d^2 k^2)\Theta. \tag{1.14b}$$

We identify

$$\mathrm{Pr} = \frac{\nu}{\kappa}, \qquad \sigma = \frac{pd^2}{\nu}, \qquad [\sigma] = 1,$$

where $\mathrm{Pr} = \nu/\kappa$ is the **Prandtl number**. Thus, Equations (1.14) become

$$\left(\partial_{\widetilde{z}}^2 - \widetilde{k}^2 - \sigma\mathrm{Pr}\right)\Theta = -\frac{\beta d^2}{\kappa}W, \tag{1.15a}$$

$$\left(\partial_{\widetilde{z}}^2 - \widetilde{k}^2\right)\left(\partial_{\widetilde{z}}^2 - \widetilde{k}^2 - \sigma\right)W = +\frac{g\alpha d^2}{\nu}\widetilde{k}^2\Theta, \tag{1.15b}$$

where $\widetilde{k} = dk$ is a dimensionless wavenumber . We combine the Θ and W-equations by taking the W-equation and operating on it with $(\partial_{\widetilde{z}}^2 - k^2 - \sigma\,\mathrm{Pr})$. We obtain

$$\left(\partial_{\widetilde{z}}^2 - \widetilde{k}^2 - \sigma\mathrm{Pr}\right)\left[\left(\partial_{\widetilde{z}}^2 - \widetilde{k}^2\right)\left(\partial_{\widetilde{z}}^2 - \widetilde{k}^2 - \sigma\right)W\right] = \left(\partial_{\widetilde{z}}^2 - \widetilde{k}^2 - \sigma\mathrm{Pr}\right)\left[\frac{g\alpha d^2}{\nu}\widetilde{k}^2\Theta\right],$$

$$= \frac{g\alpha d^2}{\nu}\widetilde{k}^2\left[\left(\partial_{\widetilde{z}}^2 - \widetilde{k}^2 - \sigma\mathrm{Pr}\right)\Theta\right],$$

$$= \frac{g\alpha d^2}{\nu}\widetilde{k}^2\left[-\frac{\beta d^2}{\kappa}W\right],$$

$$= -\frac{g\alpha\beta d^4}{\nu\kappa}\widetilde{k}^2 W.$$

We introduce

$$\mathrm{Ra} = \frac{g\alpha\beta d^4}{\nu\kappa}$$

as the **Rayleigh number** and we have the following single stability equation:

$$\left(\partial_{\widetilde{z}}^2 - \widetilde{k}^2 - \sigma\mathrm{Pr}\right)\left(\partial_{\widetilde{z}}^2 - \widetilde{k}^2 - \sigma\right)\left(\partial_{\widetilde{z}}^2 - \widetilde{k}^2\right)W = -\mathrm{Ra}\,\widetilde{k}^2 W. \tag{1.16a}$$

Exercise 1.2 *Show that the Rayleigh number is dimensionless.*

Viewing the eigenvalue problem as an equation in the single variable W, it can be noted that the

ordinary differential equation to solve is sixth order. We already have the boundary conditions

$$W = W' = 0, \qquad z = 0, 1, \tag{1.16b}$$

giving four boundary conditions. We need two more boundary conditions to close the problem. However, since $(\partial_z^2 - k^2)(\partial_z^2 - k^2 - \sigma)W = (g\alpha d^2/\nu)k^2\Theta$, and since $\Theta = 0$ on the boundaries, the remaining two boundary conditions are given by

$$\left(\partial_{\widetilde{z}}^2 - \widetilde{k}^2 - \sigma\right)\left(\partial_{\widetilde{z}}^2 - \widetilde{k}^2\right) W = 0, \qquad z = 0, 1. \tag{1.16c}$$

Thus, we have an ordinary differential equation in the eigenvalue σ. Before attempting various approaches to solve for σ as a function of k explicitly, we first of all investigate the properties of this equation using *a priori* methods. Following standard practice, in the remainder of this Chapter we omit the tildes over the dimensionless variables.

Remark 1 *A normal-mode trial solution is possible when a problem possesses translational symmetry.*

For, consider a generic linear problem

$$\frac{\partial \phi}{\partial t} = \mathcal{L}\phi,$$

where $\phi = \phi(x, t)$ is some scalar field and $\mathcal{L}$ is a linear operator depending on ∂_x and higher derivatives, such that $\mathcal{L}$ is translation invariant:

$$\mathcal{L}(x) = \mathcal{L}(x + a), \qquad \text{for all a} \in \mathbb{R}.$$

Introduce the translation operator $\mathcal{T}$:

$$\mathcal{T}_a\phi(x) = \phi(x + a).$$

Thus, $\mathcal{T}\mathcal{L}\phi = \mathcal{L}\mathcal{T}\phi$, since $\mathcal{T}$ has no effect on $\mathcal{L}$. In other words, $\mathcal{T}$ and $\mathcal{L}$ commute as operators. There is a theorem in Linear Algebra that says that if two operators commute, then they share the same eigenvectors (eigenfunctions). And, since e^{ikx} is an eigenfunction of $\mathcal{T}$, it must also be an eigenfunction of $\mathcal{L}$.

In more detail, e^{ikx} is an eigenfunction of $\mathcal{T}$ because

$$\mathcal{T}\mathrm{e}^{ikx} = \mathrm{e}^{ik(x+a)} = \mathrm{e}^{ika}\mathrm{e}^{ikx},$$

hence e^{ikx} is the eigenfunction with eigenvalue e^{ika}. ∎

1.5 A priori methods for the stability equation

Theorem 1.1 *Consider the eigenvalue problem given by Equation (1.16). The eigenvalue σ is purely real and therefore, the transition from stability to instability is given by $\sigma = 0$.*

Proof: Introduce

$$G = (\partial_z^2 - k^2)W, \qquad F = (\partial_z^2 - k^2)(\partial_z^2 - k^2 - \sigma)W,$$

hence $F = (\partial_z^2 - k^2 - \sigma)G$. The boundary conditions in Equation (1.16) imply that $F = 0$ at $z = 0$ and $z = 1$. Also, the eigenvalue equation can be rewritten as

$$(\partial_z^2 - k^2 - \operatorname{Pr}\sigma)F = -\operatorname{Ra} k^2 W.$$

We multiply both sides of this equation by F^* and integrate from $z = 0$ to $z = 1$. Now,

$$\int_0^1 F^* \partial_z^2 F \, \mathrm{d}z = -\int_0^1 |\partial_z F|^2 \, \mathrm{d}z,$$

in view of the boundary conditions on F at $z = 0$ and $z = 1$. Thus, we obtain

$$\int_0^1 \left[|\partial_z F|^2 + (k^2 + \operatorname{Pr}\sigma)|F|^2 \right] \mathrm{d}z = \operatorname{Ra} \int_0^1 F^* W \, \mathrm{d}z.$$

Now consider

$$
\begin{aligned}
\int_0^1 F^* W \, \mathrm{d}z &= \int_0^1 W(\partial_z^2 - k^2 - \sigma^*)G^* \, \mathrm{d}z, \\
&= \int_0^1 W \partial_z^2 G^* \, \mathrm{d}z - (k^2 + \sigma^*) \int_0^1 W G^* \, \mathrm{d}z, \\
&= \int_0^1 G^* \partial_z^2 W \, \mathrm{d}z - (k^2 + \sigma^*) \int_0^1 W G^* \, \mathrm{d}z, \\
&= \int_0^1 G^* \left[(\partial_z^2 - k^2) - \sigma^* \right] W \, \mathrm{d}z,
\end{aligned}
$$

where we have used integration by parts repeatedly to show that

$$\int_0^1 W \partial_z^2 G^* \, \mathrm{d}z = \int_0^1 G^* \partial_z W \, \mathrm{d}z,$$

using further the fact that $W = \partial_z W = 0$ on $z = 0, 1$. Now,

$$
\begin{aligned}
\int_0^1 F^* W \, \mathrm{d}z &= \int_0^1 G^* \left[(\partial_z^2 - k^2) - \sigma^* \right] W \, \mathrm{d}z, \\
&= \int_0^1 G^* \left(G - \sigma^* W \right) \mathrm{d}z, \\
&= \int_0^1 |G|^2 \, \mathrm{d}z - \sigma^* \int_0^1 G^* W, \\
&= \|G\|_2^2 - \sigma^* \int_0^1 \left[(\partial_z^2 - k^2) \, W^* \right] W \, \mathrm{d}z, \\
&= \|G\|_2^2 + \sigma^* \int_0^1 \left(|\partial_z W|^2 + k^2 |W|^2 \right) \mathrm{d}z
\end{aligned}
$$

Putting it all together, we have

$$
\|\partial_z F\|_2^2 + (k^2 + \Pr \sigma) \|F\|_2^2 = \mathrm{Ra} \left[\|G\|_2^2 + \sigma^* \left(\|\partial_z W\|_2^2 + k^2 \|W\|_2^2 \right) \right]
$$

Take imaginary parts on both sides of this equation:

$$
\Pr \Im(\sigma) \|F\|_2^2 = -\mathrm{Ra} \Im(\sigma) \left(\|\partial_z W\|_2^2 + k^2 \|W\|_2^2 \right),
$$

where the mysterious minus sign emerges on the right-hand side because it is σ^* that appears there, not σ. Hence,

$$
\Im(\sigma) \left[\Pr \|F\|_2^2 + \mathrm{Ra} \left(\|\partial_z W\|_2^2 + k^2 \|W\|_2^2 \right) \right] = 0.
$$

Now, the quantity inside the square brackets is positive definite, so we are forced to conclude that

$$
\Im(\sigma) = 0.
$$

For the second part of the theorem, we start with the fact that the system changes from stable to unstable when

$$
\Re(\sigma) = 0.
$$

However, σ is purely real, so this condition for a change in the stability amounts to

$$
\sigma = 0.
$$

This concludes the proof.   ∎

In stability theory it is of interest to construct the **neutral curve** $\Re(\sigma) = 0$ as a function of the problem parameters (in this case $(\mathrm{Ra}, \Pr, k)$). For the Rayleigh–Benard convection, we have shown that the neutral curve amounts to $\sigma(\mathrm{Ra}, \Pr, k) = 0$. In the next section we find semi-explicit solutions for this neutral curve.

Remark 2 *Quite generally, in linear stability theory, the condition*

$$\Re(\sigma) = 0$$

is called the **threshold** *or the point of criticality. This is where the system switches between stable and unstable states. In the case of Rayleigh–Bénard convection, the imaginary part of σ is always zero, so for this one instance only, the point of criticality is simply $\sigma = 0$. This simplifies the next piece of analysis.*

1.6 Explicit solution for the neutral curve

From the previous section, it is known that the neutral curve occurs when $\sigma = 0$. Therefore, we set $\sigma = 0$ in the eigenvalue problem (1.16) to obtain the following simplified equations:

$$\left(\partial_z^2 - k^2\right)^3 W = -\operatorname{Ra} k^2 W.$$

Instead of placing the plates at $z = 0, 1$, we instead set up the problem in a more symmetric manner, such that $z \in (-1/2, 1/2)$. Thus, the relevant boundary conditions are imposed as follows:

$$W = W' = (\partial_z^2 - k^2)^2 W = 0 \qquad \text{on } z = \pm\tfrac{1}{2}.$$

We immediately make a trial solution
$$W = \mathrm{e}^{\pm qz}$$

such that
$$(q^2 - k^2)^3 = -\operatorname{Ra} k^2.$$

We call
$$\operatorname{Ra} k^2 = \tau^3 k^6$$

hence
$$(q^2 - k^2)^3 = -\tau^3 k^6,$$

and
$$q^2 = k^2 + (-1)^{1/3}\tau k^2.$$

Note also:
$$\tau = (\operatorname{Ra}/k^4)^{1/3}.$$

The three cube roots of unity are

$$(-1)^{1/3} = -1, \qquad \tfrac{1}{2}\left(1 \pm \mathrm{i}\sqrt{3}\right),$$

hence

$$q^2 = -k^2(\tau - 1), \qquad q^2 = k^2\left[1 + \tau\tfrac{1}{2}\left(1 \pm \mathrm{i}\sqrt{3}\right)\right].$$

Taking square roots, we obtain the following six square-root solutions:

$$\pm \mathrm{i}q_0, \qquad \pm q, \qquad \pm q^*,$$

where $q_0 = k\sqrt{\tau - 1}$ and

$$\Re(q) \quad := \quad q_1 = k\left[\tfrac{1}{2}\sqrt{1 + \tau + \tau^2} + \tfrac{1}{2}\left(1 + \tfrac{1}{2}\tau\right)\right]^{1/2}, \tag{1.17a}$$

$$\Im(q) \quad := \quad q_2 = k\left[\tfrac{1}{2}\sqrt{1 + \tau + \tau^2} - \tfrac{1}{2}\left(1 + \tfrac{1}{2}\tau\right)\right]^{1/2}. \tag{1.17b}$$

Exercise 1.3 *Prove Equation* (1.17).

In view of the symmetric nature of the problem (sandwiched between $z = -1/2$ and $z = 1/2$), we can break up the solution into odd and even cases with respect to the centreline at $z = 0$. For the **even case** we have a solution

$$W = A_0 \cos(q_0 z) + A \cosh(qz) + A^* \cosh(q^*z),$$

where we have constructed a manifestly even solution via a linear superposition of component solutions. There are only three linearly independent complex coefficients in the superposition, and these can be chosen as A_0, A, and A^*, since A and A^* are linearly independent. Imposing the boundary conditions at $z = \pm 1/2$ yields

$$A_0 \cos(q_0/2) + A \cosh(q/2) + A^* \cosh(q^*/2) \;=\; 0, \tag{1.18a}$$

$$-q_0 A_0 \sin(q_0/2) + qA \sinh(q/2) + q^* A^* \sinh(q^*/2) \;=\; 0, \tag{1.18b}$$

$$A_0 \cos(q_0/2) + \tfrac{1}{2}\left(\mathrm{i}\sqrt{3} - 1\right) A \cosh(q/2) - \tfrac{1}{2}\left(\mathrm{i}\sqrt{3} + 1\right) A^* \cosh(q^*/2) \;=\; 0. \tag{1.18c}$$

This immediately leads to a determinant problem

$$
\begin{vmatrix}
\cos(q_0/2) & \cosh(q/2) & \cosh(q^*/2) \\
-q_0 \sin(q_0/2) & q \sinh(q/2) & q^* \sinh(q^*/2) \\
\cos(q_0/2) & \frac{1}{2}\left(i\sqrt{3}-1\right)\cosh(q/2) & -\frac{1}{2}\left(i\sqrt{3}+1\right)\cosh(q^*/2)
\end{vmatrix} = 0. \qquad (1.19)
$$

We divide each row of the determinant problem by the first row to obtain

$$
\begin{vmatrix}
1 & 1 & 1 \\
-q_0 \tan(q_0/2) & q \tanh(q/2) & q^* \tanh(q^*/2) \\
1 & \frac{1}{2}\left(i\sqrt{3}-1\right) & -\frac{1}{2}\left(i\sqrt{3}+1\right)
\end{vmatrix} = 0. \qquad (1.20)
$$

Next, we subtract the first row from the third row and divide the result by $-\sqrt{3}/2$ to obtain

$$
\begin{vmatrix}
1 & 1 & 1 \\
-q_0 \tan(q_0/2) & q \tanh(q/2) & q^* \tanh(q^*/2) \\
0 & \sqrt{3}-i & \sqrt{3}+i
\end{vmatrix} = 0. \qquad (1.21)
$$

Expanding this determinant yields

$$
\Im\left[\left(\sqrt{3}+i\right) q \tanh(q/2)\right] + q_0 \tan(q_0/2) = 0. \qquad (1.22)
$$

Exercise 1.4 *Fill in the blanks in the derivations of Equations* (1.18), (1.21) *and* (1.22).

Since q and q_0 are both functions of k and Ra, Equation (1.22) can be regarded as a condition of the form

$$
\Phi(\mathrm{Ra}, k) = 0,
$$

where Φ is a function of two variables. This is the implicit equation of a curve in $\mathrm{Ra} - k$ space – the neutral curve. Note that the neutral curve is independent of the Prandtl number. Thus, to determine the onset of instability, the Prandtl number is irrelevant - only the wavenumber and the Rayleigh number matter. The aim of the remainder of this section is to compute the neutral curve numerically.

There are some missing steps in Equation (1.18c). Recall, this is the boundary condition $(\partial_z^2 - k^2)^2 W = 0$, where $W = A_0 \cos(q_0 z) + A \cosh(qz) + A^* \cosh(q^* z)$. Look at the cosine component

first, and consider

$$
\begin{aligned}
(\partial_z^2 - k^2)^2 \cos(q_0 z) &= \left(\partial_z^4 - 2k^2\partial_z^2 + k^4\right)\cos(q_0 z), \\
&= (q_0^2 + 2k^2 q^2 + k^4)\cos(q_0 z), \qquad \text{(note the sign)}, \\
&= (q_0^2 + k^2)^2 \cos(q_0 z), \\
&= [(k^2\tau - k^2) + k^2]^2 \cos(q_0 z), \qquad \text{as } q_0 = k^2(\tau - 1), \\
&= k^4 \tau^2 \cos(q_0 z).
\end{aligned}
$$

Similarly, consider the cosh component $A\cosh(qz)$:

$$
\begin{aligned}
(\partial_z^2 - k^2)^2 \cosh(qz) &= (q^2 - k^2)^2 \cosh(qz), \\
&= \left[\left(k^2 + \tfrac{1}{2}\tau k^2(1 + i\sqrt{3})\right) - k^2\right]\cosh(qz), \\
&= \left(k^2\tau\omega\right)^2 \cosh(qz),
\end{aligned}
$$

where $\omega = (1 + i\sqrt{3})/2$ and

$$
\omega^2 = -\frac{1}{\omega} = \tfrac{1}{2}\left(i\sqrt{3} - 1\right).
$$

From these calculations, it is obvious that

$$
\left(\partial_z^2 - k^2\right) W = (k^2\tau)^2 A_0 \cos(q_0 z) + (k^2\tau)^2 \left[\tfrac{1}{2}\left(i\sqrt{3} - 1\right) A\cosh(qz) + +c.c.\right],
$$

from which Equation (1.18c) follows.

We write a Matlab code to solve for the neutral curve. First, for a given k-value, the critical Rayleigh number can be estimated as follows:

```matlab
function Ra=my_rayleigh_benard0(k,Ra_guess)

Ra=fzero(@myfun,Ra_guess);

function y=myfun(x)

    tau=(x/k^4)^(1/3);
    q0=k*sqrt(tau-1);
    temp=sqrt(1+tau+tau^2)+(1+(1/2)*tau);
    q1=k*sqrt(temp/2);
    temp=sqrt(1+tau+tau^2)-(1+(1/2)*tau);
    q2=k*sqrt(temp/2);

    q=q1+sqrt(-1)*q2;

    y=imag(   (sqrt(3)+sqrt(-1))*q*tanh(q/2)  )+q0*tan(q0/2);
end

end
```

rayleigh_benard/my_rayleigh_benard0.m

Next, for a range of k-values, the corresponding set of critical Rayleigh numbers can be found as follows:

```matlab
function [k_vec,Ra_vec]=my_rayleigh_benard1()

k_vec=0.1:0.05:10;
Ra_vec=0*k_vec;

Ra=my_rayleigh_benard0(k_vec(1),100000);
Ra_vec(1)=Ra;

for i=2:length(k_vec)
    Ra_guess=Ra_vec(i-1);
    Ra=my_rayleigh_benard0(k_vec(i),Ra_guess);
    Ra_vec(i)=Ra;
end

end
```

rayleigh_benard/my_rayleigh_benard1.m

This code can be used to plot the neutral curve (Figure 1.6) for the **even case**.
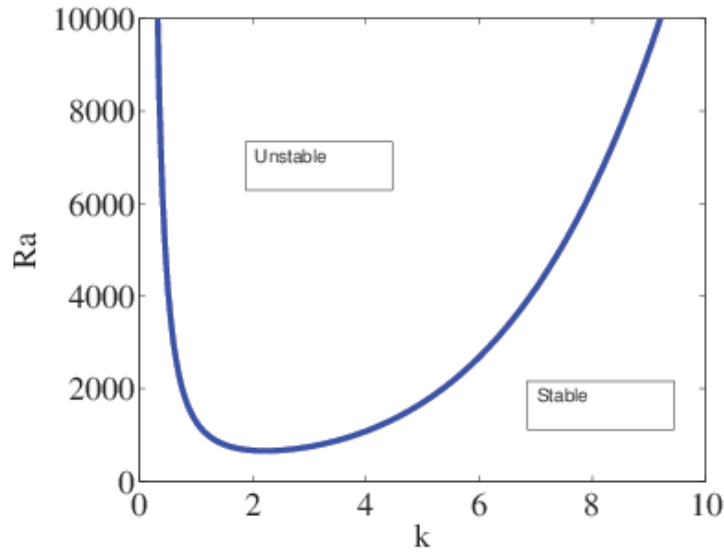
Figure 1.1: Neutral curve for the Rayleigh–Benard problem (even eigensolution)

In a similar way, the neutral curve for the odd mode is found from the root of the following equation:

$$q_0 \cot(q_0/2) = \Im\left[\left(\sqrt{3} + i\right) q \frac{\sinh(q_1) - i\sin(q_2)}{\cosh(q_1) - \cos(q_2)}\right]. \tag{1.23}$$

Exercise 1.5 *Starting with Equation (1.23), write a Matlab function to construct the neutral curve of the odd eigensolution. Then, plot the odd and even neutral curves on a single graph. Show that the critical Rayleigh number for the onset of an even unstable eigenmode is less than the corresponding critical Rayleigh number for the odd unstable eigenmode. Argue then that the even eigenmodes are more unstable than the odd ones.*

1.7   Convection patterns

We pass from two-dimensional to three-dimensional disturbances in the coodinates (x, y, z), where z is the wall-normal direction. It can be seen quite readily that the three-dimensional linearized equations of motion read

$$\frac{\partial}{\partial t}\nabla^2 w = +g\alpha\left(\frac{\partial^2\theta}{\partial x^2} + \frac{\partial^2\theta}{\partial y^2}\right) + \nu\nabla^4 w, \tag{1.24a}$$

$$\frac{\partial\theta}{\partial t} = w\beta + \kappa\nabla^2\theta \tag{1.24b}$$

where the differential operators are now in the appropriate three-dimensional form. Under a normal-mode decomposition

$$w = e^{i(k_x x + k_y y) + pt} W(z), \qquad \theta = e^{i(k_x x + k_y y) + pt} \Theta(z),$$

the eigenvalue equation derived previously **still persists**, only now the quantity k^2 in the relevant differential equation means $k^2 = k_x^2 + k_y^2$. Thus, there was no loss of generality in our previous focus on the two-dimensional case. Interestingly, the theory at this stage is by no means complete, since at the onset of **criticality** (i.e. for parameters along the neutral curve) there are many ways in which the critical wavenumber k_c^2 can be resolved into its x- and y-components. Thus, the theory so far does not tell us which pair (k_x, k_y) (with $k_x^2 + k_y^2 = k_c^2$) is selected. Indeed, any pair consistent with this condition is possible and hence, a linear superposition of all such consistent pairs is the general acceptable solution.

However, we can observe that a particular wavenumber choice corresponds to a periodic cell, replicated throughout the xy-plane. Because the problem is translationally invariant in the xy-plane, these cells should fill in the xy plane with no gaps. There is a loose analogy here with solid-state physics: translational symmetry in a discrete crystal structure implies a lattice structure, which in turn implies that the only possibility for the unit cell (in two dimensions) is a square, an equilateral triangle, or a hexagon. Thus, **only those wavenumber combinations that produce a square, equilateral triangle or a hexagon as the periodic cell are allowed by the translational symmetry of the problem.** A real hexagonal convection cell is shwon in Figure 1.2.

The complete velocity field

The complete velocity field (u, v, w) can be backed out from these considerations, albeit in a remarkably roundabout fashion. First, we note that

$$w = F(x, y) W(z),$$

where $F(x, y)$ is that combination of complex exponentials that gives the relevant periodic unit cell, such that

$$\left(\partial_x^2 + \partial_y^2 \right) F = -k^2 F.$$

Because of its ubiquity in the following, we call

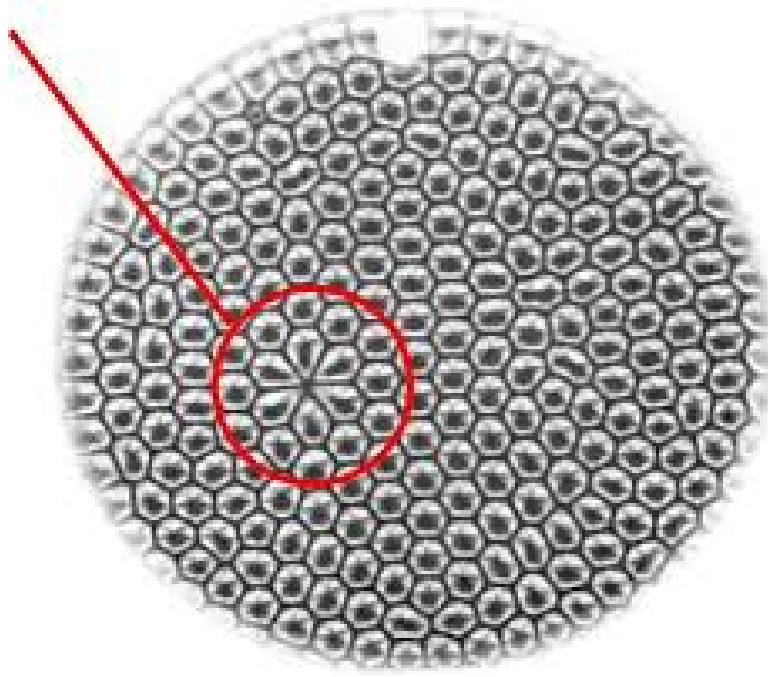$$\nabla_\perp = \left(\frac{\partial}{\partial x}, \frac{\partial}{\partial y}, 0 \right),$$

Figure 1.2: A (mostly) hexagonal array of convection cells in real-life Rayleigh–Bénard convection, from `https://www.esrl.noaa.gov/psd/outreach/education/science/convection/RBCells.html`, visited 02/02/2017.

hence $\nabla_\perp^2 F = -k^2 F$. Next, we introduce the wall-normal component of the vorticity,

$$\zeta = \hat{\boldsymbol{z}} \cdot \boldsymbol{\omega} = \partial_x v - \partial_y u.$$

We have

$$\frac{\partial \zeta}{\partial x} = \frac{\partial^2 v}{\partial x^2} - \frac{\partial^2 u}{\partial x \partial y}, \tag{1.25a}$$

$$\frac{\partial \zeta}{\partial y} = \frac{\partial^2 v}{\partial x \partial y} - \frac{\partial^2 u}{\partial y^2}. \tag{1.25b}$$

In view of the incompressibility condition $\partial_x u + \partial_y v + \partial_z w = 0$, we also have

$$\frac{\partial^2 u}{\partial x \partial y} = -\frac{\partial^2 v}{\partial y^2} - \frac{\partial^2 w}{\partial y \partial z}, \tag{1.26a}$$

$$\frac{\partial^2 v}{\partial x \partial y} = -\frac{\partial^2 u}{\partial x^2} - \frac{\partial^2 w}{\partial x \partial z}. \tag{1.26b}$$

We combine Equations (1.25)–(1.26) now to obtain

$$\frac{\partial \zeta}{\partial x} = \frac{\partial^2 v}{\partial x^2} + \frac{\partial^2 v}{\partial y^2} + \frac{\partial^2 w}{\partial y \partial z} = \nabla_\perp^2 v + \frac{\partial^2 w}{\partial y \partial z} = -k^2 v + \frac{\partial^2 w}{\partial y \partial z},$$

hence

$$v = \frac{1}{k^2}\left(\frac{\partial^2 w}{\partial y \partial z} - \frac{\partial \zeta}{\partial x}\right).$$

Also,

$$\frac{\partial \zeta}{\partial y} = -\frac{\partial^2 u}{\partial x^2} - \frac{\partial^2 w}{\partial x \partial z} - \frac{\partial^2 u}{\partial y^2} = -\nabla_\perp^2 u - \frac{\partial^2 w}{\partial y \partial z} = k^2 u - \frac{\partial^2 w}{\partial y \partial z},$$

hence

$$u = \frac{1}{k^2}\left(\frac{\partial^2 w}{\partial x \partial z} + \frac{\partial \zeta}{\partial y}\right).$$

However, quite generally, we have the vortex stretching equation, which reads

$$\frac{\partial \boldsymbol{\omega}}{\partial t} + \boldsymbol{u} \cdot \nabla \boldsymbol{\omega} = \boldsymbol{\omega} \cdot \nabla u + \nu \nabla^2 \boldsymbol{\omega},$$

the linearization of which is

$$\frac{\partial \boldsymbol{\omega}}{\partial t} = \nu \nabla^2 \boldsymbol{\omega},$$

and projecting on to the z-direction gives

$$\frac{\partial \zeta}{\partial t} = \nu \nabla^2 \zeta.$$

In normal-mode form, this gives

$$\sigma \zeta = (\partial_z^2 - k^2)\zeta.$$

However, we are at criticality, with $\sigma = 0$, hence

$$(\partial_z^2 - k^2)\zeta = 0, \qquad \zeta = 0 \text{ on } z = \pm 1/2,$$

the only solution of which is $\zeta = 0$. Hence, the wall-normal component of the vorticity vanishes in this very particular case, and we are left with

$$u = \frac{1}{k^2}\frac{\partial^2 w}{\partial y \partial z}, \qquad v = \frac{1}{k^2}\frac{\partial^2 w}{\partial x \partial z}.$$

Letting $\boldsymbol{u}_\perp = (u, v)$, we have

$$\boldsymbol{u}_\perp = \frac{1}{k^2}\frac{\partial}{\partial z}\left(\frac{\partial w}{\partial x}, \frac{\partial w}{\partial y}\right) = \frac{1}{k^2}W'\nabla_\perp F.$$

But $w = F(x, y)W(z)$, hence $F = w/W$, hence

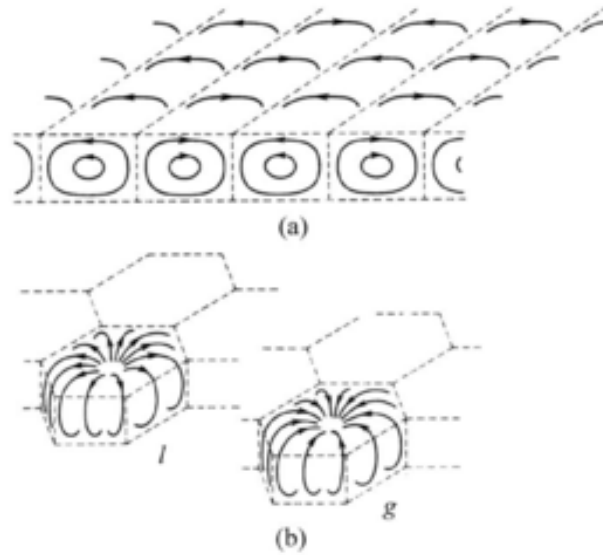$$\boldsymbol{u}_\perp = \frac{1}{k^2}\frac{W'}{W}\nabla_\perp w.$$

Figure 1.3: Typical two-dimensional and three-dimensional convection cells are compared side-by side. Schematic from Scholarpedia article on Rayleigh–Benard convection (accessed 07/01/2015).

Thus, if the gradient $\nabla_\perp w$ vanishes, then so does $\boldsymbol{u}_\perp$. We now use these results to investigate the convection cells. We examine only two-dimensional rolls in depth here: the interested reader can study Chandrasekhar's book for an in-depth treatment of the three-dimensional structures: rectangular, triangular and hexagonal cells. Typical two-dimensional and three-dimensional convection cells are compared side-by side in Figure 1.3.

Convection rolls

Remark 3 *This part was done only very briefly in class.*

The simplest convection pattern is the roll, wherein $k_y = 0$, and the problem reverts to a two-dimensional one. Let the critical wavenumber be k. Then , the size of the convection cell is $L = 2\pi/k$. The velocity profile is

$$ w = W(z)\cos(kx), \qquad k = 2\pi/L $$

where $W(z)$ is the eigenfunction corresponding to the eigenvalue $\sigma = 0$. The corresponding components of the velocity parallel to the wall are

$$ u = -\frac{1}{k}W'\sin(kx), \qquad v = 0. $$

It is clear that an appropriate streamfunction for the flow is
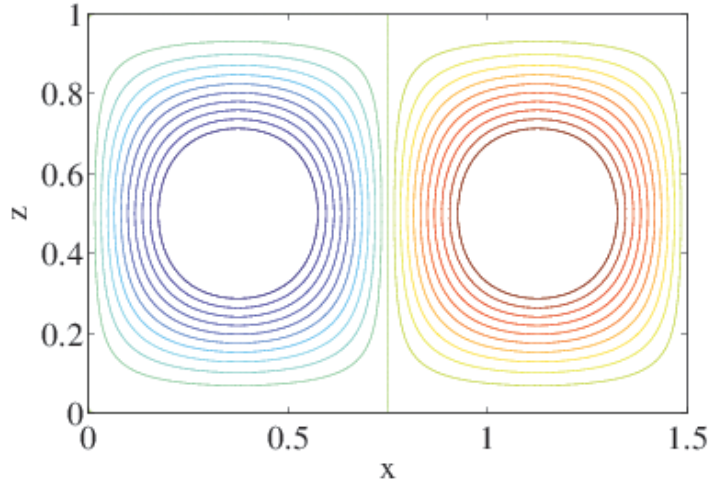
$$ \psi = -\frac{1}{k}W\sin(kx), $$

Figure 1.4: Two-dimensional convection roll in Rayleigh–Bénard convection (at criticality)

with $u = \partial_z \psi$ and $w = -\partial_x \psi$. The streamlines can be plotted as isosurfaces of the streamfunction. For the W-component of the streamfunction, I use the approximation $W \approx z^2 - 2z^3 + z^4$, which satisfies the symmetry condition (even function) and boundary conditions but is otherwise an approximation of the true eigenfunction. The result of the plot is shown in Figure 1.4. The main feature here is two counter-rotating vortices in the cell that act to redistribute the temperature. This is the essential signature of Rayleigh–Bénard convection.

1.8 Beyond linear theory – the Nusselt Number

Beyond linear theory, the exponential growth of the convection rolls will either saturate (leading to steady, laminar flow) or themselves become unstable – in which case a pattern of turbulent convection ensues. The eventual outcome of these processes depends on the Rayleigh number – the higher the Rayleigh number the less laminar the flow eventually is. In both cases, the vertical velocity represents a highly efficient means of transporting heat from bottom to top – over and above the heat transfer that can be achieved by diffusion alone. The enhancement is characterized by the Nusselt number:

$$\mathrm{Nu} = \frac{\left\langle \int_0^d \left(wT - \kappa \frac{\partial T}{\partial z} \right) \mathrm{d}z \right\rangle}{\kappa (T_{\mathrm{hot}} - T_{\mathrm{cold}})}, \tag{1.27}$$

where the angle brackets denote a space-time average (i.e. averaging over both time and the x- and y-directions), $w(x, y, z, t)$ is the instantaneous fluid velocity in the vertical (z-direction), and $T(x, y, z, t)$ is the corresponding instantaneous temperature field. Because these fields arise as solutions to the full (nonlinear) Navier–Stokes equations, there is no simple way to derive a closed form for the Nusselt number. However, some accepted correlations exist, which have been derived

rigorously from decades of experiments and also, direct numerical simulations:

$$\text{Nu} = \begin{cases} 0.54\text{Ra}^{1/4}, & 10^3 \leq \text{Ra} \leq 10^7, \qquad \text{Pr} \geq 0.7, \\ 0.15\text{Ra}^{1/3}, & 10^7 \leq \text{Ra} \leq 10^{11}, \qquad \text{all Pr} \end{cases} \tag{1.28}$$

The second of these correlations is the 'classical' Rayleigh–Bénard scaling, which applies when the convection rolls are fully turbulent. The scaling regime beyond $\text{Ra} = 10^{11}$ is the subject of current research [AGL09].

Chapter 2

Rayleigh–Taylor Instability

2.1 Overview

The idea behind the Rayleigh–Taylor instability is to take two distinct incompressible fluids separated by a flat interface, such that the heavier fluid sits on top of the lighter one. This is obviously an unstable situation: we introduce the theory that proves this. This is an important example not only for the practical applications (some of which are nefarious) but because it is the simplest possible example of a **two-phase flow instability**, the stability theory for which admits exact analytical solutions. In this chapter we will give an account not only of the inviscid theory (wherein those analytical solutions apply), but the viscous case also. The viscous case gives a nice introduction to numerical spectral methods for the solution of eigenvalue problems in two-phase flows.

2.2 Stability analysis – Inviscid case

A schematic description of the physical problem is shown in Figure 2.1. The fluid domain is $(x, y) \in \mathbb{R}^2$, and the base-state location of the interface is at $z = 0$. The density profile is

$$\rho(x, y) = \begin{cases} \rho_L, & z > 0, \\ \rho_G, & z < 0, \end{cases}$$

where ρ_G and ρ_L are both constant and $\rho_G < \rho_L$. Thus, it is as though the domain is taken up by two distinct fluids (or **phases**). Both phases are however assumed for the time being to be invsicid, with $\mu_i = 0$ and $i = L, G$. The base-state corresponds to a situation with no flow, such that $\boldsymbol{u}_i = 0$, again with $i = L, G$.

Interestingly, the equilibrium pressure field P_0 is non-trivial. The z-momentum equation in the base
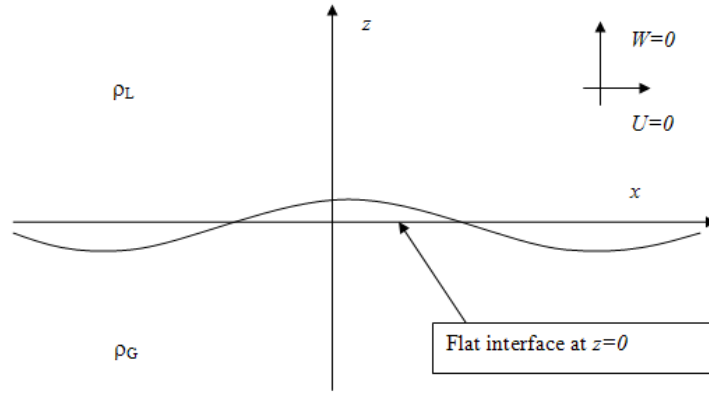
Figure 2.1: Schematic description of the base state of the Rayleigh–Taylor instability

state reads

$$0 = -\frac{dP_0}{dz} - \rho_i g,$$

hence

$$\frac{dP_0}{dz} = -\rho_i g,$$

where $g > 0$ is the acceleration due to gravity. We integrate this equation in the bottom layer $(i = G)$:

$$P_{0G}(z) - C_G = -\rho_G g z,$$

hence $P_{0G}(z) = C_G - \rho_G g z$. Similarly, in the top layer, we obtain $P_{0L}(z) = C_L - \rho_L g z$, and the two constants of integration must coincide so that the pressure is continuous. Thus, upon setting the (irrelevant) constant to zero, we obtain

$$P(x,y) = \begin{cases} -\rho_L g z, & z > 0, \\ -\rho_G g z, & z < 0, \end{cases}$$

Introduction of small-amplitude perturbations

A tiny sinuousoidal perturbation is introduced on the interface separating the phases such that the configuration of the fluid density changes:

$$\rho(x,y) = \begin{cases} \rho_L, & z > \eta(x,y,t), \\ \rho_G, & z < \eta(x,y,t). \end{cases}$$

This change induces corresponding changes in the velocity and pressure fields, to be determined now by the relevant linearized (Euler) equations of motion:

$$\frac{\partial}{\partial t} \boldsymbol{u}_i = -\frac{1}{\rho_i} \nabla \delta p_i, \qquad i = L, G,$$

where the perturbation velocities $\boldsymbol{u}_i$ satisfy the incompressibility condition

$$\nabla \cdot \boldsymbol{u}_i = 0.$$

The linearized Euler equation demonstrates conservation of vorticity:

$$\frac{\partial}{\partial t} \left(\nabla \times \boldsymbol{u}_i \right) = 0.$$

We assume a two-dimensional disturbance in the xz plane and project this conservation equation on to the y-direction to obtain

$$\frac{\partial}{\partial t} \left(\partial_x w - \partial_z u \right) = 0.$$

The incompressibility condition reads (correspondingly)

$$\partial_x u + \partial_y w = 0.$$

Thus, we introduce a streamfunction ψ, such that $u = \partial_z \psi$ and $w = -\partial_x \psi$. The conservation of vorticity equation now reads

$$\frac{\partial}{\partial t} \left(-\partial_x^2 \psi_i - \partial_z^2 \psi_i \right) = 0,$$

or

$$\frac{\partial}{\partial t} \nabla^2 \psi_i = 0,$$

hence $\nabla^2 \psi_i = \mathrm{Const.}$ But the initial configuration corresponds to no flow and no vorticity, hence

$$\nabla^2 \psi_i = 0.$$

We make a normal-mode decomposition $\psi = \mathrm{e}^{ikx + \sigma t} \Psi(z)$, hence

$$\left(\partial_z^2 - k^2 \right) \Psi_i = 0,$$

with solution

$$\Psi_i = A_i \mathrm{e}^{-k|z|}$$

(the other solutions are thrown away because they correspond to unbounded disturbances as $|z| \to \infty$).

It now remains to match the streamfunction across the interface. This is where the two-phase flow aspect of the problem enters: physical **jump conditions** need to be prescribed at the interface $z = \eta$.

Jump conditions

We demand **continuity of velocity** at the interface $z = \eta$. In particular, $w_i = -\mathrm{i}k\mathrm{e}^{\mathrm{i}kx+\sigma t}\Psi_i(z)$ is continuous across the interface:

$$
\begin{aligned}
w_L(x, z = \eta) &= w_G(x, z = \eta), \\
\Psi_L(z = \eta) &= \Psi_G(z = \eta), \\
\Psi_L(0) + \frac{\partial \Psi_L}{\partial z}\Big|_0 \eta + \cdots &= \Psi_G(0) + \frac{\partial \Psi_G}{\partial z}\Big|_0 \eta + \cdots .
\end{aligned}
$$

Linearized on to the surface $z = 0$, this continuity condition reads

$$
\Psi_L(0) = \Psi_G(0).
$$

Since $\Psi_i = A_i\mathrm{e}^{-k|z|}$, it follows that $A_L = A_G = A$.

The other condition is the **dynamic Laplace–Young condition**, which says that the jump in the normal stress across the interface must be balanced by the surface-tension force. However, the normal stress is just $-P$, where P is the total pressure, $P = P_0 + \delta p$. In other words, we have

$$
P_L(x, z = \eta) - P_G(x, z = \eta) = \gamma \kappa,
$$

where γ is the surface tension and κ is the (mean) curvature of the interface. We now work out each of these contributions:

- Interfacial pressure in the upper layer: We have

$$
\begin{aligned}
P_L(x, z = \eta) &= P_{0L}(z = \eta) + \delta p_L(x, z = \eta), \\
&= P_{0L}(0) + \frac{dP_{0L}}{dz}\Big|_0 \eta + \delta p_L(x, z = 0) + \left[\frac{\partial}{\partial z}\delta p\right]_{z=0}\eta + \cdots, \\
&= -\rho_L g\eta + \delta p_L(x, z = 0),
\end{aligned}
$$

where we have linearized again on to the surface $z = 0$.

- Interfacial pressure in the upper layer: This is similar to the upper layer, and we have

$$
P_G(x, z = \eta) = -\rho_G g\eta + \delta p_G(x, z = 0),
$$

- Mean curvature: By a standard formula, we have

$$\kappa = \frac{\eta_{xx}}{(1 + \eta_x^2)^{3/2}}.$$

Applying the linearization and the normal-mode decomposition, this is

$$\kappa = -k^2 \eta.$$

Hence, the jump condition on the pressure now reads

$$[-\rho_L g\eta + \delta p_L(x, z = 0)] - [-\rho_G g\eta + \delta p_G(x, z = 0)] = -\gamma k^2 \eta.$$

This is re-arranged as

$$\delta p_L - \delta p_G = (\rho_L - \rho_G)g\eta - \gamma k^2 \eta.$$

It remains to connect the pressure to the streamfunction and hence to write down an eigenvalue problem.

The eigenvalue problem

We return to the perturbation equation for the u-velocity:

$$\frac{\partial u_i}{\partial t} = -\frac{1}{\rho_i}\frac{\partial}{\partial x}\delta p_i.$$

Going over to the normal-mode and streamfunction representations, this equation can be written as

$$\sigma \partial_z \psi = -\frac{1}{\rho_i}\mathrm{i}k\delta p_i,$$

where $\psi = \mathrm{e}^{\mathrm{i}kx+\sigma t}\Psi(z)$ is the total streamfunction. Hence,

$$\delta p_i = \frac{1}{k}\mathrm{i}\rho_i \sigma \partial_z \psi,$$

and the jump condition on the pressure can now be rewritten as

$$\frac{1}{k}\mathrm{i}\sigma\left(\rho_L \partial_z \psi_L - \rho_G \partial_z \psi_G\right) = (\rho_L - \rho_G)g\eta - \gamma k^2 \eta.$$

We use again the fact that $\Psi_L = A\mathrm{e}^{-kz}$ and $\Psi_G = A\mathrm{e}^{kz}$ to rewrite this further as

$$-\mathrm{i}\sigma(\rho_L + \rho_G)A\mathrm{e}^{\mathrm{i}kx+\sigma t} = (\rho_L - \rho_G)g\eta - \gamma k^2 \eta, \tag{2.1}$$

Let $\eta = \eta_0 e^{ikx+\sigma t}$, where η_0 is a complex number. Hence, Equation (2.1) becomes

$$-i\sigma(\rho_L + \rho_G)\psi(0) = (\rho_L - \rho_G)g\eta_0 - \gamma k^2 \eta_0,$$

Some further work is needed to express η in terms of the streamfunction. We use **kinematic condition**, which says that fluid particles on the interface follow the motion of the interface itself:

$$\frac{\partial \eta}{\partial t} + u\frac{\partial \eta}{\partial x} = w,$$

or, in a linearized version,

$$\frac{\partial \eta}{\partial t} = w,$$

and finally, in the normal-mode and streamfunction representation,

$$\sigma \eta_0 = -ik\Psi(0),$$

hence $\eta_0 = -ik\Psi(0)/\sigma$. Thus, the jump condition can be re-expressed as

$$-i\sigma(\rho_L + \rho_G)\Psi(0) = \left[(\rho_L - \rho_G)g - k^2\gamma\right]\left[-ik\Psi(0)/\sigma\right].$$

Tidying up, the result is

$$\sigma^2 = \frac{\rho_L - \rho_G}{\rho_L + \rho_G}gk - \frac{\gamma k^3}{\rho_L + \rho_G},$$

and finally,

$$\sigma = \sqrt{\frac{\rho_L - \rho_G}{\rho_L + \rho_G}gk - \frac{\gamma k^3}{\rho_L + \rho_G}}.$$

The quantity $(\rho_L - \rho_G)/(\rho_L - \rho_G) > 0$ is called the **Atwood number**:

$$\text{At} = \frac{\rho_L - \rho_G}{\rho_L + \rho_G};$$

the relationship between the **growth rate** σ and the wavenumber k is called the **dispersion relation**:

$$\sigma(k) = \sqrt{\text{At}gk - \frac{\gamma k^3}{\rho_L + \rho_G}}. \tag{2.2}$$

Implications

When $\gamma = 0$ the surface tension vanishes, and the dispersion relation reads
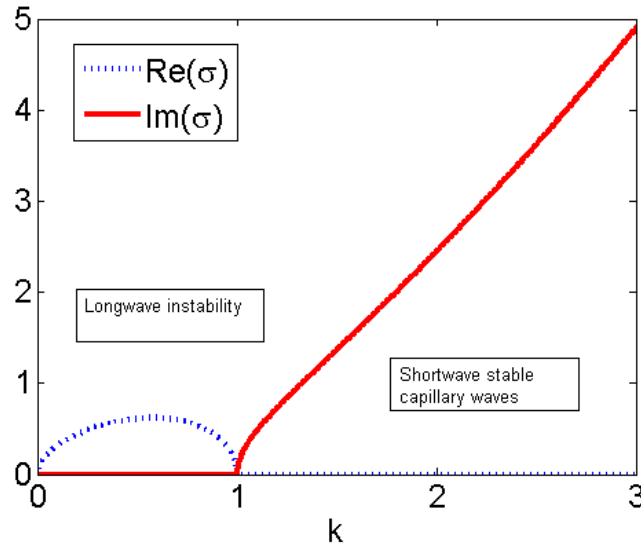
$$\sigma(k) = \sqrt{\text{At}gk}.$$

Figure 2.2: Sample dispersion relation showing the bifurcation from shortwave neutral capillary waves to longwave unstable gravitational disturbances. Model parameters: $\mathrm{At} = g = \gamma/(\rho_L + \rho_G) = 1$.

In this case, the growth rate σ is purely real and positive, and waves of arbitrary wavelength are unstable. In contrast, for $\gamma \neq 0$, there is a critical wavenumber k_0 where the radicand in Equation (2.2) changes sign:

$$\mathrm{At}g = \frac{\gamma}{\rho_L + \rho_G} k_0^2,$$

such that

$$\sigma = \begin{cases} \sqrt{\mathrm{At}gk - \frac{\gamma k^3}{\rho_L + \rho_G}}, & k < k_0, \\ \pm\mathrm{i}\sqrt{\frac{\gamma k^3}{\rho_L + \rho_G} - \mathrm{At}gk}, & k \geq k_0, \end{cases}$$

where the long-wave $(k < k_0)$ case corresponds to pure unstable motion and the short-wave case corresponds to neutral travelling capillary travelling waves. Thus, **surface tension stabilizes short-wave disturbances**. A sample dispersion relation showing this **bifurcation** in the nature of the eigensolutions is shown in Figure 2.2.

2.3 Viscous case

The base state is unchanged. The first main change is in the linearized equation of motion:

$$\frac{\partial}{\partial t}\boldsymbol{u}_i = -\frac{1}{\rho_i}\nabla\delta p_i + \frac{\mu_i}{\rho_i}\nabla^2\boldsymbol{u}_i, \qquad i = L, G,$$

which now contains a viscous term. As before, we take the curl on both sides to eliminate the pressure:

$$\frac{\partial}{\partial t}\boldsymbol{\omega}_i = \frac{\mu_i}{\rho_i}\nabla^2\boldsymbol{\omega_i},$$

and we project on to the y-direction to obtain

$$\frac{\partial}{\partial t}\left(\partial_x w - \partial_z u\right) = \frac{\mu_i}{\rho_i}\nabla^2\left(\partial_x w - \partial_z u\right).$$

As before, we introduce the streamfunction and the equation of motion reduces to

$$\frac{\partial}{\partial t}\nabla^2\psi = \frac{\mu_i}{\rho_i}\nabla^4\psi.$$

A normal-mode decomposition is made, such that $\psi = \mathrm{e}^{\mathrm{i}kx+\sigma}\Psi(z)$, and the relevant eigenvalue equation now reads

$$\sigma\left(\partial_z^2 - k^2\right)\Psi_i = \frac{\mu_i}{\rho_i}\left(\partial_z^2 - k^2\right)^4\Psi_i.$$

It is clear that the boundary conditions are

$$\Psi_i = \Psi_i' = 0, \qquad \text{as } |z| \to \infty.$$

However, we now have a fourth-order equation to match across the interface at $z = 0$, which requires four matching conditioins (previously we had two matching conditions for a second-order equation). This requires more physics.

Matching Conditions

As before, we impose continuity of velocity. Continuity of the w-component of velocity gives

$$\Psi_L(0) = \Psi_G(0).$$

We also have continuity of the u-component of velocity, where $u = \partial_z\psi$, and where $\psi = \mathrm{e}^{\mathrm{i}kx+\sigma t}\Psi(z)$ is the full streamfunction. We have

$$\begin{aligned}u_L(x, z=\eta) &= u_G(x, z=\eta),\\ \implies u_L(x, z=0) &= u_G(x, z=0),\\ \implies \partial_z\psi_L(x, z=0) &= \partial_z\psi_G(x, z=0),\end{aligned}$$

hence

$$\partial_z\Psi_L(z=0) = \partial_z\Psi_G(z=0).$$

Thus, both Ψ and its first derivative are continuous across the interface.

The next condition relevant for viscous flow is the continuity of **tangential stress** across the

interface. Recall, the stress tensor associated with the Navier–Stokes equations is

$$\mathrm{T} = -p\mathrm{I} + \mu \left(\nabla \boldsymbol{u} + \nabla \boldsymbol{u}^T \right),$$

and the tangential stress is

$$\hat{\boldsymbol{n}} \cdot \mathrm{T} \cdot \hat{\boldsymbol{t}},$$

where

$$\hat{\boldsymbol{t}} = \frac{(1, \eta_x)}{\sqrt{1 + \eta_x^2}} \approx (1, \eta_x)$$

is the unit tangent vector to the interface and

$$\hat{\boldsymbol{n}} = \frac{(-\eta_x, 1)}{\sqrt{1 + \eta_x^2}} \approx (-\eta_x, 1)$$

is the unit normal vector.

Now $\hat{\boldsymbol{n}} \cdot \mathrm{I} \cdot \hat{t} = \hat{\boldsymbol{n}} \cdot \hat{t} = 0$, so the tangential stress is

$$
\begin{aligned}
\mu \hat{\boldsymbol{n}} \cdot \left(\nabla \boldsymbol{u} + \nabla \boldsymbol{u}^T \right) \cdot \hat{\boldsymbol{t}} &= \mu \sum_{i,j=1}^{2} n_i \left(\frac{\partial u_i}{\partial x_j} + \frac{\partial u_j}{\partial x_i} \right) t_j, \\
&= \mu n_1 t_1 \left(\frac{\partial u_1}{\partial x_1} + \frac{\partial u_1}{\partial x_1} \right) + mu n_1 t_2 \left(\frac{\partial u_1}{\partial x_2} + \frac{\partial u_2}{\partial x_1} \right) + \\
&\quad \mu n_2 t_1 \left(\frac{\partial u_2}{\partial x_1} + \frac{\partial u_1}{\partial x_2} \right) + \mu n_2 t_2 \left(\frac{\partial u_2}{\partial x_2} + \frac{\partial u_2}{\partial x_2} \right)
\end{aligned}
$$

The only term that survives the linearization is proportional to $n_2 t_1$, hence the tangential stress is

$$\mu n_2 t_1 \left(\frac{\partial u_2}{\partial x_1} + \frac{\partial u_1}{\partial x_2} \right) = \mu \left(\frac{\partial w}{\partial x} + \frac{\partial u}{\partial z} \right),$$

which in streamfunction form is

$$\mu \left(\partial_z^2 + k^2 \right) \psi.$$

Hence,

$$\mu_L \left(\partial_z^2 + k^2 \right) \psi_L = \mu_G \left(\partial_z^2 + k^2 \right) \psi_G.$$

The final condition relevant for viscous flow is the familiar jump condition for **tangential stress** across the interface. The normal stress is $\hat{\boldsymbol{n}} \cdot \mathbf{T} \cdot \hat{\boldsymbol{n}}$, and the jump in the normal stress is balanced by the surface-tension force:

$$[\hat{\boldsymbol{n}} \cdot \mathbf{T} \cdot \hat{\boldsymbol{n}}]_G^L = -\gamma \kappa.$$

We now work out the linearized normal stress. Note that

$$\hat{\boldsymbol{n}} \cdot (p\mathrm{I}) \cdot \hat{\boldsymbol{n}} = p\hat{\boldsymbol{n}} \cdot \hat{\boldsymbol{n}} = p.$$

Also, each term in the sum

$$\hat{\boldsymbol{n}} \cdot \left(\nabla\boldsymbol{u} + \nabla\boldsymbol{u}^T\right) \cdot \hat{\boldsymbol{n}} = \sum_{i,j=1}^{2} n_i n_j \left(\frac{\partial u_i}{\partial x_j} + \frac{\partial u_j}{\partial x_i}\right)$$

is proportional to $n_i n_j$. The only contribution to survive in a linearization is $i = 2$ and $j = 2$ (with $n_2^2 = 1$)

$$\hat{\boldsymbol{n}} \cdot \left(\nabla\boldsymbol{u} + \nabla\boldsymbol{u}^T\right) \cdot \hat{\boldsymbol{n}} = 2\frac{\partial w}{\partial z}.$$

Thus, the linearized normal stress in the ith phase is

$$-p_i + 2\mu_i \frac{\partial w_i}{\partial z}$$

Thus, the final matching condition at the interface reads

$$\left[-p_L + 2\mu_L \frac{\partial w_L}{\partial z}\right] - \left[-p_G + 2\mu_G \frac{\partial w_G}{\partial z}\right] = \gamma k^2 \eta.$$

Re-arranging and using the by-now familiar streamfunction representation gives

$$(-p_L) - (-p_G) - \mathrm{i}k\left(2\mu_L \partial_z \psi_L - 2\mu_G \partial_z \psi_G\right) = \gamma k^2 \eta.$$

Now, the computation of the jump in pressures is the same as before, so we are left with the matching condition

$$g\left(\rho_L - \rho_G\right)\eta + \left(-\delta p_L + \delta p_G\right)_{z=0} - \mathrm{i}k\left(2\mu_L \partial_z \psi_L - 2\mu_G \partial_z \psi_G\right) = \gamma k^2 \eta,$$

or

$$\left(-\delta p_L + \delta p_G\right)_{z=0} - \mathrm{i}k\left(2\mu_L \partial_z \psi_L - 2\mu_G \partial_z \psi_G\right) = -g\left(\rho_L - \rho_G\right)\eta + \gamma k^2 \eta.$$

It now remains to work out the pressure perturbation for the viscous fluid. We start with the u-component of the velocity equation:

$$\frac{\partial}{\partial t}u_i = -\frac{1}{\rho_i}\frac{\partial}{\partial x}\delta p_i + \frac{\mu_i}{\rho_i}\nabla^2 u_i,$$

which in streamfunction-normal-mode form reads

$$\sigma\partial_z \psi = -\frac{\mathrm{i}k}{\rho_i}\delta p_i + \frac{\mu_i}{\rho_i}(\partial_z^2 - k^2)\partial_z \psi.$$

Hence,

$$\rho_i \sigma \partial_z \psi - \mu_i (\partial_z^2 - k^2) \partial_z \psi = -ik \delta p_i,$$

and finally,

$$-\frac{i}{k} \rho_i \sigma \partial_z \psi_i + \frac{i}{k} \mu_i \partial_z^3 \psi_i - ik \mu_i \partial_z \psi = -\delta p_i.$$

We assemble the results:

$$(-\delta p_L + \delta p_G) - 2ik \left(\mu_L \partial_z \psi_L - \mu_G \partial_z \psi_G \right)$$

$$= \left(-\frac{i}{k} \rho_L \sigma \partial_z \psi_L + \frac{i}{k} \mu_L \partial_z^3 \psi_L - ik \mu_L \partial_z \psi_L \right) - \left(-\frac{i}{k} \rho_G \sigma \partial_z \psi_G + \frac{i}{k} \mu_G \partial_z^3 \psi_G - ik \mu_G \partial_z \psi_G \right)$$

$$- 2ik \left(\mu_L \partial_z \psi_L - \mu_G \partial_z \psi_G \right)$$

$$= \left(-\frac{i}{k} \rho_L \sigma \partial_z \psi_L + \frac{i}{k} \mu_L \partial_z^3 \psi_L - 3ik \mu_L \partial_z \psi_L \right) - \left(-\frac{i}{k} \rho_G \sigma \partial_z \psi_G + \frac{i}{k} \mu_G \partial_z^3 \psi_G - 3ik \mu_G \partial_z \psi_G \right)$$

which is all equal to $-(\rho_L - \rho_G)\eta + \gamma k^2 \eta$:

$$\sigma \left(-\frac{i}{k} \rho_L \partial_z \psi_L + \frac{i}{k} \rho_G \partial_z \psi_G \right) + \left[\left(\frac{i}{k} \mu_L \partial_z^3 \psi_L - 3ik \mu_L \partial_z \psi_L \right) - \left(\frac{i}{k} \mu_G \partial_z^3 \psi_G - 3ik \mu_G \partial_z \psi \right) \right]$$

$$= -g(\rho_L - \rho_G)\eta + \gamma k^2 \eta$$

Multiply up by $-k/i$ for the final result:

$$\sigma \left(\rho_L \partial_z \psi_L - \rho_G \partial_z \psi_G \right) + \left[\left(3k^2 \mu_L \partial_z \psi_L - \mu_L \partial_z^3 \psi_L \right) - \left(3k^2 \mu_G \partial_z \psi_G - \mu_G \partial_z^3 \psi_G \right) \right]$$

$$= -ik \left[(\rho_L - \rho_G) - \gamma k^2 \right] \eta. \quad (2.3)$$

Now, if we used the kinematic condition here to write $\eta = -ik\psi(0)/\sigma$, we would end up with σ^2 in the matching condition. This is not advisable: we want a linear eigenvalue problem in the variable σ. Therefore, we leave Equation (2.3) as-is, and include η as an extra variable. Let us assemble the results here. We have the following ordinary differential equations in the eigenvalue σ valid in the bulk parts of the domain:

$$\sigma \rho_L \left(\partial_z^2 - k^2 \right) \Psi_L = \mu_L \left(\partial_z^2 - k^2 \right)^2 \Psi_L, \qquad z > 0, \qquad (2.4a)$$

$$\sigma \rho_G \left(\partial_z^2 - k^2 \right) \Psi_G = \mu_G \left(\partial_z^2 - k^2 \right)^2 \Psi_G, \qquad z < 0. \qquad (2.4b)$$

The following matching conditions apply at $z = 0$:

$$\Psi_L(0) = \Psi_G(0), \tag{2.4c}$$

$$\partial_z \Psi_L(0) = \partial_z \Psi_G(0), \tag{2.4d}$$

$$\mu_L \left(\partial_z^2 + k^2\right) \Psi_L = \mu_G \left(\partial_z^2 + k^2\right) \Psi_G, \tag{2.4e}$$

$$\sigma \rho_L \partial_z \Psi_L + \mu_L \left(3k^2 \partial_z \Psi_L - \mu_L \partial_z^3 \Psi_L\right) = \sigma \rho_G \partial_z \Psi_G + \mu_G \left(3k^2 \partial_z \Psi_G - \partial_z^3 \Psi_G\right)$$
$$-\mathrm{i}k \left[g(\rho_L - \rho_G)k - \gamma k^3\right] \eta_0. \tag{2.4f}$$

Here, again, $\eta = \eta_0 \mathrm{e}^{\mathrm{i}kx + \sigma t}$ and η_0 is the phase, determined by the kinematic condition

$$\sigma \eta_0 = -\mathrm{i}k \Psi(0). \tag{2.4g}$$

Finally, the following boundary conditions apply:

$$\psi_L, \partial_z \psi_L \to 0 \text{ as } z \to \infty, \qquad \psi_G, \partial_z \psi_G \to 0 \text{ as } z \to -\infty. \tag{2.4h}$$

These are the equations we now solve. Although it is possible to solve these equations semi-analytically, it is in fact more revealing (and easier) to solve them numerically. We introduce a convenient numerical method in the next chapter – numerical spectral methods.

Exercise 2.1 Rayleigh–Taylor instability in a porous medium: *Consider the stability of a basic flow in which two incompressible fluids move with a horizontal interface and uniform vertical velocity in a uniform porous medium. You are given that motion of a fluid in a porous medium is governed by Darcy's Law, namely that $\boldsymbol{u} = \nabla \phi$, where $\phi = -k(p + g\rho z)/\mu$, ρ is the density and μ the dynamic viscosity of the fluid, and k is the permeability of the medium to the fluid.*

Let the lower fluid have density ρ_1 and viscosity μ_1 and the upper fluid ρ_2 and μ_2; let the medium have permeability k_1 to the lower and k_2 to the upper fluid, and let the basic velocity be $W\hat{\boldsymbol{z}}$. Then show that the flow is stable if and only if

$$\left(\frac{\mu_1}{k_1} - \frac{\mu_2}{k_2}\right) W + g(\rho_1 - \rho_2) \geq 0.$$

Hints: Decompose the velocity potential in each phase as $\phi_i + \delta\phi_i$, where ϕ_i is the base-state contribution. Use (and prove) the following intermediate steps if necessary:

- $\nabla^2 \phi_i = \nabla^2 \delta\phi_i = 0$ *in the interior of each fluid domain.*

- *Write $\delta\phi_i = \mathrm{e}^{\lambda t + \mathrm{i}\alpha x}\Phi_i$, hence $(\partial_z^2 - \alpha^2)\Phi_i = 0$.*

- *Continuity of normal velocity across the perturbed interface at $z = \eta(x,t) = \eta_0 \mathrm{e}^{\lambda t + \mathrm{i}\alpha x}$ implies $\Phi_1 = A\mathrm{e}^{\alpha z}$ and $\Phi_2 = -A\mathrm{e}^{-\alpha z}$. Also, obtain the kinematic condition $\lambda\eta_0 = A\alpha$.*

- *Continuity of pressure across the perturbed interface implies that*

$$\left(\frac{\partial p_1}{\partial z} - \frac{\partial p_2}{\partial z} \right)\eta = \frac{\mu_1}{k_1}\delta\phi_1 - \frac{\mu_2}{k_2}\delta\phi_2.$$

Exercise 2.2 Rayleigh–Taylor stability of superposed fluids confined in a vertical cylinder: *Consider an inviscid incompressible fluid of density ρ_1 at rest beneath a similar fluid of density ρ_2, the fluids being confined by a long vertical rigid cylinder with equation $r = a$ and there being surface tension γ at the interface with equation $z = 0$. Here cylindrical polar coordinates (r, θ, z) are used and Oz is the upward vertical. Then show, much as in the analysis throughout this chapter, that small irrotational disturbances of the state of rest may be found in terms of the normal modes of the form*

$$\phi = \cos n\theta \, J_n(kr)\mathrm{e}^{-k|z| + \lambda t},$$

where ϕ is the velocity potential of the disturbance, $n = 0, 1, 2, \cdots$, and where

$$\lambda^2 = \frac{g(\rho_2 - \rho_1)k - \gamma k^3}{\rho_1 + \rho_2}.$$

Here, the wavenumber k is determined by the condition that ka equals the mth positive zero $j'_{n,m}$ of the derivative J'_n of the Bessel function for $m = 1, 2, \cdots$. Deduce that there is stability if

$$a^2 g(\rho_2 - \rho_1) < \gamma j_{1,1}^2.$$

Chapter 3

Spectral methods in fluid dynamics

3.1   Overview

We introduce numerical spectral methods in the context of a simple two-point boundary-value problem. We then extend the method to the problem of determining the eigenvalues of the viscous Rayleigh–Taylor problem. The following books might help in understanding this last chapter:

- *Chebyshev and Fourier spectral methods*, J. P. Boyd, Dover Publications (2000). Boyd himself has put a copy of this on his website and is therefore available for free in pdf form [Boy01].

- *Spectral methods in Matlab*, L. N. Trefethen, SIAM Publications (2001) [TTTD93].

3.2   A simpler problem

Consider the equation

$$\frac{d^2 f}{dy^2} = -\lambda f, \qquad y \in [-L/2, L/2], \tag{3.1}$$

which is to be solved with **vanishing boundary conditions**

$$f(-L/2) = f(L/2) = 0.$$

This is an **eigenvalue problem** in the eigenvalue λ. However, we already know the solution: it is

$$f(y) = f_n(y) = \sin(\sqrt{\lambda_n}y), \qquad \lambda_n = \frac{4\pi^2}{L^2}n^2, \qquad n = 1, 2, \cdots$$

or

$$f(y) = f_n(y) = \cos(\sqrt{\lambda_n}y), \qquad \lambda_n = \frac{4\pi^2}{L^2}\left(n + \tfrac{1}{2}\right)^2, \qquad n = 0, 1, \cdots$$

where the apparently free parameter λ is now forced to take discrete values, $\lambda = \lambda_n$.

We are now going to 'shoot a pigeon with a cannon', and solve this problem numerically. We are going to expand the solution in terms of a set of **basis functions**,

$$f(y) = \sum_{n=0}^{\infty} a_n T_n(x), \qquad x = \frac{2}{L} y,$$

where $\{T_n(x)\}_{n=0}^{\infty}$ are a complete set of basis functions on the interval $[-1, 1]$ called the Chebyshev polynomials:

$$T_n(x) = \cos(n \arccos(x)).$$

Although this does not really look like a polynomial in x, it is!. The first few are shown here:

$$
\begin{aligned}
T_0(x) &= 1, \\
T_1(x) &= x, \\
T_2(x) &= 2x^2 - 1, \\
T_3(x) &= 4x^3 - 3x, \\
T_4(x) &= 8x^4 - 8x^2 + 1.
\end{aligned}
$$

For more information on the properties of these functions, you may, in this instance, check out the Wikipedia article. I can personally vouch for this article since I have contributed to it myself!

Just as

$$\left\{ 1, \sin\left(\frac{2n\pi}{L} x\right), \cos\left(\frac{2n\pi}{L} x\right) \right\}_{n=1}^{\infty}$$

are a good set of basis functions for **periodic functions** on an interval $[-L/2, L/2]$, so too are the Chebyshev polynomials for **arbitrary functions** on the same interval. Thus, we in expanding the solution in terms of these exotic functions, instead of familiar sines and cosines, we are taking into account the fact that the solution is not necessarily periodic. Of course, we must truncate the expansion in a numerical framework, so we work with the approximate solution

$$f_N(y) = \sum_{n=0}^{N} a_n T_n(x).$$

There are $N+1$ undetermined coefficients and two boundary conditions. That leaves $N-1$ conditions to obtain. We therefore evaluate the ODE at $N-1$ interior points to give $N+1$ constraints on

the coefficients:

$$
\begin{aligned}
f_N(-L/2) &= 0, \\
\left.\frac{d^2 f_N}{dy^2}\right|_{y_1} &= -\lambda f_N(y_1), \\
\vdots \qquad &\qquad \vdots \\
\left.\frac{d^2 f_N}{dy^2}\right|_{y_{N-1}} &= -\lambda f_N(y_{N-1}), \\
f_N(+L/2) &= 0,
\end{aligned}
$$

or

$$
\begin{aligned}
\sum_{n=0}^{N} a_n T_n(-1) &= 0, \\
\sum_{n=0}^{N} a_n \left(\frac{2}{L}\right)^2 T_n''(x_1) &= -\lambda \sum_{n=0}^{N} a_n T_n(x_1), \\
\vdots \qquad &\qquad \vdots \\
\sum_{n=0}^{N} a_n \left(\frac{2}{L}\right)^2 T_n''(x_{N-1}) &= -\lambda \sum_{n=0}^{N} a_n T_n(x_{N-1}), \\
\sum_{n=0}^{N} a_n T_n(+1) &= 0.
\end{aligned}
$$

The interior points are NOT arbitrary: we evaluate at the $N-1$ points

$$
x_1,\, x_2, \cdots,\, x_{N-1} = \cos\left(\frac{\pi}{N}\right),\, \cos\left(2\frac{\pi}{N}\right), \cdots, \cos\left((N-1)\frac{\pi}{N}\right);
$$

these are the **collocation points**.

But now we have a **generalised eigenvalue problem**:

$$
L\boldsymbol{a} = \lambda M \boldsymbol{a},
$$

where

$$
L = \begin{pmatrix}
T_0(-1) & \cdots & T_N(-1) \\
(2/L)^2 T_0''(x_1) & \cdots & (2/L)^2 T_N''(x_1) \\
\vdots & & \vdots \\
(2/L)^2 T_0''(x_{N-1}) & \cdots & (2/L)^2 T_N''(x_{N-1}) \\
T_0(+1) & \cdots & T_N(+1)
\end{pmatrix},
$$

$$M = - \begin{pmatrix} 0 & \cdots & 0 \\ T_0(x_1) & \cdots & T_N(x_1) \\ \vdots & & \vdots \\ T_0(x_{N-1}) & \cdots & T_N(x_{N-1}) \\ 0 & \cdots & 0 \end{pmatrix},$$

and

$$\boldsymbol{a} = (a_0, \cdots, a_n)^T.$$

This is a standard problem, and can be solved using a numerical package, such as 'eig' in Matlab.

- Typing

  ```
  d=eig(L,M);
  ```

  in Matlab yields the first $N + 1$ eigenvalues.

- We must then check that the eigenvalues are real (a check for bugs in the code):

  ```
  plot(imag(d),'o')
  ```

- Having done that, we sort the eigenvalues in increasing order:

  ```
  d=sort(d);
  ```

- Then, we plot the results.

  ```
  plot(d,'o')
  ```

- Typically, the solver yields an accurate answer only for the first few eigenvalues. Suppose we want to find the first two eigenvalues accurately. We fix N and compute the first two eigenvalues. We then increase N and compute the eigenvalues again. We continue increasing N until the first two eigenvalues do not change upon varying N. The solver is then said to have **converged**.

Happily, these solvers such as 'eig' tell us the eigenvectors as well as the eigenvalues. Typing

```
[V,D]=eig(L,M);
```

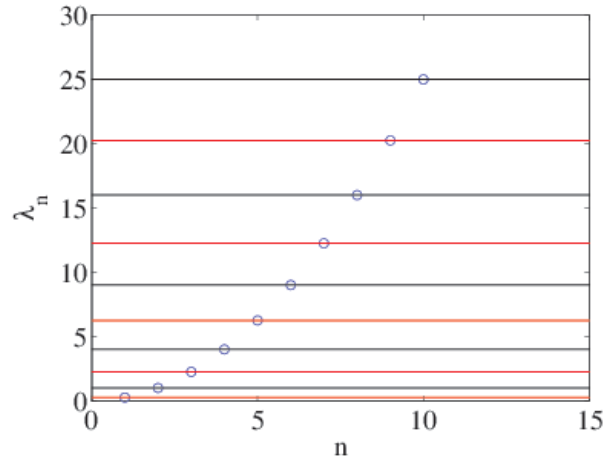gives two $(N+1) \times (N+1)$ matrices. The matrix D is diagonal and corresponds to the eigenvalues,

Figure 3.1: The spectrum of the problem $f''(y) = -\lambda f(y)$: comparison between numerical method and theory. Here $N = 100$ and $L = 2\pi$.

```
for i=1:(N+1)
   d(i)=D(i,i);
end
```

while the matrix V corresponds to the eigenvectors. Suppose we want to find the leading eigenvector. We would pick out the leading eigenvalue:

```
[maxd,imax]=max(d);
```

(do NOT sort them!). The corresponding eigenvector is

```
a=V(:,imax),
```

i.e. the $imax^{\text{th}}$ column of the matrix V. Finally then, our guess for the leading vector is

$$f_N(y) = \sum_{n=0}^{n} a_n T_n(x), \qquad x = \frac{2}{L}y.$$

The results of implementing this algorithm, with $N = 100$, are shown in Fig. 3.1. The first ten numerically-generated modes are shown in the figure (dots), along with the analytical modes: red lines for $\lambda = (n + 1/2)^2$, and black lines for $\lambda = n^2$ (Here $L = 2\pi$). The two calculations agree exactly. I have also picked out the first two modes and computed the corresponding eigenfunctions (Fig. 3.2). These eigenfunctions are $\psi = \cos(y/2)$ (lowest), and $\psi = \sin(y)$ (second lowest). Again, the exact calculation and the numerical calculation agree very well. In the next section, we answer the question, 'how well?' First, the Matlab codes used to generate the numerical solution in this section are referenced here:
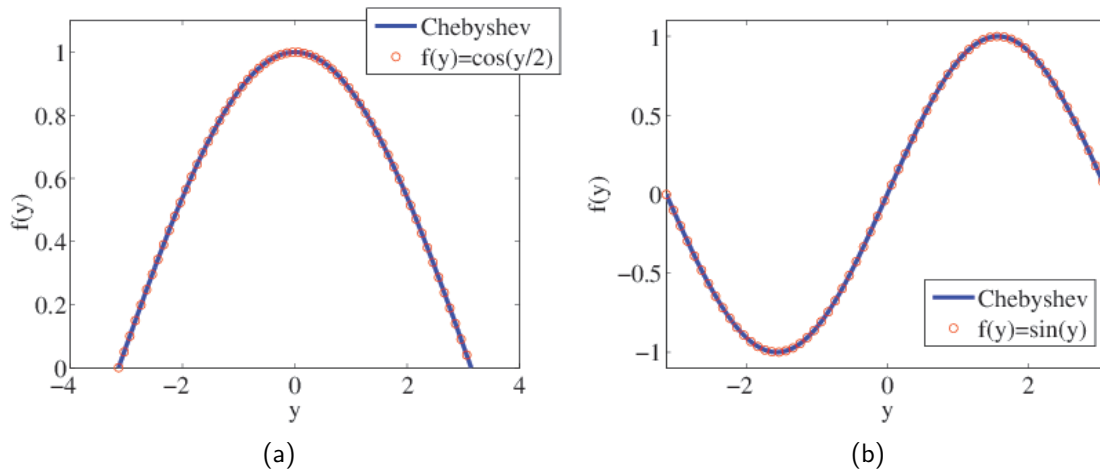
Figure 3.2: The first two eigenfunctions of the problem $f''(y) = -\lambda f(y)$. Here $N = 100$ and $L = 2\pi$.

- Calculation of eigenvalues: `simple.m`

- Calculation of eigenfunctions: `make_eigenfunction_simple`

Exercise 3.1

1. Solve the eigenvalue problem (3.1) analytically, this time with the Neuman boundary conditions

$$f'(-L/2) = f'(L/2) = 0.$$

2. Modify the Matlab codes above to solve the eigenvalue problem above in (1) numerically. Compare the analytical and numerical results, both for the eigenfunctions and eigenvalues.

3.3   Exponential convergence

In this section we examine some numerical issues surrounding the Chebyshev collocation method. So far we have been quite casual in our use of nomenclature. For definiteness, we work on the interval $[-1, 1]$. We start with the operator problem

$$\mathcal{L}f = \lambda \mathcal{M}f,$$

and construct the approximate solution

$$f(y) \approx f_N(y) = \sum_{n=0}^{N} a_n T_n(x), \qquad x \in [-1, 1].$$

Until now, we have called this a **truncation**, although really it is an **interpolation**. Let's see why the latter label is more appropriate.

First, recall the following result, due to Lagrange:

Theorem 3.1 *Let $f(x)$ be some function whose value is known at the discete points $x_0, x_1, \cdots, x_N$. Then there exist polynomials $C_0(x), C_1(x), \cdots, C_N(x)$ such that the function*

$$P_N(x) = \sum_{i=0}^{N} f(x_i) C_i(x)$$

agrees with $f(x)$ at the points $x_0, x_1, \cdots, x_N$:

$$P_N(x_i) = f(x_i), \qquad i = 0, 1, \cdots, N.$$

Proof: Take

$$C_i(x) = \prod_{j=0, j \neq i}^{N} \frac{x - x_j}{x_i - x_j}.$$

Noting that

$$C_i(x_k) = \delta_{ik},$$

the result follows. This result establishes the existence of interpolating polynomials, but does not tell us which ones are best. It turns out that the Chebyshev polynomials are among the better polynomials, and that the non-uniform Chebyshev grid is best. In what follows, we explain why.

For illustration purposes, consider the problem $\mathcal{L}f = \lambda \mathcal{M}f$ where boundary conditions are not important. We pose the interpolation approximation

$$f_N(x) = \tfrac{1}{2} b_0 T_0(x) + \sum_{n=1}^{N-1} b_n T_n(x) + \tfrac{1}{2} b_N T_N(x)$$

We impose the condition that $f_N(x)$ and $f(x)$ agree exactly at the points $x_0, x_1, \cdots, x_N$. We do not know the value of $f(x)$, but we do know the differential equation it solves. Thus, we have

$$\mathcal{L}f_N(x_k) = \lambda \mathcal{M} f_N(x_k), \qquad k = 0, 1, \cdots N.$$

Then the following theorem holds:

Theorem 3.2 *Let the interpolation grid be given by*

$$x_k = \cos(k\pi/N), \qquad k = 0, 1, \cdots N.$$

Let $f_N(x)$ be the interpolating polynomial of degree N which interpolates to $f(x)$ on this grid:

$$f_N(x) = \tfrac{1}{2} b_0 T_0(x) + \sum_{n=1}^{N-1} b_n T_n(x) + \tfrac{1}{2} b_N T_N(x),$$

$$f_N(x_k) = f(x_k)$$

Finally, let $\{\alpha_n\}_n$ be the coefficients of the exact expansion of $f(x)$ in Chebyshev polynomials:

$$f(x) = \tfrac{1}{2}\alpha_0 T_0(x) + \sum_{n=1}^{\infty} \alpha_n T_n(x)$$

Then,

$$b_n = \frac{2}{N} \left[\tfrac{1}{2} f(x_0) T_n(x_0) + \sum_{k=0}^{N-1} f(x_k) T_n(x_k) + \tfrac{1}{2} f(x_N) T_n(x_N) \right],$$

which leads to the following bound:

$$|f(x) - f_N(x)| \leq 2 \sum_{n=N+1}^{\infty} |\alpha_n|.$$

The proof of this theorem is straightforward but the reader is referred to Boyd [Boy01] for the details. We focus instead on the following corollary.

Theorem 3.3 *If the problem $\mathcal{L}f = \lambda \mathcal{M}f$ is analytic, then the convergence of the interpolation approximation in Theorem 3.2 is exponential.*

Proof: If there are no singularities in the problem $\mathcal{L}f = \lambda \mathcal{M}f$, then a power-series solution is possible, with finite radius of convergence. Continuing the power series into the complex plane gives a solution that has derivatives of all order. Thus, we may assume that

$$|f^{(p)}(x)| \leq M_p,$$

where the bound is independent of $x \in [-1, 1]$.

Next, we note that a Chebyshev series is but a Fourier series in disguise! For, let $\theta = \arccos(x)$. Then,

$$f(x) = \tfrac{1}{2}\alpha_0 + \sum_{n=1}^{\infty} \alpha_n T_n(x) = \tfrac{1}{2}\alpha_0 + \sum_{n=1}^{\infty} \alpha_n \cos(n\theta).$$

Differentiating both sides p times with respect to θ gives

$$\sum_{n=1}^{\infty} \alpha_n n^p \Re\left(i^p e^{in\theta}\right) = \frac{d^p f}{d\theta^p}.$$

But note:

$$
\begin{aligned}
\frac{df}{d\theta} &= \frac{dx}{d\theta}\frac{df}{dx} = -\sin\theta\frac{df}{dx}, \\
\frac{d^2 f}{d\theta} &= \sin^2\theta\frac{d^2 f}{dx^2} - \cos\theta\frac{df}{dx},
\end{aligned}
$$

and so on, implying that $|d^p f/d\theta^p| \le \widetilde{M_p}$, where the bound is independent of θ or x. Hence,

$$\left|\sum_{n=0}^{\infty} \alpha_n n^p \Re\left(i^p e^{in\theta}\right)\right| \le \tilde{M}_p,$$

and this is a convergent series. It follows that the general term tends to zero:

$$\lim_{n\to\infty} |\alpha_n| n^p = 0.$$

At worst,

$$|\alpha_n| \le A' e^{-\gamma' n^\delta}, \qquad n \to \infty,$$

for some positive parameters A', γ', and δ that are independent of n. Consider $\log|\alpha_n|/n$ as $n \to \infty$; this is

$$\log|\alpha_n|/n \sim -\gamma n^{\delta-1}, \text{ with } R = \lim_{n\to\infty} \log|\alpha_n|/n.$$

Three possibilities emerge:

1. $R = \infty$, corresponding to $\delta > 1$ and **supergeometric** behaviour. This implies that the true analytic eigensolution is an entire function in the complex plane (analytic continuation);

2. $R = \mathrm{Const}$, corresponding to $\delta = 1$ and **geometric** behaviour. This implies that the true analytic eigensolution that is a meromorphic in the complex plane got by analytically continuing the real solution, or has branch cuts, where these singularties are far from the (real) interval of interest.

3. $R = 0$, corresponding to **subgeometric** behaviour.

In any case, given the assumed regularity of the ODE to be solved, only cases 1 and 2 pertain, and thus, in a worst-case sceario, we have the geometric case, so we can conclude that for the problems of interest,

$$|\alpha_n| \le A e^{-\gamma n}, \qquad n \to \infty,$$

for some further positive parameters A and γ that are independent of n. Hence, there exists $N_0 \in \mathbb{N}$ such that

$$|\alpha_n| < A e^{-\gamma n}, \qquad \text{for all } n > N_0.$$

Returning to the bound in the Theorem 3.2, we have

$$
\begin{aligned}
|f(x) - f_{N_0}(x)| \;&\leq\; 2 \sum_{n=N_0+1}^{\infty} |\alpha_n|, \\
&\leq\; 2A \sum_{n=N_0+1}^{\infty} e^{-\gamma n}, \\
&\leq\; 2A e^{-\gamma(N_0+1)} \sum_{r=0}^{\infty} e^{-\gamma r}, \\
&\leq\; B e^{-\gamma N_0}
\end{aligned}
$$

The error is thus proportional to $e^{-\gamma N_0}$ and we therefore say that the Chebyshev collocation method **converges exponentially**. Typically, this result generalizes to situations where the boundary conditions are built in to the interpolation coefficients.

3.4 The Rayleigh–Taylor instability revisited

I have implemented a numerical spectral method for the computation of the eigenvalues of the Rayleigh–Taylor instability. The eigenvalue problem is solved in a finite domain $z \in [-H, H]$. In numerical methods, it is convenient to nondimesnionalize the problem. The curious thing about the Rayleigh–Taylor problem is that there is no natural unit of length, and even in the finite domain, using the scale H as the standard lengthscale is problematic. Thus, we introduce an arbitrary lengthscale h_0 and non-dimesnionalize with respect to that, as well as the typical velocity scale $U_0 = \sqrt{gh_0}$. Densities and viscosities are scaled relative to the bottom-layer density and viscosity – ρ_G and μ_G respectively. The non-dimensional problem to solve reads

$$
\sigma r_L \left(\partial_z^2 - k^2\right) \Psi_L \;=\; \frac{m_L}{Re} \left(\partial_z^2 - k^2\right)^2 \Psi_L, \qquad z \in (0, \nu_L), \tag{3.2a}
$$

$$
\sigma r_G \left(\partial_z^2 - k^2\right) \Psi_G \;=\; \frac{m_G}{Re} \left(\partial_z^2 - k^2\right)^2 \Psi_G, \qquad z \in (-\nu_G, 0). \tag{3.2b}
$$

The following matching conditions apply at $z = 0$:

$$\Psi_L(0) = \Psi_G(0), \tag{3.2c}$$

$$\partial_z \Psi_L(0) = \partial_z \Psi_G(0), \tag{3.2d}$$

$$m_L \left(\partial_z^2 + k^2\right) \Psi_L = m_G \left(\partial_z^2 + k^2\right) \Psi_G, \tag{3.2e}$$

$$\sigma r_L \partial_z \Psi_L + \frac{m_L}{Re} \left(3k^2 \partial_z \Psi_L - \partial_z^3 \Psi_L\right) = \sigma r_G \partial_z \Psi_G + \frac{m_G}{Re} \left(3k^2 \partial_z \Psi_G - \partial_z^3 \Psi_G\right)$$
$$-\mathrm{i}k \left[(r_L - r_G)k - \mathcal{S}k^3\right] \eta_0. \tag{3.2f}$$

Here, $\eta = \eta_0 \mathrm{e}^{\mathrm{i}kx + \sigma t}$ and η_0 is the phase, determined by the kinematic condition

$$\sigma \eta_0 = -\mathrm{i}k \Psi(0). \tag{3.2g}$$

Finally, the following boundary conditions apply:

$$\psi_L, \partial_z \psi_L \to 0 \text{ as } z \to \infty, \qquad \psi_G, \partial_z \psi_G \to 0 \text{ as } z \to -\infty. \tag{3.2h}$$

The dimensionless quantities are defined here as follows. First, we have $\nu_L = \nu_G = H/h_0 \in (0, \infty)$, which are variable parameters. For the densities, we have

$$r_L = \rho_L/\rho_G \in [1, \infty), \qquad r_G = \rho_G/\rho_G = 1,$$

For the viscosity parameters, we have

$$m_L = \mu_L/\mu_G \in [0, \infty), \qquad m_G = \mu_G/\mu_G = 1,$$

The Reynolds number is $Re = U_0 h_0 \rho_G/\mu_G$, also variable. Finally, $\mathcal{S} = \gamma/(\rho_G h U_0^2)$ is a dimensionless surface-tension parameter.

It is not necessary for the students to write a code to solve the RTI eigenvalue problem (I have done that already). Instead, you can take the codes

- OS_rti.m

- call_OS_rti.m

and study them yourself. In particular, carry out the following exercise:

Exercise 3.2 *Take the RTI eigenvalue solver. Take $Re = 1000$ and $m_L = m_G = 1$. Choose further appropriate values for the other parameters. Show in this parameter regime of large*
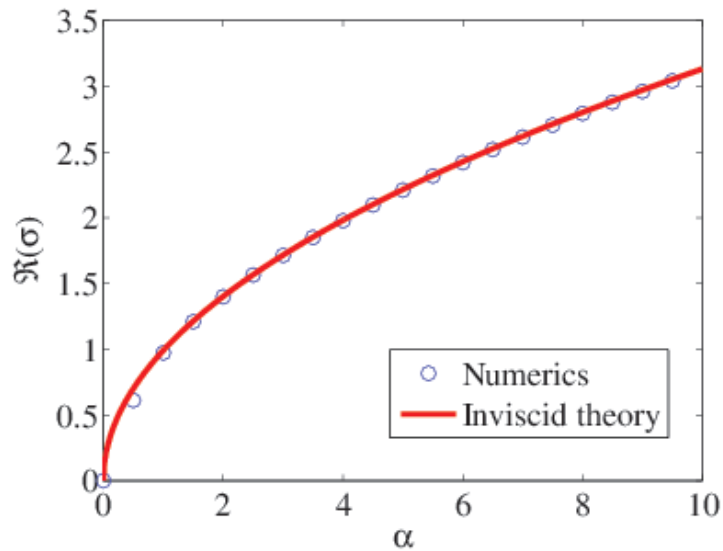
Figure 3.3: Comparison between the inviscid theory and the numerical method

Reynolds number that the numerical results agree very closely with the earlier inviscid analysis. Justify this finding.

Example: With $Re = 1000$, $m_L = m_G = 1$, $\nu_L = \nu_G = 2$, $N_L = N_G = 100$ and $\mathcal{S} = 0$ the results in Figure 3.3 were obtained. Excellent agreement is obtained. The small discrepancies at long wavelengths (small α) have been investigated by an M.Sc. student and are found to arise due to the confinement of the numerical domain.

Chapter 4

Stability of viscous parallel flow

Overview

We introduce the Orr–Sommerfeld equation for the stability of parallel flow. We demonstrate one particular instance where exact solutions for the eigenvalue problem are obtainable. We then pass over to numerical spectral methods to calculate the critical Reynolds number for the onset of instability in Poiseuille channel flow.

4.1   Parallel flow

We consider the Navier–Stokes equations for a wall-bounded flow, such that $z \in [0, H]$, and such that the velocity vanishes at $z = 0$ and $z = H$ (no-slip). Suppose that the flow is characterized by a typical velocity V. The Navier–Stokes equations then non-dimensionalize in a standard fashion:

$$\frac{\partial \boldsymbol{u}}{\partial t} + \boldsymbol{u} \cdot \nabla \boldsymbol{u} = -\nabla p + \frac{1}{Re}\nabla^2 \boldsymbol{u}, \qquad \nabla \cdot \boldsymbol{u} = 0, \tag{4.1a}$$

where $\boldsymbol{u}$ and p have their usual meanings and

$$Re = \frac{VH\rho}{\mu} \tag{4.1b}$$

is the (dimensionless) Reynolds number. Here, ρ and μ are the fluid density and viscosity respectively. We henceforth work with these non-dimensional equations of motion.

Consider now a parallel flow $U_0(z)$ shown schematically in Figure 4.1. The origin of such a flow profile will be discussed in later sections in this chapter. For now, it suffices to notice that a flow $\boldsymbol{u} = (U_0(z), 0, 0)$ is an equilibrium solution of the Navier–Stokes equation (4.1a). A small perturbation

50
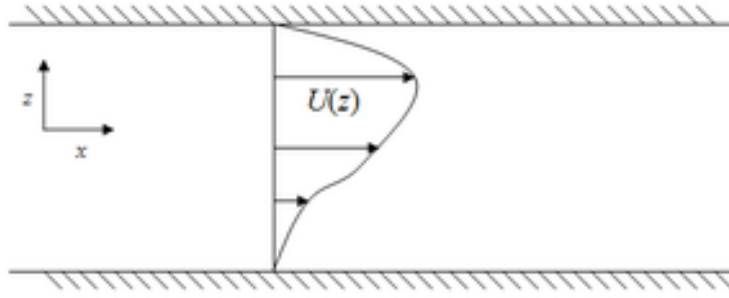
around this base state is now introduced (it suffices to consider two-dimensional perturbations in the first instance), such that the following perturbed velocity field is considered:

$$\boldsymbol{u} = (U_0(z) + u'(x, z, t), 0, w'(x, z, t))$$

This functional form for the velocity is substituted into the Navier–Stokes equations and the equations are linearized. One obtains

$$\frac{\partial u'}{\partial t} + U_0 \frac{\partial u'}{\partial x} + w' \frac{dU_0}{dz} = -\frac{\partial}{\partial x} \delta p + Re^{-1} \nabla^2 u', \tag{4.2a}$$

$$\frac{\partial w'}{\partial t} + U_0 \frac{\partial w'}{\partial x} = -\frac{\partial}{\partial z} \delta p + Re^{-1} \nabla^2 w', \tag{4.2b}$$

$$\frac{\partial u'}{\partial x} + \frac{\partial w'}{\partial z} = 0. \tag{4.2c}$$

We carry out our favourite trick by taking $\partial_z(4.2a) - \partial_x(4.2b)$. We obtain

$$\frac{\partial}{\partial t} (\partial_z u' - \partial_x w') + U_0 (\partial_{xz} u' - \partial_{xx} w') + \frac{dU_0}{dz} \left(\frac{\partial u'}{\partial x} + \frac{\partial w'}{\partial z} \right) + w' \frac{d^2 U_0}{dz^2} = Re^{-1} \nabla^2 (\partial_z u' - \partial_x w').$$

The term $(dU_0/dz)(\partial_x u' + \partial_z w')$ obviously drops out because of incompressibility. To make further progress, we introduce the streamfunction $\psi(x, z, t)$, such that $u' = \partial_z \psi$ and $w' = -\partial_x \psi$, leaving

$$\left(\frac{\partial}{\partial t} + U_0 \partial_x \right) \nabla^2 \psi - \frac{\partial \psi}{\partial x} \frac{d^2 U_0}{dz^2} = Re^{-1} \nabla^4 \psi.$$

As in previous work on stability theory, we now make a normal-mode decomposition $\psi(x, z, t) = e^{\lambda t + ikx} \Psi(z)$. One obtains

$$(\lambda + ikU_0) \left(\partial_z^2 - k^2 \right) \Psi - ikU_0'' \Psi = Re^{-1} \left(\partial_z^2 - k^2 \right)^2 \Psi.$$

It is standard to write $\lambda = -ikc$, where c is a wave speed. Thus, we obtain the following equation:

$$ik \left[(U_0 - c) \left(\partial_z^2 - k^2 \right) \Psi - U_0'' \Psi \right] = Re^{-1} \left(\partial_z^2 - k^2 \right)^2 \Psi. \tag{4.3}$$

Equation (4.3) is the celebrated Orr–Sommerfeld equation. When supplemented with the no-slip boundary conditions

$$\Psi(0) = \Psi'(0) = \Psi(1) = \Psi'(1)$$

it is an eigenvalue problem in the eigenvalue c.

4.2 Couette flow

Consider again the two parallel plates in Figure 4.1. Suppose that the upper plate moves at a constant velocity V. We work out the base state of the Navier–Stokes equations in this instance: simply

$$\nabla^2 \boldsymbol{u} = 0,$$

with $\boldsymbol{u} = (U_0, 0, 0)$ for a parallel flow, hence $d^2 U_0/dz^2 = 0$, hence $U_0 = A + Bz$. The no-slip condition at the lower wall gives $A = 0$. Now, at the upper wall, no slip means 'no relative motion': the plate and the fluid-at-the-plate should move at exactly the same velocity, hence $U_0(H) = V$, hence $BH = V$, hence

$$U_0(z) = zV/H.$$

This is the celebrated **Couette flow**. Going over to non-dimensional variables, this is simply $U_0 = z$, and the corresponding Orr–Sommerfeld equation reads

$$\mathrm{i}k\,(z - c)\left(\partial_z^2 - k^2\right)\Psi = Re^{-1}\left(\partial_z^2 - k^2\right)^2\Psi. \tag{4.4}$$

Analytical progress can be made with respect to Equation (4.4). Call $v = \left(\partial_z^2 - k^2\right)\Psi$. Then, we are left with the equation

$$\mathrm{i}k\,(z - c)\,v = Re^{-1}\left(\partial_z^2 - k^2\right)v. \tag{4.5}$$

Certainly, the trivial solution is a possibility for Equation (4.5), leaving $v = \left(\partial_z^2 - k^2\right)\Psi = 0$, hence

$$\Psi = \cosh(kz), \qquad \Psi = \sinh(kz).$$

However, because the eigenvalue equation is fourth order, two other linearly independent solutions can be found. We re-write Equation (4.5) as

$$\frac{d^2 v}{dz^2} - Re\,\mathrm{i}k\left(z - c - \frac{\mathrm{i}k}{Re}\right)v = 0.$$

Let $\widetilde{z} = z - c - ik/Re$. Hence, we obtain

$$\frac{d^2 v}{d\widetilde{z}^2} - Reik\widetilde{z}v = 0.$$

Introduce $\xi = \lambda\widetilde{z}$, where λ is constant. We have

$$\frac{d}{d\widetilde{z}} = \frac{d\xi}{d\widetilde{z}}\frac{d}{d\xi}.$$

Hence,

$$\lambda^2 \frac{d^2 v}{d\xi^2} - \frac{ikRe}{\lambda}\xi v = 0.$$

Choosing $\lambda^3 = ikRe$ gives Airy's equation:

$$\frac{d^2 v}{d\xi^2} - \xi v = 0,$$

with solutions

$$v = Ai(\xi), \qquad v = Bi(\xi).$$

We also choose the particular cube root of $i^{1/3} = e^{i\pi/6}$.

We must now solve the equations

$$(\partial_z^2 - k^2)\Psi = Ai(\xi), \qquad (\partial_z^2 - k^2)\Psi = Bi(\xi). \tag{4.6}$$

These are linear second-order inhomogeneous equations. We use the method of variation of parameters. We study first the solutions of the homogeneous problem

$$\Psi_1(z) = \cosh(kz), \qquad \Psi_2(z) = \sinh(kz).$$

Let's focus for definiteness on the case where the right-hand side is $Ai(\xi)$. We construct the Wronskian

$$W(z) = \begin{vmatrix} \Psi_1(z) & \Psi_2(z) \\ \Psi_1'(z) & \Psi_2'(z) \end{vmatrix} = \begin{vmatrix} \cosh(kz) & \sinh(kz) \\ k\sinh(kz) & k\cosh(kz) \end{vmatrix},$$

which gives $W(z) = k$. Next, we form the Wronskians $W_i(z)$, which is identical to $W(z)$ except that the ith column is replaced by $(0, Ai(\xi))^T$. We have

$$W_1(z) = \begin{vmatrix} 0 & \sinh(kz) \\ Ai(\xi) & k\cosh(kz) \end{vmatrix} = -\sinh(kz)Ai(\xi).$$

Also,

$$W_2(z) = \begin{vmatrix} 0 & \sinh(kz) \\ k\cosh(kz) & Ai(\xi) \end{vmatrix} = \cosh(kz)Ai(\xi).$$

The particular integral in the method of variation-of-parameters by given by

$$\Psi = \sum_{i=1}^{2} \Psi_i(z) \int \frac{W_i(z')}{W(z')} dz.$$

Hence,

$$\Psi = \frac{1}{k}\left[-\cosh(kz)\int \sinh(kz')Ai(\xi)dz' + \sinh(kz)\int \cosh(kz')Ai(\xi)dz'\right].$$

Using a trigonometric identity here, this becomes

$$\Psi = \frac{1}{k}\int \sinh[k(z-z')]Ai(\xi)dz'.$$

Finally, we call this solution $\xi_1(z)$ and we fill in for ξ:

$$\chi_1(z) = \frac{1}{k}\int_0^z \sinh[k(z-z')]Ai\left[(ikRe)^{1/3}\left(z'-c-\frac{ik}{Re}\right)\right]dz',$$

Here, the limits of integration have been chosen such that $\chi_1(0) = \chi_1'(0) = 0$, such that $\chi_1(z)$ satisfies the boundary conditions at $z = 0$. A similar trick can be performed when the right-hand side of Equation (4.6) is equal to $Bi(\xi)$, one obtains the solution $\chi_2(z)$, where

$$\chi_2(z) = \frac{1}{k}\int_0^z \sinh[k(z-z')]Bi\left[(ikRe)^{1/3}\left(z'-c-\frac{ik}{Re}\right)\right]dz',$$

with $\chi_2(0) = \chi_2'(0) = 0$.

We have the following solution of the eigenvalue problem:

$$\Psi = A\Psi_1(z) + B\Psi_2(z) + C\chi_1(z) + D\chi_2(z).$$

The vanishing of the streamfunction at the boundaries implies that

$$\begin{vmatrix} 1 & 0 & 0 & 0 \\ 0 & k & 0 & 0 \\ \cosh(k) & \sinh(k) & \chi_1(1) & \chi_2(1) \\ k\sinh(k) & k\cosh(k) & \chi_1'(1) & \chi_2'(1) \end{vmatrix} = 0.$$

This determinant problem simplifies dramatically to

$$k\left[\chi_1(1)\chi_2'(1) - \chi_2(1)\chi_1'(1)\right] = 0. \tag{4.7}$$

The right-hand side can be viewed as a complex-valued function of k, Re, and c (the latter a complex variable). We therefore have the condition

$$F(k, Re, c) = 0,$$

which is a rootfinding condition, with a set of roots $c_n(k, Re)$ such that $F(k, Re, c_n) = 0$.

Analytical progress based on Equation (4.7) is difficult if not impossible [DR81]. Indeed, there is a celebrated theorem due to Romanov [Rom73] that states that $c_i(k, Re) \leq 0$ for all finite real values of k and Re, indicating the unconditional **linear stability** of plane Couette flow. However, this theorem uses a completely different approach in the proof, and the dispersion relation (4.7) is therefore something of a dead end. Therefore, in a later part of this chapter, we introduce numerical spectral methods for solving the generic Orr–Sommerfeld equation.

4.3 Poiseuille flow

Consider the two parallel plates in Figure 4.1. Suppose now that both plates are stationary but that a constant pressure drop $dP/dL < 0$ is applied along the length of the channel We work out the base state of the Navier–Stokes equations in this instance:

$$\begin{aligned} 0 &= -\frac{dP}{dL} + \mu\nabla^2 u, \\ 0 &= \nabla^2 w. \end{aligned}$$

We assume only a z-dependence for the velocity, giving $d^2w/dz^2 = 0$, with $w(0) = w(H) = 0$, hence $w = 0$. Thus, the equations to solve reduce to

$$-\frac{dP}{dL} + \mu\frac{d^2U_0}{dz^2} = 0,$$

where the base state in the streamwise (x-direction) is denoted now by $U_0(z)$. The equation is integrated twice to yield

$$U_0 = A + Bz + \frac{1}{2\mu}\frac{dP}{dL}z^2.$$

The no-slip condition at the lower wall gives $A = 0$. At the upper wall $z = H$, the same condition gives

$$B = -\frac{1}{2\mu}\frac{dP}{dL}H,$$

hence

$$U_0 = -\frac{1}{2\mu}\frac{dP}{dL}\left(zH - z^2\right).$$

This is tidied up slightly here to give

$$U_0 = \frac{H^2}{2\mu}\left|\frac{dP}{dL}\right|\left[\frac{z}{H} - \left(\frac{z}{H}\right)^2\right].$$

As before, it is necessary to introduce a velocity scale V, and to nondimensionalize the problem based on the scales V and H. We choose V to be the so-called friction velocity,

$$\rho V^2 = \mu\frac{dU_0}{dz}\Big|_{z=0},$$

hence

$$\rho V^2 = \frac{1}{2}\left|\frac{dP}{dL}\right|H \implies V = \sqrt{\frac{H}{2\rho}\left|\frac{dP}{dL}\right|}.$$

Introduce also $\widetilde{z} = z/H$, such that the base-state velocity profile reads

$$U_0 = \frac{H^2}{2\mu}\left|\frac{dP}{dL}\right|\left[\frac{z}{H} - \frac{z}{H}^2\right].$$

We have

$$
\begin{aligned}
\widetilde{U_0} &= \frac{U_0}{V}, \\
&= \frac{\frac{H^2}{2\mu}\left|\frac{dP}{dL}\right|\left(\widetilde{z} - \widetilde{z}^2\right)}{\sqrt{\frac{H}{2\rho}\left|\frac{dP}{dL}\right|}}, \\
&= \frac{\frac{\rho H}{\mu}\frac{H}{2\rho}\left|\frac{dP}{dL}\right|\left(\widetilde{z} - \widetilde{z}^2\right)}{\sqrt{\frac{H}{2\rho}\left|\frac{dP}{dL}\right|}}, \\
&= \frac{\rho H}{\mu}\sqrt{\frac{H}{2\rho}\left|\frac{dP}{dL}\right|}\left(\widetilde{z} - \widetilde{z}^2\right), \\
&= \frac{\rho V H}{\mu}\left(\widetilde{z} - \widetilde{z}^2\right), \\
&= Re_*\left(\widetilde{z} - \widetilde{z}^2\right),
\end{aligned}
$$

where

$$Re_* = \frac{\rho V H}{\mu}.$$

is the Reynolds number based on the friction velocity and the channel depth H. We now omit all ornamentation over the dimensionless variables and write down the Orr–Sommerfeld equation

$$\mathrm{i}k\left[(U_0 - c)\left(\partial_z^2 - k^2\right) - U_0''\right]\Psi = Re_*^{-1}\left(\partial_z^2 - k^2\right)^2\Psi, \qquad U_0(z) = Re_* z(1 - z). \tag{4.8}$$

It is now of pressing urgency to introduce a numerical method to obtain a reliable solution of both Equation (4.8) for the Poiseuille problem, but also to illuminate the dispersion relation of the Couette flow problem in Equation (4.4). We do this in the next section.

4.4 Spectral methods for the generic Orr–Sommerfeld equation

We start with the generic Orr–Sommerfeld equation

$$\mathrm{i}k\left[(U_0 - c)\left(\partial_z^2 - k^2\right) - U_0''\right]\Psi = Re_*^{-1}\left(\partial_z^2 - k^2\right)^2\Psi, \qquad z \in (0, 1), \tag{4.9}$$

together with the necessary boundary conditions

$$\Psi(z) = \Psi'(z) = 0, \qquad z = 0, 1.$$

A trial solution

$$\Psi_N(z) = \sum_{i=0}^{N} A_n T_n(\eta)$$

is made, with $\eta = 2z - 1$, such that $\eta = 0$ and $\eta = 1$ denote the boundaries. This is substituted into Equation (4.9):

$$\sum_{n=0}^{N} A_n\left\{\mathrm{i}k\left[(U_0 - c)\left(\partial_z^2 - k^2\right) - U_0''\right]T_n(\eta)\right\} = Re^{-1}\sum_{n=0}^{N} A_n\left(\partial_z^2 - k^2\right)^2 T_n(\eta) \tag{4.10}$$

This equation is now evaluated at $N - 4$ collocation points

$$\eta_j = \cos\left(\frac{\pi j}{N - 3}\right), \qquad j = 1, \cdots, N - 3$$

and the following set of equations is obtained:

$$\lambda \sum_{j=0}^{N} A_j \left[s^2 T_n''(\eta_j) - k^2 T_n(\eta_j) \right] +$$

$$\mathrm{i}k \sum_{j=0}^{N} A_j \left[s^2 U_0(z_j) T_n''(\eta_j) - k^2 U_0(z_j) T_n(\eta_j) - U_0''(z_j) T_n(\eta_j) \right]$$

$$= Re^{-1} \sum_{n=0}^{N} A_n \left[s^4 T_n^{(\mathrm{iv})}(\eta_j) - 2k^2 s^2 T_n^2(\eta_j) + k^4 T_n(\eta_j) \right], \quad (4.11)$$

where $s = d\eta/dz = 2$ and $z_j = 2\eta_j - 1$. We now introduce a number of matrices:

$$\begin{aligned}
\mathbf{d0T}_{ij} &= T_j(\eta_i), \\
\mathbf{d2T}_{ij} &= s^2 T_j''(\eta_i), \\
\mathbf{d4T}_{ij} &= s^4 T_j^{(\mathrm{iv})}(\eta_i), \\
\mathbf{d0Td0U}_{ij} &= U_0(z_i) T_j(\eta_i), \\
\mathbf{d0Td2U}_{ij} &= U_0''(z_i) T_j(\eta_i), \\
\mathbf{d2Td0U}_{ij} &= s^2 U_0(z_i) T_j''(\eta_i), \\
\boldsymbol{A} &= (A_0, \cdots, A_N)^T,
\end{aligned}$$

such that Equation (4.11) can now be written in matrix form as follows:

$$\lambda \left(\mathbf{d2T} - k^2 \mathbf{d0T} \right) \boldsymbol{A} = -\mathrm{i}k \left(\mathbf{d2Td0U} - k^2 \mathbf{d0Td0U} - \mathbf{d0Td2U} \right) \boldsymbol{A}$$
$$+ Re^{-1} \left(\mathbf{d4T} - 2k^2 \mathbf{d2T} + k^4 \mathbf{d0T} \right) \boldsymbol{A}.$$

However, since $i = 0, 1, \cdots, N-3$ and $j = 1, 2, \cdots N+1$, this equation set is not complete (four rows are missing). We now impose the boundary conditions. $\Psi_N(0) = 0$ implies that

$$\sum_{j=0}^{N} T_j(-1) A_i = 0.$$

Similarly, $\Psi_N'(0) = 0$ implies that

$$\sum_{j=0}^{N} T_j'(-1) A_j = 0.$$

and so on for the other boundary conditions. Thus, we now form a new linear problem:

$$
\lambda
\begin{pmatrix}
0 & 0 & \cdots & 0 \\
0 & 0 & \cdots & 0 \\
& & & \\
& \mathbf{d2T} - k^2 \mathbf{d0T} & & \\
& & & \\
0 & 0 & \cdots & 0 \\
0 & 0 & \cdots & 0
\end{pmatrix}
\boldsymbol{A}
$$

$$
=
\begin{pmatrix}
T_0(-1) & T_1(-1) & \cdots & T_N(-1) \\
T_0'(-1) & T_1;(-1) & \cdots & T_N'(-1) \\
& & & \\
& -\mathrm{i}k\left(\mathbf{d2Td0U} - k^2\mathbf{d0Td0U} - \mathbf{d0Td2U}\right) & & \\
& +Re^{-1}\left(\mathbf{d4T} - 2k^2\mathbf{d2T} + k^4\mathbf{d0T}\right) & & \\
& & & \\
T_0(1) & T_1(1) & \cdots & T_N(1) \\
T_0'(1) & T_1'(1) & \cdots & T_N'(1)
\end{pmatrix}
\boldsymbol{A}
$$

or in a more abstract notation,

$$\lambda \mathbf{M}\boldsymbol{A} = \mathbf{L}\boldsymbol{A}, \tag{4.12}$$

which is now a straightforward finite-dimensional generalized-eigenvalue problem that can be solved in Matlab (or any other linear algebra package). Obviously, the number of Chebyshev polynomials N should be adjusted until numerical convergence is achieved.

Couette flow

Equation (4.12) is solved for $U_0(z) = z$ for various Reynolds numbers in the range $Re = 100$ up to $Re = 100,000$, and in each instance $N = 100$ is sufficient for convergence. The results are shown in Figure 4.1 confirming (but by no means proving) the stability of Couette flow to infinitesimal disturbances.

Poiseiulle flow

Equation (4.12) is solved for $U_0(z) = Re_* z(1-z)$ and the results shown in Figure 4.2 for $Re_* = 100$ and $Re_* = 1000$. It can be seen that for the lower Reynolds number the flow is stable at all wavenumbers, while for $Re_* = 1000$, there is a range of wavenumbers within which the flow is

Figure 4.1: Numerically-generated dispersion relation for Couette flow for range of different Reynolds numbers. Solid line: $Re = 100$. Dashed line: $Re = 1000$. Dotted line: $Re = 10,000$. Dot-dashed line: $Re = 100,000$. It can be seen that the disturbances become less stable as Re increases but the curve corresponding to the growth rate never crosses the horizontal axis, which underscores the analytical result that Couette flow is stable to infinitesimal disturbances at all finite Reynolds numbers.
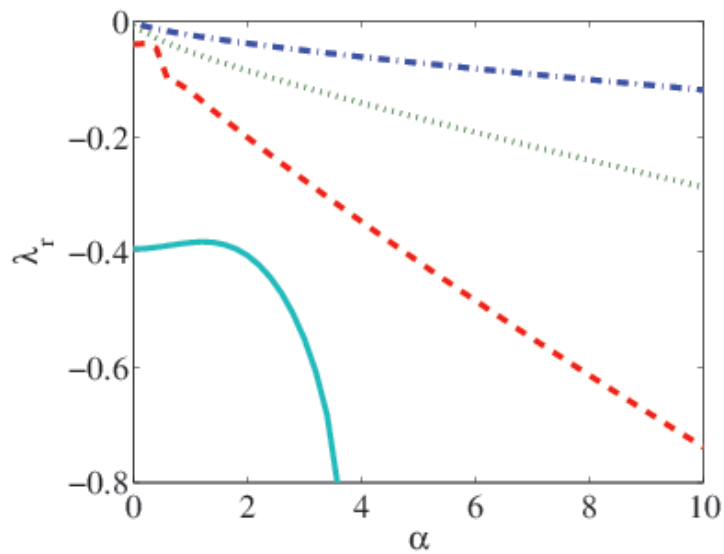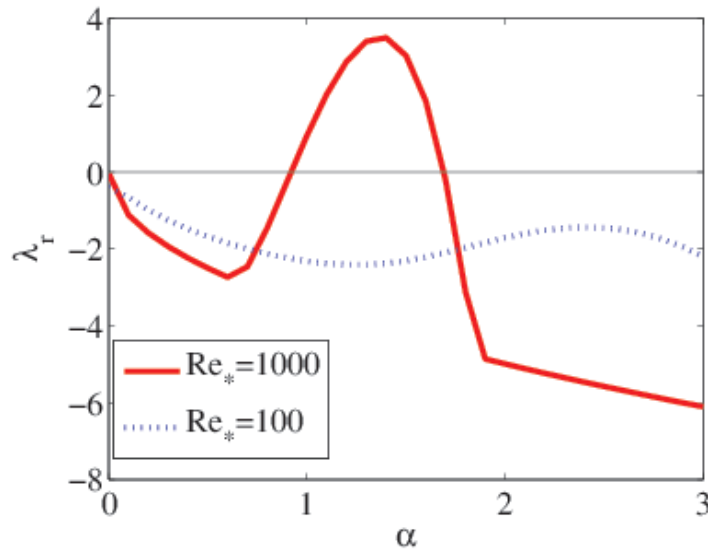

Figure 4.2: Numerically-generated dispersion relation for Poiseuille flow for range of different Reynolds numbers. Solid line: $Re = 1000$, linearly unstable. Dotted line: $Re = 100$, linearly stable. In each instance $N = 100$ is sufficient for convergence.

unstable. This therefore suggests a critical Reynolds number Re_{*c} at which the growth rate curve just barely touches the horizontal axis. The numerical code indicates that to three significant figures,

$$Re_{*c} = 214.8$$

It is of interest to examine the Reynolds numbmer

$$Re = \frac{U_{\max}(H/2)\rho}{\mu},$$

where $U_{\max}$ is the centreline velocity. Now

$$\frac{U_{\max}}{V} = Re_*/4.$$

Also,

$$
\begin{aligned}
Re &= \frac{U_{\max}(H/2)\rho}{\mu}, \\
&= \frac{VH\rho}{\mu}\left(\frac{1}{2}\frac{U_{\max}}{V}\right), \\
&= \tfrac{1}{2}Re_*\left(Re_*/4\right), \\
&= \tfrac{1}{8}Re_*^2,
\end{aligned}
$$

hence

$$Re_c = \tfrac{1}{8}Re_{*c} \approx 5772$$

to four significant figures. This is the famous and oft-quoted result of Orzag [Orz71].

4.5 Analytical validation of the numerical method by long-wave perturbation theory

How do we know that the numerical results in the previous section are correct? The answer is that they have been **validated** with respect to known analytical solutions. Those solutions are constructed in the present section and pertain to the longwave limit where $k \to 0$.

We start by looking at the case $k = 0$, where we are to solve the equation

$$\partial_z^4\Psi = Re(\mathrm{i}kz + \lambda)\partial_z^2\Psi \implies \partial_z^4\Psi = Re\lambda\partial_z^2\Psi, \qquad z \in [0,1].$$

For simplicity, we change coordinates to $\eta = z - 1/2$, and the equation to be solved now reads

$$\frac{d^4\Psi}{d\eta^4} = Re\lambda\frac{d^2\Psi}{d\eta^2}, \qquad \eta \in [-1/2, 1/2]. \tag{4.13}$$

with boundary conditions

$$\Psi(\eta) = \Psi'(\eta) = 0, \qquad \eta = \pm 1/2. \tag{4.14}$$

It is clear from Equation (4.13) and from the relevant boundary conditions that the eigenvalue problem is self-adjoint and **hence the eigenvalues are real**. Moreover, that the four linearly independent eigensolutions are

$$\Psi = 1, \qquad \eta, \qquad \cosh(k\eta), \qquad \sinh(k\eta),$$

where $k = \sqrt{\lambda Re}$. We split the eigensolutions up into odd and even cases.

$$\Psi_{\text{even}} = A + B\cosh(k\eta), \qquad \Psi_{\text{odd}} = A\eta + B\sinh(k\eta).$$

where A and B are complex constants. We consider the even case first. The boundary conditions are applied at $\eta = +1/2$ to yield

$$\begin{vmatrix} 1 & \cosh(k/2) \\ 0 & k\sinh(k/2) \end{vmatrix} = 0,$$

hence $k = 0$ or

$$\sinh(k/2) = 0$$

which has solutions $k = 2in\pi$, where $n \in \mathbb{Z}$. But $k = \sqrt{\lambda Re}$, hence

$$\lambda_{n,\text{even}} = -\frac{4n^2\pi^2}{Re}, \qquad n \in \mathbb{N},$$

where we do not include $n \leq 0$ so as to avoid double-counting.

Next for the odd case. The boundary conditions are again applied at $\eta = 1/2$ to yield

$$\begin{vmatrix} \frac{1}{2} & \sinh(k/2) \\ 1 & k\cosh(k/2) \end{vmatrix},$$

hence

$$(k/2)\cosh(k/2) = \sinh(k/2).$$

By inspection, this equation has no solution in real values of k, and complex values are ruled out because of the reality of the eigenvalues. However, purely imaginary solutions are possible, with

$k = i\hat{k}$, where $\hat{k}$ is real. We must therefore solve

$$\tfrac{1}{2}\hat{k}\cos(\hat{k}/2) = \sin(\hat{k}/2)$$

In addition to $\hat{k} = 0$, this equation has an infinite family of roots $\pm x_n$, with $x_n \in \mathbb{R}^+$, the lowest value of which is $x_1 = 8.987$. But $k = i\hat{k} = \pm i x_n = \sqrt{\lambda Re}$, hence

$$\lambda_{n,\text{odd}} = -\frac{x_n^2}{Re}, \qquad n \in \mathbb{N}.$$

We have

$$\begin{aligned}
\lambda_{1,\text{even}} &= -39.4784/Re, \\
\lambda_{2,\text{odd}} &= -80.7662/Re, \\
\lambda_{1,\text{even}} &= -157.9137/Re, \\
\lambda_{2,\text{odd}} &= -238.7025/Re.
\end{aligned}$$

Hence, the least stable mode is even, with $n = 1$, eigenvalue $\lambda = -4\pi^2/Re$ and corresponding eigenfunction

$$\Psi = \cos(2\pi\eta) + 1.$$

We now make a regular perturbation expansion

$$\lambda = \lambda_0 + k\lambda_1 + \cdots$$

and

$$\Psi = \Psi_0 + k\Psi_1 + \cdots$$

and substitute into the Orr–Sommerfeld equation. At order k^0 we obtain

$$Re\lambda_0\partial_\eta^2\Psi_0 = \partial_\eta^4\Psi_0,$$

which is precisely the eigenvalue problem at $k = 0$ with the already-computed solutions. At first order in k, the perturbation theory gives the following equation:

$$Re\left[iU_0(\eta) + \lambda_1\right]\partial_\eta^2\Psi_0 - iReU_0''\Psi_0 + \lambda_0\partial_\eta^2\Psi_1 = \partial_\eta^4\Psi_1.$$

Here is the trick: multiply both sides of this equation by Ψ_0^* and integrate from $\eta = -1/2$ to

$\eta = 1/2$. The result is

$$\mathrm{i}Re \int_{-1/2}^{1/2} U_0 \Psi_0^* \partial_\eta^2 \Psi_0 \, \mathrm{d}\eta - \mathrm{i}Re \int_{-1/2}^{1/2} U_0'' |\Psi_0|^2 \, \mathrm{d}\eta + Re\lambda_1 \langle \Psi_0, \partial_\eta^2 \Psi_0 \rangle + \lambda_0 \langle \Psi_0, \partial_\eta^2 \Psi_1 \rangle = \langle \Psi_0, \partial_\eta^4 \Psi_1 \rangle.$$

Re-arrange slightly:

$$\mathrm{i}Re \int_{-1/2}^{1/2} U_0 \Psi_0^* \partial_\eta^2 \Psi_0 \, \mathrm{d}\eta - \mathrm{i}Re \int_{-1/2}^{1/2} U_0'' |\Psi_0|^2 \, \mathrm{d}\eta + Re\lambda_1 \langle \Psi_0, \partial_\eta^2 \Psi_0 \rangle = -\langle \lambda_0 \Psi_0, \partial_\eta^2 \Psi_1 \rangle + \langle \Psi_0, \partial_\eta^4 \Psi_1 \rangle,$$

where we have used the reality of λ_0 to take it inside the inner product

$$\langle f, g \rangle = \int_{-1/2}^{1/2} f^* g \, \mathrm{d}\eta.$$

We next use the self-adjointness of the operators ∂_η^2 and ∂_η^4 with respect to the imposed boundary conditions to obtain

$$\mathrm{i}Re \int_{-1/2}^{1/2} U_0 \Psi_0^* \partial_\eta^2 \Psi_0 \, \mathrm{d}\eta - \mathrm{i}Re \int_{-1/2}^{1/2} U_0'' |\Psi_0|^2 \, \mathrm{d}\eta + Re\lambda_1 \langle \Psi_0, \partial_\eta^2 \Psi_0 \rangle = -\langle \partial_\eta^2 \lambda_0 \Psi_0, \Psi_1 \rangle + \langle \partial_\eta^4 \Psi_0, \Psi_1 \rangle,$$

or

$$\mathrm{i}Re \int_{-1/2}^{1/2} U_0 \Psi_0^* \partial_\eta^2 \Psi_0 \, \mathrm{d}\eta - \mathrm{i}Re \int_{-1/2}^{1/2} U_0'' |\Psi_0|^2 \, \mathrm{d}\eta + Re\lambda_1 \langle \Psi_0, \partial_\eta^2 \Psi_0 \rangle = \langle -\lambda_0 \partial_\eta^2 \lambda_0 \Psi_0 + \partial_\eta^4 \Psi_0, \Psi_1 \rangle,$$

where the right-hand side is now manifestly zero because Ψ_0 satisfies the lowest-order eigenvalue problem, hence

$$\lambda_1 = \mathrm{i} \frac{\int_{-1/2}^{1/2} U_0'' |\Psi_0|^2 \, \mathrm{d}\eta}{\langle \Psi_0, \partial_\eta^2 \Psi_0 \rangle} - \mathrm{i} \frac{\int_{-1/2}^{1/2} U_0 \Psi_0^* \partial_\eta^2 \Psi_0 \, \mathrm{d}\eta}{\langle \Psi_0, \partial_\eta^2 \Psi_0 \rangle},$$

or

$$\lambda_1 = -\mathrm{i} \frac{\int_{-1/2}^{1/2} U_0'' |\Psi_0|^2 \, \mathrm{d}\eta}{\langle \partial_\eta \Psi_0, \partial_\eta \Psi_0 \rangle} + \mathrm{i} \frac{\int_{-1/2}^{1/2} U_0 \Psi_0^* \partial_\eta^2 \Psi_0 \, \mathrm{d}\eta}{\langle \partial_\eta \Psi_0, \partial_\eta \Psi_0 \rangle},$$

For **Couette flow**, $U_0'' = 0$, and the correction λ_1 contains only one term. However, it is clear that the numerator is identically zero: $\Psi_0^* \partial_\eta^2 \Psi_0$ is an even function while $U_0 = \eta$ is an odd function, and the integral is over a symmetric interval, hence

$$\lambda = \lambda_0 + O(k^2)$$

for Couette flow. On the other hand, for Poiseuille flow, we have $U_0 = Re_* z - Re_* z^2$ and $U_0'' = $
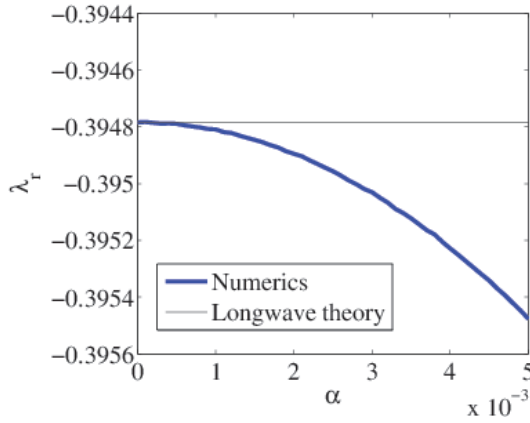
(a)   (b)

$-2Re_*$, hence $U_0 = Re_*[(1/4) - \eta^2]$ and

$$\lambda_1 = 2\mathrm{i}Re\frac{\int_{-1/2}^{1/2} |\Psi_0|^2 \,\mathrm{d}\eta}{\langle \partial_\eta \Psi_0, \partial_\eta \Psi_0 \rangle} + \tfrac{1}{4}\mathrm{i}Re\frac{\int_{-1/2}^{1/2} \Psi_0^* \partial_\eta^2 \Psi_0 \,\mathrm{d}\eta}{\langle \partial_\eta \Psi_0, \partial_\eta \Psi_0 \rangle} - \mathrm{i}Re\frac{\int_{-1/2}^{1/2} \eta^2 \Psi_0^* \partial_\eta^2 \Psi_0 \,\mathrm{d}\eta}{\langle \partial_\eta \Psi_0, \partial_\eta \Psi_0 \rangle},$$
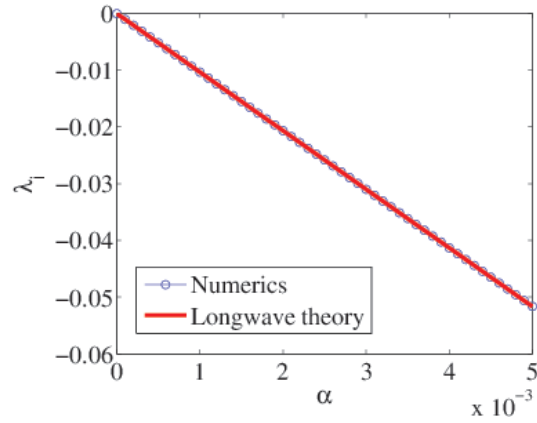
We have the following results:

$$\frac{\int_{-1/2}^{1/2} |\Psi_0|^2 \,\mathrm{d}\eta}{\langle \partial_\eta \Psi_0, \partial_\eta \Psi_0 \rangle} = \frac{\frac{3}{2}}{2\pi^2} \tag{4.15a}$$

$$\frac{\int_{-1/2}^{1/2} \Psi_0^* \partial_\eta \Psi_0 \,\mathrm{d}\eta}{\langle \partial_\eta \Psi_0, \partial_\eta \Psi_0 \rangle} = -1, \tag{4.15b}$$

$$\tag{4.15c}$$

$$\frac{\int_{-1/2}^{1/2} \eta^2 \Psi_0^* \partial_\eta^2 \Psi_0 \,\mathrm{d}\eta}{\langle \partial_\eta \Psi_0, \partial_\eta \Psi_0 \rangle} = \frac{\frac{1}{2\pi}\left(-\frac{1}{3}\pi^3 + \frac{7}{2}\pi\right)}{2\pi^2} \tag{4.15d}$$

hence

$$\lambda_1 = \mathrm{i}Re\left(\tfrac{3}{2\pi^2} - \tfrac{1}{4} + \tfrac{1}{12} - \tfrac{7}{8\pi^2}\right) = \mathrm{i}Re\left(\tfrac{5}{8\pi^2} - \tfrac{1}{6}\right) = -(0.103340926890206\cdots)\mathrm{i}Re. \tag{4.16}$$

Exercise 4.1 *Prove Equations* (4.15) *and hence prove Equation* (4.16).

These results are now examined in the context of the numerical solution for the dispersion relation Poiseuille flow (Figure 6.2). Clearly, excellent agreement is obtained, inspiring confidence in our OS solver.

Exercise 4.2 *Some analytical progress is possible for the Orr–Sommerfeld equation when $Re = \infty$. Then, the eigenvalue equation to be solved reverts to the **Rayleigh equation***:

$$(U_0 - c)\left(\partial_z^2 - k^2\right)\phi - U_0''\phi = 0, \qquad z \in (0, 1)$$

*with no-penetration boundary conditions $\phi = 0$ at $z = 0, 1$. The Rayleigh equation has a singular point if $U_0(z) = c$ somewhere, which is called a **critcal layer**. No critical layer exists if $c_i \neq 0$. In this question, assume that the flow is unstable, namely that $c_i > 0$.*

- *By rewriting the Rayleigh equation as*

$$\left(\partial_z^2 - k^2\right)\phi = \frac{U_0''}{U_0 - c}\phi,$$

  show that

$$\int_0^1 \frac{U_0''}{|U_0 - c|^2}|\phi|^2\mathrm{d}z = 0,$$

  and conclude that U_0'' must change sign at least once in $(0, 1)$.

- *Using the two results*

$$\int_0^1 \frac{U_0''(U_0 - c_\mathrm{r})}{|U - c|^2}|\phi|^2\mathrm{d}z = -\|\partial_z\phi\|_2^2 - k^2\|\phi\|_2^2,$$

  and

$$\int_0^1 \frac{U_0''}{|U_0 - c|^2}|\phi|^2\mathrm{d}z = 0,$$

  show that

$$\int_0^1 \frac{U_0''(U_0 - U_{0\mathrm{s}})}{|U_0 - c|^2}|\phi|^2\mathrm{d}z < 0, \qquad U_0''(z_\mathrm{s}) = 0, \qquad U(z_\mathrm{s}) = U_{0\mathrm{s}}$$

  *and hence conclude for an unstable flow, $U_0''(U_0 - U_{0\mathrm{s}}) < 0$ somewhere in the flow domain. This is **Fjortoft's theorem**.*

Exercise 4.3 Stability of an inviscid triangular jet: *Let $U_0(z) = 1 - |z|$ for $|z| < 1$ and $U_0(z) = 0$ for $|z| \geq 1$. Show that the eigenvalue relation for the sinuous mode (ϕ even) is*

$$2k^2c^2 + k(1 - 2k - \mathrm{e}^{-2k})c - [1 - k - (1 + k)\mathrm{e}^{-2k}] = 0.$$

Hints:

- *For the inviscid case, it suffices to solve the Rayleigh equation in region I with $z > 1$ and region II with $0 < z < 1$. At the boundary between any two regions labelled by i and j, the continuity of normal velocity implies that*

$$\phi_i = \phi_j$$

  where $\phi(z)$ is the streamfunction in a normal-mode decomposition. Continuity of pressure implies that

$$(U_{0i} - c)\frac{\partial \phi_i}{\partial z} - \phi_i U'_{0i} = (U_{0i} - c)\frac{\partial \phi_j}{\partial z} - \phi_j U'_{0j}$$

  at the same boundary.

- *At the boundary $z = 0$ the same conditions apply. Call the region $-1 < z < 0$ region III. We have $\phi_{III}(0) = \phi(0^-)$ and $\phi_{II} = \phi(0^+)$. Working with the even mode, we have*

$$\phi(0^-) = \phi(0^+), \qquad \partial_z\phi(0^-) = -\partial_z\phi(0^+).$$

Chapter 5

Absolute Instability

5.1   Overview

The response of the linearized dynamics to a delocalized plane-wave initial disturbance is obviously of great interest. However for parallel flows, a more pertinent question is to ask what is the response of the system to a localized **impulsive** forcing. In other words, we want to find out if a localized impulsive disturbance grows *in situ* at the initial source of the disturbance (absolute instability) or grows merely as it is convected downstream by the base flow (convective instability). Absolute instability can be thought of as 'more dangerous' as under such a situation the growing disturbances constantly renew themselves and contaminate the whole system for all time. In contrast, in a convective instablity the unstable disturbance does grow but is convected harmlessly downstream and eventually leaves the system. In this section we formulate a mathematical criterion that is 'usually' able to distinguish between the two types of instability.

5.2   Simplified Model Problem

Instead of starting our study with the full Orr–Sommerfeld equation for parallel flow, we begin instead with the following greatly simplified model problem, which nonetheless captures the essential features of absolute versus convective instability:

$$\frac{\partial u}{\partial t} + U_0 \frac{\partial u}{\partial x} = \mu u + \gamma \frac{\partial^2 u}{\partial x^2}, \tag{5.1}$$

where $\mu \in \mathbb{C}$, $\gamma \in \mathbb{C}$, with $\Re(\gamma) > 0$, and $U_0 \in \mathbb{R}^+$. The idea here is that $u(x,t)$ represents some disturbance that is convected by the constant base flow U_0. The problem is posed on the whole real line, with initial conditions to be prescribed in what follows.

We first of all note that Equation (5.1) is amenable to a modal analysis, wherein a normal-mode solution $u(x,t) = e^{-i\omega t + i\alpha x}$ is possible, provided the following dispersion relation is satisfied:

$$\omega = i\left(\mu - \gamma\alpha^2\right) + \alpha U_0 \tag{5.2}$$

In this context, a complex diffusion coefficient with positive imaginary part is necessary to give a growth rate $\omega_i = \mu - \gamma_r\alpha^2$ that is negative for short wavenumbers, leading to a well-posed problem. This is a minimal model of linear instability, and it includes longwave growth and shortwave stabilization. Clearly, the flow is unstable if $\mu > 0$, where instability exists for a band of wavenumbers with $\alpha^2 < \gamma_r/\mu$.

More importantly, we have a minimal model of absolute instability when the following initial condition is prescribed:

$$u(x, t = 0) = \delta(x - x_0). \tag{5.3}$$

This initial condition represents an impulsive disturbance localized at x_0. By direct computation, the solution to Equation (5.1) with the initial data (5.3) reads

$$G(x, x_0, t) = \frac{1}{2\sqrt{\pi\gamma t}} \exp\left\{ t\left[\mu - \frac{1}{4\gamma}\left(\frac{x - x_0}{t} - U \right)^2 \right] \right\}, \qquad \gamma_r > 0. \tag{5.4}$$

The flow is absolutely unstable if $\lim_{t\to\infty} G(x, x_0, t) = \infty$, i.e. if

$$\mu - \tfrac{1}{4}U^2 \Re(1/\gamma) > 0. \tag{5.5}$$

Intriguingly, the condition (5.5) can be recast as follows:

$$\omega_i(\alpha_0) > 0, \qquad \left.\frac{d\omega}{d\alpha}\right|_{\alpha_0} = 0, \tag{5.6}$$

i.e. α_0 is the (complex) saddle point of the dispersion relation (5.2). The derivation of Equations (5.2) involves the computation of a Gaussian integral over all wavenumbers. Here lies the wide applicability of CGL theory: a wide class of dispersion relations in fluid mechanics is locally quadratic in wavenumber, enabling a saddle-point approximation of the generic Green's function, such that all Green's functions in this class resemble Equation (5.4) in the limit as $t \to \infty$. Thus, for this wide class of fluid-mechanical dispersion relations, the condition for absolute instability is simply that the imaginary part of the frequency at the saddle point be positive [HM90]. Of course, there is a variety of fluid-mechanical problems where naive application of the saddle-point criterion (5.6) fails [tS13]. These issues are discussed below.

Exercise 5.1

1. *Using Fourier transforms, show that the solution of Equation* (5.1) *with the initial data* (5.4) *reads*

$$u(x,t) = \int_{-\infty}^{\infty} u_\alpha(t) \frac{\mathrm{e}^{\mathrm{i}\alpha x}}{2\pi}, \tag{5.7}$$

   where

$$\frac{du_\alpha}{dt} = \lambda_\alpha u_\alpha,$$

   where λ_α is to be determined.

2. *Evaluate the integral in Equation* (5.7). *Hence, derive Equation* (5.4)

3. *Find a formula for $u(x = 0, t)$. Hence, derive the criterion for the flow to be absolutely unstable.*

5.3   Parallel flows and the adjoint eigenvalue problem

We are interested in the following Cauchy problem:

$$\frac{\partial}{\partial t}\nabla^2\psi + U_0(z)\nabla^2\frac{\partial\psi}{\partial x} - U_0''(z)\frac{\partial\psi}{\partial x} = \frac{1}{Re}\nabla^4\psi, \tag{5.8a}$$

with boundary conditions

$$\psi = \psi_z = 0, \qquad \text{at } z = 0, 1, \tag{5.8b}$$

and

$$\lim_{|x|\to\infty}\psi = \lim_{|x|\to\infty}\psi_x = 0, \tag{5.8c}$$

subject to an initial impulsive disturbance

$$\psi(x, z, t = 0) = \delta(x - x_0)\delta(z - z_0). \tag{5.8d}$$

Obviously, a particular solution to the parallel-flow problem is the plane-wave solution $\psi(x, z, t) = \mathrm{e}^{\lambda t + \mathrm{i}\alpha x}\phi(z)$, where ϕ solves the Orr–Sommerfeld eigenvalue problem:

$$\mathcal{L}\phi = \lambda\mathcal{M}\phi, \tag{5.9a}$$

where

$$\mathcal{L} = \frac{1}{Re}\left(\partial_z^2 - \alpha^2\right)^2 - i\alpha U_0(z)(\partial_z^2 - \alpha^2) + i\alpha U_0''(z),$$ (5.9b)

and

$$\mathcal{M} = (\partial_z^2 - \alpha^2).$$ (5.9c)

Denote by (ϕ_n, λ_n) a particular eigensolution of Equation (5.9). We are interested also in the adjoint eigenvalue problem, solved by a pair $(\xi_n \, mu_n)$:

$$\mathcal{L}^+\xi_n = \mu_n\mathcal{M}^+\xi_n,$$

where the adjoint operator is obtained with respect to the usual inner product in the z-variable in the interval $[0, 1]$. We have the following theorem:

Theorem 5.1 $\langle \phi_n, \mathcal{M}\xi_m \rangle \propto \delta_{nm}$

Proof: From the definition of the adjoint operators, it is obvious that if λ_n is an eigenvalue of the direct problem, then λ_n^* is an eigenvalue of the adjoint problem[1]. Therefore, consider

$$\mathcal{L}\phi_n = \lambda_n\mathcal{M}\phi_n,$$
$$\mathcal{L}^+\xi_m = \lambda_m^*\mathcal{M}^+\xi_m,$$

Take inner products of both these equations: the first with ξ_m and the second with ϕ_n. We have:

$$\langle \xi_m, \mathcal{L}\phi_n \rangle = \lambda_n\langle \xi_m, \mathcal{M}\phi_n \rangle,$$
$$\langle \mathcal{L}^+\xi_m, \phi_n \rangle = \lambda_m\langle \mathcal{M}^+\xi_m, \phi_n \rangle,$$

Take the adjoint of the second relation to obtain the following equation pair:

$$\langle \xi_m, \mathcal{L}\phi_n \rangle = \lambda_n\langle \xi_m, \mathcal{M}\phi_n \rangle,$$
$$\langle \xi_m, \mathcal{L}\phi_n \rangle = \lambda_m\langle \xi_m, \mathcal{M}\phi_n \rangle,$$

Subtract to obtain

$$(\lambda_n - \lambda_m)\langle \xi_m, \mathcal{M}\phi_n \rangle = 0,$$

---

[1]For finite-dimensional vector spaces, this really is obvious by looking at the characteristic polynomial

or
$$\langle \xi_m, \mathcal{M}\phi_n \rangle \propto \delta_{nm},$$

and by the self-adjointness of the $\mathcal{M}$ operator (with $\mathcal{M} = \partial_z^2 - \alpha^2$), we also have

$$\langle \phi_n, \mathcal{M}\xi_m \rangle \propto \delta_{nm},$$

5.4   The solution of the Cauchy problem

Equation (5.8a) is rewritten in Orr–Sommerfeld operator form as follows:

$$\frac{\partial}{\partial t}\mathcal{M}_{OS}[\partial_x, \partial_z]\psi(x, z, t) = \mathcal{L}_{OS}[\partial_x, \partial_z]\psi(x, z, t) + F(x, z, t), \qquad \psi(x, z, t = 0) = 0. \quad (5.10)$$

Here, $F(x, z, t)$ represents the momentum source; this can either be continuous-in-time, or be an initial impulse imposed on the system. In the impulsive case, the source can be written as $\delta(t)F(x, z)$, with Laplace transform $F(x, z)$. We proceed with the general case, and specialize to the impulsive case as required. The solution can be written in terms of Fourier transforms as follows:

$$\psi(x, z, t) = \int_{-\infty}^{\infty} \frac{\mathrm{d}\alpha}{2\pi} \mathrm{e}^{\mathrm{i}\alpha x} \widetilde{\psi}_\alpha(z, t),$$

where the Fourier coefficients $\widetilde{\psi}_\alpha(z, t)$ satisfy

$$\frac{\partial}{\partial t}\mathcal{M}_{OS}[\mathrm{i}\alpha, \partial_z]\widetilde{\psi}_\alpha(z, t) = \mathcal{L}_{OS}[\mathrm{i}\alpha, \partial_z]\widetilde{\psi}_\alpha(z, t) + \widetilde{F}_\alpha(z, t).$$

Each Fourier component $\widetilde{\psi}_\alpha(z, t)$ can be decomposed further via an inverse Laplace tranform:

$$\widetilde{\psi}_\alpha(z, t) = \frac{1}{2\pi\mathrm{i}} \int_B \mathrm{d}\lambda \, \mathrm{e}^{\lambda t} \widetilde{\psi}_{\alpha\lambda}(z),$$

where B is the Bromwich contour. The components $\widetilde{\psi}_{\alpha\lambda}(z)$ of the inverse Laplace tranform in turn satisfy

$$\lambda \mathcal{M}_{OS}(\mathrm{i}\alpha, z)\widetilde{\psi}_{\alpha\lambda}(z) = \mathcal{L}_{OS}(\mathrm{i}\alpha, \partial_z)\widetilde{\psi}_{\alpha\lambda}(z) + \widetilde{F}_\alpha(z, \lambda), \quad (5.11)$$

where the Laplace transform of the force function S has been taken with respect to time. This is the **Orr–Sommerfeld eigenvalue problem**.

The (formal) solution to Equation (5.11) reads

$$\widetilde{\psi}_{\alpha\lambda}(z) = -\left[\mathcal{L}_{OS} - \lambda\mathcal{M}_{OS}\right]^{-1}\widetilde{F}_\alpha(z, \lambda)$$

This purely formal solution is understood as follows. We write the solution of Equation (5.11) as $\widetilde{\psi}_{\alpha\lambda}(z) = \sum_n a_n \phi_{\alpha n}(z)$. Here, the $\phi_{\alpha n}$'s are the eigenfunctions of the Orr–Sommerfeld equation at wavenumber α. Equation (5.11) is therefore re-written as

$$\lambda \sum_n a_n \mathcal{M}_{OS}\phi_{\alpha n}(z) = \sum_n a_n \mathcal{L}_{OS}\phi_{\alpha n}(z) + \widetilde{F}_\alpha(z,\lambda). \tag{5.12}$$

The eigenfunctions $\phi_{\alpha m}^+(z)$ of the adjoint OS problem satisfy

$$\int dz \left[\phi_{\alpha m}^+(z)\right]^* \mathcal{M}_{OS}\phi_{\alpha n}(z) = \delta_{nm}.$$

We multiply both sides of Equation (5.11) by $\left[\phi_m^+(z)\right]^*$ and integrate with respect to z; the result is

$$a_m = \frac{1}{\lambda - \lambda_m} \int dz \left[\phi_{\alpha m}^+(z)\right]^* \widetilde{F}_\alpha(z,\lambda) := \frac{1}{\lambda - \lambda_m} \langle \phi_{\alpha m}^+, \widetilde{F}_\alpha(z,\lambda)\rangle,$$

and

$$\widetilde{\psi_{\alpha\lambda}}(z) = [\mathcal{L}_{OS} - \lambda\mathcal{M}_{OS}]^{-1} \widetilde{F}_\alpha(z,\lambda) =$$
$$\sum_n \frac{\phi_{\alpha n}(z)}{\lambda - \lambda_n} \int dz \left[\phi_{\alpha n}^+(z)\right]^* \widetilde{F}_\alpha(z,\lambda) := \sum_n \frac{\phi_{\alpha n}(z)F_{\alpha n}(\lambda)}{\lambda - \lambda_n}.$$

Thus, the solution to the Cauchy problem (5.10) becomes

$$\psi(x,z,t) = \frac{1}{2\pi i} \int_{-\infty}^{\infty} \frac{d\alpha}{2\pi} e^{i\alpha x} \int_B d\lambda\, e^{\lambda t} \sum_n \frac{\phi_{\alpha n}(z)F_{\alpha n}(\lambda)}{\lambda - \lambda_n}, \tag{5.13}$$

where the Bromwich contour C is a straight line parallel to the imaginary axis, to the right of all the eigenvalues $\{\lambda_n\}$ of the Orr–Sommerfeld equation. A key property of Equation (5.13) is the absence of any contributions from a continuous spectrum: for a bounded domain $z \in [0,1]$, the spectrum of the Orr–Sommerfeld equation is entirely discrete. Using the theory of residues, one obtains for the innermost integral

$$\psi(x,z,t) = \sum_n \int_{-\infty}^{\infty} \frac{d\alpha}{2\pi} e^{i\alpha x + \lambda_n t} F_{\alpha n}(\lambda_n)\phi_{\alpha n}(z). \tag{5.14}$$

The outermost (α-) integral can be computed in certain special cases. This is discussed in the next two sections.

5.5   Explicit asymptotic solutions

5.5.1   Monochromatic forcing

For monochromatic, impulsive forcing, $F(x, z, t) = \mathrm{e}^{\mathrm{i}\alpha_0 x}\delta(t)f(z)$, $\widetilde{F}_\alpha(z, \lambda) = 2\pi f(z)\delta(\alpha - \alpha_0)$, and

$$F_{\alpha n}(\lambda) = \delta(\alpha - \alpha_0)\int \mathrm{d}z \left[\phi^+_{\alpha_0 n}(z)\right]^* f(z) := \delta(\alpha - \alpha_0)f_{\alpha_0 n}.$$

From Equation (5.14),

$$\psi(x, z, t) = \sum_n \mathrm{e}^{\mathrm{i}\alpha_0 x + \lambda_n(\alpha_0)t} f_{\alpha_0 n}\phi_{\alpha_0 n}(z). \tag{5.15}$$

Thus,

$$\lim_{t\to\infty}\psi(x, z, t) = \left[f_{\alpha_0 n_{\max}}\mathrm{e}^{\mathrm{i}\alpha_0 x + \lambda_{n_{\max}}(\alpha_0)}\right]\phi_{\alpha_0 n_{\max}}(z),$$

where $n_{\max}$ is that eigenvalue whose real part is maximal over the entire spectrum $\{\lambda_n(\alpha_0)\}$. Note also,

$$\lim_{t\to\infty}\|\psi\|_2(t) = \|\phi_{\alpha_0 n_{\max}}\|_2 |f_{\alpha_0 n_{\max}}| \, \mathrm{e}^{\Re[\lambda_{n_{\max}}(\alpha_0)]t},$$

where $\|\cdot\|_2(t)$ is the transient L^2 norm; for a function $\Phi(x, z, t)$,

$$\|\Phi\|_2(t) := \left(\iint \mathrm{d}x\mathrm{d}z|\Phi(x, z, t)|^2\right)^{1/2}.$$

Thus, as $t\to\infty$, the disturbance grows exponentially fast, at a rate

$$\Re[\lambda_{n_{\max}}(\alpha_0)].$$

This is called the **most-dangerous mode**. Obviously, if $\Re[\lambda_{n_{\max}}(\alpha_0)] > 0$ the system is (convectively) unstable. The system is completely linearly stable if $\Re[\lambda_{n_{\max}}(\alpha_0)] < 0$.

5.5.2   Localized impulsive forcing

For localized impulsive forcing, $F(x, z, t) = \delta(x)\delta(z - z_0)\delta(t)$, with $\widetilde{F}_\alpha(z, \lambda) = \delta(z - z_0)$, and

$$F_{\alpha n}(\lambda) = [\phi^+_{\alpha n}(z_0)]^*$$

Thus,

$$\psi(x, z, t) = \sum_n \int_{-\infty}^{\infty} \frac{\mathrm{d}\alpha}{2\pi}\mathrm{e}^{\mathrm{i}\alpha x + \lambda_n t}[\phi^+_{\alpha n}(z_0)]^*\phi_{\alpha n}(z). \tag{5.16}$$

This integral can be regarded as being in the form

$$\psi(x, z, t) = \frac{1}{2\pi} \sum_n \int_{-\infty}^{\infty} d\alpha \, \mathcal{F}_n(\alpha, z) e^{\lambda_n(\alpha)t},$$

where

$$\mathcal{F}_n(\alpha, z) = e^{i\alpha x} [\phi_{\alpha n}^+(z_0)]^* \phi_{\alpha n}(z)$$

This integral is now in a form where the saddle-point method can be applied. We need the following additional assumptions:

Assumption 5.5.1

1. *The phase function $\lambda_n(\alpha)$ has a single dominant saddle point;*

2. *The saddle point is not degenerate.*

3. *If the phase function or the $\mathcal{F}_n(\alpha)$'s do have singularities, they are located 'far away' from the saddle point, in the sense that they do not prevent us from deflecting the contour $\alpha \in (-\infty, \infty)$ to pass through the dominant saddle point.*

For the dominant saddle point, we compute

1. Saddle-point location: α_0, such that $(d\lambda_n/d\alpha)_{\alpha_0} = 0$.

2. The value $\lambda_n(\alpha_0)$,

3. The derivative $\lambda_n''(\alpha_0)$

4. The phase $\varphi_n = \frac{1}{2}\pi - \frac{1}{2}\arg(\lambda_n''(\alpha_0))$

5. $\mathcal{F}_n(\alpha_0)$.

Applying the saddle-point method to the integral (5.16), we get

$$\psi(x, z, t) \sim \frac{1}{2\pi} \sum_n \frac{\sqrt{2\pi} e^{i\alpha_0 x} [\phi_{\alpha_0 n}^+(z_0)]^* \phi_{\alpha_0 n}(z) e^{\lambda_n(\alpha_0)t} e^{i\varphi_n}}{|t\lambda_n''(\alpha_0)|^{1/2}} \tag{5.17}$$

We assume a dominant saddle point, taken over the full OS spectrum. We therefore take $\alpha_{0,n_{\max}}$ to be the mode corresponding to

$$\sup_n \Re \left[\lambda(\alpha_{0,n}) \right]$$

Then, the limit (5.17) simplifies further:

$$\lim_{t \to \infty} \psi(x, z, t) = \frac{e^{i\varphi_{n_{\max}}}}{\sqrt{2\pi}} \frac{[\phi_{\alpha_0 n_{\max}}^+(z_0)]^* \phi_{\alpha_0 n_{\max}}(z)}{\left| t \frac{d^2 \lambda_{n_{\max}}}{d\alpha^2} \right|_{\alpha_0}^{1/2}} e^{i\alpha_0 x + \lambda_{n_{\max}}(\alpha_0)t}. \tag{5.18}$$

Absolute instability

From Equation (5.18), we see that the instability grows (asymptotically) at the source $x = 0$ if $\Re\left[\lambda_{n_{\max}}(\alpha_0)\right] > 0$. This is the notion of linear absolute instability. Of course, the simplification that leads from Equation (5.16) to Equation (5.18) is possible only when the phase function possesses no singularities close to the saddle point, and when the saddle point is non-degenerate.

The pinching criterion

Recall the formal solution to Cauchy problem (5.10) (Equation (5.13)):

$$\psi(x, z, t) = \int_{-\infty}^{\infty} \frac{\mathrm{d}\alpha}{2\pi} \mathrm{e}^{\mathrm{i}\alpha x} \int_B \mathrm{d}\lambda \, \mathrm{e}^{\lambda t} \sum_n \frac{\phi_{\alpha n}(z) F_{\alpha n}(\lambda)}{\lambda - \lambda_n}, \tag{5.19}$$

where the λ-integration is done first. To get a self-consistent answer, it should be possible to reverse the order of integration, doing the α-integral first, to arrive at a result identical to Equation (5.18). However, only so-called **pinching saddles** satisfy this self-consistency property. A pinching saddle is one where the α-curves of constant ω (in particular, curves of constant ω, with $\omega_\mathrm{i} = \omega_\mathrm{i}(\alpha_0)$) ramify into different half-planes. See [HM90].

5.6   Example and exercise

Consider the base flow

$$U_0(z) = 1 - \Lambda + \frac{2\Lambda}{1 + \sinh^{2N}[z \sinh^{-1}(1)]},$$

where $\Lambda < 0$ and $N \geq 1$ are real parameters. This is a model for the wake flow past a bluff body and was introduced in the paper by Monkewitz [Mon88]. The boundary between absolute and convective instability in the (Λ, N) parameter space is derived in that paper and is reproduced below in Figure 5.1.

Exercise 5.2 *Download the Matlab codes from the module website. Choose one parameter set corresponding to absolute instability and another corresponding to convective instability. Run the Orr–Sommerfeld solver in each case for a range of complex-valued α-values and reproduce the saddle point(s) in both cases.*
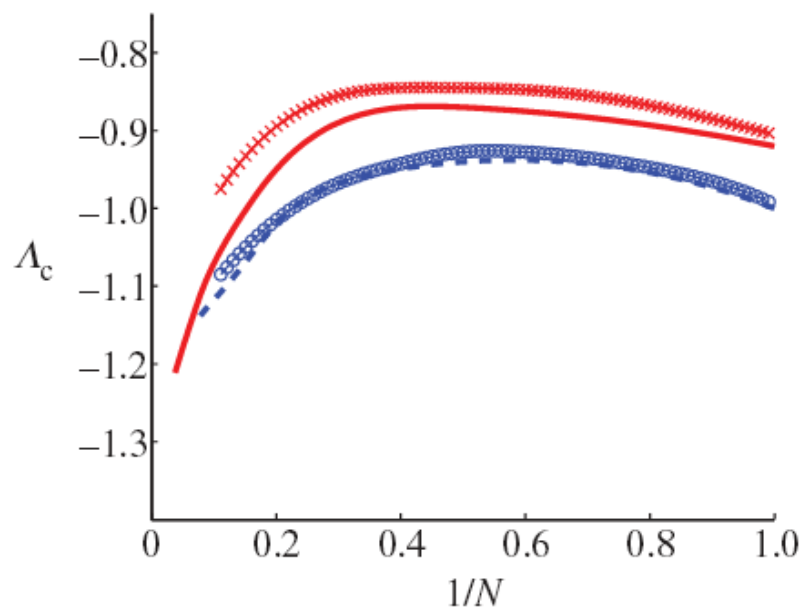
Figure 5.1: Boundary between the absolute and convective regions for differennt Reynolds numbers. Curves without symbols correspond to direct OS eigenvalue calculations in the complex α-plane and agree exactly with the results in [Mon88]. Curves with symbols correspond to the semi-analytical *cubic approximation* of [NS13]. Dashed curve: $Re = 20$; solid curve: $Re = 100$.

Chapter 6

Transient Growth

Overview

We have already seen that plane Couette flow is linearly stable at all finite Reynolds numbers, while plane Poiseuille flow is stable below a critical Reynolds number $Re \approx 5772$. However, it is well known that such linearly stable flows undergo a transition to a complicated chaotic time-dependent state (turbulence) below the threshold for the onset of linear instability. This is called the **subcritical transition to turbulence**. Below we introduce a toy model to explain this phenomenon and then connect the toy model back to the Orr–Sommerfeld equation.

6.1 The basic idea

Historically, the linear stability of a system of evolutionary equations was tackled via eigenvalue analysis. Consider a generic evolutionary system $\partial_t \boldsymbol{u} = \boldsymbol{F}(\boldsymbol{u}; \mu)$, where $\boldsymbol{u}(t)$ is a trajectory in $\mathbb{C}^n$ and μ is a real parameter. A *base state* $\boldsymbol{u}_0$ of the system is a solution of the equation $\boldsymbol{F}(\boldsymbol{u}_0; \mu) = 0$. The *linearization* around the base state refers to the following equation: $\partial_t \boldsymbol{u} = \boldsymbol{J} \boldsymbol{u}$, where $\boldsymbol{J}$ is the Jacobian matrix, with $J_{ij} = (\partial F_i / \partial u_j)_{(\boldsymbol{u}_0, \mu)}$. Let $\{\lambda_1, \cdots, \lambda_n\} = \operatorname{spec}(\boldsymbol{J})$, and let λ_0 denote the eigenvalue with largest real part. The full system is said to be linearly stable if $\Re(\lambda_0) < 0$. Suppose for a critical parameter value $\mu = \mu_c$ we have $\Re(\lambda_0) < 0$ for $\mu < \mu_c$ and $\Re(\lambda_0) > 0$ for $\mu > \mu_c$. Then the system undergoes a bifurcation from linearly stable to linearly unstable at the critical value $\mu = \mu_c$. The same analysis can usually be applied to spatially extended systems by projecting the evolutionary equation on to a set of basis functions of dimension n and taking $n \to \infty$, assuming that the weak solutions so constructed tend to a strong solution.

Such systems can exhibit transient growth in a subcritical parameter regime whereby for suitable initial conditions involving a superposition of eigenmodes, the L^2 norm (or some other more ap-

propriate measure of the energy) of the solution grows initially before eventually decaying at a rate dictated by λ_0. This can happen in two ways. If the eigenvectors do not form a complete set spanning $\mathbb{C}^n$, then the solution to the initial-value problem will involve contributions such as $t^p e^{\lambda_j t}$, where $p \geq 1$ and $j \in \{1, \cdots, n\}$, such that transient algebraic growth is possible before the onset of the asymptotic decay of the solution. We do not consider this case further here (but see Reference [SH01]). Instead, we consider situations where the eigenvectors of $\boldsymbol{J}$ do indeed span $\mathbb{C}^n$ but are non-orthogonal, corresponding to a situation where $\boldsymbol{J}$ is not a normal operator. In such a scenario, the L^2 norm of solutions involving certain combinations of eigenvectors can grow transiently before eventually decaying, with transient growth factors $\|\boldsymbol{u}(t)\|_2 / \|\boldsymbol{u}(t=0)\|_2$ that can be as high as $O(10^5)$ (e.g. Reference [CC97]). This is the phenomenon of transient growth.

6.2 The toy model

In this section a two-level system is introduced that exhibits the twin effects of non-normality and nonlinearity. The aim is to start with a set of linear equations and to quantify the influence of the non-normality on the transient growth at subcritical parameter regimes. Next, a cubic nonlinearity is introduced and an exact solution for the global mode (and its stability) is obtained. The section concludes with a crucial discussion about the physical relevance of the system in optics.

6.2.1 Non-normal linear model

We consider the following two-level system

$$i\frac{\partial u}{\partial t} = \mathcal{H}u + i\left(\mu_0 \mathbb{I} + \mathcal{G}\right)u, \qquad u \in \mathbb{C}^2, \tag{6.1}$$

where

$$\mathcal{H} = \begin{pmatrix} E_0 & A \\ A & E_0 \end{pmatrix}, \qquad \mathcal{G} = \begin{pmatrix} -g_1 & 0 \\ 0 & -g_2 \end{pmatrix},$$

where E_0, A, μ_0, g_1, g_2 are positive real numbers, and where $\mathcal{H}$ and $\mu_0\mathbb{I} + \mathcal{G}$ are Hermitian matrices, with $[\mathcal{H}, \mathcal{G}] \neq 0$, where $[\cdot, \cdot]$ denotes the matrix commutator. Note that $[\mathcal{H}, \mathcal{G}] \neq 0$ implies that the operator on the right-hand side of Equation (6.1) is non-normal. One writes down the trial solution $u(t) = u_0 e^{-i\omega t}$ to obtain the following eigenvalues:

$$\omega_{\rm r} = E_0 \pm \tfrac{1}{2}\sqrt{4A^2 - (g_1 - g_2)^2}, \qquad \omega_{\rm i} = \mu_0 - \tfrac{1}{2}(g_1 + g_2), \qquad 4A^2 > (g_1 - g_2)^2, \qquad \text{Case 1,} \tag{6.2}$$

and

$$\omega_{\rm r} = E_0, \qquad \omega_{\rm i} = \mu_0 - \tfrac{1}{2}(g_1 + g_2) \pm \tfrac{1}{2}\sqrt{(g_1 - g_2)^2 - 4A^2}, \qquad 4A^2 < (g_1 - g_2)^2, \qquad \text{Case 2,} \tag{6.3}$$

The corresponding eigenvectors for both Case 1 and Case 2 are

$$u_{0+} = \begin{pmatrix} e^{-i\varphi/2} \\ e^{i\varphi/2} \end{pmatrix}, \qquad u_{0-} = \begin{pmatrix} -e^{i\varphi/2} \\ e^{-i\varphi/2} \end{pmatrix}, \qquad \varphi = \sin^{-1}\left(\frac{g_1 - g_2}{2A} \right).$$

For Case 1, we have $|(g_1 - g_2)/2A| < 1$, hence $\varphi \in \mathbb{R}$, while for Case 2, φ is complex. For both cases, the eigenvectors are non-orthogonal; the degree of non-orthogonality is expressed by the relation $\langle u_{0+}, u_{0-} \rangle = 2i(g_2 - g_1)/2A$. Here, $\langle \cdot, \cdot \rangle$ denotes the usual scalar product on $\mathbb{C}^2$, with $\langle \boldsymbol{u}, \boldsymbol{v} \rangle = \overline{\boldsymbol{u}^T} \boldsymbol{v}$, for all column vectors $\boldsymbol{u}, \boldsymbol{v}$ in $\mathbb{C}^2$. Orthogonality of eigenvectors is regained for $g_1 = g_2$; this corresponds precisely to $[\mathcal{H}, \mathcal{G}] = 0$ and the normality of the (symmetric) operator $\mathcal{H} + i\mathcal{G}$. The crossover between Cases 1 and 2, where $(g_1 - g_2)^2 = 4A^2$ is referred to as a *diabolic point* in the literature concerning non-Hermitian quantum mechanics [Gra09, Rot09]; this point truly is fiendish, since the eigenvectors degenerate and fail to span $\mathbb{C}^2$ in this instance. However, in this work, consideration is given strictly to Case 2, for reasons given in what follows.

Exercise 6.1

1. Call $\mathcal{L} = \mathcal{H} + (\mu_0 \mathbb{I} + \mathcal{G})$. Compute explicitly $[\mathcal{L}, \mathcal{L}^\dagger]$, where the dagger denotes the Hermitian conjugate of the matrix. Hence veryify that $[\mathcal{L}, \mathcal{L}^\dagger] \neq 0$. This is the definition of a **non-normal** operator.

2. Drive the eigenvalules and eigenvectors for Case 2.

For all possible parameter values, the intrinsic non-Hermiticity of the operator in Equation (6.1) implies the following nontrivial evolution equation for the L^2 norm of the general solution $u(t)$:

$$\|u\|_2^2 := \langle u, u \rangle, \qquad \tfrac{1}{2}\frac{d}{dt}\|u\|_2^2 = \langle u, (\mu_0 + \mathcal{G}) u \rangle. \tag{6.4}$$

The quadratic form on the right-hand side can be evaluated in the eigenbasis of the operator $\mathcal{G}$ and a bound on the growth of the L^2 norm is obtained:

$$\tfrac{1}{2}\frac{d}{dt}\|u\|_2^2 \leq [\mu_0 - \min(g_1, g_2)] \|u\|_2^2. \tag{6.5}$$

In this work, we focus on models that exhibit transient growth. Since this relies on the 'mixing' of eigenstates with eigenfrequencies whose imaginary parts are distinct, we are forced by this constraint to work in Case 2 (this rules out of consideration the diabolic point). With reference to this case,

and to Equation (6.3), transient non-asymptotic growth is possible in the paramter range

$$\min(g_1, g_2) < \mu_0 < \tfrac{1}{2}(g_1 + g_2) - \sqrt{(g_1 - g_2)^2 - 4A^2}. \tag{6.6}$$

This is the 'sweet' operational range where the system is subcritical, in the sense that $\omega_i < 0$ for both eigenvalues, but where the balance between forcing and dissipation is ambiguous, so that the sign of the upper bound of the growth rate in Equation (6.5) is not definite.

6.2.2 Introduction of nonlinear terms

We add non-linearity to the problem by modifying Equation (6.1) as follows:

$$i\frac{\partial u}{\partial t} = \mathcal{H}u + i\left(\mu_0 \mathbb{I} + \mathcal{G}\right)u + a\begin{pmatrix} |u_1|^2 & 0 \\ 0 & |u_2|^2 \end{pmatrix}u, \tag{6.7}$$

where a is real. The evolution of the L^2 norm $\|u\|_2^2$ is again unchanged under the addition of the nonlinear term: the quantity $\|u\|_2^2$ still evolves according to the norm-evolution first written down for the linear problem (i.e. Equation (6.4)). However, in contrast to the linear model, Equation (6.7) has a nonlinear periodic solution, which we find by making the trial solution

$$u = Re^{-i\Omega t}u_0, \qquad \|u_0\|_2^2 = 1, \qquad \Omega \in \mathbb{R}. \tag{6.8}$$

Substitution of Equation (6.8) into Equation (6.7) yields the following eigenvalue problem for u_0:

$$\Omega u_0 = \mathcal{L}u_0 + aR^2\begin{pmatrix} |u_{01}|^2 & 0 \\ 0 & |u_{02}|^2 \end{pmatrix}u_0, \qquad \mathcal{L} = \mathcal{H} + i\left(\mu_0 \mathbb{I} + \mathcal{G}\right). \tag{6.9}$$

In general, Equation (6.9) has a family of solutions labelled by the continuous parameter R, with corresponding eigenvalues $\Omega(R)$. However, there is a finite number of R-values consistent with the requirement $\Im[\Omega(R)] = 0$; all other R-values correspond to eigensolutions of Equation (6.9) that are nonetheless inconsistent with Equation (6.8). It is as if we are solving a nonlinear double eigenvalue problem in the parameters Ω and R (the analogous double eigenvalue problem of linear algebra is addressed elsewhere [BC78]). Solutions of this double eigenvalue problem are called *self-consistent* in the remainder of this work, and can be found analytically for the simple two-level system considered in this section. Indeed, we have the following theorem:

Theorem 6.1 *Let $g_2 < \mu_0 < g_1$, and let*

$$X^2 = -\frac{(\mu_0 - g_1)(\mu_0 - g_2)}{A^2}. \tag{6.10a}$$

Assume that $X^2 < 1$. Then Equation (6.9) has the following self-consistent solution:

$$\Omega = E_0 + aR^2, \qquad R^2 = \frac{g_1 - g_2}{a}\sqrt{\frac{1}{X^2} - 1}, \qquad u_0 = \begin{pmatrix} re^{i\varphi} \\ x \end{pmatrix}, \tag{6.10b}$$

where

$$r = \sqrt{\frac{\mu_0 - g_2}{g_1 - g_2}}, \qquad x = \sqrt{\frac{g_1 - \mu_0}{g_1 - g_2}}, \qquad \varphi = -\sin^{-1}(X). \tag{6.10c}$$

Proof The so-called self-consistent nonlinear eigenvalue problem refers to the solution u_0 of Equation (6.9) with the constraint that

$$\langle u_0, (\mu_0 + \mathcal{G})u_0 \rangle = 0. \tag{6.11}$$

To obtain such a solution, we take

$$u_0 = \begin{pmatrix} re^{i\varphi(R)} \\ x \end{pmatrix}, \qquad r, \varphi, x \in \mathbb{R}, \qquad r^2 + x^2 = 1; \tag{6.12}$$

this amounts to a fixed choice for the (arbitrary) global phase of u_0. Substitution into Equation (6.11) yields

$$r^2(\mu_0 - g_1) + x^2(\mu_0 - g_2) = 0, \qquad r^2 + x^2 = 1, \tag{6.13}$$

hence

$$r = \sqrt{\frac{\mu_0 - g_2}{g_1 - g_2}}, \qquad x = \sqrt{\frac{g_1 - \mu_0}{g_1 - g_2}}, \tag{6.14}$$

where r and x are both real because $g_2 < \mu_0 < g_1$. The phase φ is not determined by this analysis; this is obtained by consideration of the full nonlinear eigenvalue problem, which is written out in full as follows:

$$\Omega re^{i\varphi} = \mathcal{L}_{11}re^{i\varphi} + \mathcal{L}_{12}x + aR^2r^3e^{i\varphi}, \tag{6.15a}$$

$$\Omega x = \mathcal{L}_{21}re^{i\varphi} + \mathcal{L}_{22}x + aR^2x^3. \tag{6.15b}$$

The imaginary part of the second equation is set to zero to yield a root-finding condition for φ:

$$\mathcal{L}_{21}^{(r)}\sin\varphi + \mathcal{L}_{21}^{(i)}\cos\varphi + \mathcal{L}_{22}^{(i)}(x/r) = 0. \tag{6.16}$$

Because the operator $\mathcal{L}$ is symmetric, setting the imaginary part of the first equation to zero yields precisely the same condition for φ. Equation (6.16) simplifies drastically, once the coefficients $\mathcal{L}_{21}^{(r)}$

etc. are filled in:

$$A \sin \varphi + (\mu_0 - g_2)(x/r) = 0.$$

Using Equations (6.13)–(6.14), this expression can be written as an explicit function of the problem parameters alone:

$$A \sin \varphi \pm (\mu_0 - g_2)\sqrt{-\frac{\mu_0 - g_1}{\mu_0 - g_2}} = 0,$$

where the two branches come from taking $x = \pm\sqrt{1 - r^2}$ in Equation (6.14), and where the radicand is positive because of the constraints on the parameters in Theorem 6.1. Hence,

$$\varphi = \mp \sin^{-1}\left(\sqrt{-\frac{(\mu_0 - g_1)(\mu_0 - g_2)}{A^2}}\right) = \mp \sin^{-1}(X), \qquad (6.17)$$

with $\varphi \in [-\pi/2, \pi/2]$. Upon satisfaction of the condition (6.17), Equations (6.15a) and (6.15b) are consistent, but only in the sense that both equations now imply that Ω is real. The equations (6.15a) and (6.15b) are made totally consistent by choosing a value of R such that the value of Ω in both these equations is the same. In terms of the explicit values of the $\mathcal{L}$-matrix, we have

$$\begin{aligned}\Omega &= E_0 + A \cos \varphi (x/r) + aR^2 r^2, \\ &= E_0 + A \cos \varphi (r/x) + aR^2 x^2.\end{aligned}$$

This is a simple quadratic equation in R, for which R has a single real positive root:

$$R^2 = \frac{g_1 - g_2}{a}\sqrt{\frac{1}{X^2} - 1}.$$

This procedure therefore picks out two isolated pairs $(\mp\varphi, R)$ that leads to a self-consistent solution of the nonlinear double eigenvalue problem. ∎

Further analytical progress is possible with respect to Equation (6.9): the family of complex-valued eigenvalues $\Omega(R)$ can be controlled in the following manner:

Theorem 6.2 *Take as given the non-linear eigenvalue problem* (6.9), *with eigenvalues* $\Omega(R) \in \mathbb{C}$ *for* $R \geq 0$. *Then*

$$(\mu_0 - g_2) - (g_1 + g_2) \leq \Im(\Omega) \leq \mu_0 - g_2.$$

Proof Take $re^{-i\varphi}$ [Eq. (6.15a)] $+ x$ [Eq. (6.15b)] to obtain

$$\Omega = E_0 + 2Arx \cos \varphi + aR^2(r^4 + x^4) + i(\mu_0 - g_1 r^2 - g_2 x^2).$$

Since $x^2 + r^2 = 1$, we have

$$\Im(\Omega) = (\mu_0 - g_2) - (g_1 + g_2)r^2,$$

with $0 \le r^2 \le 1$, hence $(\mu_0 - g_2) - (g_1 + g_2) \le \Im(\Omega) \le \mu_0 - g_2$. ∎

Thus, the range of allowed values of $\Im(\Omega)$ is bounded above and below. In order for $\Im(\Omega) = 0$ to be achievable, the upper bound must be non-negative, so that a necessary condition for the existence of a global mode is $\mu_0 > g_2$. By Equation (6.5), this is the same necessary condition as the one required for linear transient growth to occur.

6.2.3   Stability of nonlinear oscillatory state

The stability of the self-consistent oscillatory state is investigated by consideration of a trial solution

$$u = Re^{-i\Omega t} u_0 + \delta u,$$

where $R = R_{\mathrm{c}}$, and where u_0 is the solution of the nonlinear eigenvalue problem. Linearization around the periodic state yields the following ODE:

$$
\begin{aligned}
i\frac{d}{dt}\delta u &= \mathcal{L}\delta u + 2R^2 a \begin{pmatrix} |u_{01}|^2 & 0 \\ 0 & |u_{02}|^2 \end{pmatrix} \delta u + R^2 e^{-2i\Omega t} \begin{pmatrix} u_{01}^2 & 0 \\ 0 & u_{02}^2 \end{pmatrix} \overline{\delta u}, \\
&:= \mathcal{A}\,\delta u + e^{-2i\Omega t}\mathcal{B}\,\overline{\delta u}.
\end{aligned}
\tag{6.18}
$$

The manifestly time-dependent term is removed by making the trial solution $\delta u = \delta v e^{-i\Omega t}$, such that Equation (6.18) becomes

$$i\frac{d}{dt}\delta v = (\mathcal{A} - \Omega)\,\delta v + \mathcal{B}\overline{\delta v}.\tag{6.19}$$

Equation (6.19) can be further simplified by breaking it up into real and imaginary parts. We take $\delta v = (a + ib, u + iv)^T$, where a, b, u, and v are real-valued functions of t. We also take $\mathcal{B} = \widehat{\beta} + i\widehat{\gamma}$, where $\widehat{\beta}$ and $\widehat{\gamma}$ are real matrices. Similarly, we write $\Re(\mathcal{A} - \Omega) := \widehat{\mathcal{H}}$. Finally, we note that $\Im(\mathcal{A} - \Omega) = \mu_0 \mathbb{I} + \mathcal{G}$. Using this notation, we obtain the following real system of equations:

$$
\frac{d}{dt}\begin{pmatrix} a \\ b \\ u \\ v \end{pmatrix} = \begin{pmatrix} \mu_0 - g_1 + \widehat{\gamma}_{11} & \widehat{\mathcal{H}}_{11} - \widehat{\beta}_{11} & 0 & A \\ -\widehat{\mathcal{H}}_{11} - \widehat{\beta}_{11} & \mu_0 - g_1 - \widehat{\gamma}_{11} & -A & 0 \\ 0 & A & \mu_0 - g_2 + \widehat{\gamma}_{22} & \widehat{\mathcal{H}}_{22} - \widehat{\beta}_{22} \\ -A & 0 & -\widehat{\mathcal{H}}_{22} - \widehat{\beta}_{22} & \mu_0 - g_2 - \widehat{\gamma}_{22} \end{pmatrix} \begin{pmatrix} a \\ b \\ u \\ v \end{pmatrix}.\tag{6.20}
$$

The results of Theorem 6.1 are now used to fill out the entries in the matrix in Equation (6.20) with closed-form expressions involving the model parameters:

$$
\frac{d}{dt}
\begin{pmatrix} a \\ b \\ u \\ v \end{pmatrix}
=
\left(
\begin{array}{c|c|c|c}
\begin{array}{c} \mu_0 - g_1 \\ +aR^2r^2\sin 2\varphi \end{array} & \begin{array}{c} aR^2(2r^2-1) \\ -aR^2r^2\cos 2\varphi \end{array} & 0 & A \\
\hline
\begin{array}{c} -aR^2(2r^2-1) \\ -aR^2r^2\cos 2\varphi \end{array} & \begin{array}{c} \mu_0 - g_1 \\ -aR^2r^2\sin 2\varphi \end{array} & -A & 0 \\
\hline
0 & A & \mu_0 - g_2 & \begin{array}{c} -aR^2(2r^2-1) \\ -aR^2(1-r^2) \end{array} \\
\hline
-A & 0 & \begin{array}{c} aR^2(2r^2-1) \\ -aR^2(1-r^2) \end{array} & \mu_0 - g_2
\end{array}
\right)
\begin{pmatrix} a \\ b \\ u \\ v \end{pmatrix}
$$

(6.21)

Based on this expression of the stability equations, we prove the following theorem:

Theorem 6.3 *The oscillatory state in Equation* (6.10) *is asymptotically unstable.*

Proof We write $(a, b, u, v)^T = e^{\sigma t}(a_0, b_0, u_0, v_0)$, and search for eigensolutions where a_0, b_0, u_0 and v_0 are real. Calling the matrix in Equation (6.21) $\mathcal{M}$, it can be shown by direct computation that $\det(\mathcal{M}) = 0$ identically (e.g. using a symbolic algebra package), such that the characteristic equation of the matrix $\mathcal{M}$ is

$$
\sigma\left[\sigma^3 - \text{tr}(\mathcal{M})\sigma^2 + m_1\sigma + m_2\right] = 0,
\tag{6.22}
$$

where m_1 and m_2 are real constants that depend on the problem parameters. A further direct computation yields

$$
m_2 = 8A^2(1 - X^2)\left[\mu_0 - \tfrac{1}{2}(g_1 + g_2)\right].
\tag{6.23}
$$

Under the twin assumptions that we are in the operating range given by Equation (6.6) and that $0 < X^2 < 1$, we have that $m_2 < 0$, such that the cubic polynomial in the square brackets $[\cdots]$ in Equation (6.22) has at least one real *positive* root, with a corresponding real eigenvector $(a_0, b_0, u_0, v_0)^T$. The corresponding real eigenvalue therefore has $\sigma > 0$, hence the system (6.21) is asymptotically unstable. ∎

6.3   Illustrative numerical examples

It is of interest to examine whether the periodic unstable state has any bearing on the dynamics of Equation (6.7). Thus, temporal numerical simulations of the same equation are performed. We use

the parameter values

$$E_0 = 1, \qquad A = 0.1, \qquad g_2 = 0.01, \qquad g_1 = g_2 + (4A^2 + 0.01^2)^{1/2}, \qquad a = 1,$$

$$\mu_0 = 0.95 \left[\tfrac{1}{2}(g_1 + g_2) - \sqrt{(g_1 - g_2)^2 - 4A^2} \right]. \quad (6.24)$$

Also, the initial condition was taken to be $(A_0/\sqrt{2})(\mathrm{i}, 1)^T$, where A_0 is taken to be small in an appropriate sense, so that the early-stage dynamics correspond to linear theory. The parameters (6.24) correspond to a subcritical case: both eigenfrequencies of the linearized dynamics possess negative imaginary parts. However, the same parameters are appropriate for (linear) transient growth, as outlined in Equation (6.6).

The results are shown in Figure 6.1. The numerical solutions are obtained using an eight-order accurate Runge–Kutta scheme [Gov]. Solutions under the linearized dynamics are shown in Figure 6.1(a).
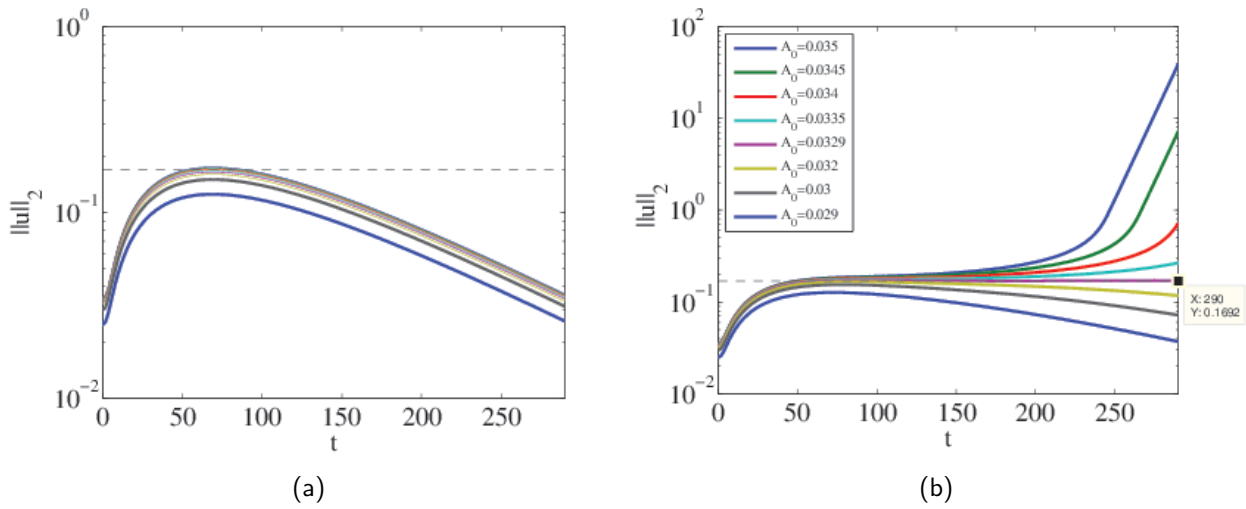

(a)   (b)

Figure 6.1: Solutions of (a) the non-Hermitian linear Schrodinger equation; (b) the non-Hermitian *nonlinear* Schrödinger equation. The initial data are the parameters are the same in (a) and (b).

Significant transient growth occurs for the initial data and parameter values in Equation (6.24), in spite of the negatativity of the linear growth rates, i.e. $\Im\left[\mathrm{spec}\left(\mathcal{L}\right)\right] \leq 0$: the maximum amplification is over 500% in the figure. In contrast, solutions under the nonlinear dynamcis are shown in Figure 6.1(b). The linear transient growth operates in the same manner as in Figure 6.1, up to $t \approx 80$. Thereafter, a range of possibilities exists, depending on the initial amplitude of the disturbance. First, one notes that there is a critical initial amplitude A_{0c} such that $\lim_{t \to \infty} \|u\|_2 = R_c$; this is precisely the critical radius for which the nonlinear oscillatory state exists, as in the analysis in Equation (6.9). Also, for initial amplitudes above this threshold, the same nonlinear oscillatory state is excited, but is subsequently destabilized, and indefinite exponential growth takes place. Finally, for initial amplitudes below the same threshold, the nonlinear oscillatory state cannot be maintained, and the linear dissipation eventually causes the disturbance to decay to zero. For the case $A_0 > A_{0c}$,

one obtains the eery result that the disturbance grows exponentially fast, in spite of the fact that the eigenfrequencies of the linearized problem possess negative imaginary parts. This is a subcritical transition to (nonlinear) instability.

These results point to the following conclusion: linear transient growth by itself is not sufficient to induce a transition from a regime of small-amplitude disturbances to one of nonlinear instability in the model equation (6.7). Rather, the transient growth must have available an excitable non-linear eigenmode, and moreover, the operating parameter regime must be such that the nonlinear eigenmode is linearly (asymptotically) unstable or neutral. These findings are consistent with the literature on a vastly more complicated system, namely the subcritical transition to turbulence in parallel shear flows [SH01, Gro00], where a combination of transient growth and the secondary instability of coherent states [Wal95, Wal98] is required for subcritical transition to turbulence.

Exercise 6.2

1. The maximum transient growth rate is defined as

$$\gamma(t) = \sup_{u \neq 0} \frac{\|e^{\mathcal{L}t}u\|}{\|u\|}, \qquad (6.25)$$

   where the L^2 norm is taken. Show that at each time t the disturbance u that realises the maximum in Equation (6.25) is the solution of the eigenvalue problem

$$e^{\mathcal{L}^\dagger t}e^{\mathcal{L}t}u_t = \lambda u_t, \qquad (6.26)$$

   where the subscript t indicates that u_t is the disturbance that maximizes the growth rate $\gamma(t)$ at the particular time t. The quantity u_t is called the **optimal disturbance** at time t.

2. Use the parameters (6.24) and the solution (6.26) to generate numerically the curve $\gamma(t)$, with $0 < t < 300$, say.

3. Download the ".m" code from the website. Run the linear and noninear version of the code with the initial condition $u(t = 0) = u_{50}$ (say). Plot the L^2 norm of the solution versus t and compare with Figure 6.1.

6.4　Interlude: Three-dimensional disturbances in plane parallel flows and Squire's Theorem

Before applying the theory of transient growth to plane parallel flows, we must first all make a digression and consider in more detail the notion of three-dimensional disturbances to a plane parallel flow $U_0(z)$, with $\boldsymbol{u} = U_0(z)\hat{\boldsymbol{x}} + \delta\boldsymbol{u}$, where $\delta\boldsymbol{u} = (\delta u, \delta v, \delta w)$, such that the perturbed velocity $\boldsymbol{u}$ has three non-trivial components. The reason for this is that we will find out that the optimal disturbance is three-dimensional.

As before, the basic non-dimensional equation of motion is

$$\frac{\partial}{\partial t}\delta\boldsymbol{u} + U_0\frac{\partial}{\partial x}\delta\boldsymbol{u} + \hat{\boldsymbol{x}}\delta w\frac{dU_0}{dz} = -\nabla p + Re^{-1}\nabla^2\delta\boldsymbol{u},$$

where δp is the perturbation pressure. We operate on both sides with the curl to obtain the linearized vorticity equation:

$$\frac{\partial}{\partial t}\delta\boldsymbol{\omega} + U_0\frac{\partial}{\partial x}\delta\boldsymbol{\omega} - U_0'\left(\hat{\boldsymbol{x}}\partial_x\delta v - \hat{\boldsymbol{y}}\partial_x\delta u\right) + U_0'\left(\hat{\boldsymbol{y}}\partial_z\delta w + \hat{\boldsymbol{z}}\partial_y\delta w\right) + \hat{\boldsymbol{y}}U_0''\delta w = Re^{-1}\nabla^2\boldsymbol{\omega}$$

Call $\eta = \hat{\boldsymbol{z}} \cdot \delta\vec{\omega}$. Clearly,

$$\frac{\partial\eta}{\partial t} + U_0\frac{\partial\eta}{\partial x} + U_0'\partial_y\delta w = Re^{-1}\nabla^2\eta. \tag{6.27}$$

Next, consider $\delta\omega_x = \hat{\boldsymbol{x}} \cdot \delta\boldsymbol{\omega}$ and $\delta\omega_y = \hat{\boldsymbol{y}} \cdot \delta\boldsymbol{\omega}$. We have

$$\frac{\partial}{\partial t}\delta\omega_x + U_0\frac{\partial}{\partial x}\delta\omega_x - U_0'\frac{\partial}{\partial x}\delta v \;=\; = Re^{-1}\nabla^2\delta\omega_x, \tag{6.28a}$$

$$\frac{\partial}{\partial t}\delta\omega_y + U_0\frac{\partial}{\partial x}\delta\omega_y + U_0'\frac{\partial}{\partial x}\delta u + U_0'\frac{\partial}{\partial z}\delta w + U_0''\delta w \;=\; Re^{-1}\nabla^2\delta\omega_y, \tag{6.28b}$$

We go over to a normal-mode decomposition with $\delta\boldsymbol{\omega} \propto e^{i\alpha x + i\beta y}$, such that $\partial_x = i\alpha$ and $\partial_y = i\beta$. Thus, the two vorticity components $\delta\omega_x$ and $\delta\omega_y$ become

$$\delta\omega_x \;=\; \partial_y\delta w - \partial_z\delta v = i\beta\delta w - \partial_z\delta v,$$

$$\delta\omega_y \;=\; \partial_z\delta u - \partial_x\delta w = -i\alpha\delta w + \partial_z\delta u.$$

Put these into Equation (6.28):

$$\frac{\partial}{\partial t}\left(i\beta\delta w - \partial_z\delta v\right) + U_0 i\alpha\left(i\beta\delta w - \partial_z\delta v\right) - U_0' i\alpha\delta v = Re^{-1}\nabla^2\left(i\beta\delta w - \partial_z\delta v\right), \tag{6.29a}$$

$$\frac{\partial}{\partial t}\left(-i\alpha\delta w + \partial_z\delta u\right) + U_0 i\alpha\left(-i\alpha\delta w + \partial_z\delta u\right)$$
$$+ U_0' i\alpha\delta u + U_0'\partial_z\delta w + U_0''\delta w Re^{-1}\nabla^2\left(-i\alpha\delta w + \partial_z\delta u\right), \quad (6.29b)$$

Take $i\beta$(6.29a):

$$\frac{\partial}{\partial t}\left(-\beta^2\delta w - i\beta\partial_z\delta v\right) + i\alpha U_0\left(-\beta^2\delta w - i\beta\partial_z\delta v\right)$$
$$- i\alpha U_0'\left(i\beta\delta v\right) = Re^{-1}\nabla^2\left(-\beta^2\delta w - i\beta\partial_z\delta v\right). \quad (6.30a)$$

Also, take $i\alpha$(6.29b):

$$\frac{\partial}{\partial t}\left(\alpha^2\delta w + i\alpha\partial_z\delta u\right) + i\alpha U_0\left(\alpha^2\delta w + i\alpha\partial_z\delta u\right)$$
$$+ i\alpha U_0'\left(i\alpha\delta u\right) + i\alpha U_0'\partial_z\delta v + i\alpha U_0''\delta w = Re^{-1}\nabla^2\left(\alpha^2\delta w + i\alpha\partial_z\delta u\right). \quad (6.30b)$$

Subtract:

$$\frac{\partial}{\partial t}\left(-\beta^2\delta w - \alpha^2\delta w - i\beta\partial_z\delta v - i\alpha\partial_z\delta u\right) + i\alpha U_0\left(-\beta^2\delta w - \alpha^2\delta w - i\beta\partial_z\delta v - i\alpha\partial_z\delta u\right)$$
$$+ i\alpha U_0'\left(-i\beta\delta v - i\alpha\delta u - \partial_z\delta v\right) - i\alpha U_0''\delta w = Re^{-1}\nabla^2\left(-\beta^2\delta w - \alpha^2\delta w - i\beta\partial_z\delta v - i\alpha\partial_z\delta u\right)$$

Use incompressibility:

$$i\alpha\delta u + i\beta\delta v + \partial_z\delta w = 0$$

hence

$$\partial_z^2\delta w - i\alpha\delta u - i\beta\delta v,$$

and thus

$$\frac{\partial}{\partial t}\nabla^2\delta w + i\alpha U_0\nabla^2\delta w - i\alpha U_0''\delta w = \nabla^4\delta w.$$

Going over to the normal-mode decomposition, this is

$$\frac{\partial}{\partial t}\left(\partial_z^2 - k^2\right)\delta w + i\alpha U_0\left(\partial_z^2 - k^2\right)\delta w - i\alpha U_0''\delta w = \left(\partial_z^2 - k^2\right)^2\delta w, \qquad k^2 = \alpha^2 + \beta^2.$$

With $\delta w \propto e^{-i\alpha ct}$ this is

$$i\alpha\left(U_0 - c\right)\left(\partial_z^2 - k^2\right)\delta w - i\alpha U_0''\delta w = Re^{-1}\left(\partial_z^2 - k^2\right)^2\delta w, \qquad (6.31a)$$

which is precisely the Orr–Sommerfeld equation. However, we have a further equation for the wall-normal vorticty (Equation (6.27)) which now reads

$$i\alpha(U_0 - c)\eta + i\beta U_0'\delta w = Re^{-1}(\partial_z^2 - k^2)\eta. \qquad (6.31b)$$

Equations (6.31) are the **Orr–Sommerfeld–Squire** equations.

Equation (6.31a) can be mapped into a two-dimensional Orr–Sommerfeld equation by the introduction of the variables

$$\alpha_{2D} \quad = \quad k = \sqrt{\alpha^2 + \beta^2}, \tag{6.32a}$$

$$Re_{2D} \quad = \quad \frac{\alpha}{\alpha_{2D}} Re = \sqrt{\frac{\alpha^2}{\alpha^2 + \beta^2}} Re. \tag{6.32b}$$

Thus, Equation (6.31a) can be rewritten as

$$i\alpha_{2D} \left(U_0 - c \right) \left(\partial_z^2 - \alpha_{2D}^2 \right) \delta w - i\alpha U_0'' \delta w = Re_{2D}^{-1} \left(\partial_z^2 - \alpha_{2D} \right)^2 \delta w,$$

which is precisely the Orr–Sommerfeld equation in two dimensions. From Equation (6.32) we have

$$Re_{2D} < Re.$$

Thus, we have shown the following result:

Lemma 6.1 *To each three-dimensional Orr–Sommerfeld–Squire mode there corresponds a two-dimensional Orr–Sommerfeld mode at a* **lower** *Reynolds number.*

This enables us to prove **Squire's theorem**:

Theorem 6.4 *Given Re_L as the critical Reynolds number for the onset of linear instability for a given (α, β), the Reynolds number Re_c below which no exponential instabilities exist for any wavenumbers satisfies*

$$Re_c := \min_{\alpha, \beta} Re_L(\alpha, \beta) = \min_{\alpha} Re_L(\alpha, 0).$$

Thus, parallel shear flows fisrt become unstable to two-dimensional wavelike perturbations at a value of the Reynolds number that is smaller than any value for which unstable three-dimensional perturbations exist. That is the reason why no generality was lost to date in studying only the two-dimensional disturbances for the plane parallel flows.

The proof of Squire's theorem follows directly from the Squire transformation (6.32): if a three-dimensional mode is unstable, then a two-dimensional mode is unstable at a lower Reynolds number.

We also have the following result for so-called pure Squire modes (A solution of the Orr–Sommerfeld–Squire equations with $w = 0$ is called a **pure Squire mode**):

Theorem 6.5 *The eigenvalues of all pure squire modes are damped, i.e. $c_i < 0$ for all α, β and Re, for all pure Squire modes*

The proof here is straightforward: we take $w = 0$ in the Squire equation (6.31b). We then multiply by η^* and integrate from $z = 0$ to $z = 1$:

$$\lambda \int_0^1 |\eta|^2 \, \mathrm{d}z + \mathrm{i}\alpha \int_0^1 U_0 |\eta|^2 = Re^{-1} \int_0^1 \eta^* \left(\partial_z^2 - k^2 \right) \eta, \qquad \lambda = -\mathrm{i}\alpha c. \qquad (6.33)$$

Since $\eta = \hat{\boldsymbol{z}} \cdot \delta\boldsymbol{\omega} = \mathrm{i}\alpha \delta v - \mathrm{i}\beta \delta u$ we have $\eta = 0$ at $z = 0$, $z = 1$. This enables us to do integration by parts on the right-hand side of Equation (6.33) and to set the boundary terms to zero. We obtain

$$\lambda \int_0^1 |\eta|^2 \, \mathrm{d}z + \mathrm{i}\alpha \int_0^1 U_0 |\eta|^2 = -Re^{-1} \int_0^1 \left(|\partial_z \eta|^2 + k^2 |\eta|^2 \right) \mathrm{d}z.$$

Taking real parts, we have
$$\lambda_{\mathrm{r}} \|\eta\|_2^2 = -Re^{-1} \left(\|\partial_z \eta\|_2^2 + k^2 \|\eta\|_2^2 \right)$$

hence $\lambda_{\mathrm{r}} \|\eta\|_2^2 < 0$, hence $c_{\mathrm{i}} < 0$ as required.

Transient behaviour

It is tempting to ask why wave introduced the Orr–Sommerfeld Squire equations when the end result has been a theorem showing that as far as eigenvalues are concerned, the three-dimensional disturbances are not important. The answer is that stability theory is about more than eigenvalues. Eigenvalue analysis is only valid as $t \to \infty$. For finite times, we must consider the full initial value problem. The initial value problem for the Squire equation reads

$$\frac{\partial \eta}{\partial t} + \mathrm{i}\alpha U_0(z)\eta + \mathrm{i}\beta U_0' \delta w = Re^{-1} \left(\partial_z^2 - k^2 \right) \eta.$$

For $\alpha = 0$ this reads
$$\frac{\partial \eta}{\partial t} + \frac{\alpha^2}{Re} \eta = \frac{1}{Re} \partial_z^2 \eta + \mathrm{i}\beta U_0' \delta w. \qquad (6.34)$$

Let us further focus on the large-Reynolds number flows, and focus on the case where we can take $Re \to \infty$, such that Equation (6.34) reads

$$\frac{\partial \eta}{\partial t} = -\mathrm{i}\beta U_0' \delta w.$$

This is a first-order separable ODE, with solution

$$\eta(z, t) = \eta(z, 0) - \mathrm{i}\beta U_0'(z) \int_0^t \delta w(z, t) \, \mathrm{d}t.$$

For short times we can take $\delta w(z,t)$ outside the integrand, leaving

$$\eta(z,t) \approx \eta(z,0) - \mathrm{i}\beta U_0' \delta w(z,0) t \tag{6.35}$$

Thus, the vorticity grows linearly with time for short times. This is the notion of a **transient instability**. Of course, what happens as $t \to \infty$ is not predicted by Equation (6.35) – that is determined by the eigenvalue analysis. But it is of interest to study in a systematic way the transient behavior of the Orr–Sommerfeld–Squire equations at finite times, i.e. before the eigenvalue analysis becomes the factor determining the time evolution. We do this in the next section.

6.5 Transient growth in plane parallel flows

6.5.1 Formulation

The Orr–Sommerfeld–Squire equation for a generic problem in the hydrodynamic stability of a parallel flow can be written down in generic form as follows:

$$\mathcal{L}\boldsymbol{\chi} = \lambda\mathcal{M}\boldsymbol{\chi}, \tag{6.36}$$

The stability problem is solved at a particular set of wavenumbers (α, β), and the Orr–Sommerfeld–Squire matrices $\mathcal{L}$ and $\mathcal{M}$ and the eigenvalue λ all depend on the wavenumbers. Recall, the state vector $\boldsymbol{\chi}$ is obtained by writing the wall-normal velocity and vorticity in a finite Chebyshev approximation:

$$w(z) = \sum_{i=0}^{N} A_i T_i(x), \qquad \eta = \sum_{i=0}^{N} B_i T_i(x), \qquad x = 2z - 1,$$

such that
$$\boldsymbol{\chi} = (A_0, \cdots, A_n, B_0, \cdots, B_n)^T.$$

Now, it can be shown that the matrices in Equation (6.36) can be used to solve the corresponding initial-value problem (e.g. Reference [ÓNSS13]). The initial-value problem is formulated as follows:

$$\frac{\partial}{\partial t}\mathcal{M}\boldsymbol{\chi} = \mathcal{L}\boldsymbol{\chi}, \qquad t > 0, \tag{6.37a}$$

with initial condition

$$\boldsymbol{\chi}(t=0) = \boldsymbol{\chi}_0, \qquad \boldsymbol{\chi}_0 = (x_0, \cdots, x_n, y_0, \cdots, y_n)^T, \tag{6.37b}$$

and where

$$x_0 = \frac{1}{\pi} \int_{-1}^{1} T_0(x) w \left(\tfrac{1}{2}(x+1), t=0 \right) \frac{\mathrm{d}x}{\sqrt{1-x^2}}, \tag{6.38a}$$

$$x_i = \frac{2}{\pi} \int_{-1}^{1} T_i(x) w \left(\tfrac{1}{2}(x+1), t=0 \right) \frac{\mathrm{d}x}{\sqrt{1-x^2}}, \qquad i \neq 0, \tag{6.38b}$$

$$y_0 = \frac{1}{\pi} \int_{-1}^{1} T_0(x) \eta \left(\tfrac{1}{2}(x+1), t=0 \right) \frac{\mathrm{d}x}{\sqrt{1-x^2}}, \tag{6.38c}$$

$$y_i = \frac{2}{\pi} \int_{-1}^{1} T_i(x) \eta \left(\tfrac{1}{2}(x+1), t=0 \right) \frac{\mathrm{d}x}{\sqrt{1-x^2}}, \qquad i \neq 0. \tag{6.38d}$$

It can be easily seen that the solution to Equation (6.37) can be written as

$$\boldsymbol{\chi}(t_n) = \mathcal{X}(t_n) \boldsymbol{\chi}_0, \qquad t_n = n \Delta t, \qquad n = 0, 1, \cdots,$$

where $\Delta t \to 0$, keeping $t_n = t$ finite. Also,

$$\mathcal{X}(t) = \lim_{\Delta t \to 0} \left[(\mathcal{M} - \Delta t \mathcal{L})^{-1} \mathcal{M} \right]^n. \tag{6.39}$$

Note that Equation (6.39) amounts to solving the linear differential algebraic equation (DAE) (6.37a) using the backward Euler method.

6.5.2 The method

The idea of the transient-growth calculation is to start with the energy norm

$$E(t) = \int_{0}^{1} \left(|\partial_z w|^2 + k^2 |w|^2 + |\eta|^2 \right) \mathrm{d}z, \qquad k^2 = \alpha^2 + \beta^2, \tag{6.40}$$

and at each point in time to optimize the energy norm subject to the constraint that $E(0) = 1$. The resulting maximum energy is called the *transient growth rate*, $G(t)$. These calculations can be done within the framework of Section 6.5.1 as follows. First, the energy norm in Equation (6.40) is identified with a scalar product on the space of admissible $\boldsymbol{\chi}$-vectors:

$$\begin{aligned}
E(t) &= \tfrac{1}{2} \int_{-1}^{1} \mathrm{d}x \left[\left| \sum_{i=0}^{N} A_i e_x T_i'(x) \right|^2 + k^2 \left| \sum_{i=0}^{N} A_i T_i(x) \right|^2 + \left| \sum_{i=0}^{N} B_i T_i(x) \right|^2 \right], \qquad e_x = \frac{\mathrm{d}x}{\mathrm{d}z} = 2, \\
&= \sum_{i,j} A_i^* A_j \left(\tfrac{1}{2} e_x^2 \int_{-1}^{1} T_i'(x) T_j'(x) \mathrm{d}x \right) + \sum_{i,j} A_i^* A_j \left(\tfrac{1}{2} k^2 \int_{-1}^{1} T_i(x) T_j(x) \mathrm{d}x \right) \\
&\quad + \sum_{i,j} B_i^* B_j \left(\tfrac{1}{2} \int_{-1}^{1} T_i(x) T_j(x) \mathrm{d}x \right).
\end{aligned}$$

Call

$$\mathbb{T}_{ij}^{(1)} = \tfrac{1}{2} e_x^2 \int_{-1}^{1} T_i'(x) T_j'(x) \mathrm{d}x,$$

$$\mathbb{T}_{ij}^{(0)} = \tfrac{1}{2} \int_{-1}^{1} T_i(x) T_j(x) \mathrm{d}x.$$

We have

$$E(t) = \sum_{i,j} A_i^* A_j \mathbb{T}_{ij}^{(1)} + k^2 \sum_{i,j} A_i^* A_j \mathbb{T}_{ij}^{(0)} + \sum_{i,j} B_i^* B_j \mathbb{T}_{ij}^{(0)},$$

$$= \left\langle \boldsymbol{\chi}, \begin{pmatrix} \mathbb{T}^{(1)} + k^2 \mathbb{T}^{(0)} & 0 \\ 0 & \mathbb{T}^{(0)} \end{pmatrix} \boldsymbol{\chi} \right\rangle,$$

$$:= \langle \boldsymbol{\chi}, \mathcal{G}\boldsymbol{\chi} \rangle.$$

Here, the brackets denote the usual scalar product on the space of $\boldsymbol{\chi}$-vectors, and the matrix $\mathcal{G}$ is symmetric positive-definite. Thus, the equation

$$E(t) = \langle \boldsymbol{\chi}, \mathcal{G}\boldsymbol{\chi} \rangle$$

defines a scalar product on the space of $\boldsymbol{\chi}$-vectors. However, we have

$$\boldsymbol{\chi} = \mathcal{X}(t)\boldsymbol{\chi}_0,$$

hence

$$E(t) = \langle \boldsymbol{\chi}_0, \mathcal{X}(t)^\dagger \mathcal{G} \mathcal{X}(t) \boldsymbol{\chi}_0 \rangle.$$

Thus, the optimization to be performed can be recast as an optimization of the functional

$$E[\chi_0] = \langle \boldsymbol{\chi}_0, \mathcal{X}(t)^\dagger \mathcal{G} \mathcal{X}(t) \boldsymbol{\chi}_0 \rangle,$$

subject to the constraint that

$$\langle \boldsymbol{\chi}_0, \mathcal{G}\boldsymbol{\chi}_0 \rangle = 1.$$

In other words, we have the following Lagrange-multiplier problem:

$$E[\chi_0] = \langle \boldsymbol{\chi}_0, \mathcal{X}(t)^\dagger \mathcal{G} \mathcal{X}(t) \boldsymbol{\chi}_0 \rangle - \lambda \left(\langle \boldsymbol{\chi}_0, \mathcal{G}\boldsymbol{\chi}_0 \rangle - 1 \right).$$

The optimum vector is obtained by setting

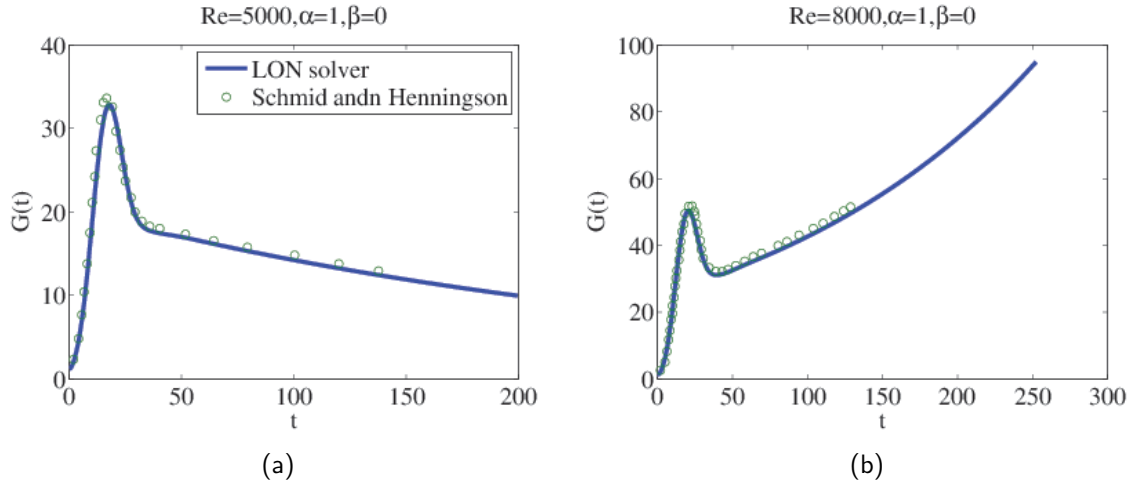$$\frac{\delta E}{\delta \boldsymbol{\chi}^*} = 0,$$

Figure 6.2: Validation of our code for the maximum transient growth rate compared to known benchmark case in the literature (data from Reference [SH01]). The small discrepancies between the two datasets are due to errors in scanning and digitizing the data from the reference text.

in other words,

$$\mathcal{X}^\dagger \mathcal{G} \mathcal{X}(t) \boldsymbol{\chi}_0 = \lambda \mathcal{G} \boldsymbol{\chi}_0. \tag{6.41}$$

Equation (6.41) is a generalized eigenvalue problem, and it is readily checked that the eigenvalues are real (both matrices appearing in the problem are Hermitian) and moreover, that the eigenvalues are non-negative. It can be further shown by a straightforward calculation (backsubstitution into the constrained functional) that

$$\sup_{\boldsymbol{\chi}_0} \left[E[\boldsymbol{\chi}_0] - \lambda \left(\langle \boldsymbol{\chi}_0, \mathcal{G} \boldsymbol{\chi}_0 \rangle - 1 \right) \right] = \max \lambda,$$

where the maximum is taken over the spectrum of the generalized eigenvalue problem (6.41). Thus, at each point in time, the transient growth rate is

$$G(t) = \max \lambda.$$

6.5.3   Results for Poiseiulle flow

We have validated this procedure against the known test case of Poiseuille flow. We work in the units used by Orzag and other later researchers for their stability calculations of single-phase Poiseuille flow [Orz71]. Thus, we take $\alpha = 1$, $\beta = 0$, and two cases for the Reynolds number: $Re = 5000$ (asymptotically stable) and $Re = 8000$ (asymptotically unstable). A comparison between known results for $G(t)$ in this instance and the results from our own calculations are shown in Figure 6.2.

It is now of interest to examine the behavior demonstrated in Figure 6.2 a little further. We go back over to our own units based on the full channel height and the friction velocity and examine the

(a) $t = 0.05$

(b) $t = 0.1$

(c) $t = 0.15$

(d) $t = 0.5$

(e) $t = 1$
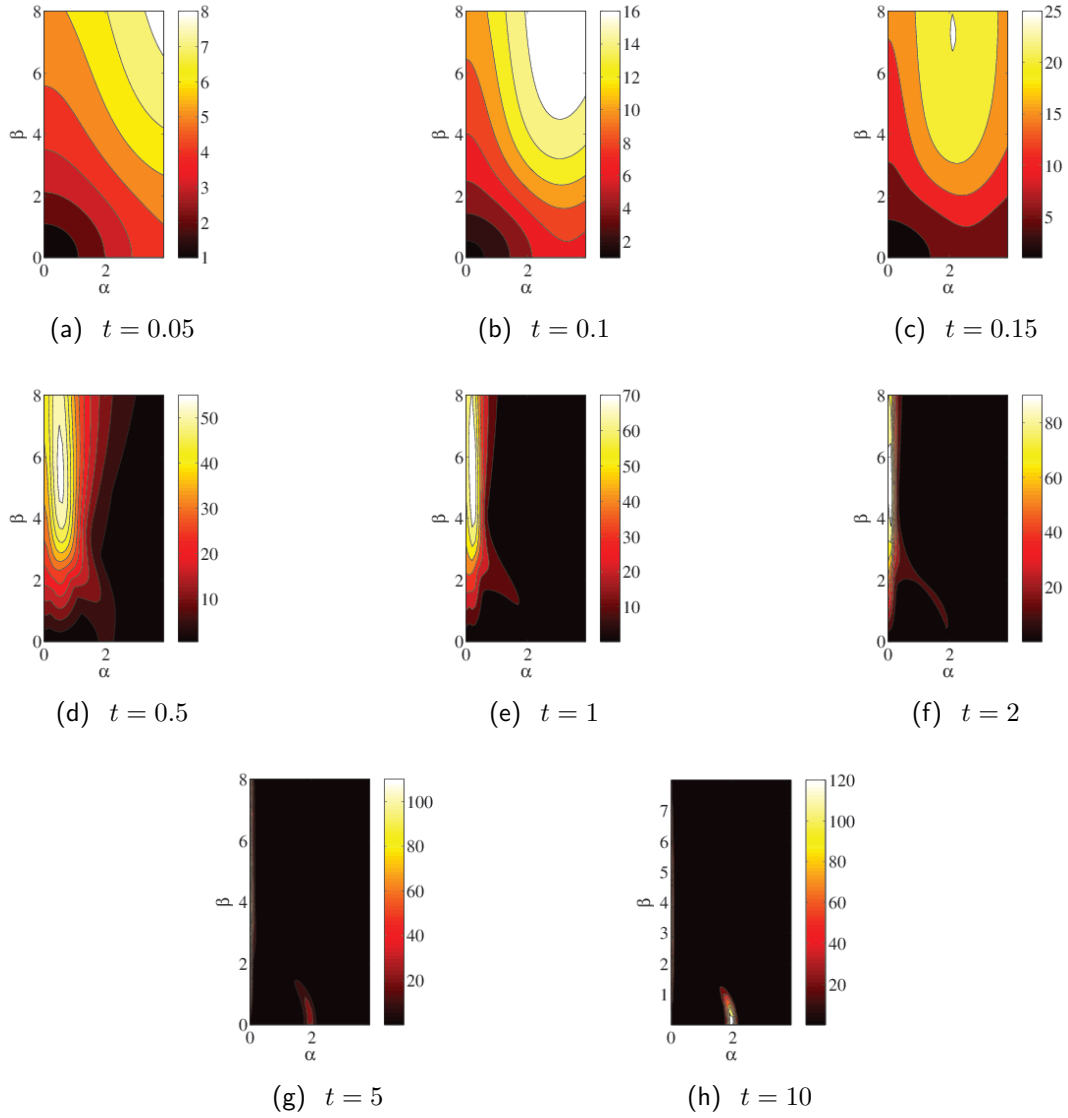

(f) $t = 2$

(g) $t = 5$

(h) $t = 10$

Figure 6.3: Time evolution of the optimal transient growth rate as a function of the wavenumbers α (streamwise) and β (spanwise). Between $t = 0.1$ and $t = 10$ the optimal disturbance moves from being spanwise-dominated to streamwise-dominated.

features of the transient growth in the supercritical case $Re = 8000$, $Re_* = \sqrt{8 \times 8000} \approx 252.9822$, for various times $t \in [0, 2]$ (corresponding to times $[0, 2] Re_*/2$ in Figure 6.2). The resulting study is presented in Figure 6.3 where it should be noticed that it is the square root of the energy of the most-amplified disturbance that is plotted in a wavenumber space, for different t-values. For very short times ($t = 0.1$) the transiently most-amplified mode has a wavevector with components in both the streamwise and spanwise directions (at $t = 0.1$, $\max_{\alpha,\beta} G_{\alpha,\beta}(t)$ occurs at $(\alpha, \beta) \approx (3, 8)$). As time goes by, the most-amplified mode moves to a more spanwise wavenumber such that by $t = 1$ the maximum value $\max_{\alpha,\beta} G_{\alpha,\beta}(t)$ occurs at $\alpha \approx 0$ and $\beta = 6$. Thereafter, there is a slow evolution of the trajectory of the most-amplified disturbance through the wavenumber space away from spanwise wavenumbers towards streamwise ones (the eigenvalue theory predicts that as $t \to \infty$
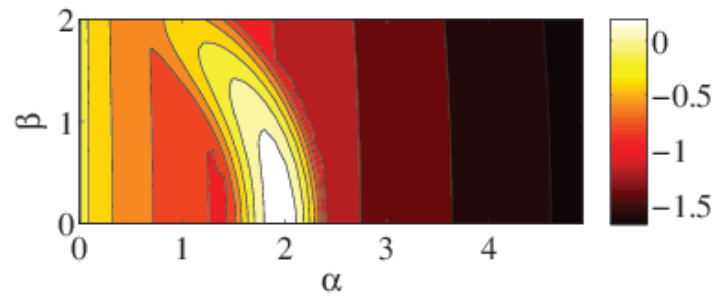
Figure 6.4: Eigenvalue of most-dangerous mode of the Orr–Sommerfeld–Squire equations, with $Re = 5000$. The most-dangerous mode according to eigenvalue analysis (valid as $t \rightarrow \infty$) is a streamwise one.

the most-amplified disturbance is a streamwise-only mode – Figure 6.4). By $t = 10$ the asymptotic state is reached and the most-amplified disturbance is indeed streamwise-only.

Chapter 7

Weakly nonlinear theory

7.1 Overview

Beyond linear theory, analytical progress can be made in certain scenarios wherein a **separation of scales** occurs. The idea here is to break up the eigenmodes of the linear theory into two sets. In the first set, the growth rates of the linear theory are $O(1)$, while in the second set, the normal modes possess large damping rates of magnitude $1/\epsilon$, so that a separation of timescales between the two sets occurs. Thus, two sets emerge, corresponding to fast dynamics and slow dynamics. The modes belonging to the fast set can be viewed as **slaved** to the slow modes, and do not evolve dynamically. Analytical expressions for the fast modes in terms of the slow modes can be derived, which in turn are substituted back into the equations for the slow modes, leading to a simplified system of differential equations for the fast modes.

7.2 Example – Cahn–Hilliard equation

We will start with an example of a nonlinear equation amenable to a weakly nonlinear analysis. The direct relevance to Fluid Dynamics here is not immediately obvious, but it serves here as an excellent example of the methodology. We therefore study the following **Cahn–Hilliard equation** in one spatial dimension:

$$\frac{\partial C}{\partial t} = \nabla^2 \left(C^3 - C - \gamma \nabla^2 C \right), \qquad t > 0, \qquad x \in (0, L), \tag{7.1}$$

with initial date $C(x, t = 0) = C_{\text{init}}(x)$ and periodic boundary conditions on the interval $(0, L)$. Also, D and γ are positive constants.

It can be seen that the Cahn–Hilliard equation is mass-conserving,

$$\frac{d}{dt} \int_0^L C(x,t)\,\mathrm{d}x = 0 \tag{7.2}$$

In this example, we take

$$\int_0^L C(x,t)\,\mathrm{d}x = 0,$$

corresponding to a **symmetric mixture**. It can also be seen that the state $C(x,t) = C_0$, with C_0 is a solution of the Cahn–Hilliard equation for a symmetric mixture, and that the state is linearly unstable with respect to small-amplitude perturbations. For, starting with the trial solution $C(x,t) = C_0 + \epsilon e^{\nu + ikx}$, the growth rate ν satisfies the dispersion relation

$$\nu = Dk^2(1 - \gamma k^2),$$

with cutoff wavenumber $k_c = \gamma^{1/2}$ and most-dangerous mode $k_{\max} = k_c/\sqrt{2}$.

We now explore the weakly nonlinear dynamcis of Equation (7.1). For simplicity, we will examine a scenario where the set of fast modes comprises a single normal mode, and that all other modes are damped according to linear theory. This corresponds to a situation just above criticality. The application of weakly nonlinear theory to this scenario where the set of fast modes contains only one element is called **Stuart–Landau theory**. Parameters appropriate for this regime are $L = 1$ and $\gamma = 1/8\pi^2$. The most-dangerous mode therefore occurs at $k_1 = 2\pi$ and the cutoff is at $k_c = \sqrt{2}k_1$, with $k_1 < k_c < 2k_1$, such that precisely one unstable mode fits inside the box.

The complete solution of Eq. (7.1) is expanded as a Fourier series,

$$C(x,t) = \sum_{n=-\infty}^{\infty} A_n(t) e^{ik_n x}, \qquad k_n = (2\pi/L)n, \qquad A_{-n} = A_n^*, \tag{7.3}$$

with $A_0 = 0$ for symmetric mixtures. The solution (7.3) is substituted into Equation (7.1). One obtains the following amplitude equations:

$$\frac{dA_n}{dt} = \nu(k_n)A_n - Dk_n^2 \sum_{p=-\infty}^{\infty} \sum_{q=-\infty}^{\infty} A_p A_q A_{n-p-q}. \tag{7.4}$$

Equation (9.5) is an example of a nonlinearity by way of a **four-wave interaction**. Four-wave interactions are the hallmark of a cubic nonlinearity. Now, for a barely-supercritical system, the fundamental mode ($n = \pm 1$) has a positive linear growth rate, while all other modes have a negative linear growth rate. Initially therefore, the fundamental dominates the evolution. Overtones will only be relevant if they couple to the fundamental. We therefore simplify Eq. (9.5) by considering the dominant modes. These will be the fundamental and a handful of overtones. In fact, we reduce

the equations down to a triple by considering the fundamental and the $n = 2, 3$ overtones, and by neglecting all other modes. A further simplification occurs in the overtone equations, wherein one considers the most-dominant interaction terms only; *i.e.* those that involve a power of A_1. One arrives at the following set of equations

$$\frac{dA_1}{dt} = \nu(k_1)A_1 - Dk_1^2 A_1 \left(6|A_2|^2 + 6|A_3|^2 + 3|A_1|^2\right) - 3Dk_1^2 A_3 A_1^{*2}, \tag{7.5a}$$

$$\frac{dA_2}{dt} = \nu(k_2)A_2 - 6Dk_2^2|A_1|^2 A_2, \tag{7.5b}$$

$$\frac{dA_3}{dt} = \nu(k_3)A_3 - Dk_3^2 A_1^3. \tag{7.5c}$$

Because of the cubic interaction, a strange thing occurs, whereby the right-hand side of the A_2 equation is proportional to A_2 itself, meaning that the amplitude $|A_2|$ can be controlled in the following manner:

$$\tfrac{1}{2}\frac{d}{dt}|A_2|^2 = \left(\nu(k_2) - 6Dk_2^2|A_1|^2\right)|A_2|^2 \leq \nu(k_2)|A_2|^2,$$

By Gronwall's inequality, we have the following further inequality:

$$|A_2(t)| \leq |A_2(0)|e^{\nu(k_2)t},$$

which is exponentially decaying because only the fundamental is linearly unstable. Thus, in the set of modes $\{A_1, A_2, A_3\}$, the mode A_2 is decaying. In contrast, the right-hand side of the A_3-equation is **not** proportional to A_3, and the corresponding amplitude is not controlled. Indeed, Equation (7.5b) is a first-order homogeneous ODE for A_2, while the corresponding equation for A_3 is first-order and inhomogeneous, with solution

$$A_3 = A_3(0)e^{\nu(k_3)t} - Dk_3^2 e^{\nu(k_3)t} \int_0^t e^{-\nu(k_3)s}[A_1(s)]^3 \, ds. \tag{7.6}$$

We now invoke the separation-of-timescales argument, assuming that $|\nu(k_1)/\nu(k_2)| \ll 1$, and $|\nu(k_1)/\nu(k_3)| \ll 1$, with $\nu(k_1) > 0$ and the other two growth rates negative. It is as if we are taking the limit $\nu(k_2) \to -\infty$ and $\nu(k_3) \to -\infty$. In this limit, the A_2 mode is damped rapidly to zero, so that under separation of scales, we have

$$A_2 = 0.$$

Consideration is given to Equation (7.6) in the same limit. In this limit, the most-rapidly varying term in the integral is $e^{-\nu(k_3)s}$, compared to which $A_1(s)$ varies slowly and can be taken outside the

integral, leaving

$$
\begin{aligned}
A_3(t) &= A_3(0)e^{\nu(k_3)t} - Dk_3^2 e^{\nu(k_3)t} \int_0^t e^{-\nu(k_3)s}[A_1(s)]^3 \, ds, \\
&\approx A_3(0)e^{\nu(k_3)t} - Dk_3^2 e^{\nu(k_3)t}[A_1(t)]^3 \int_0^t e^{-\nu(k_3)s} \, ds, \\
&= A_3(0)e^{\nu(k_3)t} + \frac{Dk_3^2}{\nu(k_2)} e^{\nu(k_3)t}[A_1(t)]^3 \left(e^{-\nu(k_3)t} - 1\right), \\
&= \frac{Dk_3^2}{\nu(k_2)}[A_1(t)]^3 + \left[A_3(0)e^{\nu(k_3)t} - \frac{6Dk_3^2}{\nu(k_2)}[A_1(t)]^3 e^{\nu(k_3)t}\right],
\end{aligned}
$$

which in the limit of infinite separation of scales reduces to

$$
A_3(t) = \frac{Dk_3^2}{\nu(k_2)}[A_1(t)]^3.
$$

Summarizing, in the limit of infinite separation of scales, we have

$$
A_2 = 0, \qquad A_3(t) = \frac{Dk_3^2}{\nu(k_2)}[A_1(t)]^3 := CA_1^3. \tag{7.7}
$$

These identities are now substituted back into Equation (7.5a) for A_1, which now is constituted in closed form:

$$
\begin{aligned}
\frac{dA_1}{dt} &= \nu(k_1)A_1 - Dk_1^2 A_1 \left(3|A_1|^2 + 6C^2|A_1|^6\right) - 3CA_1|A_1|^2, \\
&= \nu(k_1)A_1 - Dk_1^2 A_1 \left(3|A_1|^2 + 3C|A_1|^4 + 6C^2|A_1|^6\right). \tag{7.8}
\end{aligned}
$$

A solution to the A_1-equation is readily available in closed form, and backsubstitution into Equation (7.7) yields A_3. Thus, under the separation-of-scales assumption, A_3 does not evolve dynamically – it is **slaved** to the mode A_1. Also, from Equation (7.8), we can see that

$$
\tfrac{1}{2}\frac{d}{dt}|A_1|^2 = \nu(k_1)|A_1|^2 - Dk_1^2|A_1|^2 \mathcal{P}(|A_1|^2),
$$

where

$$
\mathcal{P}(x^2) = 3x^2 + 3Cx^4 + 6C^2x^6 \geq 0
$$

meaning that exponential linear growth term $\nu(k_1)|A_1|^2$ is eventually balanced by the nonlinear term $Dk_1^2|A_1|^2\mathcal{P}(|A_1|^2)$ and the nonlinearity in this instance is **saturating**.

The theory can be extended to involve the five modes $\{A_1, A_2, A_3, A_4, A_5\}$, leading to the following

amplitude equations:

$$
\begin{aligned}
\frac{dA_1}{dt} &= \nu(k_1)A_1 - Dk_1^2 A_1 \left(3|A_1|^2 + 6|A_2|^2 + 6|A_3|^2 + 6|A_4|^2 + 6|A_5|^2\right) \\
&\quad -3Dk_1^2 A_3(A_1^{*2} + 2A_2A_4^* + A_3A_5^*) - 6Dk_1^2 A_4(A_1^*A_2^* + A_2A_5^*) \\
&\quad -3Dk_1^2 A_5(A_2^{*2} + 2A_1^*A_3^*),
\end{aligned}
\tag{7.9}
$$

$$
\frac{dA_2}{dt} = \nu(k_2)A_2 - 6Dk_2^2|A_1|^2 A_2,
\tag{7.10}
$$

$$
\frac{dA_3}{dt} = \nu(k_3)A_3 - Dk_3^2 A_1^3,
\tag{7.11}
$$

$$
\frac{dA_4}{dt} = \nu(k_4)A_4 - 3Dk_2^2 A_1^2 A_2,
\tag{7.12}
$$

$$
\frac{dA_5}{dt} = \nu(k_5)A_5 - 3Dk_5^2 A_1^2 A_3,
\tag{7.13}
$$

where in the equations for the harmonics we have kept only those interaction terms that involve the highest powers of A_1 and A_1^*.

Again, in the limit of infinite separation of scales, we have $A_2 \to 0$ and hence by recursion, $A_4 \to 0$, and thus we reduce to a triple of equations for **odd modes**:

$$
\begin{aligned}
\frac{dA_1}{dt} &= \nu(k_1)A_1 - Dk_1^2 A_1 \left(3|A_1|^2 + 6|A_3|^2 + 6|A_5|^2\right) \\
&\quad -3Dk_1^2 A_3(A_1^{*2} + A_3A_5^*) - 6Dk_1^2 A_1^*A_3^*A_5,
\end{aligned}
\tag{7.14}
$$

$$
\frac{dA_3}{dt} = \nu(k_3)A_3 - Dk_3^2 A_1^3,
\tag{7.15}
$$

$$
\frac{dA_5}{dt} = \nu(k_5)A_5 - 3Dk_5^2 A_1^2 A_3.
\tag{7.16}
$$

The limit of infinite separation-of-scales is invoked again and we obtain

$$
A_3 = \frac{Dk_3^2}{\nu(k_3)} A_1^3, \qquad A_5 = \frac{3D^2 k_5^2 k_3^2}{\nu(k_3)\nu(k_5)} A_1^5.
\tag{7.17}
$$

Thus, we have $A_n \propto A_1^n$, valid clearly (by recursion) for all $n \in \{3, 5, 7, \cdots\}$. This is a hallmark of the Stuart–Landau theory: **the amplitude of the harmonics is a power of the amplitude of the fundamental**. The Stuart–Landau law (7.17) is substituted back into Equation (7.14). One obtains

$$
\frac{dA_1}{dt} = \nu(k_1)A_1 - Dk_1^2 A_1 \mathcal{Q}(|A_1|^2),
\tag{7.18}
$$

where again, $\mathcal{Q} \geq 0$ and the nonlinearity is **saturating**.

The theory in Equations (7.17)–(7.18) is now checked against numerical simulation. The numerical simulation is carried out with the FDCH parallel Cahn–Hilliard solver [NSN15]. The numerical

simulation seeded with the initial condition

$$C_{\text{init}} = \epsilon \cos(k_1 x), \qquad \epsilon = 10^{-4}. \tag{7.19}$$

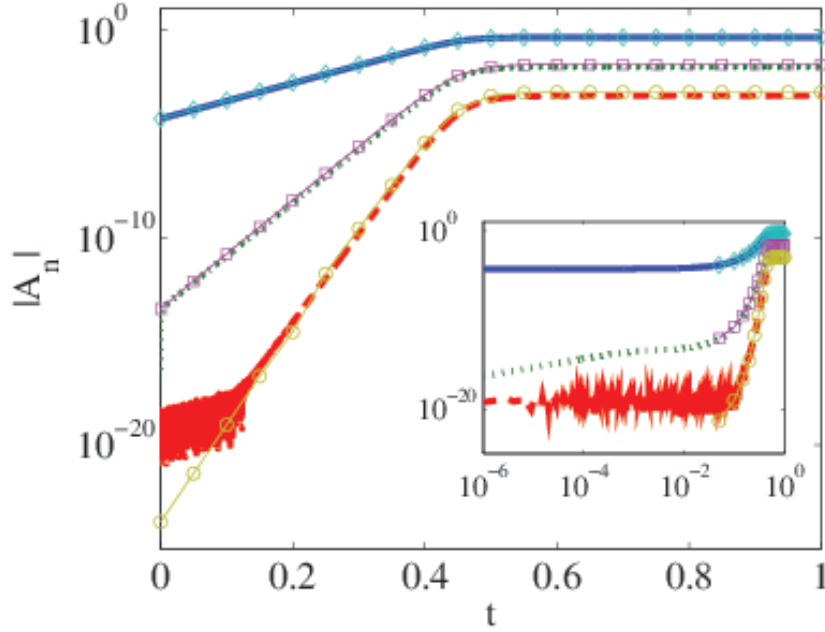A spectral analysis of the numerical solution was obtained and the results plotted in Fig. 7.1. An

Figure 7.1: (Figure from Reference [NSN15]). Comparison between weakly linear theory and direct numerical simulation. Model parameters: $D = 1$, $L = 1$, and $\gamma = 1/8\pi^2$. Simulation parameters: $\Delta x = 1/304$, $\Delta t = 10^{-8}$. The simulation results are shown in thick lines: solid line: $|A_1|$, dotted line: $|A_3|$, dashed line: $|A_5|$. The predictions from weakly nonlinear theory are shown in thin lines with symbols. Squares and circles: predictions based on Equation (7.17) for $|A_3|$ and $|A_5|$ respectively. Diamonds: prediction based on Equation (7.18) for $|A_1|$. The main figure is presented again in the inset using a log-log scale to show the initial layer of the dynamics before the onset of slaving.

additional log-log plot shown in the inset of the same figure reveals the presence of odd-numbered harmonics even at $t = 0$. This is due to roundoff error in the simulation (the simulations used the IEEE double precision format). A combination of roundoff error and numerical error also leads to the the presence of some transient noise in the amplitude $|A_5|$. However, these effects are rapidly dissipated, such that the eventual outcome of the simulation demonstrates excellent agreement between the theory based on Equations (7.17)–(7.18) and the FDCH code.

7.3   General theory

The general theory of slaving involves a set of ODEs,

$$\frac{dx}{dt} = f(x, y), \qquad x \in \mathbb{C}^n, \tag{7.20a}$$

$$\frac{dy}{dt} = -\frac{1}{\epsilon}Dy + g(x, y), \qquad y \in \mathbb{C}^m, \tag{7.20b}$$

valid for $t > 0$, with initial data

$$x(t = 0) = x_0, \qquad y(t = 0) = y_0. \tag{7.20c}$$

where D is a diagonal matrix with $D_{ii} > 0$.

An implicit solution of the y-equation is obtained as follows:

$$y_i(t) = y_i(0)e^{-tD_{ii}/\epsilon} + e^{-tD_{ii}/\epsilon} \int_0^t e^{-tD_{ii}/\epsilon} g_i(x(s), y(s)) \, ds$$

Clearly, $y_i(t)$ varies on two timescales: the rapid timescale $1/\epsilon$, and the slow timescale which is $O(1)$, and we write

$$y_i(t) = y_i(t, t/\epsilon),$$

such that

$$y_i(t) = y_i(0)e^{-tD_{ii}/\epsilon} + e^{-tD_{ii}/\epsilon} \int_0^t e^{tD_{ii}/\epsilon} g_i(x(t), y(t, t/\epsilon)) \, dt$$

suppressing the difference between the dummy variable of integration and t for the time being. We make the substitution $\tilde{t} = t/\epsilon$. Thus,

$$y_i(t) = y_i(0)e^{-tD_{ii}/\epsilon} + \epsilon e^{-tD_{ii}/\epsilon} \int_0^{t/\epsilon} e^{\tilde{t}D_{ii}} g_i(x(\epsilon\tilde{t}), y(\epsilon\tilde{t}, \tilde{t})) \, d\tilde{t}.$$

We now solve the integral equation recursively. To lowest order in ϵ, we have

$$y_i(t) = y_i(0)e^{-tD_{ii}/\epsilon} + \epsilon e^{-tD_{ii}/\epsilon} \int_0^{t/\epsilon} e^{\tilde{t}D_{ii}} g_i(x(\epsilon\tilde{t}), y_i(0)e^{-tD_{ii}\tilde{t}}) \, d\tilde{t}.$$

We take $\epsilon^a < t$, where $a < 1$. Then the first term is bounded by

$$y_i(0)e^{-D_{ii}/\epsilon^{1-a}} \to 0, \qquad \epsilon \to 0,$$

such that

$$y_i(t) \to \epsilon e^{-tD_{ii}/\epsilon} \int_0^{t/\epsilon} e^{\tilde{t}D_{ii}} g(x(\epsilon\tilde{t}), 0) d\tilde{t} = e^{-tD_{ii}/\epsilon} \int_0^t e^{tD_{ii}/\epsilon} g_i(x(t), 0) dt, \qquad \epsilon \to 0,$$

and provided $t < 1/\epsilon$ the term $g(x(t), 0)$ can be treated as a constant, leaving

$$y_i(t) \to e^{-tD_{ii}/\epsilon} g_i(x(t), 0) \int_0^t e^{tD_{ii}/\epsilon} dt \qquad \epsilon \to 0,$$

leaving

$$y_i(t) \sim \frac{\epsilon}{D_{ii}} g_i(x(t), 0), \qquad t < 1/\epsilon, \qquad \epsilon \to 0,$$

which is the final result.

7.4 Example – Kuramoto–Sivashinsky equation

Consider the following longwave model for waves on a thin film in the presence of surface tension and inertia, taken from Reference [BCF95]:

$$\frac{\partial h}{\partial t} + \frac{\partial}{\partial x} \left[c_0 h + h^2(V + hW) + Re(R + hT)\frac{\partial h}{\partial x} + M\frac{\partial^2 h}{\partial x^2} + \frac{ReS}{We}\frac{\partial^3 h}{\partial x^3} \right] = 0,$$

$$x \in (0, L), \qquad t > 0, \quad (7.21)$$

with applied periodic boundary conditions in the x direction. Here $\{c_0, V, W, Re, R, T, M, S, We\}$ are positive real constants of the model.

Exercise 7.1 *Compute the dispersion relation for the linearized equation of motion.*

Answer clue:
$$\nu = ik(-c_0 + Mk^2) + Re\, k^2 \left(R - \frac{S}{We}k^2 \right).$$

Exercise 7.2 *Show that the amplitude equation corresponding to Equation* (7.21) *is*

$$\frac{dA_n}{dt} = \nu A_n + (i\alpha + n\beta) \sum_{p=-\infty}^{\infty} pA_p A_{n-p} + i\chi \sum_{p=-\infty}^{\infty} \sum_{q=-\infty}^{\infty} pA_p A_q A_{n-p-q}, \qquad (7.22)$$

where

$$\alpha = k_1 V, \qquad \beta = \tfrac{1}{2}k_1^2 Re\, T, \qquad \chi = \tfrac{3}{4}ik_1 W$$

and where k_1 is the fundamental wavenumber.

Exercise 7.3 *Assume that the fundamental is a standing wave, with $c_0 = Mk_1^2$. By keeping only*

the first three modes, and by taking $\delta = Mk_1^3$, derive the following amplitude equations:

$$\frac{dA_1}{dt} = \sigma_1 A_1 + (\mathrm{i}\alpha + \beta)A_1^* A_2 + \mathrm{i}\chi A_1^2 A_1^*, \tag{7.23a}$$

$$\frac{dA_2}{dt} = (\sigma_2 - 6\mathrm{i}\delta)A_2 + (\mathrm{i}\alpha + 2\beta)A_1^2, \tag{7.23b}$$

$$\frac{dA_3}{dt} = (\sigma_3 - 24\mathrm{i}\delta)A_3 + 3(\mathrm{i}\alpha + 3\beta)A_1 A_2 + \mathrm{i}\chi A_1^3, \tag{7.23c}$$

where $\sigma_n = \Re[\nu(k_n)]$.

Exercise 7.4 *Working near criticality, with $\sigma_1 > 0$, $\sigma_n < 0$, and $|\sigma_n| \gg \sigma_1$ for $n \geq 2$ argue as before that*

$$A_n \propto A_1^n, \qquad n \geq 2.$$

Chapter 8

Direct numerical simulation of the incompressible Navier–Stokes equations

8.1   Overview

In this section we outline a numerical method to solve the incompressible Navier–Stokes equations. The method will be broken down piece-by-piece and numerical algorithms to solve each piece will be introduced. Analysing and implementing these algorithms will be the subject of this and future chapters. The aim is to develop a complete understanding of a parallel DNS solver called TPLS.

8.2   The basic equations

We start with the incompressible Navier–Stokes in non-dimensional form:

$$\frac{\partial \boldsymbol{u}}{\partial t} + \boldsymbol{u} \cdot \nabla u = -\nabla q + \frac{1}{Re} \nabla \cdot \left[\mu \left(\nabla \boldsymbol{u} + \nabla \boldsymbol{u}^{T} \right) \right] \qquad \nabla \cdot \boldsymbol{u} = 0, \qquad t > 0, \qquad (8.1)$$

with initial conditions

$$\boldsymbol{u}(\boldsymbol{x}, t = 0) = \boldsymbol{u}_0, \qquad q(\boldsymbol{x}, t = 0) = q_0, \qquad \nabla \cdot \boldsymbol{u}_0 = 0,$$

defined on the domain $(x, y, z) \in [0, L_x] \times [0, L_y] \times [01]$. For definiteness, we work in a channel geometry, with the following boundary conditions:

$$\boldsymbol{u}(z = 0) = \boldsymbol{u}(z = 1) = 0,$$

and with periodic boundary conditions in the other two directions. Ordinarily, the viscosity μ is a constant; however, it is treated here as a quantity that potentially varies in space and time, meaning

that our discussion is quite general, and can be extended to large-eddy simulations and Reynolds-averaged simulation modelling of turbulence. A schematic of the computational domain is illustrated
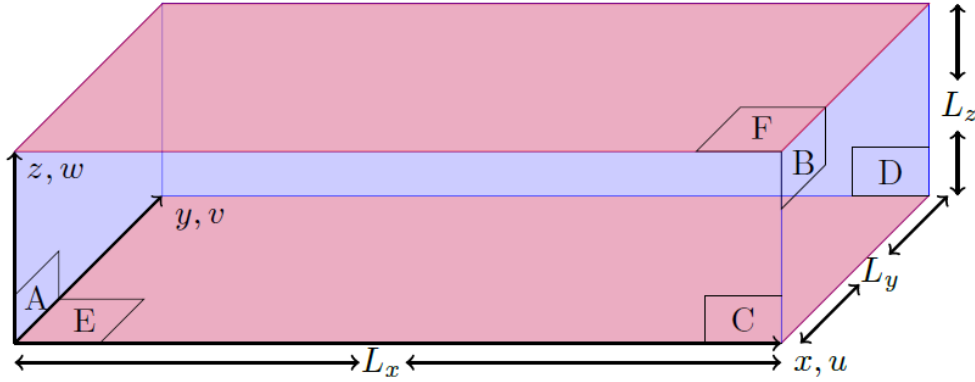

Figure 8.1: (Picture thanks to James Fannon) Computational domain $\Omega = [0, L_x] \times [0, L_y] \times [0, L_z = 1]$. Periodic boundary conditions are used in the streamwise (faces AB) and spanwise (faces CD) directions, while no-slip boundary conditions are used on faces E and F.

in figure 8.1, where the length scale is normalised with respect to the channel height i.e. $L_z = 1$.

A driving force is introduced in the streamwise (x-direction), such that

$$q(\boldsymbol{x}, t) = p(\boldsymbol{x}, t) - |dP/dL|x,$$

where $|dP/dL|$ is the constant pressure drop. Thus, the equations to be solved now read

$$\frac{\partial \boldsymbol{u}}{\partial t} + \boldsymbol{u} \cdot \nabla u = -\nabla p + \frac{1}{Re} \nabla \cdot \left[\mu \left(\nabla \boldsymbol{u} + \nabla \boldsymbol{u}^T \right) \right] + \hat{x}|dP/dL|, \qquad \nabla \cdot \boldsymbol{u} = 0, \qquad t > 0. \quad (8.2)$$

It is difficult to evolve these equations forward in time because there is no explicit equation for p. The solution to this problem is to use a **projection method**. This will be done in tandem with a finite-volume discretization.

8.3   The method

We employ a uniform finite-volume discretization. This is similar in spirit to a uniform finite-difference discretization, except that more attention is paid to the physics of each computational cell. Each cell is of size Δx^3, but now scalar quantities are defined at cell centres and vector quantities on the appropriate cell faces. In this way, the divergence of a vector flux is automatically defined at cell centres and also, is automatically computed by a centred finite difference, which has higher-order accuracy than a more naive approach, and also takes account of the physics of the fluxes flowing
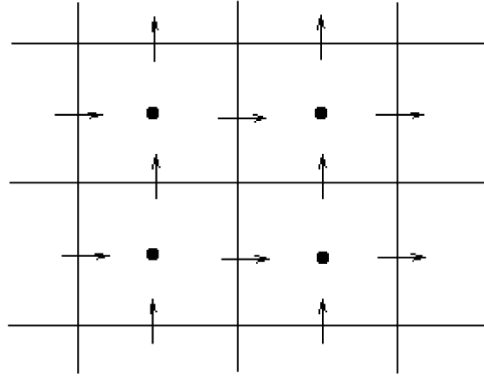
Two-dimensional staggered grid on which flow variables are defined: ↑, vertical component of velocity; →, horizontal component of velocity; •, scalar variables (pressure and volume fraction).

Figure 8.2: Schematic description of a two-dimensionial MAC grid

into and out of each computational cell. A schematic description of this setup is given in Figure 8.2. This choice of grid is called a **marker-and-cell** (MAC) grid.

To evolve the equations forward in time, operator-splitting is carried out in two distinct half-steps. In the first half-step, an intermediate velocity $\boldsymbol{u}^*$ is computed by momentarily ignoring the pressure contribution in the momentum equation:

$$\boldsymbol{u}^* - \boldsymbol{u}^n = -\boldsymbol{u} \cdot \nabla \boldsymbol{u} + \frac{1}{Re} \nabla \cdot \left[\mu \left(\nabla \boldsymbol{u} + \nabla \boldsymbol{u}^T \right) \right].$$

The precise manner in which $\boldsymbol{u}^*$ is extracted from this equation is discussed below. We first of all however describe the second half-step which is got by considering the pressure contribution:

$$\frac{\boldsymbol{u}^{n+1} - \boldsymbol{u}^*}{\Delta t} = -\nabla p^{n+1} + |dP/dL|\hat{\boldsymbol{x}}. \tag{8.3}$$

We take the divergence on both sides and impose the constraint that $\nabla \cdot \boldsymbol{u}^{n+1} = 0$, leading to

$$\nabla p^{n+1} = \frac{\nabla \cdot \boldsymbol{u}^*}{\Delta t}. \tag{8.4}$$

By solving the Poisson equation (8.4) the pressure at timestep $n+1$ is obtained. This is then substituted back into Equation (8.3) to give

$$\boldsymbol{u}^{n+1} = \boldsymbol{u}^* - \Delta t \nabla p^{n+1} + \Delta t |dP/dL|\hat{\boldsymbol{x}}.$$

We now describe in detail the implementation of the momentum half-step.

8.4   Discretzation of the momentum half-step in space and time

Recall, in the momentum half-step, the equation

$$\frac{\boldsymbol{u}^* - \boldsymbol{u}^n}{\Delta t} + \boldsymbol{u} \cdot \nabla \boldsymbol{u} = \frac{1}{Re} \nabla \cdot \left[\mu \left(\nabla \boldsymbol{u} + \nabla \boldsymbol{u}^T \right) \right] \tag{8.5}$$

is solved for $\boldsymbol{u}^*$. Here, μ is the (possibly varying) viscosity, defined at cell centres. Below we show how Equation (8.5) is disctetized in space and time.

Temporal discretization

The viscous term is broken up first of all into contributions that are more convective in nature and other contributions that can be treated are more of a diffusive character. The more convective parts are identified as

$$\frac{1}{Re} \frac{\partial}{\partial x_i} \left(\mu \frac{\partial u_i}{\partial x_j} \right), \qquad j = 1, 2, 3,$$

while the more diffusive parts are identified as

$$\frac{1}{Re} \frac{\partial}{\partial x_i} \left(\mu \frac{\partial u_j}{\partial x_i} \right) := \boldsymbol{\mathcal{D}} \left(\boldsymbol{u} \right), \qquad j = 1, 2, 3.$$

For example, for $j = 1$ (with $\boldsymbol{u} = (u, v, w)$), the more convective parts are

$$\frac{1}{Re} \left[\frac{\partial}{\partial x} \left(\mu \frac{\partial u}{\partial x} \right) + \frac{\partial}{\partial y} \left(\mu \frac{\partial v}{\partial x} \right) + \frac{\partial}{\partial z} \left(\mu \frac{\partial w}{\partial x} \right) \right]$$

and the more diffusive parts are

$$\frac{1}{Re} \left[\frac{\partial}{\partial x} \left(\mu \frac{\partial u}{\partial x} \right) + \frac{\partial}{\partial y} \left(\mu \frac{\partial u}{\partial y} \right) + \frac{\partial}{\partial z} \left(\mu \frac{\partial u}{\partial z} \right) \right] := \mathcal{D}_1(\boldsymbol{u}).$$

Thus, Equation (8.5) is rewritten as

$$\frac{\boldsymbol{u}^* - \boldsymbol{u}^n}{\Delta t} = \left[-\boldsymbol{u} \cdot \nabla \boldsymbol{u} + \frac{\boldsymbol{e}_j}{Re} \frac{\partial}{\partial x_i} \left(\mu \frac{\partial u_i}{\partial x_j} \right) \right] + \boldsymbol{\mathcal{D}} \left(\boldsymbol{u} \right). \tag{8.6}$$

where $\boldsymbol{e}_j$ is a unit vector in the jth Cartesian direction. The terms in the square bracket are now bundled together as a convective term $\boldsymbol{\mathcal{C}}$ and Equation (8.6) is discretized in time using Adams–Bashforth discretization on convective terms and Crank–Nicholson discretization on the diffusive

contribution, giving

$$\boldsymbol{u}^* = \boldsymbol{u}^n + \Delta t \left(\boldsymbol{C}^n - \tfrac{4}{3}\boldsymbol{C}^{n-1} + \tfrac{5}{12}\boldsymbol{C}^{n-2}\right) + \tfrac{1}{2}\Delta t \left[\boldsymbol{\mathcal{D}}(\boldsymbol{u}^*) + \boldsymbol{\mathcal{D}}(\boldsymbol{u}^n)\right],$$

where $\mathcal{D}(\cdot)$ is identified as a linear operator. Thus,

$$\left[\mathbb{I} - \tfrac{1}{2}\Delta t \boldsymbol{\mathcal{D}}\right] \boldsymbol{u}^* = \Delta t \left(\boldsymbol{C}^n - \tfrac{4}{3}\boldsymbol{C}^{n-1} + \tfrac{5}{12}\boldsymbol{C}^{n-2}\right) + \tfrac{1}{2}\Delta t \boldsymbol{\mathcal{D}}(\boldsymbol{u}^n) := \mathrm{RHS},$$

or

$$\left[\mathbb{I} - \tfrac{1}{2}\Delta t \boldsymbol{\mathcal{D}}\right] \boldsymbol{u}^* = \mathrm{RHS}. \tag{8.7}$$

Spatial discretization

Equation (8.7) is now discretized, using a flux-conservative treatment for the diffusion terms. What this means is explained in the context of the particular equation in the x-direction. Here, we are working on the u-grid. We have

$$\mathcal{D}_1(u) = \frac{\mu_{+(1/2)x}\frac{\partial u}{\partial x}\big|_{+1/2} - \mu_{-(1/2)x}\frac{\partial u}{\partial x}\big|_{+1/2}}{\Delta x} + \frac{\mu_{+(1/2)y}\frac{\partial u}{\partial y}\big|_{+1/2} - \mu_{-(1/2)y}\frac{\partial u}{\partial y}\big|_{+1/2}}{\Delta y}$$
$$+ \frac{\mu_{+(1/2)z}\frac{\partial u}{\partial z}\big|_{+1/2} - \mu_{-(1/2)z}\frac{\partial u}{\partial z}\big|_{+1/2}}{\Delta z},$$

where

$$\mu_{+(1/2)x} = \mu_{i+1,j+1,k+1},$$
$$\mu_{-(1/2)x} = \mu_{i,j+1,k+1},$$
$$\mu_{+(1/2)y} = \tfrac{1}{4}\left[\mu_{i,j+1,k+1} + \mu_{i+1,j+1,k+1} + \mu_{i,j+2,k+1} + \mu_{i+1,j+2,k+1}\right],$$
$$\mu_{-(1/2)y} = \tfrac{1}{4}\left[\mu_{i,j+1,k+1} + \mu_{i+1,j+1,k+1} + \mu_{i,j,k+1} + \mu_{i+1,j,k+1}\right],$$
$$\mu_{+(1/2)z} = \tfrac{1}{4}\left[\mu_{i,j+1,k+1} + \mu_{i+1,j+1,k+1} + \mu_{i,j+1,k+2} + \mu_{i+1,j+1,k+2}\right],$$
$$\mu_{-(1/2)z} = \tfrac{1}{4}\left[\mu_{i,j+1,k+1} + \mu_{i+1,j+1,k+1} + \mu_{i,j+1,k} + \mu_{i+1,j+1,k}\right]$$

are the viscosity interpolated linearly on to the u-grid, and

$$
\left.\frac{\partial u}{\partial x}\right|_{+1/2} = \frac{u_{i+1,j,k} - u_{i,j,k}}{\Delta x},
$$

$$
\left.\frac{\partial u}{\partial x}\right|_{-1/2} = \frac{u_{i,j,k} - u_{i-1,j,k}}{\Delta x},
$$

$$
\left.\frac{\partial u}{\partial y}\right|_{+1/2} = \frac{u_{i,j+1,k} - u_{i,j,k}}{\Delta y},
$$

$$
\left.\frac{\partial u}{\partial y}\right|_{-1/2} = \frac{u_{i,j,k} - u_{i,j-1,k}}{\Delta y},
$$

$$
\left.\frac{\partial u}{\partial z}\right|_{+1/2} = \frac{u_{i,j,k+1} - u_{i,j,k}}{\Delta z},
$$

$$
\left.\frac{\partial u}{\partial z}\right|_{-1/2} = \frac{u_{i,j,k} - u_{i,j,k-1}}{\Delta z},
$$

Putting these rules together with Equation (8.7), the linear equation to solve is

$$
\left[1 + \mu_{+(1/2)x}(\alpha/2) + \mu_{-(1/2)x}(\alpha/2) + \mu_{+(1/2)y}(\alpha/2) + \mu_{-(1/2)y}(\alpha/2) + \mu_{+(1/2)z}(\alpha/2) + \mu_{-(1/2)z}(\alpha/2)\right] u^*_{ijk}
$$
$$
= \mathrm{RHS}_{ijk} + (\alpha/2)\mu_{+(1/2)x}u^*_{i+1,j,k} + (\alpha/2)\mu_{-(1/2)x}u^*_{i-1,j,k} + (\alpha/2)\mu_{+(1/2)y}u^*_{i,j+1,k} + (\alpha/2)\mu_{-(1/2)y}u^*_{i,j-1,k} +
$$
$$
(\alpha/2)\mu_{+(1/2)z}u^*_{i,j,k+1} + (\alpha/2)\mu_{-(1/2)z}u^*_{i,j,k-1},
$$

where $\alpha = \Delta t/\Delta x^2$, and $\Delta x = \Delta y = \Delta z$. Calling

$$
\mathrm{Diagonal} = 1 + \mu_{+(1/2)x}(\alpha/2) + \mu_{-(1/2)x}(\alpha/2) + \mu_{+(1/2)y}(\alpha/2) + \mu_{-(1/2)y}(\alpha/2) + \mu_{+(1/2)z}(\alpha/2) + \mu_{-(1/2)z}(\alpha/2)
$$

we have

$$
u^*_{ijk} = \frac{(\alpha/2)\mu_{+(1/2)x}u^*_{i+1,j,k} + (\alpha/2)\mu_{-(1/2)x}u^*_{i-1,j,k} + (\alpha/2)\mu_{+(1/2)y}u^*_{i,j+1,k} + (\alpha/2)\mu_{-(1/2)y}u^*_{i,j-1,k}}{\mathrm{Diagonal}}
$$
$$
+ \frac{(\alpha/2)\mu_{+(1/2)z}u^*_{i,j,k+1} + (\alpha/2)\mu_{-(1/2)z}u^*_{i,j,k-1} + \mathrm{RHS}_{ijk}}{\mathrm{Diagonal}} \quad (8.8)
$$

Boundary condition

In a MAC grid, the x-index will range from $i = 0, \cdots, \ell$, the y-index from $j = 0, \cdots, m$, and the z-index from $k = 0, \cdots, n$ **at cell centres**. However, each velocity grid will have its own range of indices; in particular, the index k ranges from $k = 0$ to $k = n - 2$ on the u-grid. A sketch of the MAC grid (e.g. the schematic diagram in Section 8.5, below) indicates that u at $k = 0$ and $n - 2$ corresponds to a location half a grid-spacing away from the wall. Thus, it is not physical to

implement a no-slip condition at $k = 0$ and $n - 2$. Instead, we use linear interpolation to define u at 'ghost' cells at fictitious sites at $k = -1$ and $k = n - 1$ as follows. If $k = 0$, then we are at $z = \Delta x/2$ away from the bottom wall, and we therefore take

$$u_{-z} = \begin{cases} -2u_{i,j,0} + \frac{1}{3}u_{i,j,1}, & k = 0, \\ u_{i,j,k-1}, & \text{otherwise.} \end{cases} \tag{8.9}$$

If $k = n - 2$, then we are at at $z = 1 - \Delta x/2$ away from the top wall, and we therefore take

$$u_{+z} = \begin{cases} -2u_{i,j,n-2} + \frac{1}{3}u_{i,j,n-3}, & k = n - 2, \\ u_{i,j,k+1}, & \text{otherwise.} \end{cases} \tag{8.10}$$

These identifications are then used to compute $(\partial u/\partial z)_{+1/2}$ and $(\partial u/\partial z)_{-1/2}$, e.g.

$$\left.\frac{\partial u}{\partial z}\right|_{+1/2} = \frac{u_{+z} - u_{ijk}}{\Delta z},$$

and

$$\left.\frac{\partial u}{\partial z}\right|_{-1/2} = \frac{u_{ijk} - u_{-z}}{\Delta z},$$

The aim of subsequent chapters is an abstract study of the Helmoholtz equation (8.7) and Poisson equation (8.4). When this is complete we will apply our knowledge to solving these particular equations and thus, to constructing a functioning flow solver.

8.5 Detailed description of a notional two-dimensional MAC grid

Two-dimensional MAC Grid

$u = m \times (n-1)$ matrix

$= 20 \times 9$ matrix

$P = (m+1) \times (n+1)$ matrix

$= 21 \times 11$ matrix

Row of fictitious u's (implicit): $u_f = -u(:,n-1)$

$u = 0$ here (no slip)

Inlet conditions

Row of fictitious pressures

Col $u(20,:)$ updated diagnostically: $u(20,:) = u(19,:)$
$\frac{\partial u}{\partial x}\big|_{19} = 0$

This col $(u(1,:))$ is a fixed inlet condition

Row of fictitious pressure

$u = 0$ (no slip)

Row of fictitious u's (implicit): $u_f = -u(:,1)$

Two-dimensional MAC Grid

$W = (m-1) \times n$ matrix

$U = 19 \times 10$ matrix

$P = (m+1) \times (n+1) = 21 \times \ldots$ matrix

f W

This row is zero (no slip)

Row of fictious pressures

Row of fictious pressure

fictious col of u's (implied): $uf = W(20,:) \ldots$ implements no flux; $\partial w/\partial x |_{19} = 0$

fictious col of w's (implied): $wf = 0$

This row is zero (no slip)

Chapter 9

Simplified model problems involving Poisson and Helmholtz equations

Overview

We consider analytical solutions to a two-dimensional diffusion problem. The reason for examining this particular problem are manifold: it is a minimal model that nonetheless has a small amount of complexity sufficient to warrant the use of a number of interesting numerical methods. Also, analytical solutions in this section will be used as benchmarks for future numerical simulation studies. Throughout this chapter and beyond, the problem considered in herein be referred to as the **model diffusion equation**.

9.1 Boundary conditions – review

For this discussion, let

$$\frac{\partial C}{\partial t} = a(x,t)\frac{\partial^2 C}{\partial x^2} + b(x,t)\frac{\partial C}{\partial x} + c(x,t)C + d(x,t), \qquad x \in (0,L), \qquad t > 0,$$

be a parabolic partial differential equation in one space dimension, on $x \in (0, L)$, with smooth initial conditions

$$C(x, t = 0) = C_{\text{init}}(x), \qquad x \in [0, L].$$

Then the following boundary conditions are possible.

1. **Dirichlet conditions** The function $C(x, t > 0)$ is specified on the boundaries:

$$
\begin{aligned}
C(0, t > 0) &= g_1(t), \\
C(L, t > 0) &= g_2(t).
\end{aligned}
$$

If the functions $g_1 = g_2 = 0$, then we have **homogeneous Dirichlet conditions**:

$$
\begin{aligned}
C(0, t > 0) &= 0, \\
C(L, t > 0) &= 0.
\end{aligned}
$$

2. **Neumann conditions**: The **derivative** $C_x(x, t > 0)$ is specified on the boundaries:

$$
\begin{aligned}
C_x(0, t > 0) &= g_1(t), \\
C_x(L, t > 0) &= g_2(t).
\end{aligned}
$$

If the functions $g_1 = g_2 = 0$, then we have **homogeneous Neumann conditions**, corresponding to **no flux through the boundaries**.

3. **Mixed conditions**: As the name suggests, this set is a mixture of Dirichlet and Neumann conditions:

$$
\begin{aligned}
\alpha_1 C_x(0, t > 0) + \alpha_2 C(0, t > 0) &= g_1(t), \\
\alpha_3 C_x(L, t > 0) + \alpha_4 C(L, t > 0) &= g_2(t).
\end{aligned}
$$

4. **Periodic boundary conditions**: The function $C(x, t > 0)$ has the same value on either boundary point:

$$
C(0, t) = C(L, t), \qquad t > 0.
$$

In practice, these are not very realistic boundary conditions but they are used in numerical experiments because they are easy to implement. However, they can be used to mimic an infinite domain, if the periodic length L is made long enough.

9.2   The model diffusion equation

We are interested in solving the following partial differential equation (PDE) for diffusion, given here in non-dimensional form as follows:

$$
\frac{\partial C}{\partial t} = \nabla^2 C + s(x, z), \qquad (x, z) \in \Omega, \tag{9.1a}
$$

where

$$\Omega = (0, L_x) \times (0, 1), \tag{9.1b}$$

and $\nabla^2 = \partial_x^2 + \partial_z^2$ is the Laplacian. The partial differential equation is subject to the following boundary conditions:

$$\frac{\partial C}{\partial z} = 0, \qquad z = 0, \qquad z = 1, \tag{9.1c}$$

together with periodic boundary conditions in the x direction:

$$C(x = 0, z, t) = C(x = L_x, z, t). \tag{9.1d}$$

Finally, an initial condition is prescribed:

$$C(x, z, t = 0) = C_{\text{init}}(x, z), \qquad (x, z) \in \overline{\Omega}, \tag{9.1e}$$

where $C_{\text{init}}(x, z)$ is a continuous function. Here, the system of equations (10.1) is made non-dimensional on the channel depth L_z (herein set to unity), and the diffusive timescale $\tau = L_z^2/D$, where D is the diffusion coefficient.

9.3   Physical interpretation

Physically, Equation (10.1) is a model for diffusion of particles in the presence of a source. The amount of matter in the system changes over time, due to contributions from the source $s(x, y, z)$. There are no contributions from the boundary conditions. For, consider the following evolution equation for the total system mass

$$M = \int_\Omega \mathrm{d}^2x \, C(x, z, t).$$

We have

$$\begin{aligned}
\frac{dM}{dt} &= \int_\Omega \mathrm{d}^2x \, \frac{\partial C}{\partial t}, \\
&= \int_\Omega \mathrm{d}^2x \, \left[\nabla^2 C + s(x, z)\right], \\
&= \int_\Omega \mathrm{d}^2x \, s(s, z) + \int_{\partial\Omega} \mathrm{d}\ell \boldsymbol{n} \cdot \nabla C,
\end{aligned}$$

where $\partial\Omega$ is the boundary of the set Ω, $\mathrm{d}\ell$ is a line element on the boundary, and $\boldsymbol{n}$ is the outward-pointing unit normal to $\partial\Omega$. We compute

$$
\int_{\partial\Omega} \mathrm{d}A\, \boldsymbol{n}\cdot\nabla C \;=\; \int_0^{L_x} \mathrm{d}x\, \left.\frac{\partial C}{\partial z}\right|_{z=1} - \int_0^{L_x} \mathrm{d}x\, \left.\frac{\partial C}{\partial z}\right|_{z=0}
$$

$$
+ \int_0^{L_z} \mathrm{d}z\, \left.\frac{\partial C}{\partial x}\right|_{x=L_x} - \int_0^{L_z} \mathrm{d}z\, \left.\frac{\partial C}{\partial x}\right|_{x=0}.
$$

However, all of these terms cancel, either because of the no-flux boundary condition $(\partial C/\partial z)(z = 0, 1) = 0$, or because of periodicity, meaning that

$$
\frac{dM}{dt} = L_x L_z \langle s \rangle, \qquad \langle s \rangle := \frac{1}{L_x L_z} \int_\Omega \mathrm{d}^2 x\, s(s, z). \tag{9.2}
$$

9.4   Decomposition

In view of the formula (9.2), it is sensible to split the solution into two parts:

$$
C = \langle C \rangle(t) + C'(x, z, t), \qquad s = \langle s \rangle + s'(x, z).
$$

By linearity,

$$
\frac{\partial}{\partial t}\langle C \rangle \;=\; \nabla^2\langle C \rangle + \langle s \rangle,
$$
$$
\frac{\partial C'}{\partial t} \;=\; \nabla^2 C' + s'.
$$

Indeed, the solution to the mean contribution is known:

$$
\langle C \rangle(t) = \langle C \rangle(t = 0) + \langle s \rangle t = \langle C_{\mathrm{init}} \rangle + \langle s \rangle t.
$$

while the PDE for the fluctuations inherits all the properties of the basic PDE (10.1), such that

$$
\frac{\partial C'}{\partial t} = \nabla^2 C' + s'(x, z), \qquad (x, z) \in \Omega, \tag{9.3a}
$$

subject to the following boundary conditions:

$$
\frac{\partial C'}{\partial z} = 0, \qquad z = 0, \qquad z = 1, \tag{9.3b}
$$

together with periodic boundary conditions in the x-direction:

$$
C'(x = 0, z, t) = C'(x = L_x, z, t). \tag{9.3c}
$$

Finally, an initial condition is prescribed:

$$C'(x, z, t = 0) = C_{\text{init}}(x, z) - \langle C_{\text{init}} \rangle, \qquad (x, z) \in \overline{\Omega}, \tag{9.3d}$$

9.5 Analytical solution

We prove the following theorem:

Theorem 9.1 *Equation* (9.3) *has at least one smooth solution, namely*

$$C'(x, z, t) = \sum_{n=1}^{\infty} \sum_{i=-\infty}^{\infty} \left\{ e^{-k_{in}^2 t} \left[a_{in}(0) - \frac{s_{in}}{k_{in}^2} \right] + \frac{s_{in}}{k_{in}^2} \right\} e^{i[(2\pi/L_x)ix]} \cos\left(\frac{n\pi z}{L_z} \right), \tag{9.4a}$$

where

$$a_{in}(0) = \frac{2}{L_x L_z} \int_0^{L_x} \int_0^{L_z} d^2 x \, e^{-i[(2\pi/L_x)ix]} \cos\left(\frac{n\pi z}{L_z} \right) \left[C_{\text{init}}(x, z) - \langle C_{\text{init}} \rangle \right], \tag{9.4b}$$

and where we have restored the definition of L_z for clarity's sake.

Proof: Take Equation (9.1a), multiply by $\cos(n\pi z/L_z)$ (with $n = 1, 2, \cdots$) and integrate with respect to z. The result is

$$\partial_t \int_0^{L_z} C' \cos\left(\frac{n\pi z}{L_z} \right) dz = \partial_x^2 \int_0^{L_z} C' \cos\left(\frac{n\pi z}{L_z} \right) dz + \int_0^{L_z} \left(\frac{\partial^2 C'}{\partial z^2} \right) \cos\left(\frac{n\pi z}{L_z} \right) dz$$
$$+ \int_0^{L_z} s(x, z) \cos\left(\frac{n\pi z}{L_z} \right) dz.$$

We call

$$\widehat{C}_n(x, t) := \frac{2}{L_z} \int_0^{L_z} C'(x, t) \cos\left(\frac{n\pi z}{L_z} \right) dz, \qquad \widehat{s}_n(x) := \frac{2}{L_z} \int_0^{L_z} s(x, z) \cos\left(\frac{n\pi z}{L_z} \right) dz;$$

hence, we have

$$\frac{\partial \widehat{C}_n}{\partial t} = \partial_x^2 \widehat{C}_n + \frac{2}{L_z} \int_0^{L_z} \left(\frac{\partial^2 C'}{\partial z^2} \right) \cos\left(\frac{n\pi z}{L_z} \right) dz + \widehat{s}_n(x). \tag{9.5}$$

Consider now the following (with $k_n = n\pi/L_z$):

$$
\begin{aligned}
\int_0^{L_z} \left(\frac{\partial^2 C'}{\partial z^2} \right) \cos\left(\frac{n\pi z}{L_z} \right) \mathrm{d}z &= \int_0^{L_z} \left\{ \frac{\partial}{\partial z}\left[\cos\left(\frac{n\pi z}{L_z} \right) \frac{\partial C'}{\partial z} \right] + k_n \sin\left(\frac{n\pi z}{L_z} \right) \frac{\partial C'}{\partial z} \right\} \mathrm{d}z, \\
&= \left[\cos\left(\frac{n\pi z}{L_z} \right) \frac{\partial C'}{\partial z} \right]_{z=0}^{z=L_z} + k_n \int_0^{L_y} \sin\left(\frac{n\pi z}{L_z} \right) \frac{\partial C'}{\partial z} \, \mathrm{d}z, \\
&= 0 + k_n \int_0^{L_z} \sin\left(\frac{n\pi z}{L_z} \right) \frac{\partial C'}{\partial z} \, \mathrm{d}z, \\
&= k_n \int_0^{L_z} \left\{ \frac{\partial}{\partial z}\left[\sin\left(\frac{n\pi z}{L_z} \right) C' \right] - k_n \cos\left(\frac{n\pi z}{L_z} \right) C' \right\} \mathrm{d}z, \\
&= \left[\sin\left(\frac{n\pi z}{L_z} \right) C' \right]_{z=0}^{z=L_z} - k_n^2 \int_0^{L_z} \cos\left(\frac{n\pi z}{L_z} \right) C'(x,z,t) \, \mathrm{d}z.
\end{aligned}
$$

Hence,

$$
\frac{2}{L_z} \int_0^{L_z} \left(\frac{\partial^2 C'}{\partial z^2} \right) \cos\left(\frac{n\pi z}{L_z} \right) \mathrm{d}z = -k_n^2 \, (2/L_z) \int_0^{L_z} \cos\left(\frac{n\pi z}{L_z} \right) C'(x,z,t) \, \mathrm{d}z = -k_n^2 \hat{C}_n.
$$

Thus, Equation (9.1a) is transformed – via Equation (9.5) to

$$
\frac{\partial \widehat{C}_n}{\partial t} + k_n^2 \widehat{C}_n = \partial_x^2 \widehat{C}_n + \widehat{s}_n(x). \tag{9.6}
$$

However, this is now a standard diffusion problem in one (periodic) dimension, which can be solved by standard Fourier-series methods: we propose

$$
\widehat{C}_n(x,t) = \sum_{i=-\infty}^{\infty} a_{in}(t) \mathrm{e}^{\mathrm{i}[(2\pi/L_x)ix]};
$$

we also decompose $\widehat{s}_n(x)$ as

$$
\widehat{s}_n(x) = \sum_{i=-\infty}^{\infty} s_{in} \mathrm{e}^{\mathrm{i}[(2\pi/L_x)ix]}.
$$

Thus, the following amplitude equations are obtained:

$$
\frac{da_{in}}{dt} = -k_{in}^2 a_{in} + s_{in}, \tag{9.7}
$$

where

$$
k_{in} = \left[\left(\frac{2\pi}{L_x} \right)^2 i^2 + \left(\frac{\pi}{L_z} \right)^2 n^2 \right]^{1/2}.
$$

Equation (9.7) has solution

$$
a_{in}(t) = \begin{cases} e^{-k_{in}^2 t} \left[a_{in}(0) - \frac{s_{in}}{k_{in}^2} \right] + \frac{s_{in}}{k_{ijn}^2}, & k_{in} \neq 0, \\ a_0(0) + s_0 t, & k_{in} = 0, \end{cases}
$$

where the second case follows because $k_{in} = 0$ if and only if $i = n = 0$. However, this case is ruled out because $n \neq 0$. Thus, the solution for $\widehat{C}_n(x, t)$ is therefore

$$
\widehat{C}_n(x, t) = \sum_{i=-\infty}^{\infty} \left\{ e^{-k_{in}^2 t} \left[a_{in}(0) - \frac{s_{in}}{k_{in}^2} \right] + \frac{s_{in}}{k_{in}^2} \right\} e^{i[(2\pi/L_x)ix]}.
$$

We now note that a cosine transform has been taken in the z-direction:

$$
\widehat{C}_n(x, t) = \frac{2}{L_z} \int_0^{L_z} \cos\left(\frac{n\pi z}{L_z}\right) C'(x, z, t)\, \mathrm{d}z, \qquad n \neq 0.
$$

However, since

$$
\left\{ \cos\left(\frac{n\pi z}{L_z}\right) \right\}_{n=1}^{\infty}
$$

is a basis for **mean-zero** continuous functions whose first derivative vanishes at $z = 0, L_z$, meaning that the cosine transform can be reversed:

$$
C'(x, z, t) = \sum_{n=1}^{\infty} \widehat{C}_n(x, t) \cos\left(\frac{n\pi z}{L_z}\right).
$$

Hence,

$$
C'(x, z, t) = \sum_{n=1}^{\infty} \sum_{i=-\infty}^{\infty} \left\{ e^{-k_{in}^2 t} \left[a_{in}(0) - \frac{s_{in}}{k_{in}^2} \right] + \frac{s_{in}}{k_{in}^2} \right\} e^{i[(2\pi/L_x)ix]} \cos\left(\frac{n\pi z}{L_z}\right).
$$

Finally, it is of interest to determine the coefficients $a_{ijn}(0)$. We have

$$
C_{\mathrm{init}}(x, z) - \langle C_{\mathrm{init}} \rangle = \sum_{n=1}^{\infty} \sum_{i=-\infty}^{\infty} a_{ij}(0) e^{i[(2\pi/L_x)ix]} \cos\left(\frac{n\pi z}{L_z}\right),
$$

hence, by Fourier transformation,

$$
a_{in}(0) = \frac{2}{L_x L_z} \int_0^{L_x} \int_0^{L_z} \mathrm{d}^2 x\, e^{-i[(2\pi/L_x)ix]} \cos\left(\frac{n\pi z}{L_z}\right) \left[C_{\mathrm{init}}(x, z) - \langle C_{\mathrm{init}} \rangle \right].
$$

(the factor of 2 comes from the cosine series). Having constructed a solution to Equation (9.3), it is also the case that this is the only such smooth solution:

Theorem 9.2 *Equation* (9.4) *is the unique smooth solution of Equation* (9.3).

Exercise 9.1 *Prove Theorem* (9.2).

9.6 The model Poisson problem

We shall also consider a simpler problem than the diffusion problem posed previously. It will be referred to throughout the course as the **model Poisson problem**, given here as follows:

$$\nabla^2 C_0 + s(x, z) = 0, \qquad (x, z) \in \Omega, \tag{9.8a}$$

where

$$\Omega = (0, L_x) \times (0, 1), \tag{9.8b}$$

with boundary conditions

$$\frac{\partial C_0}{\partial z} = 0, \qquad z = 0, \qquad z = 1, \tag{9.8c}$$

and

$$C_0(x = 0, z, t) = C_0(x = L_x, z, t). \tag{9.8d}$$

9.7 Solvability condition and explicit solution

Consider Equation (9.8a). Integrate both sides over x and z and apply the boundary conditions on C. The result is

$$0 = \int_0^{L_x} \mathrm{d}x \int_0^{L_z} \mathrm{d}z\, s(x, z).$$

Thus, in order to get a self-consistent solution, we require that the source should have zero mean:

$$\langle s \rangle := \frac{1}{L_x L_z} \int_0^{L_x} \mathrm{d}x \int_0^{L_z} \mathrm{d}z\, s(x, z) = 0.$$

This is referred to as the **solvability condition**.

Assuming that Equation (9.8) satisfies the solvability condition, a solution is available through a Fourier-cosine series:

$$C_0(x) = \sum_{n=1}^{\infty} \sum_{i=-\infty}^{\infty} \frac{s_{in}}{k_{in}^2} \mathrm{e}^{\mathrm{i}[(2\pi/L_x)ix]} \cos\left(\frac{n\pi z}{L_z}\right), \tag{9.9}$$

where k_{in} and s_{in} are defined as in Section 9.2.

9.8 Relation between model diffusion and Poisson problems

It is clear from Equation (9.9) that

$$\lim_{t\to\infty} C'(x, z, t) = C_0(x, z),$$

where $C'(x, z, t)$ (LHS) is the fluctuating part of the solution of the model diffusion problem, and $C_0(x)$ (RHS) here denotes the solution of the model Poisson problem. Thus, the following theorem is shown:

Theorem 9.3 *Let $\langle s \rangle = 0$ in the model diffusion equation. Then the solution $C(x, z, t)$ of the model diffusion equation – given smooth initial data – converges to the solution of the model Poisson problem, as $t \to \infty$:*

$$\lim_{t\to\infty} C(x, z, t) = C_0(x, z), \qquad \nabla^2 C_0(x, z) + s(x, z) = 0.$$

Exercise 9.2 *Prove Theorem 9.3 using a second approach: show first that*

$$\frac{\partial}{\partial t}(C - C_0) = \nabla^2(C - C_0),$$

and hence show that

$$\lim_{t\to\infty} C(x, z, t) = C_0(x, z). \tag{9.10}$$

Non-uniqueness of solutions

Consider again the model Poisson problem with solution (9.9). It is clear that $C_0 + \text{Const.}$ is also a solution, since $\nabla^2(\text{Const.}) = 0$, and $C_0 + \text{Const.}$ also satisfies the boundary conditions (hybrid periodic–Neumann). The solution (9.9) is therefore not unique. This is because the operator ∇^2, equipped with the hybrid periodic–Neumann boundary conditions has a non-trivial kernel – the set of all constant functions is a one-dimensional vector subspace and is the non-trivial kernel of the PDE.

Exercise 9.3 *What happens to the kernel of ∇^2 if the boundary conditions are modified to be a mixture of periodic BCs in the x-direction and homogeneous Dirichlet conditions in the z-direction?*

Chapter 10

Simplified model problems – numerical setup

Overview

In this chapter we consider numerical solutions of the model equations We introduce centred differencing in space as a way of approximating the Laplace operator numerically. For the model diffusion equation, we introduce Crank–Nicholson temporal discretization as a way of discretizing the temporal derivative $\partial/\partial t$. Crank–Nicholson is a so-called **implicit method**, which means that a certain equation must be inverted in order to evolve the numerical solution forward in time, stepping from one time step to the next. For this reason, Jacobi iteration is introduced as a method for solving such implicit (linear) equations.

10.1 Diffusion equation

We are interested in solving the PDE from Chapter 8, recalled here to be

$$\frac{\partial C}{\partial t} = \nabla^2 C + s(x, z), \qquad (x, z) \in \Omega, \tag{10.1a}$$

where

$$\Omega = (0, L_x) \times (0, 1), \tag{10.1b}$$

and $\nabla^2 = \partial_x^2 + \partial_z^2$ is the Laplacian. The partial differential equation is subject to the following boundary conditions:

$$\frac{\partial C}{\partial z} = 0, \qquad z = 0, \qquad z = 1, \tag{10.1c}$$

together with periodic boundary conditions in the x- and y-directions:

$$C(x = 0, z, t) = C(x = L_x, z, t). \tag{10.1d}$$

Finally, an initial condition is prescribed:

$$C(x, z, t = 0) = C_{\text{init}}(x, z), \qquad (x, z) \in \overline{\Omega}, \tag{10.1e}$$

where $C_{\text{init}}(x, z)$ is a continuous function. Here, the system of equations (10.1) is made non-dimensional on the channel depth L_z (herein set to unity), and the diffusive timescale $\tau = L_z^2/D$, where D is the diffusion coefficient.

10.2   The discretization

We discretize the PDE and compute its approximate numerical solution on a discrete grid:

$$x_i = (i - 1)\Delta x, \qquad i = 1, \cdots n_x,$$
$$z_j = (j - 1)\Delta z, \qquad j = 1, \cdots n_z,$$

such that

$$(n_x - 1)\Delta x = L_x, \qquad \Delta x = L_x/(n_x - 1),$$

and similarly, $\Delta z = L_z/(n_z - 1)$. The PDE is also discretized in time, such that the solution is only available at discrete points in time $t_n = n\Delta t$, with $n = 0, 1, \cdots$. The solution at t_n and $\boldsymbol{x} = (i\Delta x, y\Delta j)$ is written as C_{ij}^n. The diffusion operator in the PDE (10.1) is approximated by **centred differences**:

$$\left(\nabla^2 C\right)_{ij} \approx \frac{C_{i+1,j} + C_{i-1,j} - 2C_{ij}}{\Delta x^2} + \frac{C_{i,j+1} + C_{i,j-1} - 2C_{ij}}{\Delta z^2} := \mathcal{D}(C_{ij})$$
$$i = 2, 3, \cdots, n_x - 1, \qquad j = 2, 3, \cdots, n_z - 1.$$

The discretization in time is done using a **Crank–Nicholson** scheme:

$$\frac{C_{ij}^{n+1} - C_{ij}^n}{\Delta t} = \tfrac{1}{2}\left[\mathcal{D}(C_{ij}^n) + \mathcal{D}(C_{ij}^{n+1})\right] + s_{ij}, \qquad i = 2, 3, \cdots, n_x - 1, \qquad j = 2, 3, \cdots, n_z - 1.$$

Re-arrange:

$$\left[1 - \tfrac{1}{2}\Delta t \mathcal{D}\right]\left(C_{ij}^{n+1}\right) = \left[1 + \tfrac{1}{2}\Delta t \mathcal{D}\right]\left(C_{ij}^{n}\right) + \Delta t s_{ij},$$

$$i = 2, 3, \cdots, n_x - 1, \qquad j = 2, 3, \cdots, n_z - 1. \quad (10.2)$$

On the left-hand side, the quantity $\left[1 - \tfrac{1}{2}\Delta t \mathcal{D}\right]$ is in fact a matrix operator, and the solution is available only in **implicit** form: an inversion needs to be performed to extract C_{ij}^{n+1} from this implicit equation:

$$C_{ij}^{n+1} = \left[1 - \tfrac{1}{2}\Delta t \mathcal{D}\right]^{-1}\left\{\left[1 + \tfrac{1}{2}\Delta t \mathcal{D}\right]\left(C_{ij}^{n}\right) + \Delta t s_{ij}\right\}. \quad (10.3)$$

The implicit equation (10.2) is written out in more detail now:

$$\left(1 + a_x + a_y\right)C_{ij}^{n+1} - \tfrac{1}{2}a_x\left(C_{i+1,j}^{n+1} + C_{i-1,j}^{n+1}\right) - \tfrac{1}{2}a_z\left(C_{i,j+1}^{n+1} + C_{i,j-1}^{n+1}\right) = \left[1 + \tfrac{1}{2}\Delta t \mathcal{D}\right]\left(C_{ij}^{n}\right) + s_{ij} := \mathrm{RHS}_{ij}^{n},$$

where $a_x = \Delta t/\Delta x^2$ and $a_z = \Delta t/\Delta z^2$. Tidy up:

$$\left(1 + a_x + a_y\right)C_{ij}^{n+1} - \tfrac{1}{2}a_x\left(C_{i+1,j}^{n+1} + C_{i-1,j}^{n+1}\right) - \tfrac{1}{2}a_z\left(C_{i,j+1}^{n+1} + C_{i,j-1}^{n+1}\right) = \mathrm{RHS}_{ij}^{n}. \quad (10.4)$$

This is an implicit equation for C_{ij}^{n+1} that we must now endavour to solve.

10.3 Jacobi method

The focus of this course is on the use of **iterative methods** to solve problems such as Equation (10.3) or equivalently, Equation (10.4). The idea is to make an initial guess for the solution, plug this into some algorithm for refining the guess, and continue until this iterative procedure converges.

The simplest and most naive iterative method os the so-called **Jacobi method**. Let $v \equiv C^{n+1}$ be the array to be found by solving Equation (10.3):

$$\left(1 + a_x + a_y\right)v_{ij} - \tfrac{1}{2}a_x\left(v_{i+1,j} + v_{i-1,j}\right) - \tfrac{1}{2}a_z\left(v_{i,j+1} + v_{i,j-1}\right) = \mathrm{RHS}_{ij}.$$

This can be re-arranged simply as

$$v_{ij} = \frac{\tfrac{1}{2}a_x\left(v_{i+1,j} + v_{i-1,j}\right) + \tfrac{1}{2}a_z\left(v_{i,j+1} + v_{i,j-1}\right) + \mathrm{RHS}_{ij}}{1 + a_x + a_z}. \quad (10.5)$$

The idea of the Jacobi method is to take a guess for v, say v^N, and to create a new guess v_{N+1} via the formula

$$v_{ij}^{N+1} = \frac{\tfrac{1}{2}a_x\left(v_{i+1,j}^{N} + v_{i-1,j}^{N}\right) + \tfrac{1}{2}a_y\left(v_{i,j+1}^{N} + v_{i,j-1}^{N}\right) + \mathrm{RHS}_{ij}}{1 + a_x + a_y}. \quad (10.6)$$

If this iterative scheme converges, then $\lim_{N\to\infty} v^N = \lim_{N\to\infty} v^{N+1}$, and the approximate solutions v^N and v^{N+1} can be replaced in Equation (10.6) with some identical array v^*, thereby forcing Equation (10.6) to be identical to Equation (10.5).

10.4   Boundary conditions

The idea to solve the PDE (10.1a) is to do implement a Crank–Nicholson-centred difference scheme at interior points. Inversion of the resulting implicit problem is then achieved by the Jacobi method. However, this approach can only be used at **interior points**

$$i = 2, 3, \cdots, n_x - 1, \qquad j = 2, 3, \cdots, n_z - 1.$$

At boundary points, the boundary conditions are enforced: $\partial C/\partial z = 0$ at $z = 0, 1$, and periodic boundary conditions in the x-direction. These are implemented numerically in a straightforward fashion. The Neumann conditions at $z = 0, L_z$ are implemented as

$$C_{i,j=1} = C_{i,j=2}, \qquad C_{i,j=n_y} = C_{i,j=n_y-1},$$

while the periodicity conditions at $x = 0, L_x$ are implemented as follows

- $i = 1$: $C(i - 1, j) = C(n_x - 1, j)$,

- $i = n_x$: $C(i + 1, j) = C(2, j)$.

Thus, the points $i = 1$ and $i = n_x$ are identified.

10.5   The algorithm

We can now assemble an algorithm to solve Equation (10.1a) numerically:

1. Set up a discretization scheme with Δx, Δz, and Δt defined by the user. Also, prescribe an initial condition $C_{\mathrm{init}}(x, z)$ and a source function $s(x, z)$.

2. Obtain $C_{ij}^{n=1}$ from C_{ij}^0 at interior points using centred differences, the Crank–Nicholson temporal discretization, and Jacobi iteration.

3. Implement many iterations of the Jacobi method, until the method has converged to some user-defined tolerance.

4. Implement the boundary conditions on $C^{n=1}$.

5. Repeat steps 2–4 for the desired number of timesteps.

Matlab codes to implement this problem are given in Appendix A.

Chapter 11

Analysis of numerical setup

Overview

The idea of this chapter is to take a generic linear problem $\boldsymbol{Ax} = \boldsymbol{b}$, and to formulate a sufficient condition on $\boldsymbol{A}$ that guarantees the success of the Jacobi iterative method. It turns out that this sufficient condition is something called **diagonal dominance**, which means that the diagonal elements of $\boldsymbol{A}$ should be large (in some sense) compared to the off-diagonal ones.

11.1 Generic discussion

Consider the Jacobi scheme for solving

$$\boldsymbol{Av} = \boldsymbol{b}, \qquad (\boldsymbol{A})_{ij} = a_{ij} \in \mathbb{R}.$$

The idea is to write $\boldsymbol{A} = \mathbf{D} + \mathbf{R}$, where

$$\mathbf{D} = \operatorname{diag}\left(a_{11}, a_{22}, \cdots, a_{nn}\right), \qquad n \in \mathbb{N},$$

and where

$$\mathbf{R} = \boldsymbol{A} - \mathbf{D}.$$

Then, the iterations $\boldsymbol{v}^N, \boldsymbol{v}^{N+1}$ that generate approximate solutions are obtained as follows:

$$\mathbf{D}\boldsymbol{v}^{N+1} = -\mathbf{R}\boldsymbol{v}^N + \boldsymbol{b},$$

for a given starting-guess v^0. Assume that

$$\lim_{N \to \infty} = v^*.$$

Thus,

$$\mathbf{D}v^{N+1} = -\mathbf{R}v^N + b,$$
$$\mathbf{D}v^* = -\mathbf{R}v^* + b.$$

Subtract:

$$\mathbf{D}\left(v^{N+1} - v^*\right) = -\mathbf{R}\left(v^N - v^*\right),$$

or

$$\mathbf{D}r^{N+1} = -\mathbf{R}r^N, \tag{11.1}$$

where $r^N = v^N - v^*$ is the **residual vector** at level N. Take L^2 vector norms on both sides:

$$\|r^{N+1}\|_2 = \|\mathbf{D}^{-1}\mathbf{R}r^N\|_2.$$

Now, use the L^2 operator norm:

$$\|r^{N+1}\|_2 \leq \|\mathbf{D}^{-1}\mathbf{R}\|_2\|r^N\|_2.$$

Telescope this result:

$$\|r^N\|_2 \leq \left(\|\mathbf{D}^{-1}\mathbf{R}\|_2\right)^N \|r^0\|_2.$$

By requiring that $\|\mathbf{D}^{-1}\mathbf{R}\|_2 < 1$, we obtain

$$\lim_{N \to \infty} \|r^N\|_2 = 0,$$

hence

$$\lim_{N \to \infty} r^N = 0,$$

hence

$$\lim_{N \to \infty} v^n = v^*.$$

Thus, we have shown the following theorem:

Theorem 11.1 *A sufficient condition for the convergence of the Jacobi iteration algorithm*

$$\mathbf{D}v^{N+1} = -\mathbf{R}v^N + b, \qquad v^{N=0} = v_0,$$

is the following bound on the L^2 operator norm:

$$\|\mathbf{D}^{-1}\mathbf{R}\|_2 < 1. \tag{11.2}$$

For systems with entries on the diagonal that are relatively large (in absolte-value terms) compared to entries off the diagonal, this constraint is usually satisfied, and the Jacobi iteration converges. However, this is a relatively vague criterion, which is of limited use. In addition, the L^2 operator norm is difficult to compute numerically, so in practice it is not known *a priori* – using Theorem (11.1) alone – whether the Jacobi method will converge. For that reason, we need a more rigorous notion of diagonal dominance.

11.2   Diagonal dominance

Definition 11.1 (L^∞ matrix norm) *Let $\mathbf{M} \in \mathbb{R}^{n \times n}$. Then*

$$\|\mathbf{M}\|_\infty = \sup_{\|x\|_\infty = 1} \|\mathbf{M}x\|_\infty,$$

where $\|x\|_\infty$ denotes the ordinary L^∞ norm for vectors: for $x = (x_1, \cdots, x_n) \in \mathbb{R}^n$,

$$\|x\|_\infty = \max_i |x_i|.$$

Lemma 11.1 (Consistency of the L^∞ norm) *Let $\mathbf{M}_1$ and $\mathbf{M}_2$ be square matrices in $\mathbb{R}^{n \times n}$. Then*

$$\|\mathbf{M}_1\mathbf{M}_2\|_\infty \leq \|\mathbf{M}_1\|_\infty \|\mathbf{M}_2\|_\infty.$$

Proof: It suffices to consider the case with $\|\mathbf{M}_1\mathbf{M}_2\|_\infty \neq 0$.

$$
\begin{aligned}
\|\mathbf{M}_1\mathbf{M}_2\|_\infty &= \sup_{\|\boldsymbol{x}\|_\infty = 1} \|\mathbf{M}_1\mathbf{M}_2\boldsymbol{x}\|_\infty, \\
&= \|\mathbf{M}_1\mathbf{M}_2\boldsymbol{x}_0\|_\infty, \\
&= \|\mathbf{M}_1\boldsymbol{y}\|_\infty, \qquad \boldsymbol{y} = \mathbf{M}_2\boldsymbol{x}_0 \neq 0, \\
&= \left(\frac{\|\mathbf{M}_1\boldsymbol{y}\|_\infty}{\|\boldsymbol{y}\|_\infty}\right) \|\boldsymbol{y}\|_\infty, \\
&\leq \left[\sup_{\boldsymbol{y} \neq 0} \left(\frac{\|\mathbf{M}_1\boldsymbol{y}\|_\infty}{\|\boldsymbol{y}\|_\infty}\right)\right] \|\boldsymbol{y}\|_\infty, \\
&= \|\mathbf{M}_1\|_\infty \|\boldsymbol{y}\|_\infty, \\
&= \|\mathbf{M}_1\|_\infty \|\mathbf{M}_2\boldsymbol{x}_0\|_\infty, \\
&\leq \|\mathbf{M}_1\|_\infty \|\mathbf{M}_2\|_\infty.
\end{aligned}
$$

Definition 11.2 *Let $\mathbf{M} \in \mathbb{R}^{n \times n}$. The spectral radius $\rho(\mathbf{M})$ refers to that $\mathbf{M}$-eigenvalue with maximal absolute value:*

$$\rho(\mathbf{M}) = \max_i \left(|\lambda_i|\right), \qquad \mathbf{M}\boldsymbol{x}_i = \lambda_i\boldsymbol{x}_i.$$

Theorem 11.2 (Bound on the spectral radius) *Let* $\mathbf{M} \in \mathbb{R}^{n \times n}$. *Then*

$$\rho(\mathbf{M}) \leq \|\mathbf{M}\|_\infty.$$

Proof: Let $\mathbf{M}\boldsymbol{x} = \lambda\boldsymbol{x}$, with $\boldsymbol{x} \neq 0$. Let

$$\mathbf{X} = \begin{pmatrix} | & & | \\ \boldsymbol{x} & \cdots & \boldsymbol{x} \\ | & & | \end{pmatrix}.$$

Thus,

$$\mathbf{M}\mathbf{X} = \lambda\mathbf{X}.$$

Take L^∞ norms on both sides:

$$|\lambda|\|\mathbf{X}\|_\infty = \|\mathbf{M}\boldsymbol{x}\|_\infty \leq \|\mathbf{M}\|_\infty\|\mathbf{X}\|_\infty,$$

hence

$$|\lambda| \leq \|\mathbf{M}\|_\infty,$$

for any eigenvalue λ, and the result is shown:

$$\rho(\mathbf{M}) \leq \|\mathbf{M}\|_\infty.$$

Now, by this stage, I am tired of proving theorems, so I shall simply state this last and crucial theorem:

Theorem 11.3 *Let* $\mathbf{M} \in \mathbb{R}^{n \times n}$. *Then*

$$\|\mathbf{M}\|_\infty = \max_i \left(\sum_{k=1}^n |m_{ik}| \right). \tag{11.3}$$

 Note the sum over columns!

Putting it all together

We now apply these results to $\mathbf{M} = \mathbf{D}^{-1}\mathbf{R}$. In view of Theorem 11.2 and Theorem 11.3, we have

$$\rho\left(\mathbf{D}^{-1}\mathbf{R}\right) \leq \|\mathbf{D}^{-1}\mathbf{R}\|_\infty = \max_i \left(\sum_{k=1}^n |(\mathbf{D}^{-1}\mathbf{R})_{ik}| \right)$$

But

$$\mathbf{D}^{-1}\mathbf{R} = \begin{pmatrix} 0 & \frac{a_{12}}{a_{11}} & \cdots & \frac{a_{1,n-1}}{a_{11}} & \frac{a_{1n}}{a_{11}} \\ \vdots & & & & \\ \frac{a_{n1}}{a_{nn}} & \cdots & & \frac{a_{n,n-1}}{a_{nn}} & 0 \end{pmatrix},$$

hence

$$\rho\left(\mathbf{D}^{-1}\mathbf{R}\right) \leq \|\mathbf{D}^{-1}\mathbf{R}\|_\infty = \max_i \left(\frac{1}{|a_{ii}|} \sum_{\substack{k=1 \\ k \neq i}}^n |a_{ik}| \right).$$

This motivates a definition:

Definition 11.3 *A matrix $A \in \mathbb{R}^{n \times n}$ is diagonally dominant if*

$$\frac{1}{|a_{ii}|} \sum_{\substack{k=1 \\ k \neq i}}^n |a_{ik}| < 1,$$

for each $i = 1, 2, \cdots, n$.

Along the way, we have established the following facts for a diagonally-dominant matrix:

Theorem 11.4 *Let $A \in \mathbb{R}^{n \times n}$ be diagonally dominant. Then*

$$\rho\left(\mathbf{D}^{-1}\mathbf{R}\right) \leq \|\mathbf{D}^{-1}\mathbf{R}\|_\infty = \max_i \left(\frac{1}{|a_{ii}|} \sum_{\substack{k=1 \\ k \neq i}}^n |a_{ik}| \right) < 1,$$

where $\mathbf{D}$ and $\mathbf{R}$ have their usual meanings.

We now consider a final theorem:

Theorem 11.5 *Let $\boldsymbol{Av} = \boldsymbol{b}$ be a linear problem, where $\boldsymbol{A} \in \mathbb{R}^{n \times n}$ is diagonally dominant. Then the Jacobi iteration method converges.*

Proof: Start with the definition of the Jacobi residuals, Equation (11.1) or, equivalently,

$$\boldsymbol{r}^{N+1} = -\mathbf{D}^{-1}\mathbf{R}\boldsymbol{r}^N, \tag{11.4}$$

Telescope the result:

$$\boldsymbol{r}^N = (-1)^N \left(\mathbf{D}^{-1}\mathbf{R}\right)^N \boldsymbol{r}^0.$$

Write

$$\mathbf{D}^{-1}\mathbf{R} = \mathbf{P}^{-1}\mathbf{JP},$$

where $\mathbf{J}$ is the Jordan normal form associated with $\mathbf{D}^{-1}\mathbf{R}$. We have

$$\begin{aligned}
\boldsymbol{r}^N &= (-1)^N \left(-\mathbf{D}^{-1}\mathbf{R}\right)^N \boldsymbol{r}^0, \\
&= (-1)^N \left(\mathbf{P}^{-1}\mathbf{JP}\right)^N \boldsymbol{r}^0, \\
&= (-1)^N \left(\mathbf{P}^{-1}\mathbf{J}^N\mathbf{P}\right) \boldsymbol{r}^0.
\end{aligned}$$

We now use the fact that $\rho(\mathbf{D}^{-1}\mathbf{R}) \leq \|\mathbf{D}^{-1}\mathbf{R}\|_\infty < 1$ as in the hypothesis of the theorem. Thus, all the eigenvalues have modulus less than one. Hence, each block in the Jordan matrix, raised to the Nth power, tends to zero as $N \to \infty$. It follows that

$$\lim_{N\to\infty} \mathbf{J}^N = 0. \tag{11.5}$$

Therefore, finally,

$$\lim_{N\to\infty} \boldsymbol{r}^N = 0.$$

11.3   Operation count

An elementary (non-iterative) method of solving linear problems is Gaussian elimination. The operation count of Gaussian elimination is $O(n^3)$, meaning that the number of operations (addition, multiplication etc.) required to invert the matrix is proprtional to the cube of the size of the matrix. This can be regarded as a relatively good performance result, since it compares very favourably with the operation count of determinant-type calculations, the latter being another candidate method for matrix inversion. However, for massive calculations (e.g. $n \sim 10^6$), even the relatively good performance of Gaussian elimination ($O(n^3)$) is not satisfactory. For such large calculations, iterative methods such as the Jacobi scheme are preferred; clearly in such iterative methods, the count is

$O(n_c n^2)$, where n_c is the number of iterations required for the method to converge, with $n_c \ll n$ for n large.

Recall theorem (11.4) above: given a diagonally-dominant problem $\boldsymbol{Ax} = \boldsymbol{b}$, the Jacobi iteration method will converge. In this module, we are always working with such systems. Thus, the Jacobi method will always work for us. However, its convergence is quite poor. In other words, a relatively large number of iterations is required in order to obtain a sufficiently converged solution. In this section we outline a new method. Superficially, it is a straightforward extension of the Jacobi method; however, on deeper reflection, the improved method represents a conceptual leap. This is the method of **successive over-relaxation** (SOR).

11.4   SOR

Start with the generic problem

$$\boldsymbol{Ax} = \boldsymbol{b}.$$

Recall the Jacobi solution:

$$\mathbf{D}\boldsymbol{v}^{N+1} = -\mathbf{R}\boldsymbol{v}^{N} + \boldsymbol{b}.$$

In index notation,

$$v_i^{N+1} = \frac{1}{a_{ii}} \left(-\sum_{j=1}^{n} R_{ik} v_k^{N} + b_i \right). \tag{11.6}$$

The idea behind SOR is to retrospectively improve the 'old guess' $\boldsymbol{v}^{N}$ that goes into formulating the 'new guess'. If the 'old guess' can be retrospectively improved, then this makes the new guess even better. To do this, the right-hand side of the Jacobi equation (11.6) is updated with just-recently-created values of $\boldsymbol{v}^{N+1}$. Where this is not possible, the old values of $\boldsymbol{v}^{N}$ are used. The result is the following iterative scheme:

$$v_i^{N+1} = -\frac{1}{a_{ii}} \sum_{k=1}^{i-1} R_{ik} v_k^{N+1} - \frac{1}{a_{ii}} \sum_{k=i}^{n} R_{ik} v_k^{N} + \frac{b_i}{a_{ii}}. \tag{11.7}$$

But $R_{ii} = 0$, and $R_{ij} = a_{ij}$ otherwise. Hence, Equation (11.7) can be replaced by

$$v_i^{N+1} = \frac{1}{a_{ii}} \left[b_i - \sum_{k=1}^{i-1} a_{ik} v_k^{N+1} - \sum_{k=i+1}^{n} a_{ik} v_k^{N} \right]. \tag{11.8}$$

Equation (11.8) is not yet optimal (however, it is already the Gauss–Seidel method for solving a linear system). Instead, we introduce an extra degree of freedom, which allows us to weight how much or how little retrospective improvement of the old guess is implemented in the $(N+1)^{\text{th}}$

iteration step. This is done by a simple modification of Equation (11.8):

$$v_i^{N+1} = (1 - \omega) v_i^N + \frac{\omega}{a_{ii}} \left[b_i - \sum_{k=1}^{i-1} a_{ik} v_k^{N+1} - \sum_{k=i+1}^{n} a_{ik} v_k^N \right] \tag{11.9a}$$

The factor ω is restricted to the range

$$0 < \omega < 2; \tag{11.9b}$$

this preserves the diagonal-dominance of the system and hence ensures convergence. The exact choice of ω can be made by trial-and-error in order to speed up convergence.

Chapter 12

Elements of turbulence theory

Overview

We give a qualitative definition of turbulence and introduce the phenomenological Kolmogorov theory of the turbulent spectrum in three dimensions.

We discuss averaging techniques to reduce the complexity of the fully turbulent Navier–Stokes equations. These are exemplified in the theory of wall-bounded turbulent flows and the famous 'law of the wall', Finally, we introduce large-eddy simulations as a half-way house between the full direct numerical simulation (DNS) of the turbulent Navier–Stokes equations and the relatively crude averaging techniques. At the end of the chapter, the students will be asked to carry out a large-eddy simulation of a wall-bounded flow and to extract various turbulent statistics from the simulation data.

Much of the description in this chapter is taken quite directly from the book by Pope [Pop00].

12.1 Turbulence phenomenology

Turbulence is defined here as a particular kind of fluid motion characterized by a velocity field that varies in space and time in a complicated way, with the following two essential features:

- In the spatial domain, turbulent motion is characterized by the presence of many lengthscales, from the domain scale (whereupon an external forcing is typically applied), down to small lengthscales where viscous motion dominates.

- In the temporal domain, the velocity field is characterized by a non-periodic, non-constant variation in time (i.e. chaotic motion).

Note that by itself the existence of a chaotic temporal dynamics is not sufficient to characterize turbulence: it is possible for example to observe chaotic advection in laminar flows [Are84].

Because turbulence is generated from an underlying deterministic set of equations (i.e. the Navier–Stokes equations), it can be characterized in a deterministic fashion. However, the system contains a large number of degrees of freedom. Focusing for definiteness (but without loss of generality) on the case wherein the domain is a periodic box, the Fourier modes of the system form a complete discrete set of degrees of freedom, all interacting nonlinearly to produce the complicated dynamics alluded to in the definition. In this way, the discrete modes can be thought of as analogous to particles in a gas: each particle can be thought of as obeying deterministic Newtonian dynamics, but on the macroscopic level, a statistical description of the collection of gas particles (all possibly interacting) is possible and indeed, desirable. Thus, in the case of a turbulent velocity field, we introduce a statistical description of the flow, characterized by a probability distribution function $f(\boldsymbol{V}; \boldsymbol{x}, t)$ for the velocity field $\boldsymbol{U} = (U_1, U_2, U_3)$, such that

$$
\mathrm{Prob}\begin{pmatrix} a_1 < U_1 < b_1 \\ a_2 < U_2 < b_2 \ ; \boldsymbol{x}, t \\ a_3 < U_3 < b_3 \end{pmatrix} = \int_{a_1}^{b_1} \int_{a_2}^{b_2} \int_{a_3}^{b_3} f(\boldsymbol{V}; \boldsymbol{x}, t)\, \mathrm{d}V_1\, \mathrm{d}V_2\, \mathrm{d}V_3.
$$

The average velocity is therefore

$$
\langle \boldsymbol{U}(\boldsymbol{x}, t) \rangle = \iiint \mathrm{d}^3 V\, f(\boldsymbol{V}; \boldsymbol{x}; t)\boldsymbol{V},
$$

and the **fluctuation velocity** is defined as

$$
\boldsymbol{u}(\boldsymbol{x}, t) = \boldsymbol{U}(\boldsymbol{x}, t) - \langle \boldsymbol{U}(\boldsymbol{x}, t) \rangle.
$$

The probability distribution function relates to quantities evaluated at a single point in space and time. Of interest also are so-called N-point statistics: let

$$
f_N\left(\boldsymbol{V}^{(1)}, \boldsymbol{x}^{(1)}, t^{(1)}; \boldsymbol{V}^{(2)}, \boldsymbol{x}^{(2)}, t^{(2)}; \cdots ; \boldsymbol{V}^{(N)}, \boldsymbol{x}^{(N)}, t^{(N)} \right)
$$

be the joint probability distribution for the velocity random-variable $\boldsymbol{V}$ at space-time points

$$
(\boldsymbol{x}^{(1)}, t^{(1)}), \cdots, (\boldsymbol{x}^{(N)}, t^{(N)}).
$$

It should be noted that turbulent velocity fields are found **not** to be Gaussian: a Gaussian field is be fully characterized by the mean $\langle \boldsymbol{U}(\boldsymbol{x}, t) \rangle$ and by the covariances $\langle u_i(\boldsymbol{x}^{(1)}, t^{(1)}) u_j(\boldsymbol{x}^{(2)}, t^{(2)}) \rangle$.

The random field $\boldsymbol{U}(\boldsymbol{x}, t)$ is **statistically stationary** if the N-point correlation function is invariant

under a shift in time:

$$f_N \left(\boldsymbol{V}^{(1)}, \boldsymbol{x}^{(1)}, t^{(1)} + T; \boldsymbol{V}^{(2)}, \boldsymbol{x}^{(2)}, t^{(2)} + T; \cdots ; \boldsymbol{V}^{(N)}, \boldsymbol{x}^{(N)}, t^{(N)} + T \right)$$
$$= f_N \left(\boldsymbol{V}^{(1)}, \boldsymbol{x}^{(1)}, t^{(1)}; \boldsymbol{V}^{(2)}, \boldsymbol{x}^{(2)}, t^{(2)}; \cdots ; \boldsymbol{V}^{(N)}, \boldsymbol{x}^{(N)}, t^{(N)} \right).$$

Similarly, $\boldsymbol{U}(\boldsymbol{x}, t)$ is **statistically homogeneous** if the N-point correlation function is invariant under a shift in the coordinate:

$$f_N \left(\boldsymbol{V}^{(1)}, \boldsymbol{x}^{(1)} + \boldsymbol{y}, t^{(1)}; \boldsymbol{V}^{(2)}, \boldsymbol{x}^{(2)} + \boldsymbol{y}, t^{(2)}; \cdots ; \boldsymbol{V}^{(N)}, \boldsymbol{x}^{(N)} + \boldsymbol{y}, t^{(N)} \right)$$
$$= f_N \left(\boldsymbol{V}^{(1)}, \boldsymbol{x}^{(1)}, t^{(1)}; \boldsymbol{V}^{(2)}, \boldsymbol{x}^{(2)}, t^{(2)}; \cdots ; \boldsymbol{V}^{(N)}, \boldsymbol{x}^{(N)}, t^{(N)} \right).$$

Then, in particular, the distribution function $f(\boldsymbol{V}; \boldsymbol{x}, t)$ is itself translation invariant, and we obtain

$$\langle \boldsymbol{U}(\boldsymbol{x}, t) \rangle = \iiint \mathrm{d}^3 V \, f(\boldsymbol{V}; \boldsymbol{x}; t) \boldsymbol{V}, \iiint \mathrm{d}^3 V \, f(\boldsymbol{V}; \boldsymbol{x} + \boldsymbol{y}; t) \boldsymbol{V} = \langle \boldsymbol{U}(\boldsymbol{x} + \boldsymbol{y}, t) \rangle$$

for all $\boldsymbol{y} \in \mathbb{R}^3$ and hence, the average velocity field is constant in space. Obviously this is quite restrictive: too restrictive in fact. We therefore define a **homogeneous turbulence** to correspond to a turbulent velocity field wherein the N-point distribution function for the **fluctuations** is homogeneous (translation invariant). Later on, in the context of Reynolds-averaging, we shall show that for homogeneous turbulence, the mean strain rates $(\partial/\partial x_j)\langle U_i \rangle$ are uniform (but can depend on time).

Because the distributional averages, e.g. $\langle \boldsymbol{U}(\boldsymbol{x}, t) \rangle = \iiint \mathrm{d}V \, f(\boldsymbol{V}; \boldsymbol{x}, t) \boldsymbol{V}$ are equivalent to ensemble averages, e.g.

$$\langle \boldsymbol{U}(\boldsymbol{x}, t) \rangle = \lim_{N \to \infty} \frac{1}{N} \sum_{i=1}^{N} \boldsymbol{U}^{(i)}(\boldsymbol{x}, t),$$

where the superscript denotes the ith realisation of the velocity field in a set of N identical experiments, it follows that the averaging and the derivatives commute, i.e.

$$\frac{\partial}{\partial t} \langle U_i \rangle = \left\langle \frac{\partial U_i}{\partial t} \right\rangle, \tag{12.1a}$$

and

$$\frac{\partial}{\partial x_j} \langle U_i \rangle = \left\langle \frac{\partial U_i}{\partial x_j} \right\rangle. \tag{12.1b}$$

These facts will be crucial in the next section concerning Reynolds-averaging.

12.2   Reynolds averaging

We take the instantaneous Navier–Stokes equations and we perform the averaging operation, using the properties 12.1. We obtain

$$\frac{\partial}{\partial t}\langle U_i\rangle + \langle \boldsymbol{U}\cdot\nabla U_i\rangle = -\nabla\langle p\rangle + \frac{1}{Re}\nabla^2\langle U_i\rangle.$$

The problematic term here is the quantity

$$
\begin{aligned}
\langle \boldsymbol{U}\cdot\nabla U_i\rangle &= \langle U_j\frac{\partial U_i}{\partial x_j}\rangle, \\
&= \left\langle [\langle U_j\rangle + u_j]\left[\frac{\partial}{\partial x_j}\langle U_i\rangle + \frac{\partial u_i}{\partial x_j}\right]\right\rangle, \\
&= \left\langle \langle U_j\rangle\frac{\partial}{\partial x_j}\langle U_i\rangle\right\rangle + \left\langle \langle U_j\rangle\frac{\partial u_i}{\partial x_j}\right\rangle + \left\langle u_j\frac{\partial}{\partial x_j}\langle U_i\rangle\right\rangle + \left\langle u_j\frac{\partial u_i}{\partial x_j}\right\rangle.
\end{aligned}
$$

We use the obvious properties

$$\langle\langle a\rangle\rangle = \langle a\rangle, \qquad \langle u_i\rangle = 0,$$

to obtain

$$
\begin{aligned}
\langle \boldsymbol{U}\cdot\nabla U_i\rangle &= \langle U_j\rangle\frac{\partial}{\partial x_j}\langle U_i\rangle + \left\langle u_j\frac{\partial u_i}{\partial x_j}\right\rangle, \\
&= \langle \boldsymbol{U}\rangle\cdot\nabla\langle U_i\rangle + \frac{\partial}{\partial x_j}\langle u_iu_j\rangle.
\end{aligned}
$$

We introduce

$$\tau_{ij} = -\langle u_iu_j\rangle$$

as the **Reynolds stress tensor**. Then, the averaged equations of motion become

$$\frac{\partial}{\partial t}\langle U_i\rangle + \langle \boldsymbol{U}\rangle\cdot\nabla\langle U_i\rangle = -\nabla\langle p\rangle + \frac{\partial \tau_{ij}}{\partial x_j} + \frac{1}{Re}\nabla^2\langle U_i\rangle, \qquad \nabla\cdot\langle \boldsymbol{U}\rangle = 0. \qquad (12.2)$$

These are the Reynolds-averaged Navier–Stokes (RANS) equations.

12.3   Closure problem

The Reynolds stresses cannot be determined a priori – this is the **closure problem** of turbulence. Certainly, one can write down a transport equation for the Reynolds stresses themselves, e.g.

$$\left(\frac{\partial}{\partial t} + \langle \boldsymbol{U}\rangle\cdot\nabla\right)\tau_{ij} = \cdots,$$

but the right-hand side will involve tensors of at least rank three built out of the fluctuating velocities. To constitute these tensors, one needs a further transport equation and so on, *ad infinitum*. Additional knowledge from outside the set of RANS equations is needed to break this infinite chain of equations. At the very simplest level, this is done by **constitutive modelling** of the Reynolds stress tensor; at higher levels of detail, tensors of higher rank are modelled and fed back into the transport equations for the tensors of lower rank, thereby closing the problem. Consideration is given herein to the simple approach.

Eddy viscosity model

In the simplest possible closure model, the Reynolds stresses themselves are modelled. The conceptual approach is to identify the total stress tensor in the RANS equations:

$$T_{ij} = -p\delta_{ij} + Re^{-1}\left(\partial_i\langle U_j\rangle + \partial_j\langle U_i\rangle\right) - \langle u_i u_j\rangle,$$

and to assume an analogy between molecular diffusion and the effects of turbulence. Namely, on a small scale, one pictures a fluid parcel undergoing thermal fluctuations due to molecular diffusion, and further fluctuations due to the small-scale motions of the neighbouring turbulent eddies. One assumes that these effects are similar, such that on average, the effects of the turbulence can be modelled as though they were somehow viscous in nature, with

$$\tau_{ij} = \nu_T\left(\partial_i\langle U_j\rangle + \partial_j\langle U_i\rangle\right),$$

where ν_T is the **eddy viscosity**. Dimensional analysis then suggests

$$\nu_T = C\mathcal{S}\ell^2,$$

where $\mathcal{S}$ is the mean rate of strain,

$$\mathcal{S} = \sqrt{2S_{ij}S_{ij}}, \qquad S_{ij} = \tfrac{1}{2}\left(\frac{\partial}{\partial x_i}\langle U_j\rangle + \frac{\partial}{\partial x_j}\langle U_i\rangle\right)$$

and ℓ is the so-called **mixing length**, which in turn must be constituted and depends on the geometry of the problem.

12.4 Eddy-viscosity model for channel flows

In wall-bounded channel flows (e.g. Figure 12.1), the mixing length cannot exceed the size of the largest eddy, which in turn cannot exceed the distance to the nearest wall, hence $\nu_T \propto z$. This
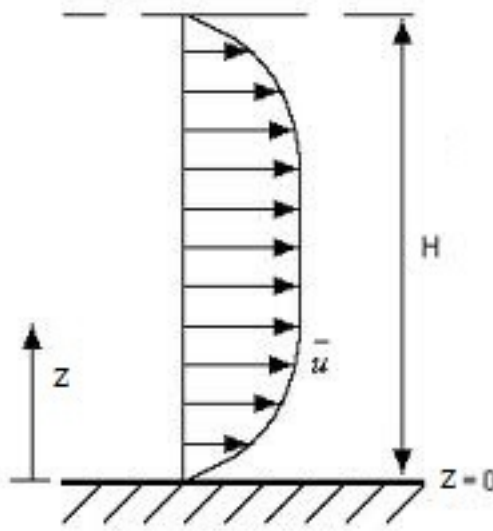
Figure 12.1: Schematic diagram of turbulent channel flow

is the Prandtl theory of wall-bounded turbulence. Suppose that an applied pressure $dP/dL < 0$ drop drives the flow from left to right in Figure 12.1. Then on average, the flow will only be in the x-direction. Once a balance between the forcing and the dissipation is established, the flow will also be (statistically) steady. Thus,

$$\boldsymbol{U}(\boldsymbol{x}, t) = (U_0(z), 0, 0)$$

(Compare with laminar Poiseuille flow). Then, the Reynolds-averaged Navier–Stokes equations reduce to

$$-\frac{dP}{dL} + \frac{\partial T_{i1}}{\partial x_i} = 0,$$

But the only non-trivial derivative is now $\partial/\partial z$, since the flow is (on average) translation-invariant in the x- and y-directions, hence the RANS equation reads

$$-\frac{dP}{dL} + \frac{dT_{12}}{dz} = 0,$$

where we have used the symmetry of the stress tensor. Integrating once, we have

$$T_{12}(z) = \tau_* - |dP/dL|z.$$

We have

$$T_{12} = Re^{-1}\frac{dU_0}{dz} + \tau_R, \qquad \tau_R = -\langle uw \rangle.$$

hence

$$Re^{-1}\frac{dU_0}{dz} + \tau_R = \tau_* - |dP/dL|z.$$

where τ_* is the **wall shear stress**, to be determined. Using the mixing-length theory, we obtain

$$\tau_R = \kappa^2 \left| \frac{dU_0}{dz} \right| z,$$

and thus the RANS balance equation reads

$$Re^{-1} \frac{dU_0}{dz} + \kappa^2 z^2 \frac{dU_0}{dz} \left| \frac{dU_0}{dz} \right| = \tau_* - |dP/dL|z.$$

This equation contains a lot more information than is apparent superficially. We identify a **viscous sublayer** where the viscous stress dominates over the Reynolds stress, which will exist for $z \to 0$, wherein the dominant balance reads

$$\rho \nu \frac{dU_0}{dz} \sim \tau_* := \rho u_*^2,$$

hence

$$\nu \frac{dU_0}{dz} \sim u_*^2$$

where we have momentarily restored the dimensional variables. The typical velocity scale in this zone is u_* and the typical lengthscale is the friction scale d_*, giving

$$\frac{\nu u_*}{d_*} \sim u_*^2,$$

hence $d_* = \nu/u_*$, where the friction velocity u_* is to be determined. The range $0 \leq z \lesssim d_*$ is therefore called the **viscous sublayer** of the flow. We next identify a region $d_* \ll z \ll H/2$ where the dominant balance in the RANS equation reads

$$\rho \kappa^2 z^2 \frac{dU_0}{dz} \left| \frac{dU_0}{dz} \right| \sim \tau_* = \rho u_*^2$$

hence

$$\kappa z \frac{dU_0}{dz} \sim u_*,$$

where we have assumed that we are near the bottom wall, such that $dU_0/dz > 0$ (the same arguments will apply near the top wall, by symmetry around the channel centreline). Integration now gives

$$U_0 \sim \frac{u_*}{\kappa} \log z + \mathrm{Const.}$$

which is the famous **law of the wall** of turbulence theory.

It would be useful to find an expression for the friction velocity in terms of the problem parameters, and at the same time, to solve for the velocity profile $U_0(z)$ throughout the entire domain $0 \leq z \leq H$. This is done now here a very simple eddy-viscosity model. However, before presenting this model, it

is useful to understand the scaling of the Reynolds stress (and hence the base-state velocity profile) near the wall at $z = 0$. We therefore Taylor-expand the velocity fluctuations near the bottom wall:

$$
\begin{aligned}
u(x, y, z, t) &= a_0(x, y, t) + a_1(x, y, t)z + a_2(x, y, t)z^2 + \cdots \\
v(x, y, z, t) &= b_0(x, y, t) + b_1(x, y, t)z + b_2(x, y, t)z^2 + \cdots \\
w(x, y, z, t) &= c_0(x, y, t) + c_1(x, y, t)z + c_2(x, y, t)z^2 + \cdots
\end{aligned}
$$

The no-slip condition obviously gives $a_0 = b_0 = c_0$, hence

$$
\begin{aligned}
u(x, y, z, t) &= a_1(x, y, t)z + a_2(x, y, t)z^2 + \cdots \\
v(x, y, z, t) &= b_1(x, y, t)z + b_2(x, y, t)z^2 + \cdots \\
w(x, y, z, t) &= c_1(x, y, t)z + c_2(x, y, t)z^2 + \cdots
\end{aligned}
$$

The same condition gives

$$
\frac{\partial w}{\partial x} = \frac{\partial w}{\partial y} = \frac{\partial v}{\partial x} = \frac{\partial v}{\partial y} = \frac{\partial u}{\partial x} = \frac{\partial u}{\partial y}
$$

at $z = 0$ and hence, by incompressibility,

$$
\frac{\partial w}{\partial z} = 0
$$

at $z = 0$. Therefore, $c_1 = 0$ identically, and hence,

$$
\begin{aligned}
uw &= \left(a_1(x, y, t)z + a_2(x, y, t)z^2 + \cdots\right)\left(c_2(x, y, t)z^2 + \cdots\right), \\
&= a_1 c_2 z^3 + \cdots,
\end{aligned}
$$

hence

$$
\tau_R = -\langle uw \rangle = -\langle a_1 c_2 \rangle z^3 + O(z^4),
$$

as $z \to 0$.

12.4.1   The model

Instead of starting from the mixing-length theory, we start from scratch, and derive the eddy viscosity using an alternative approach. We first of all introduce from first principles the non-dimensionaliztion scheme for the RANS balance equation. Thus, we introduce a **velocity scale**

$$
U_p = \sqrt{|dP/dL|h/\rho}
$$

and the Reynolds number

$$Re_p = \rho U_p h / \mu$$

The problem contains a further, apparently unknown parameter, Re_*, based on the friction velocity:

$$Re_* = \frac{\rho U_* h}{\mu}, \qquad \rho U_*^2 = \mu \frac{d\overline{U}_0}{dz}\bigg|_{z=0}.$$

which will be determined by the model. These considerations therefore suggest the following functional form for the (dimensionless) eddy viscosity:

$$\mu_T(z) = Re_* F(z/h)$$

where henceforth we use z for z/h. We are therefore dealing with an **algebraic closure model**. We make the inspired guess

$$F = \kappa \psi_{\mathrm{w}}(z) \psi_{\mathrm{w}}(1-z) G(z),$$

where

$$G(z) = z(1-z) \left[\frac{1 - 3z(1-z)}{1 - z(1-z)} \right], \tag{12.3}$$

and where

$$\psi_{\mathrm{w}}(z) = 1 - \mathrm{e}^{-\alpha z^2 Re_*^2},$$

is a **wall function** (See References [Bib07, NSMZ11]). The parameter α is fixed such that

$$U(z = 5d_*) = 0.95(u_*^2 z/\nu)_{z=5d_*} = 0.95 \times 5\, u_*.$$

Thus, the velocity is obtained through the relation

$$U(z) = \frac{Re_*^2}{Re_0} \int_0^z \frac{\left(1 - \frac{Re_0^2}{Re_*^2} s\right) \mathrm{d}s}{1 + \kappa Re_* G(s) \psi_{\mathrm{w}}(s) \psi_{\mathrm{w}}(1-s)} \tag{12.4}$$

The friction velocity is thus obtained through the following root-finding condition for Re_*:

$$U(z = 1; Re_*) = 0.$$

The clever thing about the choice (12.3) for the algebraic closure is that the correct scaling is recovered for $U(z)$ in the log layer and in the viscous sublayer. Also, the model is symmetric around the centreline, with $G(z) = G(1-z)$.
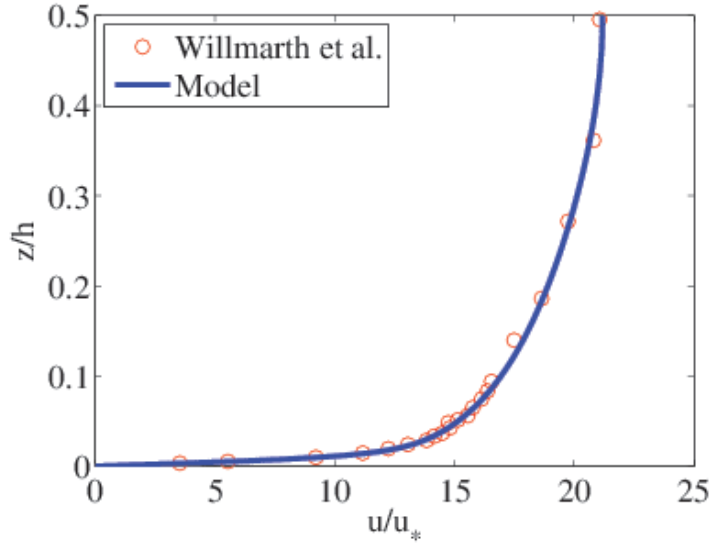
Figure 12.2: A comparison with Reference [WWL87] for single-phase channel flow. In the experiment, the Reynolds number based on the friction velocity was 1.143×10^3, which corresponds to a model Reynolds number $Re_p = \sqrt{2} \times 1.143 \times 10^3$. The mean Reynolds number in the experiment was $Re_{\mathrm{m}} = 2.158 \times 10^4$ – a Reynolds number based on the mean velocity and channel depth. For comparison, the corresponding mean Reynolds number in the model is $Re_{\mathrm{m}} = 2130 \times 10^4$.

Exercise 12.1 *Work though the derivation of Equation* (12.4) *explicitly. Implement the velocity profile numerically and compute* Re_* *for a given Reynolds number. Show also a plot of the dependence of* Re_* *on the input parameter* Re. *The computations can be validated with the data in Figure 12.2.*

We have compared the model an experimental paper [WWL87], and the model gives excellent agreement: both the curve $U_0(z)$ and the interfacial shear stress are predicted well (Figure 12.2).

12.5   Turbulence intensity

The turbulence intensity is defined as

$$k = \tfrac{1}{2}\langle u^2 + v^2 + w^2 \rangle, \qquad \rho = 1.$$

We derive a transport equation for the turbulent kinetic energy, writing the Navier–Stokes equations in the following decomposition:

$$\frac{\partial}{\partial t}\left(\langle \boldsymbol{U}\rangle + \boldsymbol{u}\right) + \left(\langle \boldsymbol{U}\rangle + \boldsymbol{u}\right)\cdot\nabla\left(\langle \boldsymbol{U}\rangle + \boldsymbol{u}\right) = -\nabla\langle p\rangle - \nabla p' + \frac{1}{Re}\nabla^2\langle U\rangle + \frac{1}{Re}\nabla^2\boldsymbol{u}.$$

But we also have the RANS equation

$$\frac{\partial}{\partial t}\langle \boldsymbol{U}\rangle + \langle \boldsymbol{U}\rangle\cdot\nabla\langle \boldsymbol{U}\rangle = -\nabla\langle p\rangle + \frac{1}{Re}\nabla^2\langle U\rangle + \nabla\cdot\boldsymbol{\tau}.$$

Subtract these equations and take components to obtain

$$\left[\frac{\partial}{\partial t} + \left(\langle \boldsymbol{U}\rangle + \boldsymbol{u}\right)\cdot\nabla\right]u_i = -u_j\frac{\partial}{\partial x_j}\langle U_i\rangle + \frac{\partial}{\partial x_j}\langle u_i u_j\rangle - \frac{\partial p'}{\partial x_i} + \frac{1}{Re}\nabla^2 u_i.$$

Multiply both sides by u_i, sum over i and average. On the LHS we obtain

$$
\begin{aligned}
\left\langle u_i\left[\frac{\partial}{\partial t} + \left(\langle \boldsymbol{U}\rangle + \boldsymbol{u}\right)\cdot\nabla\right]u_i\right\rangle &= \frac{\partial k}{\partial t} + \langle U_j\rangle\left\langle u_i\frac{\partial u_i}{\partial x_j}\right\rangle + \left\langle u_i u_j\frac{\partial u_i}{\partial x_j}\right\rangle, \\
&= \frac{\partial k}{\partial t} + \langle \boldsymbol{U}\rangle\cdot\nabla k + \left\langle u_i u_j\frac{\partial u_i}{\partial x_j}\right\rangle, \\
&= \frac{\partial k}{\partial t} + \langle \boldsymbol{U}\rangle\cdot\nabla k + \tfrac{1}{2}\frac{\partial}{\partial x_j}\langle |\boldsymbol{u}|^2 u_j\rangle.
\end{aligned}
$$

where we have used

$$\left\langle u_i u_j\frac{\partial u_i}{\partial x_j}\right\rangle = \left\langle u_i\frac{\partial}{\partial x_j}\left(u_i u_j\right)\right\rangle = \tfrac{1}{2}\frac{\partial}{\partial x_j}\langle u_i u_i u_j\rangle,$$

On the right-hand side, we work on each term individually. We identify the **production** of turbulent kinetic energy:

$$\mathcal{P} = -\langle u_i u_j\rangle\frac{\partial}{\partial x_j}\langle U_i\rangle = \boldsymbol{\tau} : \nabla\langle \boldsymbol{U}\rangle.$$

Also,

$$\left\langle u_i\frac{\partial p'}{\partial x_i}\right\rangle = \frac{\partial}{\partial x_i}\langle u_i p'\rangle.$$

Finally, the term $\langle u_i\nabla^2 u_i\rangle$ is re-arranged as

$$\langle u_i\nabla^2 u_i\rangle = \frac{\partial}{\partial x_j}\left\langle u_i\frac{\partial u_i}{\partial x_j}\right\rangle - \left\langle \frac{\partial u_i}{\partial x_j}\frac{\partial u_i}{\partial x_j}\right\rangle.$$

We identify the dissipation of turbulent intensity:

$$\epsilon := -\frac{1}{Re}\left\langle \frac{\partial u_i}{\partial x_j}\frac{\partial u_i}{\partial x_j}\right\rangle \leq 0.$$

Thus, the equation for the turbulent kinetic energy reads

$$\left(\frac{\partial}{\partial t} + \langle \boldsymbol{U} \rangle \cdot \nabla\right) k + \nabla \cdot \boldsymbol{R} = \mathcal{P} - \epsilon, \tag{12.5}$$

where the vector $\boldsymbol{R}$ represents redistribution of turbulent intensity:

$$R_i = \tfrac{1}{2}\langle |\boldsymbol{u}|^2 u_i \rangle + \langle u_i p' \rangle - \frac{1}{Re}\left\langle u_j \frac{\partial u_j}{\partial x_i}\right\rangle.$$

These results give great insight into the energy budget that underlies turbulence generation: it is the interaction between the Reynolds stresses and the mean flow that generates turbulence via the production term $\boldsymbol{\tau} : \nabla\langle \boldsymbol{U} \rangle$, while the turbulence is dissipated via molecular dissipation.

Exercise 12.2 *Show that Equation* (12.5) *can be rewritten in the following (equivalent) way:*

$$\left(\frac{\partial}{\partial t} + \langle \boldsymbol{U} \rangle \cdot \nabla\right) k + \nabla \cdot \boldsymbol{R}' = \mathcal{P} - \epsilon', \tag{12.6}$$

where the meaning of $\mathcal{P}$ is unchanged, but where

$$R_i' = \tfrac{1}{2}\langle |\boldsymbol{u}|^2 u_i \rangle + \langle u_i p' \rangle - (2/Re)\langle u_j s_{ij} \rangle,$$

and

$$\epsilon' = (2/Re)\langle s_{ij} s_{ij} \rangle.$$

Also, s_{ij} is the rate-of-strain tensor associated with the fluctuating velocities,

$$s_{ij} = \tfrac{1}{2}\left(\frac{\partial u_i}{\partial x_j} + \frac{\partial u_j}{\partial x_i}\right).$$

We now use this theory to prove an important result:

Theorem 12.1 *For homogeneous turbulence, the most general form for the mean velocity profile is*

$$\langle U_i \rangle = a_i(t) + b_{ij}(t) x_j$$

Recall, the definition of homogeneous turbulence means that the statistics of the turbulent velocity **fluctuations** are translation invariant. Thus, for homogeneous turbulence, we have

$$k = \tfrac{1}{2}\langle |\boldsymbol{u}|^2 \rangle, \qquad R_i = \tfrac{1}{2}\langle |\boldsymbol{u}|^2 u_i \rangle + \langle u_i p' \rangle - \left\langle u_i \frac{\partial u_i}{\partial x_j}\right\rangle, \qquad \epsilon = -\frac{1}{Re}\left\langle \frac{\partial u_i}{\partial x_j}\frac{\partial u_i}{\partial x_j}\right\rangle,$$
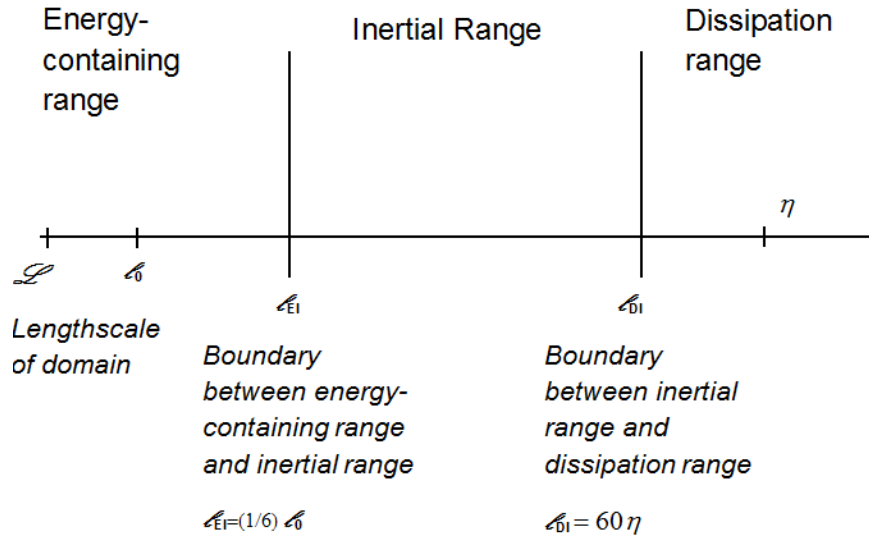
Figure 12.3: Schematic description of the different lengthscales involved in turbulence

all independent of space. We substitute these results into the turbulent kinetic energy equation to obtain

$$\frac{\partial k}{\partial t} + \epsilon = \mathcal{P}$$

and it follows that the production is independent of spatial coordinates, i.e.

$$-\langle u_i u_j \rangle \frac{\partial}{\partial x_j} \langle U_i \rangle$$

is independent of space. But $-\langle u_i u_j \rangle$ is independent of space also, and so $(\partial/\partial x_i)\langle U_j \rangle$ is independent of space. It therefore follows that

$$\langle U_i \rangle = a_i(t) + b_{ij}(t)x_j,$$

such that $(\partial/\partial x_i)\langle U_j \rangle = b_{ij}(t)$, independent of space, as required.

Having now understood something of the mechanisms underlying the production, transport, and dissipation of turbulence intensity, we can now study a more detailed (but phenomenological) theory for these processes, which underscores the multiscale nature of these turbulence mechanisms.

12.6   K-41 theory

The idea of the Kolmogorov-1941 (K-41) theory is to break up the motion into three ranges (Figure 12.3).

Energy-containing range

On these scales, the motion is made up of large-scale coherent motions called 'eddies'. A typical eddy in this range is of size ℓ_0, with $\ell_0 \sim \mathcal{L}$, where $\mathcal{L}$ is the lengthscale of the domain. The characteristic velocity of the eddies will be $u_0 = u(\ell_0)$, with $u_0 = [(2/3)k]^{1/2}$, where k is the turbulence intensity, which in turn is comparable to $\mathcal{U}$, the typical flow magnitude on the domain scale. We have $Re_0 = u_0 \ell_0 / \nu$, which is the Reynolds number associated with the large eddy. Also, $Re_0 \sim Re$, where $Re = \mathcal{U}\mathcal{L}/\nu$, which is the Reynolds number associated with the domain scales.

The large eddies interact with the smaller eddies via the nonlinear term in the NS equation, leading to a transfer of energy from the larger eddies to the smaller ones. This process continues (in three dimensions) down to the smallest scales where dissipation dominates over inertia in the Navier–Stokes equation, such that energy is eventually dissipated from the system.

The large eddies have an energy of order u_0^2 and a timescale $\tau_0 = \ell_0/\nu_0$, so the rate of transfer of energy can be supposed to scale as $u_0^2/\tau_0 = u_0^3/\ell_0$. Because the dissipation is controlled by the transfer, it can also be supposed that the **dissipation rate** ϵ scales as u_0^3/ℓ_0, independent (shockingly) of ν!!

Inertial and dissipation ranges

In the inertial range and the dissipation range, Kolmogorov's similarity hypotheses are assumed to hold:

- At sufficiently high Reynolds number, the small-scale turbulent motions ($\ell \ll \ell_0$) are statistically isotropic.

- In every turbulent flow a t sufficiently high Reynolds number, the statistics of the small-scale motions ($\ell < \ell_{EI}$) have a **universal form** that is uniquely determined by ν and ϵ.

In the **dissipation range**, dimensional analysis gives

$$\begin{aligned}
\eta &= (\nu^3/\epsilon)^{1/4} \cdots \text{lengthscale} \\
u_\eta &= (\epsilon\nu)^{1/4} \cdots \text{velocity scale} \\
\tau_\eta &= (\nu/\epsilon)^{1/2} \cdots \text{time scale.}
\end{aligned}$$

Note that

$$Re_\eta = 1,$$

meaning that dissipation is important (not surprisingly!) in the dissipation range. The ratio of the smallest to largest scales is thus given by

$$
\begin{aligned}
\frac{\eta}{\ell_0} &= \frac{\nu^{3/4}}{\ell_0 \epsilon^{1/4}}, \\
&= \frac{\nu^{3/4}}{\ell_0 (u_0^3/\ell_0)^{1/4}}, \\
&= \frac{\nu^{3/4}}{u_0^{3/4} \ell_0^{1-(1/4)}}, \\
&= (\nu/u_0\ell_0)^{-3/4}, \\
&\sim Re^{-3/4},
\end{aligned}
$$

hence $\eta/\ell_0 \sim Re^{-3/4}$. Similarly,

$$
u_\eta/u_0 \sim Re^{-1/4}, \qquad \tau_\eta/\tau_0 \sim Re^{-1/2}.
$$

Thus, at very high Reynolds numbers, the scales of motion (length, velocity and time) are all much smaller in the small eddies in the dissipative range than in the larger eddies in the energy-containing range.

Crucially for direct numerical simulation of turbulence, the numerical simulation must resolve down to the dissipative scales, such that

$$
\Delta x \leq \eta,
$$

hence

$$
\Delta x/\ell_0 \leq (\eta/\ell_0) \sim Re^{-3/4}.
$$

The number of gridpoints in the problem is $N = (\ell_0/\Delta x)^3$ for a full three-dimensional simulation and hence,

$$
N \sim Re^{9/4}
$$

is the number of grid points required in a three-dimensional direct numerical simulation of turbulence.

A further consequence of the formula $\eta/\ell_0 \sim Re^{-3/4}$ is the obvious fact that $\eta \ll \ell_0$ at high Reynolds numbers, meaning that there is a range of lengthscales ℓ, with

$$
\eta \ll \ell \ell_0
$$

which correspond neither to the dissipative range nor the energy-containing range. This is the **inertial range**. Again, in this range, it is expected that the Kolmogorov hypotheses should hold, giving

$$
u(\ell) = (\epsilon\ell)^{1/3} = \epsilon^{1/3}\ell^{1/3}.
$$

But

$$u_\eta \eta^{1/3} = \frac{(\epsilon\nu)^{1/4}}{[(\nu^3/\epsilon)^{1/4}]^{1/3}},$$

$$= \left[\frac{(\epsilon\nu)^{3/4}}{(\nu^3/\epsilon)^{1/4}}\right]^{1/3},$$

$$= \left[\frac{\epsilon^{3/4}\nu^{3/4}\epsilon^{1/4}}{\nu^{3/4}}\right]^{1/3},$$

$$= \epsilon^{1/3},$$

hence

$$u(\ell) = u_\eta(\ell/\eta)^{1/3}.$$

We have

$$u_\eta(\ell/\eta)^{1/3} = u_0(u_\eta/u_0)(\ell_0/\ell_\eta)^{1/3}(\ell/\ell_0)^{1/3},$$

$$= u_0(\ell/\ell_0)^{1/3}(u_\eta/u_0)(\ell_0/\ell_\eta)^{1/3},$$

$$= u_0(\ell/\ell_0)^{1/3}Re^{-1/4}Re^{1/4},$$

$$= u_0(\ell/\ell_0)^{1/3},$$

hence $u(\ell) \sim u_0(\ell/\ell_0)^{1/3}$. Similarly,

$$u(\ell) \sim u_0(\ell/\ell_0)^{1/3}, \qquad \tau(\ell) \sim \tau_0(\ell/\ell_0)^{2/3}, \tag{12.7}$$

such that, in the inertial range, the velocity scales $u(\ell)$ and timescales $\tau(\ell)$ decrease as ℓ decreases.

The energy cascade

The rate at which energy is transferred from a scale ℓ to (smaller) scales is denoted by $\mathcal{T}(\ell)$ and is expected to scale as

$$\mathcal{T}(\ell) \sim u(\ell)^2/\tau(\ell).$$

By Equation (12.7), we have

$$\mathcal{T}(\ell) \sim \frac{u_0^2\ell^{2/3}\ell_0^{-2/3}}{\tau_0\ell^{2/3}\ell_0^{-2/3}} = \frac{u_0^2}{\tau_0} = \epsilon,$$

and thus, the transfer rate is independent of the scale: **the transfer rate is the same on all lengthscales**.

The energy spectrum

The energy spectrum is introduced as follows, starting with the total **turbulent** kinetic energy:

$$
\begin{aligned}
E &= \int d^3x \left(\tfrac{1}{2} |\boldsymbol{u}|^2 \right), \\
&= \tfrac{1}{2} \int \frac{d^3k}{(2\pi)^3} |\widehat{\boldsymbol{u}}_{\boldsymbol{k}}|^2, \\
&= \int_0^\infty dk \left(\tfrac{1}{2} k^2 \int_\Omega d\Omega \, |\widehat{\boldsymbol{u}}_{\boldsymbol{k}}|^2 \right), \\
&:= \int_0^\infty dk \, E(k),
\end{aligned}
$$

and $E(k)$ is called the energy spectrum.

In the inertial range, by Kolmogrovo's similarity hypotheses, the energy spectrum is determiend entirely by ϵ and ν: we have

$$
E(k) = \epsilon^a \nu^b k^c,
$$

and dimensional analysis gives

$$
\begin{aligned}
2a + 3b - c &= 3, \\
3a + b &= 2.
\end{aligned}
$$

The system of equations is underdetermined. However, in the inertial range, the viscosity does not have a direct effect on the eddies. This can be seen as follows:

$$
\begin{aligned}
Re(\ell) &= \frac{u_0 (\ell/\ell_0)^{1/3} \ell}{\nu}, \\
&= \frac{u_0 \ell_0}{\nu} (\ell/\ell_0)^{1/3} (\ell/\ell_0), \\
&= Re_0 (\ell/\ell_0)^{4/3} \gg 1,
\end{aligned}
$$

with $Re(\ell) = 1$ at the onset of th dissipation range. This direct viscous effects are negligible in the inertial range, and we therefore take $b = 0$, hence $a = 2/3$ and $c = -5/3$, giving

$$
E(k) = C \epsilon^{2/3} k^{-5/3},
$$

which is the celebrated Kolmogorov spectrum of turbulence.

The Kolmogorov spectrum is a fairly well-established feature of three-dimnensional turbulence (e.g. Figure 12.4). To understand this figure fully, consider for definiteness a channel flow with walls bounding the flow in the z direction, with $(x, y, z) \in [0, L_x] \times [0, L_y] \times [0, H]$. One starts with the
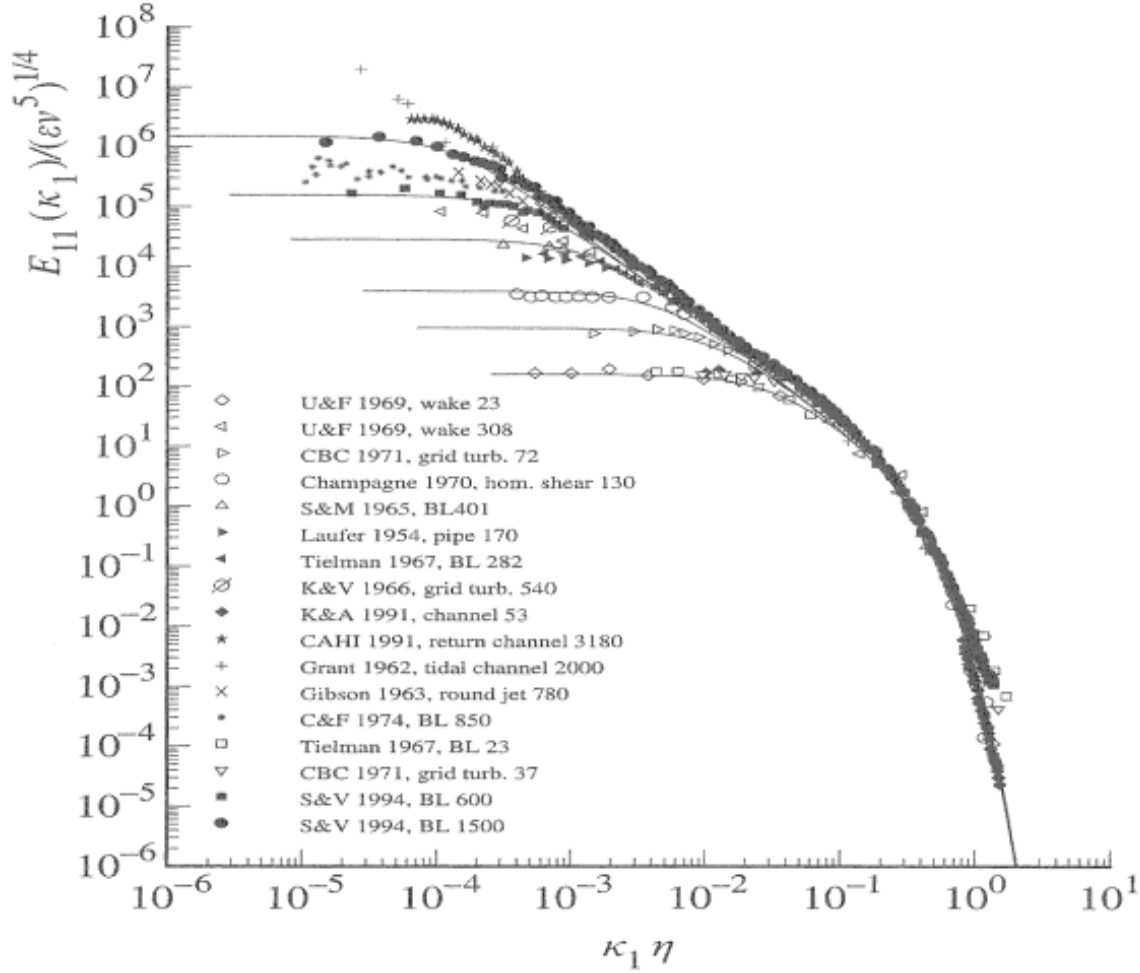
Figure 12.4: Experimental validation of the Kolmogorov spectrum in the inertial range for a variety of different turbulent flows, taken from Reference [Pop00]. As the statistics of turbulence are universal in the inertial and dissipative ranges, it is expected that the Kolmogorov spectrum will hold, not matter what are the details of the large-scale geometry and forcing.

following two-point correlation function in real space:

$$R_{ij}(x, y, z) = \frac{1}{t_2 - t_1} \frac{1}{L_x L_y} \int_{t_1}^{t_2} \mathrm{d}t \int_0^{L_x} \mathrm{d}x' \int_0^{L_y} \mathrm{d}y' U_i(x+x', y+y', z) U_j(x', y', z) - \langle U_i \rangle(z) \langle U_j \rangle(z);$$

$$\text{(12.8)}$$

Then, based on Equation (12.8), one takes a Fourier transform in plane parallel to the walls at location z, defined as follows:

$$\hat{R}_{ij}(k_x, k_y, z) = \iint_{[0,L_x] \times [0,L_y]} \mathrm{d}x \mathrm{d}y \, e^{-ik_x x - i k_y y} R_{ij}(x, y, z).$$

The vertical axis in Figure 12.4 shows $E_{11}(k_x, z) := |\hat{R}_{ij}(k_x, 0, z)|$. For a channel flow, this would be typically taken at the channel midpoint $z = H/2$. Because turbulence is homogeneous and isotropic at sufficiently small scales, it shouldn't matter that we are looking at a Fourier transform involving only the k_x-wavenumbers. Also, it shouldn't matter that we are looking at the correlation function in the particular directions $i = j = 1$. Thus, it is expected that the famous Kolmogorov scaling law $E_{11}(k_x) \sim k_x^{-5/3}$ should apply, as indeed it does in Figure 12.4 – in the window where the spectrum exhibits the straight-line behaviour on the loglog scale – to a wide range of different experiments at different (sufficiently high) Reynolds numbers. For sufficiently small scales, and across the range of experiments on show, the spectrum exhibits exponential decay (or possibly faster-than-exponential decay), corresponding to the dissipation range.

The Kolmogorov scaling theory is also self-consistent, in the following sense. For, taking $E(k) = Ak^{-p}$, the energy contained in a wavenumber range $k \in (k_0, \infty)$ is

$$\text{Energy}[k \in (k_0, \infty)] = \int_{k_0}^{\infty} E(k) \mathrm{d}k = \frac{A}{p-1} k_0^{-(p-1)},$$

meaning that $p > 1$ for a finite energy. Also, the total dissipation can be expressed as

$$\epsilon = 2\nu \int \mathrm{d}^3 x \, s_{ij} s_{ij}, \qquad s_{ij} = \frac{1}{2} \left(\frac{\partial u_i}{\partial x_j} + \frac{\partial u_j}{\partial x_i} \right)$$

where S_{ij} is the instantaneous rate-of-strain tensor. Using Parseval's identity, this is

$$\epsilon = 2\nu \int_0^{\infty} \mathrm{d}k \, k^2 E(k),$$

and the amount of dissipation occuring in the scales $k \in (0, k_0)$ is thus

$$\text{Dissipation}[k \in (0, k_0)] = 2\nu \int_0^{k_0} \mathrm{d}k \, m^2 E(k) = \frac{2\nu A}{3-p} k_0^{3-p}.$$

Therefore, in order for the dissipation in the scales $(0, k_0)$ to remain finite as $k_0 \to 0$, we need

$p < 3$. Thus, we need $1 < p < 3$, and the K-41 theory is definitely consistent with this requirement. Indeed, with the K-41 theory, we have

$$\text{Energy}[k \in (k_0, \infty)] \sim k_0^{-2/3},$$

which properly deceases as one goes to larger k_0 (smaller lengthscales), and

$$\text{Dissipation}[k \in (0, k_0)] \sim k_0^{4/3},$$

which also properly decreases as one goes to smaller k_0 (larger lengthscales).

The second-order structure function

We introduce the following two-point correlation called the **structure function**:

$$D_{ij}(\boldsymbol{r}, \boldsymbol{x}, t) = \langle [U_i(\boldsymbol{x} + \boldsymbol{r}, t) - U_i(\boldsymbol{x}, t)] [U_j(\boldsymbol{x} + \boldsymbol{r}, t) - U_j(\boldsymbol{x}, t)] \rangle.$$

For homogeneous turbulence, we have

$$D_{ij}(\boldsymbol{r}, \boldsymbol{x}, t) = D_{ij}(\boldsymbol{r}, t)$$

only, and we therefore have the following fact:

Theorem 12.2 *For the second-order structure function in homogeneous turbulence, we have*

$$\frac{\partial D_{ij}(\boldsymbol{r}, t)}{\partial r_i} = 0.$$

Proof: We have

$$D_{ij}(\boldsymbol{r}, t) = \langle U_i(\boldsymbol{x}+\boldsymbol{r}, t)U_j(\boldsymbol{x}+\boldsymbol{r}, t) \rangle - \langle U_i(\boldsymbol{x}+\boldsymbol{r}, t)U_j(\boldsymbol{x}, t) \rangle - \langle U_i(\boldsymbol{x}, t)U_j(\boldsymbol{x}+\boldsymbol{r}, t) \rangle + \langle U_i(\boldsymbol{x}, t)U_j(\boldsymbol{x}, t) \rangle.$$

Hence,

$$\frac{\partial D_{ij}(\boldsymbol{r}, t)}{\partial r_i} = \left\langle \left[\frac{\partial}{\partial r_i} U_i(\boldsymbol{x} + \boldsymbol{r}, t) \right] U_j(\boldsymbol{x} + \boldsymbol{r}, t) \right\rangle + \left\langle U_i(\boldsymbol{x} + \boldsymbol{r}, t) \left[\frac{\partial}{\partial r_i} U_j(\boldsymbol{x} + \boldsymbol{r}, t) \right] \right\rangle$$
$$- \left\langle \left[\frac{\partial}{\partial r_i} U_i(\boldsymbol{x} + \boldsymbol{r}, t) \right] U_j(\boldsymbol{x}, t) \right\rangle - \left\langle U_i(\boldsymbol{x}, t) \left[\frac{\partial}{\partial r_i} U_j(\boldsymbol{x} + \boldsymbol{r}, t) \right] \right\rangle$$

A few of these terms are obviously zero because of incompressibility, and we are left with

$$
\begin{aligned}
\frac{\partial D_{ij}(\boldsymbol{r},t)}{\partial r_i} &= \left\langle U_i(\boldsymbol{x}+\boldsymbol{r},t)\left[\frac{\partial}{\partial r_i}U_j(\boldsymbol{x}+\boldsymbol{r},t)\right]\right\rangle - \left\langle U_i(\boldsymbol{x},t)\left[\frac{\partial}{\partial r_i}U_j(\boldsymbol{x}+\boldsymbol{r},t)\right]\right\rangle \\
&= \left\langle [U_i(\boldsymbol{x}+\boldsymbol{r},t)-U_i(\boldsymbol{x},t)]\left[\frac{\partial}{\partial r_i}U_j(\boldsymbol{x}+\boldsymbol{r},t)\right]\right\rangle
\end{aligned}
$$

We break up these terms into the fluctuating component and the mean component, remembering that

$$
\langle U_i\rangle = a_i(t)+b_{ij}(t)r_j
$$

for homogeneous turbulence. Thus,

$$
\begin{aligned}
U_i(\boldsymbol{x}+\boldsymbol{r},t)-U_i(\boldsymbol{x},t) &= [u_i(\boldsymbol{x}+\boldsymbol{r},t)-u_i(\boldsymbol{x},t)]+b_{ik}r_k, \\
\frac{\partial}{\partial r_i}U_j(\boldsymbol{x}+\boldsymbol{r},t) &= \frac{\partial}{\partial r_i}u_j(\boldsymbol{x}+\boldsymbol{r},t)+b_{im}x_m
\end{aligned}
$$

Hence,

$$
\begin{aligned}
\frac{\partial D_{ij}(\boldsymbol{r},t)}{\partial r_i} &= \left\langle [(u_i(\boldsymbol{x}+\boldsymbol{r},t)-u_i(\boldsymbol{x},t))+b_{ik}r_k]\left[\frac{\partial}{\partial r_i}u_j(\boldsymbol{x}+\boldsymbol{r},t)+b_{ij}\right]\right\rangle, \\
&= \left\langle [(u_i(\boldsymbol{x}+\boldsymbol{r},t)-u_i(\boldsymbol{x},t))]\left[\frac{\partial}{\partial r_i}u_j(\boldsymbol{x}+\boldsymbol{r},t)\right]\right\rangle + \langle [(u_i(\boldsymbol{x}+\boldsymbol{r},t)-u_i(\boldsymbol{x},t))]b_{ij}\rangle \\
&\quad + \left\langle b_{ik}r_k\left[\frac{\partial}{\partial r_i}u_j(\boldsymbol{x}+\boldsymbol{r},t)\right]\right\rangle + \langle b_{ik}b_{ij}r_k\rangle.
\end{aligned}
$$

Hence,

$$
\begin{aligned}
\frac{\partial D_{ij}(\boldsymbol{r},t)}{\partial r_i} &= \left\langle r_k\left[\frac{\partial}{\partial x_k}u_i(\boldsymbol{x})\right]\left[\frac{\partial}{\partial r_i}u_j(\boldsymbol{x}+\boldsymbol{r},t)\right]\right\rangle + \tfrac{1}{2}\left\langle r_k r_m\left[\frac{\partial^2}{\partial x_k x_m}u_i(\boldsymbol{x})\right]\left[\frac{\partial}{\partial r_i}u_j(\boldsymbol{x}+\boldsymbol{r},t)\right]\right\rangle + \cdots \\
&\quad + \left\langle r_k\left[\frac{\partial}{\partial x_k}u_i(\boldsymbol{x})\right]b_{ij}\right\rangle + \tfrac{1}{2}\left\langle r_k r_m\left[\frac{\partial^2}{\partial x_k x_m}u_i(\boldsymbol{x})\right]b_{ij}\right\rangle \\
&\quad + \left\langle b_{ik}r_k\left[\frac{\partial}{\partial r_i}u_j(\boldsymbol{x}+\boldsymbol{r},t)\right]\right\rangle + \langle b_{ik}b_{ij}r_k\rangle.
\end{aligned}
$$

and these correlations now involve only the (homogeneous) fluctuations and are therefore independent of $\boldsymbol{r}$. We can therefore set $\boldsymbol{r}=0$ everywhere, giving

$$
\frac{\partial D_{ij}(\boldsymbol{r},t)}{\partial r_i} = 0.
$$

We now return to the structure function $D_{ij}(\boldsymbol{r},t)$ for **homogeneous isotropic** turbulence. Now, the only second-order homogeneous isotropic tensors that can be formed from the vector $\boldsymbol{r}$ are δ_{ij}

and $r_i r_j$, hence

$$D_{ij}(\boldsymbol{r}, t) = D_{NN}(r, t)\delta_{ij} + [D_{LL}(r, t) - D_{NN}(r, t)]\frac{r_i r_j}{r^2}.$$

Using $\partial_i D_{ij}(\boldsymbol{r}, t) = 0$, we obtain

$$D_{NN}(r, t) = D_{LL}(r, t) + \tfrac{1}{2}r\frac{\partial}{\partial r}D_{LL} \tag{12.9}$$

Exercise 12.3 *Prove Equation* (12.9).

Now, it follows from the Kolmogorov similarity hypotheses that any kind of turbulence is homogeneous and isotropic on the small scales, and thus the previous arguments will apply to any kind of turbulence for r sufficiently small. Therefore, in the inertial range and below, for any kind of turbulence, and using the second similarity hypothesis, we have

$$D_{LL}(r, t) = (\epsilon r)^{2/3}\widehat{D}_{LL}(r/\eta).$$

where $\widehat{D}_{LL}$ is a dimensionless universal function. In the inertial range, where the effects of the viscosity are only indirect, we will have

$$D_{LL}(r, t) = C(\epsilon r)^{2/3},$$

where C is a universal constant. Using Equation (12.9) above, we will also have $D_{NN} = (4/3)D_{LL}$ and hence, in the inertial range,

$$D_{ij} = C_2(\epsilon r)^{2/3}\left(\tfrac{4}{3}\delta_{ij} - \tfrac{1}{3}\frac{r_i r_j}{r^2}\right).$$

12.7   Direct numerical simulation (DNS)

As the name would suggest, the full three dimensional and time dependent Navier–Stokes equations are solved on a computational mesh which is fine enough to resolve the smallest length scale eddies present in the flow, and for a domain which is large enough to allow the largest eddies to develop. The main drawback of this method is its associated computational cost, and it cannot be applied to large Reynolds number flows which are of interest (e.g. for the flow about an airplane with a characteristic velocity of 30 m/s, the Reynolds number is typically 2×10^7 requiring in excess of 10^{17} grid points). However, due to the resolution used, they provide the most accurate computational results attainable, which can then be compared to direct experimental results in certain cases

12.8   Large-eddy simulation

With thanks to James Fannon who provided text for this section.

LES can be thought of as a middle road in terms of complexity between RANS and DNS. Main idea behind an LES is to obtain a so-called filtered velocity $\overline{\boldsymbol{u}}$ by forming a convolution between the full velocity field and a given homogeneous (i.e. space independent) filter function $G(\boldsymbol{r})$ such that:

$$\boldsymbol{u}(\boldsymbol{x},t) = \int_{\Omega} G(\boldsymbol{r})\,\boldsymbol{u}(\boldsymbol{x}-\boldsymbol{r},t)\,d^{n}x \tag{12.10}$$

where the integral is taken over the domain Ω. Typical examples of such filter functions are the box filter:

$$G(\boldsymbol{r}) = \begin{cases} \frac{1}{L}, & |\boldsymbol{r}| \leq \frac{L}{2} \\ 0, & |\boldsymbol{r}| > \frac{L}{2} \end{cases}$$

and Gaussian filter:

$$G(\boldsymbol{r}) = \frac{1}{\sqrt{\pi}L}\exp\left(\frac{-\boldsymbol{r}^2}{L^2}\right)$$

which allow for local averages of $\mathbf{u}(\mathbf{x},t)$ in the neighbourhood of $\mathbf{x}$ to be computed, where the average is taken over a length scale L [Dav09]. The effect of this process is to allow for the larger, energy carrying eddies to be resolved exactly while filtering out the small-scale eddies (Figure 12.5). Although these eddies are not simulated directly, their effect on the rest of the flow is modelled [Dav09]. As such, a LES is more accurate than a RANS simulation as the unsteady large-scale eddies are computed exactly, while it is not as computationally expensive as a full DNS as the smaller scales are not resolved. Thus, it provides a very useful middle ground between both methods. According to Reference [Pop00], the four main steps involved in a LES are given by:

1. A filtering operation is applied to the full velocity field in order to form the filtered velocity $\overline{\boldsymbol{u}}(\boldsymbol{x},t)$, which describes the motion of large-scale eddies, and the fluctuating velocity field $\boldsymbol{u}'(\boldsymbol{x},t)$ which describes the motion of the smaller, unresolved eddies.

2. Obtain the governing equations for $\overline{\boldsymbol{u}}(\boldsymbol{x},t)$ from the NSE. These contain an additional term known as the residual stress tensor.

3. The residual stress tensor is modelled in such a way that it takes into account the effect of the unresolved eddies on the rest of the flow. Hence closure is obtained.

4. The governing equations, which are now closed, are then solved numerically. This allows for the large-scale eddies in the flow to be computed exactly.

We now place our focus on deriving the governing equations for $\overline{\mathbf{u}}(\mathbf{x},t)$, for a general form of the filtered velocity as defined by equation 12.10. Let us apply the filtering process to the dimensionless
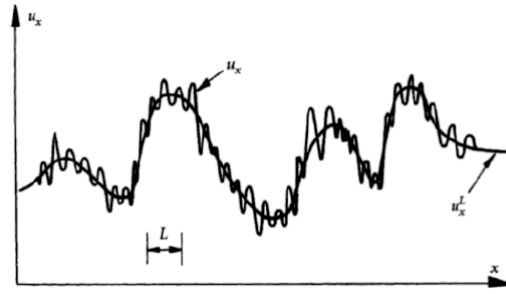
Figure 12.5: Application of a filtering process to the full velocity field u_x yields a filtered velocity u_x^L which accurately represents the large-scale features but removes the small-scale fluctuations [Dav09].

NSE. We apply the filtering operation (as defined by equation 12.10) to these equations and use the fact that the operations of filtering (denoted by the barred variables) and differentiation commute (Technically, this is only true for homogeneous filters [Pop00]), i.e.:

$$\overline{\left(\frac{\partial u_i}{\partial t}\right)} = \frac{\partial \overline{u_i}}{\partial t}, \quad \overline{\left(\frac{\partial u_i}{\partial x_j}\right)} = \frac{\partial \overline{u_i}}{\partial x_j}$$

and similarly for the pressure. Hence one obtains:

$$\frac{\partial \overline{u_i}}{\partial t} + \frac{\partial}{\partial x_j}\left(\overline{u_i u_j}\right) = -\frac{\partial \overline{p}}{\partial x_i} + \frac{1}{Re_*}\frac{\partial^2 \overline{u_i}}{\partial x_j \partial x_j}$$

$$\frac{\partial \overline{u_i}}{\partial x_i} = 0$$

By rewriting the first equation and using the incompressibility condition, we arrive at the filtered equations of motion [San09]:

$$\frac{\partial \overline{u_i}}{\partial t} + \overline{u_j}\frac{\partial \overline{u_i}}{\partial x_j} = -\frac{\partial \overline{p}}{\partial x_i} + \frac{1}{Re_*}\frac{\partial^2 \overline{u_i}}{\partial x_j \partial x_j} - \frac{\partial \overline{\tau_{ij}}}{\partial x_j} \tag{12.11}$$

$$\frac{\partial \overline{u_i}}{\partial x_i} = 0 \tag{12.12}$$

where we define the residual stress tensor as:

$$\overline{\tau_{ij}} = \overline{u_i u_j} - \overline{u_i}\,\overline{u_j} \tag{12.13}$$

Note that these equations are analogous to the RANS equations derived previously, but the interpretation of what the variables signify is very different. In the RANS equations, $\overline{u_i}$ represents the mean flow, while in the filtered equations of motion, the variable $\overline{u_i}$ represents the motion of large-scale eddies and hence can be thought of as the mean flow plus the large-scale turbulent motion [Dav09].

As the residual stress term contains the unknown variable u_i, it remains to formulate an appropriate method of modelling this term so to achieve closure of the system.

Over the past 40 years, LES have proved to be an invaluable tool for researchers interested in studying turbulent flow. The method was first implemented in Reference [Dea70] who, despite using a resolution of only 6720 grid points, obtained some promising results, and paved the way for a number of future researchers e.g. Reference [Sch75] and Reference [Pio93]. Despite the positive aspects of LES, its main weakness, as stated in the critical review carried out in Reference [Mas94], occurs at near surface regions where the turbulent length scales become small in relation to the filter width (the filter width associated with a LES is the cut-off length scale beyond which no eddies are resolved). Here, a much finer computational mesh would be needed to take into account the effect of these small-scale eddies. Ideally, one would use an adaptive grid when solving the NSE computationally, where the grid spacing itself is a function of position. In such a scheme, a higher resolution would be used close to surfaces than would be used in the rest of the domain.

12.9 LES method – implementation

The filter function $G(\mathbf{r})$ as discussed in section 12.8 is incorporated implicitly into a numerical simulation by means of the resolution of the computational mesh itself i.e. the grid spacing provides a natural filter for defining the smallest length scale eddies resolvable in the simulation. As such, it remains to model the residual stress term (also known as the Subgrid-Scale (SGS) term):

$$\overline{\tau_{ij}} = \overline{u_i u_j} - \overline{u_i}\,\overline{u_j}$$

In a turbulent flow, the net transfer of energy from large to small eddies appears as an energy loss or dissipation from the large-scale eddies. As such, the primary function of the SGS term is to remove energy from the resolved eddies at an appropriate rate, and thus the proposed model for it should be dissipative in nature [AB97]. The most common method of modelling this term is that proposed by [Sma63], known as the eddy-viscosity model:

$$\overline{\tau_{ij}} = -2\nu_t \overline{\mathbf{s}_{ij}}$$

where ν_t is the so-called eddy viscosity, while the rate of strain tensor with respect to the filtered velocity is given by:

$$\overline{\mathbf{s}_{ij}} = \frac{1}{2}\left(\frac{\partial \overline{u_i}}{\partial x_j} + \frac{\partial \overline{u_j}}{\partial x_i}\right)$$

The eddy viscosity should be determined by the most energetic of the unresolved eddies in the simulation [Dav09]. As such, let Δ denote the characteristic length scale of the largest, and hence most

energetic, unresolved eddies. According to [Dea70], this length scale is proportional to $(\Delta x \Delta y \Delta z)$, and here we take the value as quoted by [AB97]:

$$\Delta = 2 \left(\Delta x \Delta y \Delta z \right)^{1/3} \tag{12.14}$$

On dimensional grounds, one knows that $[\nu_t] = [\text{Length}]^2 / \text{Time}$, and thus a natural proposition for ν_t is of the form:

$$\nu_t \sim \Delta \left(v_\Delta \right)$$

where v_Δ is a velocity scale for eddies of size Δ. [Sma63] took this velocity scale to be:

$$v_\Delta = \Delta \left| \bar{\mathbf{s}} \right|, \quad \text{where} \ \left| \bar{\mathbf{s}} \right| = \sqrt{2 \left(\bar{\mathbf{s}}_{ij} \right) \left(\bar{\mathbf{s}}_{ij} \right)}$$

As such, the eddy viscosity term becomes:
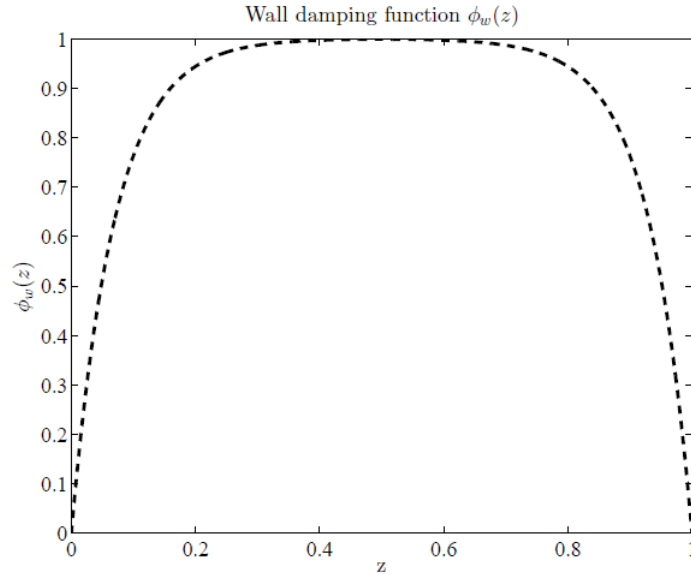
Figure 12.6: Plot of $\phi_w \left(z \right)$ for $p = q = 1$, $A = 25$ and $Re_* = 360$, the Reynolds number used in the LES.

$$\nu_t = C_S^2 \Delta^2 \left| \bar{\mathbf{s}} \right| \tag{12.15}$$

where C_S is a dimensionless constant known as the Smagorinsky coefficient, usually taken to be $C_S = 0.1$ [Dav09]. Furthermore, in order to take into account the turbulence near the walls $z = 0, 1$, where the largest unresolved eddies decrease in size, we use the method of near wall modelling (NWM). This method amounts to introducing a wall damping function $\phi_w \left(z \right)$, which is

given by [San09]:

$$\phi_w(z) = \begin{cases} \left(1 - \exp\left[\left(\frac{-zRe_*}{A}\right)\right]^p\right)^q, & z \le \frac{1}{2} \\ \left(1 - \exp\left[\frac{-(1-z)Re_*}{A}\right]^p\right)^q, & z \ge \frac{1}{2} \end{cases} \tag{12.16}$$

as an additional prefactor for the length scale Δ. In this LES, we take the values $p = q = 1$ and $A = 25$, in keeping with the standard Van Driest components. A plot of the wall damping function for the parameters of interest is given in figure 12.6. The use of this function is both simple to implement numerically and saves computational cost, as compared to introducing a finer mesh grid at the wall which would provide a much more accurate means of modelling the turbulence there. As such, by incorporating the wall damping function, the eddy viscosity term to be implemented numerically is given by:

$$\nu_t = (C_S \Delta \phi_w)^2 \, |\bar{\mathbf{s}}| \tag{12.17}$$

Now substituting the model for the SGS term:

$$\overline{\tau_{ij}} = -\nu_t \left(\frac{\partial \overline{u_i}}{\partial x_j} + \frac{\partial \overline{u_j}}{\partial x_i}\right) \tag{12.18}$$

into Equation (12.11), we find that:

$$\frac{\partial \overline{u_i}}{\partial t} + \overline{u_j} \frac{\partial \overline{u_i}}{\partial x_j} = -\frac{\partial \overline{p}}{\partial x_i} + \frac{1}{Re_*} \frac{\partial^2 \overline{u_i}}{\partial x_j \partial x_j} - \frac{\partial}{\partial x_j}\left(-\nu_t \left(\frac{\partial \overline{u_i}}{\partial x_j} + \frac{\partial \overline{u_j}}{\partial x_i}\right)\right)$$

which can be rewritten as:

$$\frac{\partial \overline{u_i}}{\partial t} + \overline{u_j} \frac{\partial \overline{u_i}}{\partial x_j} = -\frac{\partial \overline{p}}{\partial x_i} + \frac{\partial}{\partial x_j}\left(\left(\frac{1}{Re_*} + \nu_t\right)\left(\frac{\partial \overline{u_i}}{\partial x_j} + \frac{\partial \overline{u_j}}{\partial x_i}\right)\right)$$

again using the incompressibility condition.

12.9.1 Initialization

The turbulence initialization technique which will be implemented in this study is that presented by [BGC04] and [BBP08]. A summary of the method and its numerical implementation will be presented below. First, the initial velocity field to be constructed ($\mathbf{u}(\mathbf{x})$) is written as a vector potential:

$$\boldsymbol{u}(\boldsymbol{x}) = \nabla \times (\boldsymbol{A}(\boldsymbol{x}) f(z)) \tag{12.19}$$

where the function $f(z)$ is an appropriate scaling function of the vector field $\boldsymbol{A}(\boldsymbol{x})$ which ensures that the no-slip boundary conditions at $z = 0, 1$ are enforced. Expanding Equation (12.19) we have:

$$\boldsymbol{u} = f(z)(\nabla \times \boldsymbol{A}(\boldsymbol{x})) + (\nabla f) \times \boldsymbol{A}(\boldsymbol{x})$$

$$\implies \boldsymbol{u} = f(z) \begin{vmatrix} \hat{\mathbf{x}} & \hat{\mathbf{y}} & \hat{\mathbf{z}} \\ \partial_x & \partial_y & \partial_z \\ A_x & A_y & A_z \end{vmatrix} + \begin{vmatrix} \hat{\mathbf{x}} & \hat{\mathbf{y}} & \hat{\mathbf{z}} \\ 0 & 0 & f_z \\ A_x & A_y & A_z \end{vmatrix}$$

and hence each component of $\boldsymbol{u}(\boldsymbol{x})$ is given by:

$$u = f(z)(\partial_y A_z - \partial_z A_y) - A_y \frac{df}{dz} \tag{12.20}$$

$$v = f(z)(\partial_z A_x - \partial_x A_z) + A_x \frac{df}{dz} \tag{12.21}$$

$$w = f(z)(\partial_x A_y - \partial_y A_x) \tag{12.22}$$

As such, in order to ensure that each component vanishes at $z = 0, 1$ we use the following form for the scaling function:

$$f(z) = \frac{1}{2} + \frac{1}{2}\sin\left(\frac{2\pi z}{L_z} - \frac{\pi}{2}\right) \implies \frac{df}{dz} = \frac{\pi}{L_z}\cos\left(\frac{2\pi z}{L_z} - \frac{\pi}{2}\right) \tag{12.23}$$

where $L_z = 1$ is included explicitly for completeness. It now remains to define the velocity field $\boldsymbol{A}(\boldsymbol{x})$. There are a number of features which we want this field to have:

1. As we wish to initialize the system with a turbulent velocity field, the field $\boldsymbol{A}$ should incorporate some randomness.

2. It must satisfy the periodic boundary conditions in the streamwise and spanwise directions.

This suggests that we take a Fourier sum for each component of the field (where $i = x, y, z$):

$$A_i(\boldsymbol{x}) = \sum_{k_x=1}^{C_{k_x}} \sum_{k_y=1}^{C_{k_y}} \sum_{k_z=1}^{C_{k_z}} [S_i(k_x, k_y, k_z)\sin(\mathbf{k} \cdot \mathbf{x}) + C_i(k_x, k_y, k_z)\cos(\boldsymbol{k} \cdot \boldsymbol{x})] \tag{12.24}$$

where we have a sum over the wavenumber **k**:

$$\boldsymbol{k} = \left(\frac{2\pi}{L_x}k_x, \frac{2\pi}{L_y}k_y, \frac{2\pi}{L_z}k_z\right)$$

and the constants $S_i(k_x, k_y, k_z)$ and $C_i(k_x, k_y, k_z)$ are random numbers between 0 and 1.

12.10   TPLS

TPLS stands for Two-phase Levelset, and is a code created by the present author (along with Dr Prashant Valluri, University of Edinburgh), for simulating two-phase flows. This code solves the Navier–Stokes equations for two fluids, simulating the interface between the two phases using a levelset formulation. The code, written in Fortran 90, is fully parallelized using the MPI and OpenMP parallelisation schemes, so that it can be run on thousands of CPU cores, and has been rigorously validated. A single-phase version also exists and is capable of simulating turbulence using LES with the Smagorinsky model above – see

```
https://sourceforge.net/p/tpls/code/HEAD/tree/trunk/s-tpls/
```

Exercise 12.4 *Obtain the single-phase turbulent version of TPLS. Configure and compile a version on whatever multicore machine you can find. Run the code for a sufficient length of time to generate turbulent statistics. Plot the average streamwise turbulent velocity field.*

Appendix A

M codes

A numerical method for solving the model diffusion problem is implemented below.

```matlab
function [xx,yy,C,time_vec,norm_decay]=test_diffusion_jacobi()

% Numerical method to solve
% (d/dt)C=[D_{xx}+D_{yy}]C+s(x,y),
% subject to periodic boundary conditions in the x-direction,
% and Neuman boundary conditions at y=0 and y=L_y.

% ****************************************************************************
% Simulation parameters

[Nx,Ny,~,~,A0,dx,dy,kx0,ky0,dt,~,n_timesteps]=fix_all_parameters();

% max_iteration for diffusion:
max_iteration=30;

% ****************************************************************************
% Poisson solution:

  [~,~,C_poiss,~,~]=test_poisson_jacobi();

% ****************************************************************************
% Initialise source and concentration fields.
% Initialize source and concentration fields.

s_source=zeros(Nx,Ny);
C=zeros(Nx,Ny);

xx=0*(1:Nx);
yy=0*(1:Ny);
```

```matlab
30
31  kx=kx0;
32  ky=3*ky0;
33
34  for i=1:Nx
35      for j=1:Ny
36          x_val=(i-1)*dx;
37          y_val=(j-1)*dy;
38
39          xx(i)=x_val;
40          yy(j)=y_val;
41
42          s_source(i,j)=A0*cos(kx*x_val)*cos(ky*y_val);
43          C(i,j)=cos(kx0*x_val)*cos(ky0*y_val)+cos(2*kx0*x_val)*cos(ky0*y_val)+cos(
                  kx0*x_val)*cos(4*ky0*y_val);
44      end
45  end
46
47  % **************************************************************************
          Enter into time loop now
48  % Enter into time loop now
49
50  norm_decay=0*(1:n_timesteps);
51  time_vec=(1:n_timesteps)*dt;
52
53  for iteration_time=1:n_timesteps
54
55      RHS= get_RHS(C,dt,dx,dy,Nx,Ny);
56      RHS=RHS+dt*s_source;
57
58      for jacobi_iteration=1:max_iteration
59          C_old=C;
60
61          C=do_jacobi_C(C_old,RHS,dt,dx,dy,Nx,Ny);
62
63          % Implement Neumann conditions at y=0,y=L_y.
64          C(:,1)=C(:,2);
65          C(:,Ny)=C(:,Ny-1);
66      end
67
68      err1= get_diff(C,C_old,Nx,Ny);
69      if(mod(iteration_time,100)==0)
70          display(strcat(num2str(iteration_time),': Residual is ...', num2str(err1
                  )))
71          [~,myhandle]=contourf(xx,yy,C');
```

```matlab
72          set(myhandle,'edgecolor','none');
73          colorbar
74          drawnow
75      end
76
77      norm_decay(iteration_time)=sqrt(sum(sum(C-C_poiss).^2)/(Nx*Ny));
78
79 end
80
81 end
82
83 % ****************************************************************************
    Enter into time loop now
84 % ****************************************************************************
    Enter into time loop now
85
86 function RHS=get_RHS(C,dt,dx,dy,Nx,Ny)
87
88 ax=dt/(dx*dx);
89 ay=dt/(dy*dy);
90
91 Diffusion=zeros(Nx,Ny);
92
93 for j=2:Ny-1
94     for i=1:Nx
95
96         if(i==1)
97             im1=Nx-1;
98         else
99             im1=i-1;
100         end
101
102         if(i==Nx)
103             ip1=2;
104         else
105             ip1=i+1;
106         end
107
108         Diffusion(i,j)=ax*( C(ip1,j)+C(im1,j)-2.d0*C(i,j))+ay*( C(i,j+1)+C(i,j
                -1)-2.d0*C(i,j)  );
109     end
110 end
111
112 RHS=C+0.5d0*Diffusion;
113
```

```matlab
114  end
115
116  % ************************************************************************
         Enter into time loop now
117
118  function C=do_jacobi_C(C_old,RHS,dt,dx,dy,Nx,Ny)
119
120  ax=dt/(dx*dx);
121  ay=dt/(dy*dy);
122  diag_val=1+ax+ay;
123
124  C=zeros(Nx,Ny);
125
126  for j=2:Ny-1
127      for i=1:Nx
128
129      if(i==1)
130          im1=Nx-1;
131      else
132          im1=i-1;
133      end
134
135      if(i==Nx)
136          ip1=2;
137      else
138          ip1=i+1;
139      end
140
141      temp_val=(ax/2.d0)*(C_old(ip1,j)+C_old(im1,j))+(ay/2.d0)*(C_old(i,j+1)+C_old
             (i,j-1))+RHS(i,j);
142      C(i,j)=temp_val/diag_val;
143      end
144  end
145
146  end
147
148  % ************************************************************************
         Enter into time loop now
149
150  function err1=get_diff(C,C_old,~,~)
151
152  err1=max(max(abs(C-C_old)));
153
154  end
```

m_codes/diffusion_matlab/test_diffusion_jacobi.m

Subordinate subroutines

It can be noted taht the code calls two subordinate subroutines, which can be downloaded from the website. One is obvious: it is a global subroutine to fix all the parameter values. The second subroutine computes the solution of the model poisson problem to which the solution of the diffusion equation relaxes. Thus, the relaxation to the equilbrium can be monitored as a diagnostic to keep track of the accuracy of the solution. The solution to the model Poisson problem is included herein (below) for completeness.

For completeness, a numerical method for solving the mode **Poisson problem** is also provided herein (below).

```matlab
function [xx,yy,C,C_true,res_it]=test_poisson_jacobi()

% Numerical method to solve
% [D_{xx}+D_{yy}]C+s(x,y)=0,
% subject to periodic boundary conditions in the x-direction,
% and Neuman boundary conditions at y=0 and y=L_y.

[Nx,Ny,~,~,A0,dx,dy,kx0,ky0]=fix_all_parameters();
iteration_max=5000;

dx2=dx*dx;
dy2=dy*dy;

s_source=zeros(Nx,Ny);

% Initialise source

kx=kx0;
ky=3*ky0;

for i=1:Nx
    for j=1:Ny
        x_val=(i-1)*dx;
        y_val=(j-1)*dy;
        s_source(i,j)=A0*cos(kx*x_val)*cos(ky*y_val);
    end
end
```

```matlab
28
29 % Compute analytic solution ***********************************
30
31
32 xx=0*(1:Nx);
33 yy=0*(1:Ny);
34 C_true=zeros(Nx,Ny);
35
36 for i=1:Nx
37     for j=1:Ny
38         xx(i)=(i-1)*dx;
39         yy(j)=(j-1)*dy;
40
41         C_true(i,j)=(A0/(kx*kx+ky*ky))*cos(kx*xx(i))*cos(ky*yy(j));
42
43     end
44 end
45
46 % Iteration step ***********************************************
47 % Initial guess for C:
48 C=zeros(Nx,Ny);
49
50 res_it=0*(1:iteration_max);
51
52 for iteration=1:iteration_max
53
54     C_old=C;
55
56     for i=1:Nx
57
58         % Periodic BCs here.
59         if(i==1)
60             im1=Nx-1;
61         else
62             im1=i-1;
63         end
64
65         if(i==Nx)
66             ip1=2;
67         else
68             ip1=i+1;
69         end
70
71         for j=2:Ny-1
72
```

```
73              diagonal=(2.d0/dx2)+(2.d0/dy2);
74              tempval=(1.d0/dx2)*(C_old(ip1,j)+C_old(im1,j))+(1.d0/dy2)*(C_old(i,j
                    +1)+C_old(i,j-1))+s_source(i,j);
75              C(i,j)=tempval/diagonal;
76
77          end
78      end
79
80      % Implement Dirichlet conditions at y=0,y=L_y.
81      C(:,1)=C(:,2);
82      C(:,Ny)=C(:,Ny-1);
83
84      res_it(iteration)=max(max(abs(C-C_old)));
85
86  end
87
88  end
```

m_codes/diffusion_matlab/test_poisson_jacobi.m

Appendix B

Introduction to Fortran

Overview

I am going to try an example-based introduction to Fortran, wherein I provide you with a sample code, and then tell you about it. I will then ask you to some tasks based on the code, and to modify it.

B.1   Preliminaries

A basic Fortran code is written in a single file with a `.f90` file extension. It conists of a **main part** together with **subroutine** definitions. A subroutine is like a subfunction in Matlab or C, with one key difference that I will explain below.

The main part

The main code is enclosed by the following declaration pair:

```
program mainprogram
...
end program mainprogram
```

At the top level, all variables that are to be used must be declared (otherwise compiler errors will ensue). Variables can be declared as integers or as double-precision numbers (other types are possible and will be discussed later on). Before variable declarations are made, a good idea is to type `implicit none`. This means that Fortran will **not** assume that symbols such as i have an

177

(implicit) type. It is best to be honest with the compiler and tell it upfront what you are going to do. Equally, it is not a good idea for the compiler to try to guess what you mean.

An array of double-precision numbers is defined as follows:

```
integer :: Nx,Ny
parameter (Nx = 201, Ny = 101)
double precision, dimension(1:Nx,1:Ny) :: my_array
```

This creates an array of double-precision numbers where the indices go from $i = 1, 2, \cdots, 201$, and $j = 1, 2, \cdots, 101$. there is nothing special in Fortran about starting arrays with $i = 1$: they can start from any integer whatsoever (positive or negative).

After defining all arrays and all other variables operations are performed on them using standard manipulations. These typically include 'do' loops (the Fortran equivalent of 'for' loops), and 'if' and 'if-else' statements. The syntax for these operatiosn is given below in the sample code (Section B.2).

Column-major ordering

To understand column-major ordering, consider the following array:

$$A = \begin{bmatrix} 1 & 2 & 3 \\ 4 & 5 & 6 \end{bmatrix}$$

If stored in contiguous memory in a column-major format, this array will take the following form in memory:

$$1\ 4\ 2\ 5\ 3\ 6.$$

Suppose that elements of the array A are denoted by A_{ij} (i for rows, j for columns). When these elements are accessed sequentially in contiguous memory, it is the row index that increases the fastest. Thus, in Fortran, a do loop for manipulations on the array A should be written out as follows:

```
do j=1,2
  do i=1,3
    ! manipulations on A(i,j) here
    ...
  end do
end do
```

Subroutines

Subroutines contain discrete tasks that are repeated many times. Instead of having a main code that contains multiple copies of the same piece of code, such code-tasks are relegated to subroutines. The advantages are economy-of-code and computational efficiency. Unlike in C, arrays can be passed to subroutines in a blindly straightforward manner. Examples of such subroutines can be found in the sample code (Section B.2).

As mentioned previously, a subroutine in Fortran is like a subfunction in C or Matlab. However, there is one key difference: **formally, a subroutine produces no explicit outputs**. Thus, suppose we want to operate on a variable x with an operation f to give a result y (formally, $y = f(x)$). In Fortran, we view x and y as **inputs** to a subroutine wherein y is assigned the value $f(x)$ as part of the subroutine's implementation. This will become clearer in examples.

Output

Finally, the result of these manipulations should be sent to a file, for subsequent reading. The values in an array my_array of size $(1, \cdots, N_x) \times (1, \cdots N_y)$ can be written to a file as follows:

```
open(unit=20,file='myfile.dat',status='UNKNOWN')

do j=1,Ny
  do i=1,Nx
    write(20,*) my_array(i,j)
  end do
  end do
close(unit=20, status='KEEP')
```

B.2   The code

The following code solves the model Poisson problem using SOR iteration. If done correctly, it should reproduce exactly the results obtained previously in Matlab. An output file called 'oned.dat' is produced. I cannot remember why I called the output file by this name. However, these things are rather arbitrary.

```fortran
! *************************************************************

program mainprogram
        implicit none

        integer :: Nx,Ny
        parameter (Nx = 201, Ny = 101)

        double precision :: dx,dy,x_val,y_val,Lx,Ly,pi=3.1415926535
        double precision :: ax,ay,diag_val,relax,tempval,err1,err2,A0
        double precision, dimension(1:Nx,1:Ny) :: f_source,C,C_old

        integer :: i,j,im1,ip1,iteration,max_iteration=1000

        Lx=2.d0
        Ly=1.d0

        A0=10.d0

        dx=Lx/dble(Nx-1)
        dy=Ly/dble(Ny-1)

        ax=1.d0/(dx*dx)
        ay=1.d0/(dy*dy)
        diag_val=2.d0*ax+2.d0*ay
        relax=1.5d0

! *************************************************************
! compute source, initialise guess

        f_source=0.d0
        C=0.d0
        C_old=0.d0

        write (*,*) 'getting source'
        call get_f_periodic(f_source,Nx,Ny,dx,dy,Lx,Ly,A0)
        write (*,*) 'done'
```

```fortran
! **********************************************************
! sor steps

      do iteration=1,max_iteration
        err1 = 0.0

        ! for keeping track of the error
        C_old=C

        do j = 2,Ny-1
          do i = 1,Nx

            if(i.eq.1)then
              im1=Nx-1
            else
              im1=i-1
            end if

            if(i.eq.Nx)then
              ip1=2
            else
              ip1=i+1
            end if

            tempval=ax*(C(ip1,j)+C(im1,j))+ay*(C(i,j+1)+C(i,j-1))-f_source(i,j
              )
            C(i,j)=(1-relax)*C(i,j)+relax*tempval/diag_val

          end do
        end do

        ! Implement Dirichlet conditions at y=0,y=L_y.
        C(:,1)=C(:,2)
        C(:,Ny)=C(:,Ny-1)

        if(mod(iteration,100)==0)then
          call get_diff(C,C_old,Nx,Ny,err1)
          write(*,*) iteration, ' Difference is ', err1
        end If

      end do

      write(*,*) ' Difference is ', err1

!
```

```fortran
! ****************************************************************
! write result to file

          write(*,*) 'writing to file'
          open(unit=20,file='oned.dat',status='UNKNOWN')

          do j=1,Ny
            do i=1,Nx
                x_val=(i-1)*dx
                y_val=(j-1)*dy
                Write(20,*) x_val, y_val, C(i,j)
              end do
            end do
          close(unit=20, status='KEEP')
          write(*,*) 'done'

end program mainprogram


! ****************************************************************
! ****************************************************************

   subroutine get_f_periodic(f_src,Nx,Ny,dx,dy,Lx,Ly,A0)
   implicit none

   integer ::i,j,Nx,Ny
   double precision :: dx,dy,Lx,Ly,x_val,y_val, pi=3.1415926535
   double precision :: kx0,ky0,kx,ky,A0
   double precision :: f_src(1:Nx,1:Ny)

   kx0=2.d0*pi/Lx
   ky0=pi/Ly

   kx=kx0
   ky=3.d0*ky0

   f_src=0.d0
   do j=1,Ny
     do i=1,Nx
        x_val=(i-1)*dx
        y_val=(j-1)*dy
        f_src(i,j)=A0*cos(kx*x_val)*cos(ky*y_val)
     end do
   end do
```

```fortran
128       return
129       end subroutine get_f_periodic
130
131 ! ************************************************************
132
133       subroutine get_diff(C,C_old,Nx,Ny,diff)
134       implicit none
135
136       double precision :: diff,sum
137       integer :: Nx,Ny,i,j
138       double precision, dimension(1:Nx,1:Ny) :: C, C_old
139
140       sum = 0.0D0
141       Do j = 1, Ny
142         Do i = 1, Nx
143           sum = sum + (C(i,j)-C_old(i,j))**2
144         End Do
145       End Do
146       diff = sum
147
148       Return
149       End subroutine get_diff
150
151 ! ************************************************************
152 ! ************************************************************
```

m_codes/poisson_code/main_periodic_sor.f90

B.3   Porting Output into Matlab

It can be useful to examine the data in a file such as 'oned.dat' in Matlab. There are many ways of
doing this. Below is my favourite way:

```matlab
function [X,Y,C]=open_dat_file()

% We need to specify the size of the computational domain, as this can't be
% inferred from the datafile.

Nx=201;
Ny=101;

% Here I create a character array called "filename".  This should
% correspond to the name of the Fortran-generated file.

filename='oned.dat';

% Here is the number of lines in the datafile.
n_lines=Nx*Ny;

% Open the file.  Here, fid is a label that labels which line in the file
% is being read.  Obviously, upon opening the file, we are at line 1.

fid=fopen(filename);

% Preallocate some arrays for storing the data.

X=0*(1:n_lines);
Y=0*(1:n_lines);
C=0*(1:n_lines);

% Loop over all lines.

for i=1:n_lines
    % Grab the data from the current line.  Once the data is grabbed, the
    % label fix automatically moves on to the next line.
    % The data from the current line is grabbed into a string - here called
    % c1.
    c1=fgetl(fid);

    % Next I have to convert the three strings on any given line into three
    % doubles.  This is done by scanning the string into an array of
    % doubles, using the "sscanf" command:
    vec_temp=sscanf(c1,'%f');
```

```
41
42      % Now  it  is  simple :  just  assign  each  double  to  a  value  x ,  y ,  or  C .
43      x_temp=vec_temp ( 1 ) ;
44      y_temp=vec_temp ( 2 ) ;
45      C_temp=vec_temp ( 3 ) ;
46
47      % Read  the  x−,  y−,  and  C−values  into  their  own  arrays .
48      X( i )=x_temp ;
49      Y( i )=y_temp ;
50      C( i )=C_temp ;
51  end
52
53  % Finally ,  reshape  these  arrays  into  physical ,  two−dimensional  arrays .
54
55  X=reshape (X, Nx , Ny ) ;
56  Y=reshape (Y, Nx , Ny ) ;
57  C=reshape (C, Nx , Ny ) ;
58
59  % Important !  Close  the  file  so  that  it  is  not  left  dangling .   Not  closing  a
60  % file  properly  means  that  in  future ,  it  will  be  difficult  to  manipulate
61  % it .    For  example ,  it  is  impossible  to  delete  or  rename  a  a  currently −open
62  % file .
63
64  fclose ( fid ) ;
65
66  end
```

m_codes/poisson_code/open_dat_file.m

This file should be stored int he same directory as 'oned.dat'. Then, at the command line, type

```
[X,Y,C]=open_dat_file();
```

The results can be visualized as usual:

```
[h,c]=contourf(X,Y,C);
set(c,'edgecolor','none')
```

Provided the source function and domain size are the same in both cases, this figure should agree exactly with the one generated previously using only Matlab (Figure B.1). Here,

$$s(x, y) = A_0 \cos(k_x x) \cos(k_y y), \tag{B.1}$$

with $k_x = k_{x0}$ and $k_y = 3k_{y0}$, and $A_0 = 10$. Further details: $k_{x0} = (2\pi/L_x)$ is the fundamental wavenumber in the x-direction, and $k_{y0} = \pi/L_y$ is the fundamental wewavenumber in the y-direction. The domain geometry is chosen to be $L_x = 2$ and $L_y = 1$.
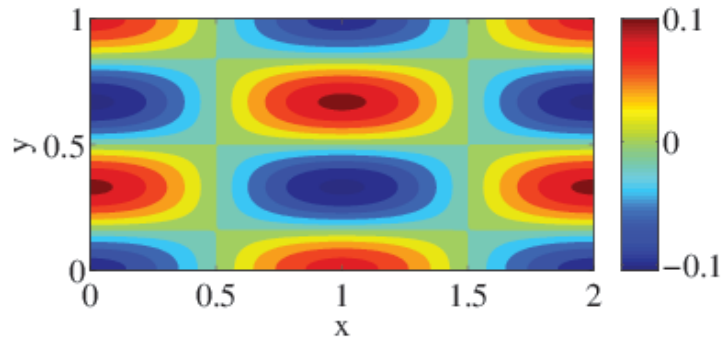

Figure B.1: Solution of the Poisson problem for the source (B.1). Grid size: $N_x = 201$ and $N_y = 101$.

Bibliography

[AB97]   M. B. Abbott and R. Basco. *Computational Fluid Dynamics – An Introduction for Engineers*. Longman, 1997.

[AGL09]   Guenter Ahlers, Siegfried Grossmann, and Detlef Lohse. Heat transfer and large scale dynamics in turbulent rayleigh-bénard convection. *Rev. Mod. Phys.*, 81:503–537, 2009.

[Are84]   Hassan Aref. Stirring by chaotic advection. *Journal of fluid mechanics*, 143:1–21, 1984.

[BBP08]   C. Benocci, J. V. Beeck, and U. Piomelli. Large eddy simulation and related techniques theory and applications, 2008. VKI Lecturer Series.

[BC78]   E. K. Blum and A. F. Chang. A numerical method for the solution of the double eigenvalue problem. *IMA J. Appl. Math.*, 22:29–42, 1978.

[BCF95]   Pierre Barthelet, François Charru, and Jean Fabre. Experimental study of interfacial long waves in a two-layer shear flow. *Journal of Fluid Mechanics*, 303:23–53, 1995.

[BGC04]   Paul Batten, Uriel Goldberg, and Sukumar Chakravarthy. Interfacing statistical turbulence closures with large-eddy simulation. *AIAA journal*, 42(3):485–492, 2004.

[Bib07]   D. Biberg. A mathematical model for two-phase stratified turbulent duct flow. *Multiph. Sci.Tech.*, 19:1, 2007.

[Boy01]   J. P. Boyd. *Chebyshev and Fourier Spectral Methods*. Dover, 2001.

[CC97]   C. Cossu and J. M. Chomaz. Global measures of local convective instabilities. *Phys. Rev. Lett.*, 78:4387–4390, 1997.

[Cha61]   S. Chandrasekhar. *Hydrodynamic and Hydromagnetic Stability*. Dover, New York, 1961.

[Dav09]   P. A. Davidson. *Turbulence – An Introduction for Scientists and Engineers*. Oxford University Press, 2009.

[Dea70]   James W Deardorff. A numerical study of three-dimensional turbulent channel flow at large reynolds numbers. *Journal of Fluid Mechanics*, 41(02):453–480, 1970.

[DR81]   P. G. Drazin and W. H. Reid. *Hydrodynamic Stability*. Cambridge University Press, Cambridge, UK, 1981.

[Gov]   V. Govorukhin. Computer code, ode87 integrator. Downloaded at `http://www.mathworks.com/matlabcentral/fileexchange/3616-ode87-integrator`.

[Gra09]   E.-M. Graefe. *Quantum-Classical Correspondence for a Bose-Hubbard dimer and its non-Hermitian generalisation*. PhD thesis, Technische Universität Kaiserslautern, 2009.

[Gro00]   S. Grossmann. The onset of shear flow turbulence. *Rev. Mod. Phys.*, 72:603–618, 2000.

[HM90]   P. Huerre and P. A. Monkewitz. Local and global instability in spatially developing flows. *Ann. Rev. Fluid Mech.*, 22:473–537, 1990.

[Mas94]   Paul J Mason. Large-eddy simulation: A critical review of the technique. *Quarterly Journal of the Royal Meteorological Society*, 120(515):1–26, 1994.

[Mon88]   P. A. Monkewitz. The absolute and convective nature of instability in two-dimensional wakes at low Reynolds numbers. *Phys. Fluids*, 31:999, 1988.

[NS13]   Lennon Ó Náraigh and Peter DM Spelt. An analytical connection between temporal and spatio-temporal growth rates in linear stability analysis. *Proceedings of the Royal Society A: Mathematical, Physical and Engineering Science*, 469(2156):20130171, 2013.

[NSMZ11] L Ó Náraigh, Peter DM Spelt, OK Matar, and TA Zaki. Interfacial instability in turbulent flow over a liquid film in a channel. *International Journal of Multiphase Flow*, 37(7):812–830, 2011.

[NSN15]   Lennon Ó Náraigh, Selma Shun, and Aurore Naso. Flow-parametric regulation of shear-driven phase separation in two and three dimensions. *Physical Review E*, 91:062127, 2015.

[ÓNSS13] Lennon Ó Náraigh, Peter DM Spelt, and Stephen J Shaw. Absolute linear instability in laminar and turbulent gas–liquid two-layer channel flow. *Journal of Fluid Mechanics*, 714:58–94, 2013.

[Orz71]   S. A. Orzag. Accurate solution of the Orr–Sommerfeld equation. *J. Fluid Mech.*, 50:689, 1971.

[Pio93]   Ugo Piomelli. High reynolds number calculations using the dynamic subgrid-scale stress model. *Physics of Fluids A: Fluid Dynamics (1989-1993)*, 5(6):1484–1490, 1993.

[Pop00]   S. B. Pope. *Turbulent Flows*. Cambridge University Press, Cambridge, UK, 2000.

[Rom73]   VA Romanov. Stability of plane-parallel couette flow. *Functional analysis and its applications*, 7(2):137–146, 1973.

[Rot09]   I. Rotter. A non-hermitian hamilton operator and the physics of open quantum systems. *J. Phys. A: Math. Theor.*, 42:153001, 2009.

[San09]   K. Sangodoyin. Computational fluid dynamics of turbulent stratified flow. Master's thesis, Imperial College London, 2009.

[Sch75]   Ulrich Schumann. Subgrid scale model for finite difference simulations of turbulent flows in plane channels and annuli. *Journal of computational physics*, 18(4):376–404, 1975.

[SH01]   P. J. Schmid and D. S. Henningson. *Stability and Transition in Shear Flows*. Springer, New York, 2001.

[Sma63]   Joseph Smagorinsky. General circulation experiments with the primitive equations: I. the basic experiment*. *Monthly weather review*, 91(3):99–164, 1963.

[tS13]   L. Ó Náraigh and P. D. M. Spelt. An analytical connection between temporal and spatio-temporal growth rates in linear stability analysis. *Proceedings of the Royal Society A*, 469(2156), 2013.

[TTTD93] N. L. Trefethen, A. E. Trefethen, S. C. Teddy, and T. A. Driscoll. Hydrodynamic stability without eigenvalues. *Science*, 561:578, 1993.

[Wal95]   F. Waleffe. Transition in shear flows. nonlinear normality verus nonnormal linearity. *Phys. Fluids*, 7:3060–3066, 1995.

[Wal98]   F. Waleffe. Three-dimensional coherent states in plane shear flows. *Phys. Rev. Lett.*, 81:4140–4143, 1998.

[WWL87]   W. W. Willmarth, T. Wei, and C. O. Lee. Laser anemometer measurements of reynolds stress in a turbulent channel flow with drag reducing polymer additives. *Phys. Fluids*, 30:933, 1987.